

# **Bioactive Constituents from Traditional Chinese Medicines Targeting Neurodegenerative Diseases**

**Chunping Tang**

*B.Sc., M.Sc.*

Eskitis Institute for Drug Discovery

School of Natural Sciences

Griffith Sciences

Submitted in fulfilment of the requirements of the degree of  
Doctor of Philosophy

November 2016



## ABSTRACT

This thesis described a proof-of-concept to translate ancient traditional Chinese medicines to modern drugs. Taking TCMs targeting neurodegenerative diseases, the thesis presented a data mining of ancient literature, physicochemical analysis of known drugs and TCM compounds, and chemical analysis, and phenotypic screening of TCM extracts, fractions and compounds, and early development of a target identification method.

Chapter 1 started with an introduction of traditional Chinese medicines and neurodegenerative diseases. It pointed out that the formula is the essence of TCM, and that herb pairs are a starting point of many formulas. It summarized the natural products used for the treatment of neurodegenerative diseases. It presented an unmet medical need that required new therapeutics. It provided a foundation for the further investigations.

Chapter 2 described a selection of 15 herbs and 5 herb pairs from the TCM formulas that have long been used for the treatment of brain-related disorders. It also included a review of physicochemical analysis of major compounds from the selected herbs using Lipinski's rule of five, ChemGPS-NP, and *in silico* prediction of the BBB permeability. Comparison of TCM compounds and current anti-AD and anti-PD drugs from the physicochemical perspective revealed an amazing convergence between TCM components and modern medicinal chemistry.

Chapter 3 gave details about the preparation of TCM samples. A total of 171 samples including 24 extracts, 48 fractions, 90 compounds and 9 artificial mixtures were prepared from the selected herbs and herb pairs. The chemical composition of all samples was analyzed by HPLC-ELSD, LC-MS, or LC-NMR methods. The results

disclosed chemical correlation among compound, fraction and extract obtained from the same herb or herb pair, including the differences caused by different extraction method. The chemical profiling of these samples provided information for data analysis in the next phenotypic screening.

Chapter 4 described phenotypic screening of all TCM samples by an established multidimensional profiling method. Twenty-eight parameters selected from known cellular pathways and organelles implicated in PD such as mitochondria, lysosomes, apoptosis, and autophagy were used to profile the biological responses of a sample on a PD patient derived cell model. By comparing the phenotypic signatures, we revealed the relationship between different samples, the synergistic effect of the mixture, the impact of the extraction method, and the influence of the ratio of individual compounds on the bioactivity of the combination. More importantly, by cluster analysis, we found almost 2/3 of the total samples showed the same biological effect on the lysosome parameters, which was established as a unique feature for TCM samples from the selected herbs and herb pairs. We concluded that the lysosome effects are highly correlated with brain perturbations, and worthy of in-depth investigations to unlock the mechanism underlying neurodegenerative diseases.

Chapter 5 presented preliminary studies to use a small molecule as a bait to identify the noncovalent ligand-protein complexes from a hONS cell lysate by using native mass spectrometry ESI-FTICR-MS. The results showed the impacts of several important instrument parameters including skimmer 1, time of flight and incubation time on the mass spectra, and tentatively proved the feasibility to detect the noncovalent complexes in the background of the highly complex cell lysate.

Chapter 6 provided a general conclusion from ancient knowledge and wisdom to modern medicine, and pointed out that integration of new technologies will greatly benefit research of the complex TCM system. Our goal is to promote the modernization

of TCMs and provide modern TCM drugs with reliable efficacy, clear chemical composition, definite mechanism, and controllable quality. The coexistence of TCM and western medicine and usage of them in a complementary way are believed to greatly benefit the health of human beings.

## **Statement of Originality**

*This work has not previously been submitted for a degree or diploma in any university.*

*To the best of my knowledge and belief, the thesis contains no material previously published or written by another person except where due reference is made in the thesis itself.*

(Signed) \_\_\_\_\_

Chunping Tang

# Contents

<b>CHAPTER 1</b>	<b>Introduction.....</b>	<b>1</b>
1.1	<b>Traditional Chinese Medicine .....</b>	<b>1</b>
1.1.1	Traditional Chinese Medicine, medical classics and Chinese Pharmacopoeia .....	1
1.1.2	TCM formula.....	5
1.1.3	TCM and natural products.....	7
1.1.4	Modernization of traditional Chinese medicines: TCM-based drug discovery .....	9
1.1.5	Herb pair: a cutting point for in-depth research of TCM .....	13
1.2	<b>Neurodegenerative disease.....</b>	<b>15</b>
1.2.1	Neurodegenerative disease and urgent need for effective therapies .....	15
1.2.2	Natural products used to treat neurodegenerative diseases .....	17
1.3	<b>Research objectives.....</b>	<b>19</b>
1.4	<b>outline of the program.....</b>	<b>20</b>
1.5	<b>References.....</b>	<b>22</b>
<b>CHAPTER 2</b>	<b>Selection of herbs and herb pairs and physicochemical analysis of major compounds from the selected herbs .....</b>	<b>26</b>
2.1	<b>Selection of herbs and herb pairs targeting neurodegenerative disease.....</b>	<b>26</b>
2.1.1	Selection of herbs frequently used to treat PD and AD .....	26
2.1.2	Selection of herb pairs.....	32
2.2	<b>Physicochemical analysis of major compounds from the 15 selected herbs .....</b>	<b>34</b>
2.2.1	Methods used for physicochemical analysis .....	34
2.2.1.1	Lipinski's rule of five .....	34
2.2.1.2	ChemGPS-NP .....	35
2.2.1.3	<i>In silico</i> prediction of the BBB permeability .....	35
2.2.2	Physicochemical analysis of major compounds from the selected herbs.....	36
2.3	<b>Conclusion .....</b>	<b>57</b>
2.4	<b>References.....</b>	<b>57</b>
<b>CHAPTER 3</b>	<b>Sample preparation and chemical profiling.....</b>	<b>59</b>
3.1	<b>Preparation of TCM samples .....</b>	<b>59</b>
3.1.1	Herb materials .....	59
3.1.2	Sample preparation.....	60
3.1.2.1	Extracts and fractions.....	61
3.1.2.2	Compounds .....	62
3.2	<b>HPLC analysis of TCM samples .....</b>	<b>70</b>
3.2.1	Extracts and fractions .....	70
3.2.2	Pure compounds .....	73
3.2.3	Herbs and herb pairs.....	74
3.2.4	Herbs and herb pairs treated with different extraction methods .....	78
3.2.5	Artificial mixtures .....	80
3.3	<b>TCM samples for screening .....</b>	<b>81</b>
3.4	<b>Experimentals .....</b>	<b>81</b>
3.4.1	Preparation of extracts and fractions.....	81
3.4.2	HPLC SOP for extracts and fractions .....	82
3.4.3	LC-MS check for compounds .....	82
3.4.4	LC-MS analysis for herb pair and its constitutive herbs .....	83
3.5	<b>References.....</b>	<b>84</b>

<b>CHAPTER 4 Image-Based Phenotypic Profiling</b>	<b>85</b>
<b>4.1 Introduction</b>	<b>85</b>
4.1.1 Phenotypic profiling	85
4.1.2 A multidimensional image-based phenotypic screening on a PD patient derived cell model	87
<b>4.2 Experimental</b>	<b>89</b>
4.2.1 Materials and reagents	89
4.2.2 Cell line and cell culture	90
4.2.3 Sample transfer for biological assay	91
4.2.4 Cell staining	91
4.2.5 Imaging and image analysis	92
<b>4.3 Results and discussion</b>	<b>93</b>
4.3.1 Clustering of TCM samples based on phenotypic responses	93
4.3.2 Phenotypic descriptions of seven bioclusters	95
4.3.2.1 Biocluster 1	95
4.3.2.2 Biocluster 2	96
4.3.2.3 Biocluster 3	97
4.3.2.4 Biocluster 4	97
4.3.2.5 Biocluster 5	98
4.3.2.6 Biocluster 6	98
4.3.2.7 Biocluster 7	100
4.3.3 Analysis of biological signatures from different respective	100
4.3.3.1 An overview	101
4.3.3.2 Extract VS fraction	104
4.3.3.3 Fraction VS compound	106
4.3.3.4 Impact of stereochemistry	108
4.3.3.5 Impact of extract method	110
4.3.4 Analysis of herb and herb pair	113
4.3.4.1 Herb pair 6+7	114
4.3.4.2 Herb pair 6+8	121
4.3.4.3 Herb pair 9+14	128
4.3.4.4 Herb pair 10+11	133
4.3.4.5 Herb pair 12+13	136
4.3.5 A summary	141
<b>4.4 Conclusions from phenotypic analysis</b>	<b>142</b>
4.4.1 Common features of TCM samples behind clustering	143
4.4.2 Biological responses related with cell toxicity	145
4.4.3 Unique features of TCM samples	146
<b>4.5 References</b>	<b>148</b>
<b>CHAPTER 5 Mass-based target identification</b>	<b>150</b>
<b>5.1 Introduction</b>	<b>150</b>
5.1.1 Target identification	150
5.1.2 ESI-FTICR-MS in study of noncovalent complex	151
5.1.3 Identify direct protein-ligand interactions from cell lysate	152
<b>5.2 Experimental</b>	<b>153</b>
5.2.1 Materials and reagents	153
5.2.2 Cell line and cell culture	154
5.2.3 Cell lysis	154

5.2.4 Protein quantification in the cell lysate .....	154
5.2.5 Buffer exchange and lysate concentration .....	155
5.2.6 Sample preparation.....	155
5.2.7 ESI-FTICR analysis .....	155
<b>5.3 Results and discussion.....</b>	<b>156</b>
5.3.1 Cell lysis and buffer exchange .....	156
5.3.2 ESI-MS conditions optimization.....	157
5.3.2.1 Time of flight.....	158
5.3.2.2 Skimmer 1 .....	159
5.3.2.3 Incubation time .....	160
5.3.3 Search for protein-ligand complexes.....	161
<b>5.4 Future work .....</b>	<b>166</b>
<b>5.5 References.....</b>	<b>167</b>
<b>CHAPTER 6 General conclusions and perspectives.....</b>	<b>169</b>
<b>6.1 General conclusions.....</b>	<b>169</b>
<b>6.2 Integration of new technologies will benefit TCM research.....</b>	<b>170</b>
<b>Supporting Information .....</b>	<b>173</b>
<b>Appendix I .....</b>	<b>180</b>
<b>Appendix II.....</b>	<b>187</b>

## LIST OF FIGURES

<b>Figure 1.1</b> The symbol of yin and yang (left), and the relationship of five elements (right). .....	2
<b>Figure 1.2</b> The cover of Pharmacopoeia of the People's Republic of China, Volume I, English Edition, 1997 (left); Descriptions of the TCM Baibu (right). .....	4
<b>Figure 1.3</b> All new approved drugs 1981–2014; n = 1562. B-biological macromolecule; N-unaltered natural product; NB-botanical drug (defined mixture); ND-natural product derivative; S-synthetic drug; S*-synthetic drug with NP pharmacophore; V-vaccine; NM-mimic of natural product. ....	8
<b>Figure 1.4</b> Descriptions about how to use Qinghao to treat malaria in Zhou-Hou-Ji-Bei-Fang (肘后备急方), an ancient medicinal book written by Hong Ge in the Eastern Jin Dynasty (317 AD – 420 AD). <i>Copyright not required</i> . ....	10
<b>Figure 1.5</b> Herb pairs have acted as a transitional role in the evolution of multi-herb formulae, and may play a key role in the development of herb formulae R&D. ....	15
<b>Figure 1.6</b> Percentage changes in selected causes of death (all ages) between 2000 and 2013. Created from data from the National Center for Health Statistics. ....	16
<b>Figure 1.7</b> Chemical structures of huperzine A, galantamine and baicalein. ....	18
<b>Figure 1.8</b> Bar charts of distribution of publication records about traditional Chinese medicine (left, blue); and traditional Chinese medicine herb pair (right, red) from 2006 to 2015. ....	19
<b>Figure 1.9</b> General flowchart of the PhD program. ....	21
<b>Figure 3.1</b> Strategy of preparation of extracts, fractions and compounds for screening. ....	60
<b>Figure 3.2</b> Flowchart of preparation of extract and fraction. ....	61
<b>Figure 3.3</b> Chemical structures of 90 compounds. ....	69
<b>Figure 3.4</b> The overlay report of E1 (total extract), E1-1 (water-soluble fraction) and E1-2 (fat-soluble fraction) from <u>Ginseng Radix</u> (herb 1). ....	71
<b>Figure 3.5</b> The overlay report of 30 Ginsenosides purchased from market and comparison with the fat-soluble fraction E1-2 of herb 1. ....	72
<b>Figure 3.6</b> Overlaid report for the fat-soluble fraction of <u>Polygoni Multiflori Radix</u> (herb 4) and five major components purchase from market: J01: aloe emodin, J02: chrysophanol, J03: physcion, J04: emodin, J05: 2,3,5,4'-tetrahydrosytilene-2-O-β-D-glucopyranoside. ....	72
<b>Figure 3.7</b> Above: HPLC chromatograms: ELSD, UV, negative total ion, positive total ion; Below: negative and positive ion chromatograms of peak at retention time around 6.06 min. ....	73
<b>Figure 3.8</b> Above: ELSD chromatogram of the herb pair 9+14 (1:1); Middle: ELSD chromatogram of the herb <u>Puerariae Lobatae Radix</u> ; Below: ELSD chromatogram of the herb <u>Salviae Miltiorrhizae Radix et Rhizoma</u> . ....	74
<b>Figure 3.9</b> Above: ELSD chromatogram of the herb pair 6+8 (1:4); Middle: ELSD chromatogram of the herb <u>Chuanxiong Rhizoma</u> ; Below: ELSD chromatogram of the herb <u>Gastrodiae Rhizoma</u> . ....	75
<b>Figure 3.10</b> Above: ELSD chromatogram of the herb pair 12+13 (1:1); Middle: ELSD chromatogram of the herb <u>Ziziphi Spinosa Semen</u> ; Below: ELSD chromatogram of the herb <u>Platycladi Semen</u> . ....	76
<b>Figure 3.11</b> Above: ELSD chromatogram of the herb pair 6+7 (3:4); Middle: ELSD chromatogram of the herb <u>Ramulus Uncariae Cum Uncis</u> ; Below: ELSD chromatogram of the herb <u>Gastrodiae Rhizoma</u> . ....	76
<b>Figure 3.12</b> Above: ELSD chromatogram of the herb pair 10+11 (1:1); Middle: ELSD	

chromatogram of the herb <i>Polygalae Radix</i> ; Below: ELSD chromatogram of the herb <i>Acori Tatarinowii Rhizoma</i> .....	77
<b>Figure 3.13</b> ELSD chromatogram comparison of the ethanol and water extracts for herb 6 (above), herb 8 (middle), and herb pair 6+8 (below). .....	79
<b>Figure 4.1</b> General strategy of the established multidimensional profiling method. ....	87
<b>Figure 4.2</b> Heatmap depicting the cytological profiles of 171 TCM samples. Based on the log <sub>2</sub> compound/DMSO ratio, with pertinent clusters highlighted. Samples were hierarchically clustered based on their pairwise Pearson coefficients and 7 clusters with an uncentered correlation superior to 0.7 were defined from the dendrogram. Uncentered correlation coefficient/cluster: 0.845/1, 0.727/2, 0.714/3, 0.718/4, 0.738/5, 0.736/6, and 0.761/7. Individual compounds are presented on the y-axis with 28 cytological parameters on the x-axis. Cytological parameters: 1- nucleus marker texture, 2- nucleus marker intensity, 3-nucleus area, 4- nucleus roundness, 5- nucleus width (μm), 6- nucleus length (μm), 7- nucleus ratio width to length, 8- cell area (μm <sup>2</sup> ), 9- cell roundness, 10- cell width (μm), 11- cell length (μm), 12- cell ratio width to length, 13- tubulin marker texture, 14- tubulin marker intensity in cytoplasm, 15- tubulin marker intensity in outer region of cytoplasm, 16- tubulin marker intensity in inner region of cytoplasm, 17- mitochondria marker texture, 18- mitochondria marker intensity in cytoplasm, 19- mitochondria marker intensity in outer region of cytoplasm, 20- mitochondria marker intensity in inner region of cytoplasm, 21- LC3b marker texture, 22- LC3b marker intensity in cytoplasm, 23- LC3b marker intensity in outer region of cytoplasm, 24- LC3b marker intensity in inner region of cytoplasm, 25- lysosomes marker texture, 26- lysosome marker intensity in cytoplasm, 27- lysosome marker intensity in outer region of cytoplasm, 28- lysosome marker intensity in inner region of cytoplasm. Yellow represents positive effect. Blue represents negative effects. The data were the average of triplicate measurements. ....	94
<b>Figure 4.3</b> Heatmap depicting the cytological profile of samples in biocluster 1, based on the log <sub>2</sub> compound/DMSO ratio. Individual compounds are presented on the y-axis with individual features on the x-axis. The parameters are the same as described fully in Figure 4.2. ....	96
<b>Figure 4.4</b> Heatmap depicting the cytological profile of samples in biocluster 2, based on the log <sub>2</sub> compound/DMSO ratio. Individual compounds are presented on the y-axis with individual features on the x-axis. The parameters are the same as described fully in Figure 4.2. ....	96
<b>Figure 4.5</b> Heatmap depicting the cytological profile of samples in biocluster 3, based on the log <sub>2</sub> compound/DMSO ratio. Individual compounds are presented on the y-axis with individual features on the x-axis. The parameters are the same as described fully in Figure 4.2. ....	97
<b>Figure 4.6</b> Heatmap depicting the cytological profile of samples in biocluster 4, based on the log <sub>2</sub> compound/DMSO ratio. Individual compounds are presented on the y-axis with individual features on the x-axis. The parameters are the same as described fully in Figure 4.2. ....	97
<b>Figure 4.7</b> Heatmap depicting the cytological profile of samples in biocluster 5, based on the log <sub>2</sub> compound/DMSO ratio. Individual compounds are presented on the y-axis with individual features on the x-axis. The parameters are the same as described fully in Figure 4.2. ....	98
<b>Figure 4.8</b> Heatmap depicting the cytological profile of samples in biocluster 6, based on the log <sub>2</sub> compound/DMSO ratio. Individual compounds are presented on the y-axis with individual features on the x-axis. The parameters are the same as described fully in Figure 4.2. ....	99
<b>Figure 4.9</b> Heatmap depicting the cytological profile of samples in biocluster 7, based on the log <sub>2</sub> compound/DMSO ratio. Individual compounds are presented on the y-axis with individual features on the x-axis. The parameters are the same as described fully in Figure 4.2. ....	100

<b>Figure 4.10</b> Heatmap depicting the cytological profiles of 171 TCM samples (A), samples from five herb pairs 6+7 (B), 6+8 (C), 9+14 (D), 10+11 (E), and 12+13 (F), and 90 pure compounds (G), 46 compounds from 5 herb pairs (H), and the extracts of 15 herbs and 5 herb pairs (I).	103
<b>Figure 4.11</b> Phenotypic signatures of the extract and its fractions obtained from 15 herbs and 5 herb pairs. HP–herb pair; Ext–extract; WF–water-soluble fraction; FF–fat-soluble fraction.	105
<b>Figure 4.12</b> Phenotypic signatures of the extract, fractions and 30 compounds obtained from herb 1. Ext–extract; WF–water-soluble fraction; FF–fat-soluble fraction; Cpd–compound. The numbers after Cpd are consistent with those in Table 3.3.	106
<b>Figure 4.13</b> Phenotypic signatures of the extract, fractions and characteristic compounds obtained from herb 2 (A) and herb 3 (B). Ext–extract; WF–water-soluble fraction; FF–fat-soluble fraction; Cpd–compound. The numbers after Cpd are consistent with those in Table 3.3.	108
<b>Figure 4.14</b> Phenotypic signatures of the extract, fractions and characteristic compounds obtained from herb 5. Ext–extract; WF–water-soluble fraction; FF–fat-soluble fraction; Cpd–compound. The numbers after Cpd are consistent with those in Table 3.3.	108
<b>Figure 4.15</b> Phenotypic signatures of three pairs of stereoisomeric compounds and two pairs of racemic and non-racemic compounds obtained from herb 1. Cpd–compound. The numbers after Cpd are consistent with those in Table 3.3.	109
<b>Figure 4.16</b> Phenotypic signatures of the extract and fractions obtained from herb 6, herb 8 and herb 6+8 using ethanol and water extraction. Ext–extract; WF–water-soluble fraction; FF–fat-soluble fraction; W–water extraction method.	110
<b>Figure 4.17</b> Bar charts of log <sub>2</sub> ratio values of the extracts of herb 6 (A), herb 8 (B), and herb pair 6+8 (C) using ethanol (Blue) and water (Red) extraction methods. The parameters are the same as described fully in Figure 4.2.	111
<b>Figure 4.18</b> Bar charts of log <sub>2</sub> ratio values of the extracts of five herb pairs. The parameters are the same as described fully in Figure 4.2.	113
<b>Figure 4.19</b> Phenotypic signatures of all samples from herb 6, herb 7 and herb pair 6+7 (A), and bar chart of log <sub>2</sub> ratio values of samples from herb 6 (red), herb 7 (green) and herb pair 6+7 (blue) (B). The parameters are the same as described fully in Figure 4.2.	114
<b>Figure 4.20</b> Phenotypic signatures of extracts of herb 6, herb 7 and herb pair 6+7 (A), and bar chart of log <sub>2</sub> ratio values of the extracts of herb 6, herb 7 and herb pair 6+7. The parameters are the same as described fully in Figure 4.2.	115
<b>Figure 4.21</b> Bar chart of log <sub>2</sub> ratio values of gastrodin ( <b>42</b> ) and the extract of herb 6 (A), and bar chart of log <sub>2</sub> ratio values of compounds <b>43-46</b> . The parameters are the same as described fully in Figure 4.2.	116
<b>Figure 4.22</b> Bar chart of log <sub>2</sub> ratio values of artificial mixtures AM1 and AM2. The parameters are the same as described fully in Figure 4.2.	118
<b>Figure 4.23</b> Bar chart of log <sub>2</sub> ratio values of AM1 and its mimic (A), and AM2 and its mimic (B). The parameters are the same as described fully in Figure 4.2.	119
<b>Figure 4.24</b> Bar chart of log <sub>2</sub> ratio values of the extract of herb7 and compounds <b>47</b> and <b>48</b> isolated from herb 7. The parameters are the same as described fully in Figure 4.2.	120
<b>Figure 4.25</b> Phenotypic signatures of all samples from herb 6, herb 8 and herb pair 6+8 (A), and bar chart of log <sub>2</sub> ratio values of samples from herb 6 (red), herb 8 (green) and herb pair 6+8 (blue) (B). The parameters are the same as described fully in Figure 4.2.	121
<b>Figure 4.26</b> Phenotypic signatures of extracts of herb 6, herb 8 and herb pair 6+8 (A), and bar chart of log <sub>2</sub> ratio values of the extracts of herb 6, herb 8 and herb pair 6+8 (B). The parameters are the same as described fully in Figure 4.2.	122
<b>Figure 4.27</b> Bar chart of log <sub>2</sub> ratio values of the extract and fractions obtained from herb 8	

(A), and bar chart of log <sub>2</sub> ratio values of compounds <b>50</b> and <b>56</b> and the fat-soluble fraction of herb 8. The parameters are the same as described fully in Figure 4.2. ....	124
<b>Figure 4.28</b> Phenotypic signatures of compounds <b>49-56</b> from herb 8 (A), and bar chart of log <sub>2</sub> ratio values of compounds <b>52-53</b> and the extract of herb 8 (B). The parameters are the same as described fully in Figure 4.2. ....	124
<b>Figure 4.29</b> Bar chart of log <sub>2</sub> ratio values of compound <b>55</b> . The parameters are the same as described fully in Figure 4.2. ....	125
<b>Figure 4.30</b> Bar chart of phenotypic signatures of compounds <b>50</b> and <b>56</b> , and the artificial mixture of AM3 (A), and the mimic AM3 (B). The parameters are the same as described fully in Figure 4.2. ....	126
<b>Figure 4.31</b> Bar chart of log <sub>2</sub> ratio values of artificial mixtures AM4 and AM5. The parameters are the same as described fully in Figure 4.2. ....	127
<b>Figure 4.32</b> Bar chart of log <sub>2</sub> ratio values of artificial mixtures AM4 and its mimic (A), and AM5 and its mimic (B). The parameters are the same as described fully in Figure 4.2. ....	127
<b>Figure 4.33</b> Phenotypic signatures of all samples from herb 9, herb 14 and herb pair 9+14 (A), and bar chart of log <sub>2</sub> ratio values of samples from herb 9 (green), herb 14 (red) and herb pair 9+14 (blue) (B). The parameters are the same as described fully in Figure 4.2. ....	128
<b>Figure 4.34</b> Phenotypic signatures of extracts of herb 9, herb 14 and herb pair 9+14 (A), and bar chart of log <sub>2</sub> ratio values of the extracts of herb 9, herb 14 and herb pair 9+14 (B). The parameters are the same as described fully in Figure 4.2. ....	129
<b>Figure 4.35</b> Bar chart of log <sub>2</sub> ratio values of compounds of the fat-soluble group (A), and compounds of the water-soluble group (B). The parameters are the same as described fully in Figure 4.2. ....	130
<b>Figure 4.36</b> Bar chart of log <sub>2</sub> ratio values of compound <b>58</b> and water-soluble and fat-soluble fractions of herb 9. The parameters are the same as described fully in Figure 4.2. ....	131
<b>Figure 4.37</b> Bar chart of log <sub>2</sub> ratio values of compound <b>86</b> and the extract of herb 9. The parameters are the same as described fully in Figure 4.2. ....	132
<b>Figure 4.38</b> Bar chart of log <sub>2</sub> ratio values of AM6 and its mimic. The parameters are the same as described fully in Figure 4.2. ....	132
<b>Figure 4.39</b> Phenotypic signatures of all samples from herb 10, herb 11 and herb pair 10+11 (A), and bar chart of log <sub>2</sub> ratio values of samples from herb 10 (red), herb 11 (green) and herb pair 10+11 (blue) (B). The parameters are the same as described fully in Figure 4.2. ....	133
<b>Figure 4.40</b> Phenotypic signatures of extracts of herb 10, herb 11 and herb pair 10+11 (A), and bar chart of log <sub>2</sub> ratio values of the extracts of herb 10, herb 11 and herb pair 10+11 (B). The parameters are the same as described fully in Figure 4.2. ....	134
<b>Figure 4.41</b> Bar chart of log <sub>2</sub> ratio values of the extract and fractions of herb 10 (A), and compounds <b>68-71</b> (B). The parameters are the same as described fully in Figure 4.2. ....	135
<b>Figure 4.42</b> Bar chart of log <sub>2</sub> ratio values of compounds <b>72-76</b> from herb 11. The parameters are the same as described fully in Figure 4.2. ....	136
<b>Figure 4.43</b> Phenotypic signatures of all samples from herb 12, herb 13 and herb pair 12+13 (A), and bar chart of log <sub>2</sub> ratio values of common compounds <b>81-84</b> of herbs 12 and 13 (red), and samples from herb 12 (green), herb 13 (orange) and herb pair 12+13 (blue) (B). The parameters are the same as described fully in Figure 4.2. ....	136
<b>Figure 4.44</b> Phenotypic signatures of extracts of the extracts of herb 12, herb 13 and herb pair 12+13 (A), and bar chart of log <sub>2</sub> ratio values of the extracts of herb 12, herb 13 and herb pair 12+13 (B). The parameters are the same as described fully in Figure 4.2. ....	137
<b>Figure 4.45</b> Phenotypic signatures of extracts of compounds <b>77-80</b> (A), and bar chart of	

log2 ratio values of compounds <b>77-80</b> (B). The parameters are the same as described fully in Figure 4.2. ....	138
<b>Figure 4.46</b> Phenotypic signatures of extracts of compounds <b>81-84</b> (A), and bar chart of log2 ratio values of compounds <b>81-84</b> (B). The parameters are the same as described fully in Figure 4.2. ....	139
<b>Figure 4.47</b> Phenotypic signatures of extracts of artificial mixtures AM7, AM8 and AM9 (A), and bar chart of log2 ratio values of artificial mixtures AM7, AM8 and AM9 (B). The parameters are the same as described fully in Figure 4.2. ....	140
<b>Figure 4.48</b> Bar chart of log2 ratio values of AM7 and its mimic (A), AM8 and its mimic (B), and AM9 and its mimic (C). The parameters are the same as described fully in Figure 4.2. ....	141
<b>Figure 4.49</b> Stacking chart of percentages of samples in biocluster 6 and biocluster 2...144	144
<b>Figure 4.50</b> Bar chart of mean values of  log2 ratio  of all samples on 28 parameters. The parameters are the same as described fully in Figure 4.2. ....	145
<b>Figure 4.51</b> Bar chart of samples with similar signatures of biocluster 6 (blue), and samples with positive deviations of lysosome (red) from TCM, marine, and nature bank. ....	147
<b>Figure 5.1</b> Target identification connects bioactive small molecules with the biological phenotypes they induce and can facilitate the elucidation of the underlying molecular mechanisms of their biological activities. ....	150
<b>Figure 5.2</b> General strategy of using a molecule as a bait to identify the protein binder. ....	152
<b>Figure 5.3</b> Spectra of the lysates obtained from the treatment with RIPA buffer (red), and M-PER reagent (blue). ....	156
<b>Figure 5.4</b> Spectra of the M-PER lysates measured using different values of time of flight (skimmer 1=130 V) ....	158
<b>Figure 5.5</b> Spectra of the M-PER lysates measured using different values of skimmer 1 (time of flight = 3.0). ....	159
<b>Figure 5.6</b> Spectra of the M-PER lysates incubated with DSI in different times (skimmer 1 = 130 V, time of flight = 3.0 ms). ....	160
<b>Figure 5.7</b> Expanded spectra ( <i>m/z</i> 1,500-2,500) of the M-PER lysates incubated with DSI in different times (skimmer 1 = 130 V, time of flight = 3.0 ms). ....	161
<b>Figure 5.8</b> Spectra ( <i>m/z</i> 200-6,000) of the M-PER lysate and the lysate incubated with DSI in different times (skimmer 1 = 130 V, time of flight = 2.0 ms, incubation time = 24 h). ....	162
<b>Figure 5.9</b> Spectra of native proteins (above) and peptides (below) extracted from the spectrum of the M-PER lysate (skimmer 1 = 130 V, time of flight = 2.0 ms). ....	162
<b>Figure 5.10</b> Expanded spectra of the lysate (blue) and the lysate incubated with DSI (red) containing the “extra” peaks. (skimmer 1 = 130 V, time of flight = 2.0 ms, incubation time = 24 h). ....	164
<b>Figure 5.11</b> Expanded spectra ( <i>m/z</i> 2,150-2,190) of the lysate (blue) and the lysate incubated with DSI (red) containing the “extra” peaks. (skimmer 1 = 130 V, time of flight = 2.0 ms, incubation time = 24 h). ....	164
<b>Figure 5.12</b> Expanded spectra ( <i>m/z</i> 1,935-1,970) of the lysate (blue) and the lysate incubated with DSI (red) containing the “extra” peaks. (skimmer 1 = 130 V, time of flight = 2.0 ms, incubation time = 24 h). ....	165

## LIST OF TABLES

<b>Table 1.1</b> English translation and explanation of the prescription of Liuwei Dihuang Wan (六味地黄丸).*	6
<b>Table 2.1</b> Commonly used formulas used clinically for PD and AD in descending order.	27
<b>Table 2.2</b> Top 20 materials with frequency recorded in formulas used to treat PD during 1987-2007.	28
<b>Table 2.3</b> Top 10 materials with frequency recorded in 132 prescriptions used to treat dementia or AD.	29
<b>Table 2.4</b> Top 12 materials with frequency recorded in 100 prescriptions used to treat AD published during 1979-2006.	29
<b>Table 2.5</b> Top 14 materials recorded in 141 prescriptions used to treat dementia during the Ming dynasty and the Qing dynasty.	30
<b>Table 2.6</b> 15 selected TCMs commonly used to treat neurodegenerative diseases.	31
<b>Table 2.7</b> 5 Selected herb pairs used to treat neurodegenerative diseases.	32
<b>Table 3.1</b> Photos of 15 selected TCM herb materials purchased from Tong-Ren-Tang. The herb numbers here are consistent with those in Table 2.6.	59
<b>Table 3.2</b> Detailed information about preparation of extracts and fractions.	61
<b>Table 3.3</b> Detailed information of 90 compounds from the selected herbs.	63
<b>Table 3.4</b> Plant 6, plant 8 and the herb pair 6+8 treated by different extraction methods.	78
<b>Table 3.5</b> Nine artificial mixtures generated from the herbs and herb pairs	80
<b>Table 4.1</b> 38 parameter used in the multi-parameter phenotypic profiling.	88
<b>Table 4.2</b> Extracts of 15 herbs and 5 herb pairs and their biocluster.	102
<b>Table 4.3</b> Statistical data of clustering of samples from five herb pairs.	143
<b>Table 4.4</b> Percentage of samples with positive deviations of lysosome or similar biological signatures with biocluster 6 from TCM, marine and nature bank.	147

## ABBREVIATIONS

[ $\alpha$ ] <sub>D</sub>	specific rotation
°C	degrees Celsius
1D	one dimensional
2D	two dimensional
AchE	acetylcholinesterase
AD	Alzheimer's disease
APP	amyloid precursor protein
A $\beta$	amyloid beta
C18	octadecyl bonded silica
ChAT	choline acetyltransferase
CNS	central nervous system
DMSO	dimethyl sulfoxide
EPO	hematopoietin
ERK	extracellular signal-regulated kinase
ESI-MS	electrospray ionization mass spectrometry
FBS	foetal bovine serum
FTICR	Fourier transform ion cyclotron resonance
HBA	hydrogen bond acceptor
HBD	hydrogen bond donor
HD	Huntington's disease
hONS	human olfactory neurosphere-derived
HPLC	high-pressure liquid chromatography
I/R	ischemia/reperfusion
LDH	lactate dehydrogenase
MAO-B	Monoamine oxidase B
Mark3	MAP/microtubule affinity-regulating kinase3
MPTP	1-methyl-4-phenyl-1,2,3,6-tetrahydropyridine
MS	mass spectrometry
NGF	neuron growth factor
NMR	nuclear magnetic resonance
NOS	nitric oxide synthetase
NT-3	neurotrophin-3
PBS	phosphate buffered saline
PD	Parkinson's disease
PDI	protein disulfide isomerase
PSA	polar surface area

Ro5	rule-of-five
Rpgrip1	retinitis pigmentosa GTPase regulator interacting protein1
TCM	traditional Chinese medicine
μg	microgram
μL	microlitre
μm	micrometre
μM	micromolar

## ACKNOWLEDGEMENTS

I would like to express the deepest appreciations to my supervisors, Professor Ronald James Quinn, Professor Yang Ye, and Dr Yunjiang Feng. They gave me invaluable supervisions during my PhD program. They steered me to explore a new and fantastic field, and made the whole PhD program a magic journey. They had unusual curiosity, enthusiasm and passion about science, which greatly inspired me. Without their guidance and persistent help this dissertation would not have been possible.

I would like to thank Professor George D. Mellick, Associate Professor Stephen A. Wood, and Miss Marie-Laure Vial for their assistance and help in the biological part of this program. Miss Marie-Laure Vial taught me operation procedures of tissue culture, phenotypic screening, and data analysis.

I am grateful to Dr Hoan Vu and Dr Wendy Loa-Kum-Cheung, who taught me everything about the ESI-FTICR-MS and gave me a lot of valuable suggestions. Without their support, I could not finish the mass spectrometry part of this thesis.

Thanks are given to Dr Sheng Yao, Mr Changqiang Ke, Miss Jinan Li, Mrs Jin Liu, and Mrs Ping Ji in Shanghai Institute of Materia Medica (SIMM), Chinese Academy of Sciences. They assisted me to collect the raw materials, prepare the samples, and finish the chemical analysis. The chemical profiling part was completed in SIMM.

Thanks are also given to all staff and students in Eskitis Institute for Drug Discovery. They make the Eskitis Institute a warm and friendly place. Thank Mrs Sheila Twilley for organizing a lot of things for me. Thank Dr Ngoc Pham from Nature Bank and Mrs Moana Simpson from Compounds Australia for registering the samples and supplying the plates for experiments.

This thesis would not have been possible without a GUIPRS scholarship support

from Griffith University.

Last but not the least, my special gratitude is given to my beloved family. Thank you to my husband, Dr Jiafeng Zeng, for his understanding and taking care of everything during my PhD program. Thank you to my daughter Candy who always encouraged me to do something I am really interested in. Special gratitude was presented to my past mother, Mrs Zhenxiu Zhang, who insisted that I should pursue a doctor degree and always told me it is never too late to learn.

## **ALL PAPERS INCLUDED ARE CO-AUTHORED**

### **Acknowledgement of Papers included in this Thesis**

Section 9.1 of the Griffith University Code for the Responsible Conduct of Research (“Criteria for Authorship”), in accordance with Section 5 of the Australian Code for the Responsible Conduct of Research, states:

To be named as an author, a researcher must have made a substantial scholarly contribution to the creative or scholarly work that constitutes the research output, and be able to take public responsibility for at least that part of the work they contributed. Attribution of authorship depends to some extent on the discipline and publisher policies, but in all cases, authorship must be based on substantial contributions in a combination of one or more of:

- conception and design of the research project
- analysis and interpretation of research data
- drafting or making significant parts of the creative or scholarly work or critically revising it so as to contribute significantly to the final output.

Section 9.3 of the Griffith University Code (“Responsibilities of Researchers”), in accordance with Section 5 of the Australian Code, states:

Researchers are expected to:

- Offer authorship to all people, including research trainees, who meet the criteria for authorship listed above, but only those people.
- accept or decline offers of authorship promptly in writing.
- Include in the list of authors only those who have accepted authorship
- Appoint one author to be the executive author to record authorship and manage correspondence about the work with the publisher and other interested parties.
- Acknowledge all those who have contributed to the research, facilities or materials but who do not qualify as authors, such as research assistants, technical staff, and advisors on cultural or community knowledge. Obtain written consent to name individuals.

Included in this thesis is a paper in *Chapter 2* which is co-authored with other researchers. My contribution to this co-authored paper is outlined at the front of the relevant chapter. The bibliographic details for this paper including all authors, are:

Chapter 2:

TCM, brain function and drug space

Chunping Tang,<sup>abc</sup> Yang Ye,<sup>bc</sup> Yunjiang Feng<sup>ac</sup> and Ronald J. Quinn<sup>\*ac</sup>

<sup>a</sup>Eskitis Institute for Drug Discovery, Griffith University, Brisbane, QLD 4111, Australia.

<sup>b</sup>State Key Laboratory of Drug Research, Shanghai Institute of Materia Medica, Chinese Academy of Sciences, Shanghai 201203, China

<sup>c</sup>Eskitis-SIMM Joint Laboratory for Drug Discovery, Australia

This paper has been published in *Natural Product Reports* (2016, **33**, 6-25).

Appropriate acknowledgements of those who contributed to the research but did not qualify as authors are included in the paper.

(Signed) \_\_\_\_\_ (Date) \_\_\_\_\_

Chunping Tang

(Countersigned) \_\_\_\_\_ (Date) \_\_\_\_\_

Supervisor: Ronald J. Quinn



## **CHAPTER 1 Introduction**

### **1.1 Traditional Chinese Medicine**

#### **1.1.1 Traditional Chinese Medicine, medical classics and Chinese Pharmacopoeia**

Traditional Chinese Medicine or TCM (中医) is a comprehensive holistic medical system that dates back thousands of years. Different from western medicine, it is based on Chinese philosophies like the principles of yin and yang (阴阳), which are negative and positive polarities, and the five elements (五行), which are wood (木), fire (火), earth (土), metal (金), and water (水) (with the elements are seasons, colors, and internal organs that correspond to them) (**Fig. 1.1**). TCM sees the human body as a whole, but with separate parts. All parts are designed to work with each other in harmony. The illness/disease is considered as the result of the loss of balance, and the whole objective for TCM therapy is to bring the balance back. TCM takes its approach from aspects of nature and applies it to the human body in treating illness and disease. The practice basically involves treatment and prevention of various illnesses through herbal medicines and different mind and body practices like meditation, tai chi, moxibustion, cupping, and acupuncture.

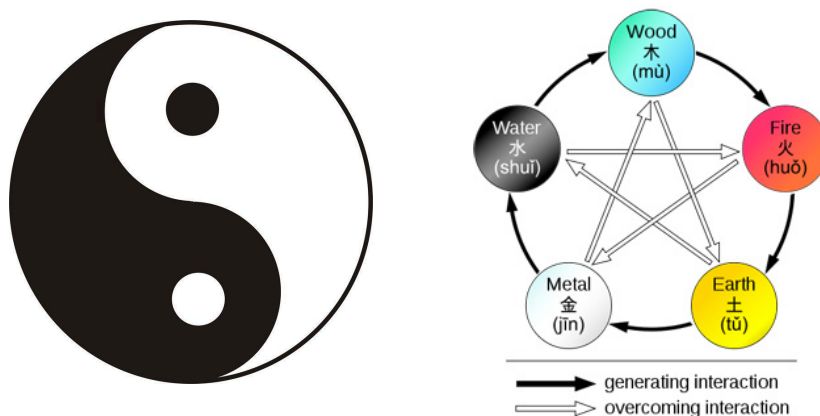


**Figure 1.1** The symbol of yin and yang (left), and the relationship of five elements (right).

TCM has proven to be effective in the treatment and management of various ailments in its long practical history. The accumulative knowledge of medical science, theory, diagnostic methods, prescriptions and cures was passed from generation to generation by oral teaching and written records. The doctors in different dynasties compiled a number of medical texts and some of them are still used as textbooks nowadays.

The Yellow Emperor's Inner Canon (黄帝内经)\*\* is one of the first, and undoubtedly the most important, classic in the history of Chinese medicine, which had an enormous influence on the medical thoughts in later centuries. This multi-volume treatise encompassed every possible aspect of diagnostics, pathology, acupuncture, and moxibution, including both theory and practice. The principles of yin and yang, the five elements, and qi (气) were described, as well as the function of the human body and the physical world that remained the basic ideas believed by traditional medicine practitioners.

The Treatise on Cold Diseases (伤寒杂病论) was compiled by Zhang Zhongjing (张仲景) (about 150–219 AD) in the late Eastern Han Dynasty. It brought up the causes of the Cold Disease and differentiated the duration and nature of various types

---

\*\* The completion time of the Yellow Emperor's Inner Canon is not clear until now. Some people believe that this book was compiled during the period of Yellow Emperor (~2600 BC), some believe it was written during the Spring and Autumn and the Warring States Periods (770 BC-221 BC), and now most experts **accept** that it was finally completed in the middle to late Western Han Dynasty (99 BC-26 BC).

according to the principles of yin and yang. It developed specific therapeutic principles and prescriptions for each type of disease. This treatise recorded 269 prescriptions involving 214 medicines. Many prescriptions such as Mahuang Tang (麻黄汤) and Guizhi Tang (桂枝汤) are used by Chinese doctors as basic formulas until now.

Another influential text is Compendium of Materia Medica (本草纲目), which was written in the middle of the Ming Dynasty era (1368–1644 AD) by Li Shizhen (李时珍, 1518–1593 AD). This text is considered as the most important traditional work on herbs and drugs. Li Shizhen recorded 1,892 pharmaceutical objects with 1,109 illustrations. 1,095 of them (about 58%) were made of plants while 276 were made of minerals, and 444 out of parts of animals. The main part of the book focused on the detailed descriptions of a huge number of pharmaceutical drugs. The description of each drug was systematically divided into eight parts. It began with an analysis of different names of the drug (Shiming, 释名), followed by the places of origin (Jijie, 集解), the general appearance, the collecting methods of the drug, preparation methods (Xiuzhi, 修治), flavor and taste (Qiwei, 氣味), therapeutic effects (Zhuzhi, 主治), and "enlightenments" (Faming, 發明). It also had detailed discussions of doubts (Bianyi, 辨疑) and corrections of errors occurring in the older texts (Zhengwu, 正誤). The therapeutic application of each drug and different prescriptions (Fufang, 附方) containing the drug were also included in the appendix of the book. A total of 11,096 prescriptions were recorded in this text.

Currently, the Pharmacopoeia of the People's Republic of China (PPRC, also known as Chinese Pharmacopoeia) is an official compendium of drugs covering both traditional Chinese and western medicines. It is compiled by the Pharmacopoeia Commission of the Ministry of Health of the People's Republic of China and provides information on the standards of purity, description, test, dosage, precaution, storage, and

the strength for each drug. Since the first edition was issued in 1953, the Chinese Pharmacopoeia was revised every five to ten years (**Fig. 1.2**). The newest 10th edition was released in 2015. The 2015 edition has four volumes. Volume I contains 2,598 monographs of Chinese material medica (药材) and pared slice (饮片), vegetable oil/fat and its extract (植物油和提取物), Chinese traditional patent medicines (成方制剂), and single ingredient of Chinese crude drug preparations (单味制剂). Volume II records 2,603 chemical drugs. Volume III collects 137 biological products. Volume IV includes 270 pharmaceutical adjuvants.<sup>1</sup> It is compulsory that every herb, extract, or herbal medicine sold in the market has to meet the requirements and standards recorded in the Chinese Pharmacopoeia.

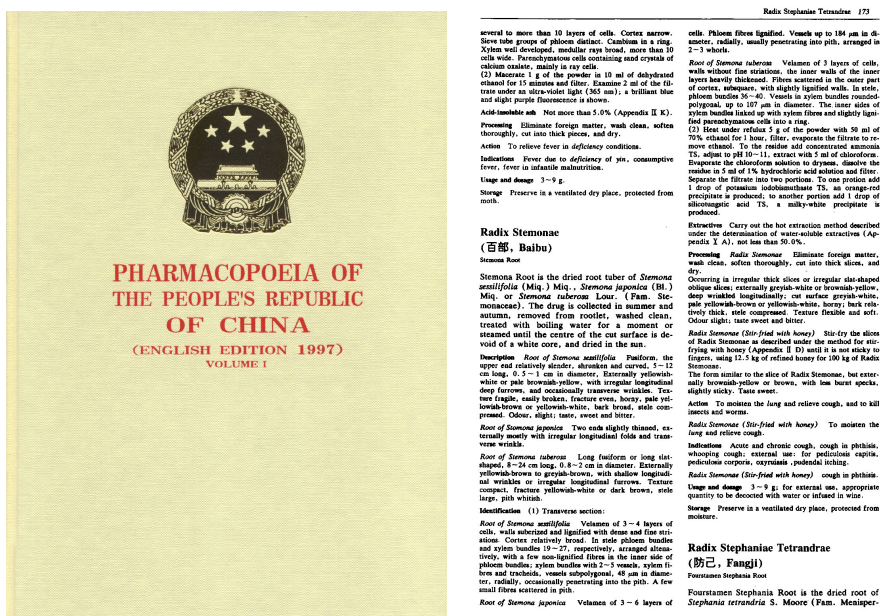


**Figure 1.2** The cover of Pharmacopoeia of the People's Republic of China, Volume I, English Edition, 1997 (left); Descriptions of the TCM Baibu (right).

Compared with the ancient classics, the Chinese Pharmacopoeia preserves traditional descriptions for a drug, such as property, flavor, channel tropism, origin, collection, processing method, therapeutic effects, and storage. On the basis of these descriptions, the Chinese Pharmacopoeia incorporates microscopic identification for raw materials, chemical constituents reported from the original plants, and modern

pharmacological effects on cell and animal models. The modern technologies such as UV, IR, TLC, HPLC, LC-MS are applied for raw material identification and quality control rather than individual experiences.

In recent years, the Chinese Pharmacopoeia was revised every five years in order to incorporate new information and new methods as quickly as possible. Compared with the 2010 edition, for example, the 2015 edition collected 440 new Chinese material medica, a 22.8% increasing in number, and 517 items, about 20% of the total, were revised.<sup>1</sup> LC-MS analysis was used, for the first time, for authentic identification of raw materials. Quantitative analysis of multi-components by single-marker (QAMS) was introduced to identify Danshen (丹参), Lingzhi (灵芝), and Gonglaomu (功劳木).

### **1.1.2 TCM formula**

In addition to the detailed descriptions of single drugs, the classic books and the Chinese Pharmacopoeia recorded a lot of prescriptions used to treat specific diseases. Except for a few prescriptions such as Dushen Tang (独参汤), the decoction of Ginseng, almost all prescriptions comprise two or more drugs, and this type of prescription is known as a formula (复方). A formula has more or less the same combination of herbs, processing method and usage, and directs to one or several specific diseases. Generally, a complete formula includes four types of drugs, principal (君), assistant (臣), complement (佐) and guide (使) drugs. The combination of different drugs in a formula is called compatibility (配伍). It is believed that multiple components could hit multiple targets and exert synergistic therapeutic efficacies when different types of drugs in a formula work together. This is the very essence and soul of TCM.

Many formulas have been approved to be effective in the long practical history and were passed from generation to generation, and until now, were recorded in Chinese Pharmacopoeia. Take a famous formula Liuwei Dihuang Wan (六味地黄丸) as an

example. The prescription (处方) in the 2015 Edition is shown as “熟地黄 160 g 酒萸肉 80 g 牡丹皮 60 g 山药 80 g 茯苓 60 g 泽泻 60 g”.<sup>2</sup> For the English translation and explanation see **Table 1.1**.

**Table 1.1** English translation and explanation of the prescription of Liuwei Dihuang Wan (六味地黄丸).\*

Drug		Weight (g)	Identification Standard	Remarks
Chinese Name	English Name			
熟地黄	<u>Rehmanniae Radix Praeparata</u>	160	Standard herb	
酒萸肉	<u>Corni Fructus</u>	80	Morroniside Loganin	Processed with yellow wine according to General Regulation 0213
牡丹皮	<u>Moutan Cortex</u>	60	Paeonol	
山药	<u>Dioscoreae Rhizoma</u>	80	Standard herb	
茯苓	<u>Poria</u>	60	Standard herb	
泽泻	<u>Alismatis Rhizoma</u>	60	Standard herb	

\* All information is obtained from the Chinese Pharmacopoeia (2015 Edition), and only sorted into a table and translated into English.

The prescription of Liuwei Dihuang Wan shows that the formula consists of six drugs with specific mass ratios. Except for “酒萸肉”, five of them are recorded in the Chinese Pharmacopoeia as material medica. “酒萸肉” is listed under the material medica Corni Fructus as pared slice, which means it must be processed before use.

Processing (炮制) plays a very important role in TCM and the raw material are generally being processed before use with different methods. Rehmanniae Radix Praeparata is actually a processed product of Rehmanniae Radix. After processing, Rehmanniae Radix Praeparata is regarded as a different material medica, having the properties of “sweet, slightly warm”, while the properties of Rehmanniae Radix is “sweet, cold”. Accordingly, they have different functions and are used to treat different diseases.<sup>3</sup>

When compared with the records in the ancient classics about the same formula, the Chinese Pharmacopoeia does not make changes in the compatibility of the formula, but

it uses modern technologies to guarantee the consistent quality produced by different manufacturers. Microscopic identification is used to identify the five raw materials except for Rehmanniae Radix Praeparata. Thin-layer chromatography is used to identify the raw materials by comparing with respective standard herbs or standard compounds morroniside, loganin and paeonol (**Table 1.1**). HPLC is performed to determine the content of morroniside and loganin in Corni Fructus, and paeonol in Moutan Cortex as quality control.

### 1.1.3 TCM and natural products

In contrast to TCM, western medicine is quite different. Western medicine has almost exclusively looked for a single molecule responsible for the biological activity of a plant or extract. Natural products are regarded as a major source of new drugs due to their highly diversified structures and specific biological activities.

In a recent review summarizing natural products as sources of new drugs (**Fig. 1.3**), Newman and Cragg figured out that in the area of cancer, over the time frame from around the 1940s to the end of 2014, of the 175 small molecules approved, 131, or 75%, are other than “S” (synthetic), with 85, or 49%, actually being either natural products or directly derived therefrom. In other areas, the influence of natural product structures is quite marked, with, as expected from prior information, the anti-infective area being dependent on natural products and their structures.<sup>4</sup>

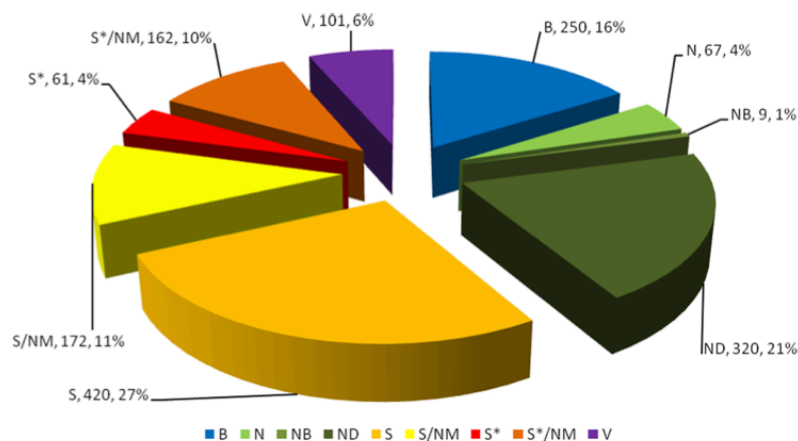


**Figure 1.3** All new approved drugs 1981–2014; n = 1562. B-biological macromolecule; N-unaltered natural product; NB-botanical drug (defined mixture); ND-natural product derivative; S-synthetic drug; S\*-synthetic drug with NP pharmacophore; V-vaccine; NM-mimic of natural product.

*This is an open access article published under an ACS AuthorChoice License, which permits copying and redistribution of the article or any adaptations for non-commercial purposes.*

From the perspective of the origin of the materials, traditional Chinese medicines can be regarded as individual plants containing natural products with diverse structures and bioactivities. So, at the early stage, TCMs were explored mainly as plants with little consideration of their therapeutic use in history. The application of modern technologies on these materials resulted in the discovery of an array of bioactive molecules and lead compounds.

Huperzine A, for example, is a well-known, reversible acetylcholinesterase inhibitor and used to treat Alzheimer's disease. It was first isolated from *Huperzia serrate* (蛇足石杉), which, in traditional Chinese medicine, was used for the treatment of traumatic injuries, venomous snakebites, and burns and scalds.<sup>5,6</sup> It is obvious that the effects of huperzine A have no correlation with those of the original plant.

Some compounds were separated for the sake of their novel structures first, but in the following assays they exhibited the bioactivities related to the traditional functions of the original plants that they came from. Baibu (百部), first recorded in Shennong Bencao Jing (神农本草经, ~1 BC), is a traditional medicine long been used as an anti-cough and an insecticidal agent. Due to their novel and diverse structures, more than 80 *Stemona* alkaloids were obtained from the *Stemona* plants since 1950s, but the relationship between these compounds and its traditional functions did not initiate until 1990s.<sup>7-12</sup> Stemofoline and its analogues, which were separated from the leaves of the *Stemona* plants, exhibited agonistic effects in electrophysiological *in vitro* tests on the insect nicotinic acetylcholine receptor.<sup>8</sup> Other types of *Stemona* alkaloids, including stemoninine-, croomine-, and tuberostemonine-type, were reported to exhibit significant antitussive activity in the guinea pig cough model induced by citric acid aerosol

stimulation.<sup>9-12</sup> An extract from the roots of *Stemona sessilifolia* was granted a patent to be used as an anti-cough agent.<sup>13</sup> These findings embody the drug discovery based on natural products rather than traditional Chinese medicines.

#### **1.1.4 Modernization of traditional Chinese medicines: TCM-based drug discovery**

Drug discovery based on TCM is one of the most important parts of modernization of traditional Chinese medicine. Modernization of traditional Chinese medicine is a concept brought up three decades ago, and draws more and more attention with economic development in China. So far, this concept has not been distinctly defined, but it is generally accepted that traditional Chinese medicine can evolve by using modern methods and technologies, and be accepted globally by following the strict standards of western medicine. It includes many aspects such as standardized manufacturing, advanced identification methods, and systematic research tools. TCM-based drug discovery is one aspect of the modernization and aims to provide new therapies that are different from conventional medicines.

As mentioned, TCM is a complex and centuries-old system, featuring usage of drugs in a form of formula. It is the characteristic of TCM, but at the same time the barrier that keeps TCM from being accepted globally due to unclear chemical constituents, unveiled mechanisms of action, and unidentified adverse effects of the mixture. The goal of TCM-based drug discovery is to use western-accepted scientific evidence to explain traditional Chinese medicine, and eventually develop active principles with specific chemical structures and identified targets as safe and efficient therapies.

It is generally accepted that drug discovery based on TCM is guided by the theories and accumulated knowledge of TCM, and its search for active principles, no matter a single or a combination of compounds, is based on the proven therapeutic effects in the

long practical history. A lot of efforts have been made in the past decades, from searching for one single active compound to identifying a combination of compounds, and recently turning to study a formula.

One of the success stories is the discovery of artemisinin (Qinghaosu, 青蒿素) from *Artemisia annua* (黄花蒿). Artemisinin is an effective anti-malaria therapy that has saved millions of lives around the world. Youyou Tu, "for her discoveries concerning a novel therapy against Malaria" (nobelprize.org), shared the Nobel Prize in Physiology or Medicine 2015 with two other scientists.

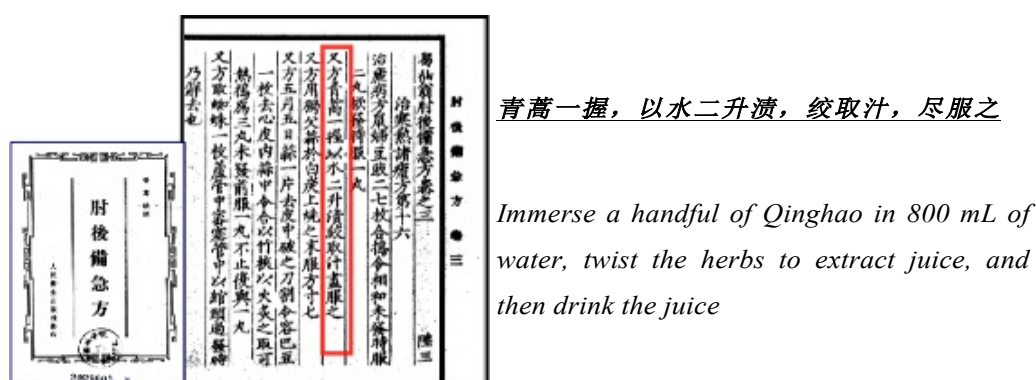


**Figure 1.4** Descriptions about how to use Qinghao to treat malaria in Zhou-Hou-Ji-Bei-Fang (肘后备急方), an ancient medicinal book written by Hong Ge in the Eastern Jin Dynasty (317 AD – 420 AD). *Copyright not required.*

Youyou Tu narrated the story about the discovery of artemisinin and its development into a drug in Nature Medicine.<sup>14</sup> She said the medicinal herb Qinghao (青蒿) was one of the most frequently used herbs for the treatment of malaria after investigating more than 2,000 Chinese herbal prescriptions. In an ancient medicinal text *Zhou-Hou-Bei-Ji-Fang* (肘后备急方) written by a famous Taoist Hong Ge (284 AD~364 AD), she found some key descriptions about how to use Qinghao (**Fig. 1.4**), which inspired her to extract the herbs with ethyl ether at room temperature rather than cook them in water – a common way used for most herbs and formulas. Professor Tu saw artimisinin as “a true gift from old Chinese medicine”.<sup>14</sup> Drawn from valuable research experiences in developing artemisinin, the Nobel laureate believes that

"Chinese medicine and pharmacology are great treasures that should be explored and raised to a higher level."

Another representative example is the discovery of depside salts (丹参多酚酸盐) from the roots of *Salvia miltiorrhiza* (Danshen, 丹参). Danshen is a popular traditional Chinese medicinal herb, and has been widely used in clinics to improve blood circulation, relieve blood stasis, and treat coronary heart disease.<sup>15-18</sup> Professor Lijiang Xuan and his collaborators studied thoroughly the well-known medicine and found that depside salts, a mixture in which magnesium lithospermate B and its 5 analogs are the active components.<sup>19</sup> They studied the pharmacokinetics, tissue distribution, metabolism, and excretion of three of the major components by using liquid chromatography-tandem mass spectrometry following intravenous administration in rats. They found the main metabolites in the serum.<sup>19</sup> In order to set a high quality control, HPLC–UV and HPLC–MS techniques were used in fingerprint analysis of Danshen injection and its raw materials.<sup>20, 21</sup>

Depside salts is regarded as an example of novel TCM having defined therapeutic effect and high quality control from raw material to the product. China's State Food and Drug Administration (SFDA) granted a new drug license for this mixture and its injectable form in May 2005 for the treatment of angina and other cardiovascular diseases. Since the injection of depside salts was put into market in 2006, the accumulated sales revenue has reached to as high as 17 billion RMB, and now is among the Top 10 drugs used in Chinese hospitals.<sup>22</sup> Professor Zhibi Hu, a member of the Chinese Academy of Engineering, commented the invention of depside salts and said in *Nature Biotechnology*, "This success means China's biopharmaceutical industry can develop innovative drugs by investigating the chemical ingredients of TCMs whose clinical effects have long been observed. Compared with developing new compounds from scratch, the approach is potentially more rapid and less expensive".<sup>23</sup>

Unremitting attempts to disclose the mystery of TCM formula have been made by Chinese scientists in the recent years. Wang et al investigated the working mechanism of a Realgar-Indigo naturalis formula (RIF).<sup>24</sup> This formula has been proven to be very effective in treating human acute promyelocytic leukemia. It consists of realgar, *Indigo naturalis*, and *Salvia miltiorrhiza*, with tetraarsenic tetrasulfide, indirubin, and tanshinone IIA as major active ingredients, respectively. They disclosed the synergic effect of three active components of RIF at the cellular level, and verified the rationality of the formula: mutual reinforcement of the compounds and reduction of adverse effects. The authors finally concluded, “we show that the dissection of the mode of action of clinically well established TCM formulae such as RIF should be possible by combined application of both analytical and synthetic research approaches at the molecular, cellular, and organism levels. This study may be considered a useful pilot trial in exploring the value of traditional formulae on a larger scale and in helping to bridge Western and the Eastern medicines in the era of systems biology.”<sup>24</sup>

This is a successful story and an excellent start when it comes to TCM formulas. However, this story needs some preconditions: relatively simple composition of the formula; identified active major components; well-established cell and molecular models. In most circumstances, the formula is much more complicated, the chemical and biological study of the formula are much more challenging. For example, one formula could compose more than 20 raw materials, and the active principles that can represent the therapeutic effects may be unknown. More importantly, the descriptions of therapeutic effects for TCM are quite different from those for western medicine, and it is challenging to establish suitable molecular, cell and animal models.

### 1.1.5 Herb pair: a cutting point for in-depth research of TCM

The more components in a formula, the more complicated it becomes. Therefore, the simplest form of a formula, the herb pair (药对), a formula of two components, provides a simple starting point. Herb pair consists of two relatively fixed Chinese herbs. That means, these two herbs are used together in many formulas and to some extent, they have been regarded as the minimum unit. Many Chinese doctors believe that in a formula, the minimal unit is an herb pair rather than an individual herb. Take Tianma Gouteng San (天麻钩藤散) as an example, Gastrodiae Rhizoma (天麻) and Ramulus Uncariae Cum Uncis (钩藤) are used together, and the pair of these two herbs is regarded as the principal drug in this classic formula.<sup>25</sup> Given its relative simplicity, the herb pair is a good starting point for in-depth research of TCM.

Yitao Wang and his research team published a series of papers reviewing not only recent advances in the theoretical foundation of herb pairs but also the results of investigations on different herb pairs.<sup>26-32</sup> Wang indicated that herb pairs ingeniously express the basic theories of TCM formula, and research about herb pairs is the foundation in the investigation of prescription compatibility since they have similar feature in essence. He also pointed out that modern technologies and methods such as informatics and systems biology are powerful tools to study the complex TCM system.<sup>27</sup> By using modern techniques and reasonable methods, pharmacodynamics and pharmacokinetics studies of herb pairs can improve the accuracy of herbal decoction in clinical application, and further help understand the characteristics of TCM. Meanwhile, it will lay theory foundation for merging systems biology into the philosophy of herb pairs.<sup>28</sup> Wang did data mining from results of three classical herb pairs, *Coptis chinensis* and *Euodia rutaecarpa* (黄连吴茱萸), *Salvia miltorrhiza* and *Panax notoginseng* (丹参三七), and *Radix astragali* and *Angelica sinensis* (黄芪当归). He

found that the combination of two drugs with different ratio showed differences not only in potency but also in function and indications.<sup>26, 30-32</sup>

The herb pair consisting of *Salvia miltiorrhiza* (SM) and *Panax notoginseng* (PN) was taken as an example. When the two herbs decocted together, the saponins of PN might promote the dissolution of the effective ingredients in SM.<sup>33</sup> Zeng *et al* investigated the protective effects of SM, PN and different weight ratios of SM/PN on a hypoxia/reoxygenation(H/R)-induced human umbilical vein endothelial cells (HUVECs) injury model. The leakage rate of lactate dehydrogenase (LDH) in the cultured medium of HUVECs was measured by an automatic biochemistry analyser. The results showed that the LDH leakage rates of normal and H/R model groups were 0.212 and 0.309, respectively, indicating that H/R would increase the LDH leakage rate of HUVECs. Samples with the ratios of SM/PN being 10:0, 10:1, 5:1, 5:3, 1:1, 3:5, 1:5, 1:10 and 0:10 would decrease the LDH leakage rate of H/R induced HUVECs to a level of 0.218, 0.227, 0.240, 0.247, 0.239, 0.230, 0.241, 0.247 and 0.242, respectively, in which only the ratios of 10:1, 5:3, 1:1 and 0:10 had the statistical significance when compared with the model group. That means, SM, PN and the herb pair with ratios of 5:3 or 1:1 (SM/PN) showed protective effects on H/R-induced human umbilical vascular endothelial cells.<sup>32</sup>

Until now, herb pair is less known to many researchers outside China. Even in China, the investigations are fragmental and unsystematic on this topic. Nevertheless, herb pair is drawing more and more attention and considered being able to play a key role in the evolution of TCM from single herb to multi-herb formula (**Fig. 1.5**). At the same time, more experiments need to be done in this field.

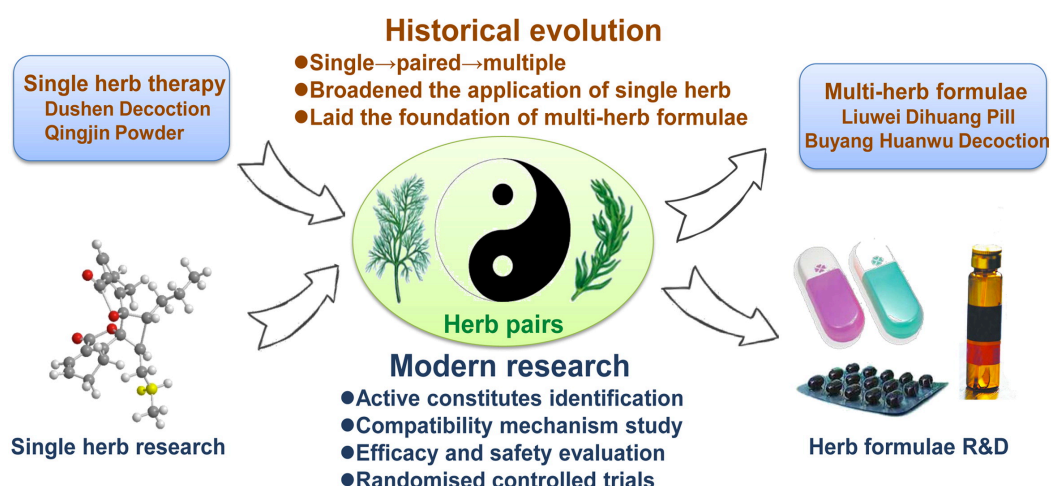


**Figure 1.5** Herb pairs have acted as a transitional role in the evolution of multi-herb formulae, and may play a key role in the development of herb formulae R&D.

*Reuse with permission from Elsevier.*

From herb pair to multi-herb formula, the concept “*multiple component, multiple target*” has been accepted gradually. Increasing evidence demonstrates that, when treating illnesses, e.g. cancer<sup>34</sup> and HIV<sup>35</sup>, therapies containing multiple drugs with distinct but related mechanisms can usually amplify the therapeutic efficacies of each agent, leading to maximal therapeutic efficacy with minimal adverse effects. The complexity of TCM, particularly TCM formula, poses a great challenge for all researchers, but at the same time, it presents an opportunity to search new therapies for complex and uncured conditions such as neurodegenerative diseases.

## 1.2 Neurodegenerative disease

### 1.2.1 Neurodegenerative disease and urgent need for effective therapies

Neurodegenerative disease, such as Alzheimer’s (AD), Parkinson’s (PD), and Huntington’s disease (HD), is an umbrella term for a range of conditions that primarily affect the neurons in the human brain. These diseases are believed to relate directly to human brain function and have a lot of symptoms like dementia, memory loss, problems in writing or speaking, poor judgment, anxiety, agitation, and sleep disturbances. Patients have to live through years of morbidity as the diseases progress.

Neurodegenerative disease has been recognized as the most common cause of dementia, as well as a major cause of death. In 2016, the Alzheimer’s Association released a report describing the public health impact of Alzheimer’s disease and pointed out that as the population of the United States ages, Alzheimer’s is becoming a more common cause of death.<sup>36</sup> Although deaths from other major causes have decreased significantly, official records indicate that deaths from Alzheimer’s disease have increased significantly. Between 2000 and 2013, deaths resulting from stroke, heart disease, and prostate cancer decreased 23%, 14%, and 11%, respectively, whereas deaths from Alzheimer’s disease increased 71% (**Fig. 1.6**).<sup>36</sup>

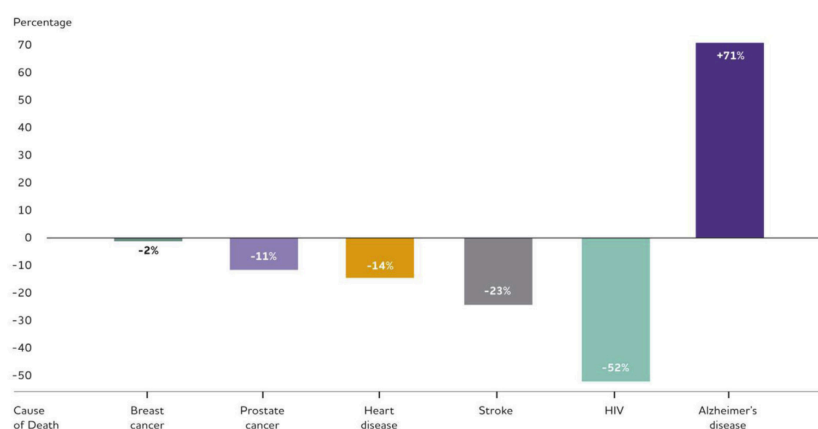


**Figure 1.6** Percentage changes in selected causes of death (all ages) between 2000 and 2013. Created from data from the National Center for Health Statistics.

*Reuse with permission from Elsevier.*

According to the statistics released by the Alzheimer’s Disease International (ADI) in its World Alzheimer Report 2015: The Global Impact of Dementia, almost 47 million people now live with this group of diseases.<sup>37</sup> The authors estimate that 74.7 million people will have dementia in 2030, and 131.5 million in 2050, roughly a doubling in numbers every 20 years. Also in this report, worldwide incidence estimates for dementia have risen to 9.9 million new cases each year, up from 7.7 million in the 2012 World Health Organization/ADI report, *Dementia: A Public Health Priority*. It also puts a dollar amount on the global cost of dementia—\$818 billion dollars in 2015, up 35 percent from \$604 billion in 2010. The authors estimate that this will climb to \$1 trillion in 2018 and \$2 trillion by 2030.<sup>37</sup>

These figures revealed that with the increase in the aging population, neurodegenerative diseases are becoming a major social and economic burden worldwide. There is an urgent need to develop more effective therapeutic strategies to treat people suffering neurodegenerative disease. In its report *Changing the Trajectory of Alzheimer's Disease: How a Treatment by 2025 Saves Lives and Dollars*, the Alzheimer's Association estimated that a treatment in 2025 that delays the onset of Alzheimer's by five years would reduce significantly the total number of people suffering AD, and save \$367 billion under the current trajectory in 2050, a decreasing of 33 percent from \$1.101 trillion.<sup>38</sup>

Due to the fact that the causes of AD, PD and other neurodegenerative diseases are not fully understood, current treatments only temporarily improve symptoms, but patients still experience progressive deterioration in cognitive capability, psychosis, agitation, and depression.<sup>39</sup> On the other hand, even as the number of patients grows by millions, the number of experimental Alzheimer's drugs in the clinic has dropped over the past 5 years.<sup>40</sup> In the field of Alzheimer's R&D, the trial failure rate hits an 'astounding' 99.6%.<sup>40</sup> Late-stage Alzheimer's research has been a disaster zone for the big pharmaceuticals, e.g. Eli Lilly's solanezumab and bapineuzumab at J&J and Pfizer, both failing in Phase III tests. The failures suggested that neurodegenerative disease is so complicated that it needs more sophisticated tools or advanced methods to search for novel therapies.

### **1.2.2 Natural products used to treat neurodegenerative diseases**

Of current drugs used against AD and PD, huperzine A, galantamine, and baicalein (**Fig. 1.7**) are natural products for the treatment of dementia, memory loss and other cognitive impairments according to the data obtained from Thomson Reuters Cortellis.<sup>41</sup> Huperzine A was first isolated from *Huperzia serrate*, and is a well-known,

reversible acetylcholinesterase inhibitor.<sup>5, 6</sup> Galantamine is an alkaloid obtained from the bulbs and flowers of *Galanthus caucasicus*, *Galanthus woronowii* and related genera such as *Narcissus* and *Lycoris*. It is a specific, competitive, and reversible acetylcholinesterase inhibitor, and also an allosteric modulator at nicotinic cholinergic receptor sites potentiating cholinergic nicotinic neurotransmission.<sup>42</sup> Baicalein is a flavone originally isolated from the roots of *Scutellaria baicalensis* and *Scutellaria lateriflora*. A recent paper reported that the neuroprotective effects of baicalein in a murine (MPTP) model of PD were due to attenuated astrocyte activation through suppressing the 1-methyl-4-phenylpyridine-induced nuclear translocation of nuclear factor- $\kappa$ B and reduced the activations of JNK and ERK.<sup>43</sup>

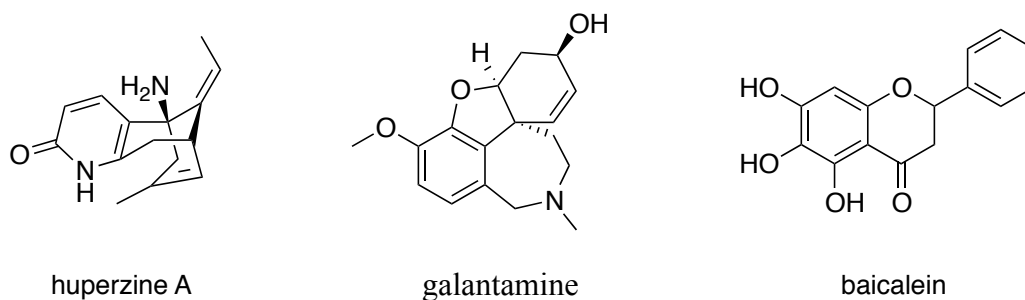


**Figure 1.7** Chemical structures of huperzine A, galantamine and baicalein.

Moreover, some naturally occurring compounds, as well as some herb extracts, were reported to have potential to treat this type of diseases. For example, the pomegranate extract, which is a rich source of polyphenols, can help prevent the development of Alzheimer's disease.<sup>44</sup> A new phase II study has shown that high doses of purified resveratrol, a polyphenol found in some foods, appear to stabilize levels of amyloid beta ( $A\beta$ ) in cerebrovascular fluid (CSF) and in plasma in patients with mild to moderate Alzheimer disease (AD) and are safe and well tolerated.<sup>45</sup>

There are strong evidences to support that it is a rational and indispensable way to discover new treatments from natural sources including TCM in the battle against neurodegenerative disease.

### 1.3 Research objectives

Although TCM has been practiced for thousands of years and proven by the long-term clinical trials, the scientific effects and benefits of TCM are still being debated due to lack of scientific evidence in terms of their biological effects and chemical constituents.

Searching “traditional Chinese medicine” in Thomson Reuters Web of Science, 15,850 literatures were found, of which 96.5% were in English, and 2.5% in Chinese. The top 3 countries or regions affiliated are China (69.3%), USA (10.5%) and Taiwan (7.9%). The distribution of the number of literatures published in the past decade (2006-2015) shows a steady but not sharp increasing curve (**Fig. 1.8**).

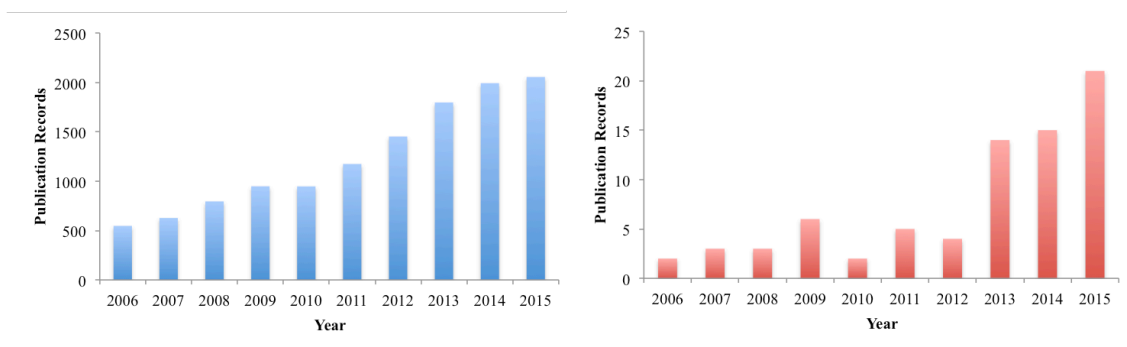


**Figure 1.8** Bar charts of distribution of publication records about traditional Chinese medicine (left, blue); and traditional Chinese medicine herb pair (right, red) from 2006 to 2015.

Searching “traditional Chinese medicine” and “herb pair” in the same database, only 90 publications were given. Few publications were found before 2006, but there has been rapid growth since 2013 (**Fig. 1.8**). Of the 90 scientific papers, 93.3% come from Chinese affiliations and the rest from the USA institutions. Considering the language obstacle, another attempt to search “中药药对” (herb pair of traditional Chinese medicine) in China National Knowledge Infrastructure (CNKI) was made, affording only 61 results. Part of the results overlap with those from Web of Science. Therefore, there is an urgent need to investigate the traditional Chinese medicine and

unlock the ancient wisdom, starting from the simple form, herb and herb pair, and finally turning to the multi-herb formula, to meet the challenges that our healthcare systems are facing.

Our research objectives are, through studying the TCM targeting the neurodegenerative diseases, to prove the following concepts:

1. Accumulated TCM knowledge could be used to guide TCM-based drug discovery.
2. TCM mixture, like the single compound in western medicine, could be an option for new drug discovery.
3. Modern technologies such as phenotypic assay and the fourier transform ion cyclotron resonance mass spectrometer (FTMS) are useful tools to study the complex system like TCM. They could supply scientific evidence to support the traditional usages of TCM, and finally contribute to a better understanding of TCM.

## **1.4 outline of the program**

This project will take advantage of the TCM knowledge accumulated in thousands of years' clinical practices. Through studying the formulas recorded in classic medicinal books and literatures, those with proven therapeutic effects on the neurodegenerative diseases will be collected. From these formulas, the principal herbs and herb pairs will be selected. The samples from the selected herbs and herb pairs, including extracts, fractions, and pure compounds, will be prepared. All samples will be assayed on an in house established cell-based profiling platform using confocal cell imaging system. The phenotypic screening of the TCM samples will give the imaging profiling fingerprints to every sample. The correlations between the phenotypic changes and the samples will be interpreted by statistical analysis, affording the sample of interest. The sample of

interest will be used to identify the potential targets through the fourier transform ion cyclotron resonance mass spectrometer (FTICR-MS). The general strategy of this program is summarized in **Fig. 1.9**.

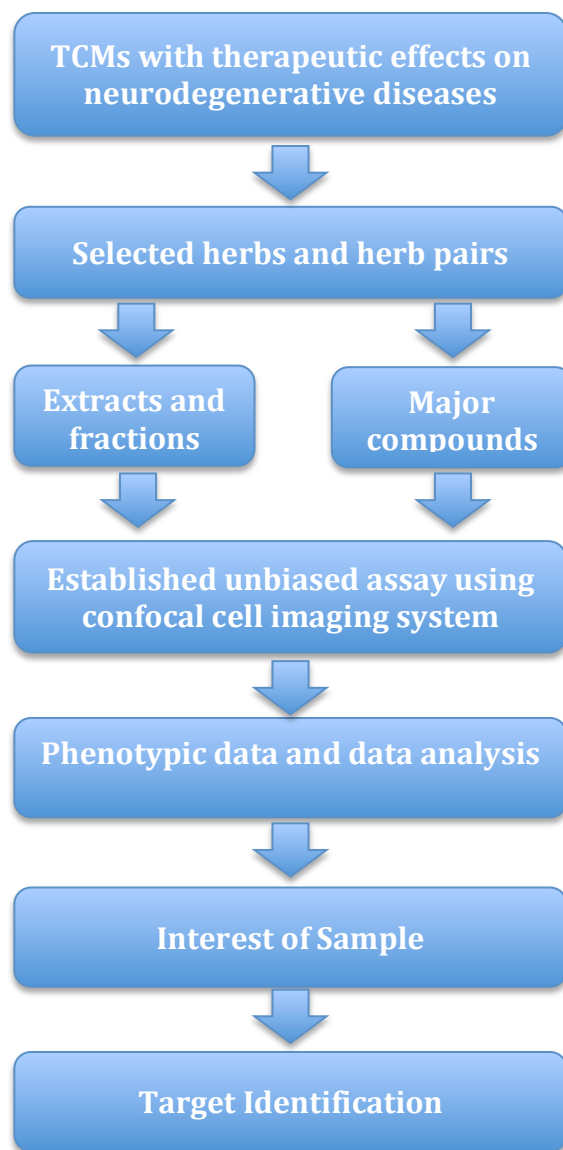


**Figure 1.9** General flowchart of the PhD program

Outline of the following chapters includes:

Chapter 2 will deal with selection of herbs and herb pairs, and physicochemical analysis of major compounds from the selected herbs.

Chapter 3 will describe preparation of all samples and chemical profiling of every sample.

Chapter 4 will focus on assay of every sample by the phenotypic imaging profiling method and the data analysis.

Chapter 5 will describe a preliminary study of target identification using a bait molecule through native mass spectrometry.

Chapter 6 will present a general conclusion and perspectives for in-depth research of TCM.

## 1.5 References

1. Wang, Y., Major Features and Changes of the 2015 Edition of Chinese Pharmacopoeia. *Progress in Pharmaceutical Sciences* **2016**, 40, (2), 118-121.
2. Pharmacopoeia of Peoples Republic of China. In 2015 ed.; National Commission of Chinese Pharmacopoeia, Ed. 中国医药科技出版社: Beijing, 2015; pp 704-705.
3. Pharmacopoeia of Peoples Republic of China. In 2015 ed.; National Commission of Chinese Pharmacopoeia, Ed. 中国医药科技出版社: Beijing, 2015; pp 124-126.
4. Newman, D. J.; Cragg, G. M., Natural Products as Sources of New Drugs from 1981 to 2014. *Journal of natural products* **2016**, 79, (3), 629-61.
5. Liu, J.-S.; Zhu, Y.-L.; Yu, C.-M.; Zhou, Y.-Z.; Han, Y.-Y.; Wu, F.-W.; Qi, B.-F., The structures of huperzine A and B, two new alkaloids exhibiting marked anticholinesterase activity. *Can. J. Chem.* **1986**, 64, 837-839.
6. Wang, Y.-e.; Yue, D.-x.; Tang, X.-c., Anti-cholinesterase activity of huperzine A. *Acta Pharmacol. Sin.* **1986**, 7, (2), 110-113.
7. Greger, H., Structural relationships, distribution and biological activities of Stemona alkaloids. *Planta Med.* **2006**, 72, (02), 99-113.
8. Tang, C.-P.; Chen, T.; Velten, R.; Jeschke, P.; Ebbinghaus-Kintscher, U.; Geibel, S.; Ye, Y., Alkaloids from stems and leaves of *Stemona japonica* and their insecticidal activities. *J. Nat. Prod.* **2007**, 71, (1), 112-116.
9. Lin, L.-G.; Zhong, Q.-X.; Cheng, T.-Y.; Tang, C.-P.; Ke, C.-Q.; Lin, G.; Ye, Y., Stemoninines from the Roots of *Stemona tuberosa*. *J. Nat. Prod.* **2006**, 69, (7), 1051-1054.
10. Lin, L.-G.; Li, K. M.; Tang, C.-P.; Ke, C.-Q.; Rudd, J. A.; Lin, G.; Ye, Y., Antitussive stemoninine alkaloids from the roots of *Stemona tuberosa*. *J. Nat. Prod.* **2008**, 71, (6), 1107-1110.
11. Lin, L.-G.; Leung, H. P.-H.; Zhu, J.-Y.; Tang, C.-P.; Ke, C.-Q.; Rudd, J. A.; Lin, G.; Ye, Y., Croomine- and tuberostemonine-type alkaloids from roots of *Stemona tuberosa* and their antitussive activity. *Tetrahedron* **2008**, 64, (44), 10155-10161.
12. Yang, X.-Z.; Zhu, J.-Y.; Tang, C.-P.; Ke, C.-Q.; Lin, G.; Cheng, T.-Y.; Rudd, J. A.; Ye, Y., Alkaloids from roots of *Stemona sessilifolia* and their antitussive activities. *Planta Med.* **2009**, 75, (02), 174-177.
13. 叶阳; 唐春萍; 李希强; 林鸽; 林理根; 柯昌强; 约翰·安东尼·鲁德 总生物碱提取物及其提取方法和在制备治疗咳嗽药物中的用途 CN101406649 A, 2009.
14. Tu, Y. Y., The discovery of artemisinin (qinghaosu) and gifts from Chinese medicine. *Nat. Med.* **2011**, 17, (10), 1217-1220.
15. Pharmacopoeia of Peoples Republic of China. In 2005 ed.; National Commission of Chinese Pharmacopoeia, Ed. Chemical Industry Press: Beijing, 2005.

16. Li, L.-N., Biologically active components from traditional Chinese medicines. *Pure Appl. Chem.* **1998**, 70, (3), 547-554.
17. Ling, S.; Dai, A.; Guo, Z.; Yan, X.; Komesaroff, P. A., Effects of a Chinese herbal preparation on vascular cells in culture: Mechanisms of cardiovascular protection. *Clin. Exp. Pharmacol. Physiol.* **2005**, 32, (7), 571-578.
18. Ji, X.; Tan, B. K. H.; Zhu, Y. C.; Linz, W.; Zhu, Y. Z., Comparison of cardioprotective effects using ramipril and DanShen for the treatment of acute myocardial infarction in rats. *Life Sci.* **2003**, 73, (11), 1413-1426.
19. Li, X.; Yu, C.; Lu, Y.; Gu, Y.; Lu, J.; Xu, W.; Xuan, L.; Wang, Y., Pharmacokinetics, tissue distribution, metabolism, and excretion of deposite salts from *Salvia miltiorrhiza* in rats. *Drug Metab. Dispos.* **2007**, 35, (2), 234-9.
20. Zhang, J. L.; Cui, M.; He, Y.; Yu, H. L.; Guo, D. A., Chemical fingerprint and metabolic fingerprint analysis of Danshen injection by HPLC-UV and HPLC-MS methods. *J. Pharm. Biomed. Anal.* **2005**, 36, (5), 1029-35.
21. Liu, A. H.; Lin, Y. H.; Yang, M.; Guo, H.; Guan, S. H.; Sun, J. H.; Guo, D. A., Development of the fingerprints for the quality of the roots of *Salvia miltiorrhiza* and its related preparations by HPLC-DAD and LC-MS(n). *J. Chromatogr. B Analyt. Technol. Biomed. Life Sci.* **2007**, 846, (1-2), 32-41.
22. 许琦敏 果德安带领团队探索科学解读中药的方法 .  
<http://sh.eastday.com/m/20160516/u1ai9373380.html>
23. China approves active ingredient of traditional medicine. *Nat. Biotechnol.* **2005**, 23, (7), 771-772.
24. Wang, L.; Zhou, G. B.; Liu, P.; Song, J. H.; Liang, Y.; Yan, X. J.; Xu, F.; Wang, B. S.; Mao, J. H.; Shen, Z. X.; Chen, S. J.; Chen, Z., Dissection of mechanisms of Chinese medicinal formula Realgar-Indigo naturalis as an effective treatment for promyelocytic leukemia. *Proc. Natl. Acad. Sci. U. S. A.* **2008**, 105, (12), 4826-4831.
25. Anonymous, 小儿卫生总微论方. In Huaxia Press: Beijing, 1997.
26. Wang, S.; Hu, Y.; Tan, W.; Wu, X.; Chen, R.; Cao, J.; Chen, M.; Wang, Y., Compatibility art of traditional Chinese medicine: from the perspective of herb pairs. *J. Ethnopharmacol.* **2012**, 143, (2), 412-23.
27. Wang, S.; Chen, M.; Wang, Y., Systematic Study of Chinese Medicine Herb Pairs (I)-Theory and Material Basic Study. *World Science and Technology/Modernization of Traditional Chinese Medicine and Mateira Medica* **2012**, 14, (2), 1317-1321.
28. Wang, S.; Hu, Y.; Chen, R.; Zhong, Z.; Chen, M.; Wang, Y., Systematic Study of Chinese Medicine Herb Pairs (II)-Pharmacodynamics and Pharmacokinetics Study. *World Science and Technology/Modernization of Traditional Chinese Medicine and Mateira Medica* **2012**, 14, (2), 1322-1328.
29. Gong, J.; Wang, S.; Chen, M.; Wang, Y., Systematic Study of Chinese Medicine Herb Pairs (III)-Pharmaceutical Theory and Novel Herb-pair Formulation. *World Science and Technology/Modernization of Traditional Chinese Medicine and Mateira Medica* **2012**, 14, (2), 1328-1333.
30. Chen, R.; Hu, Y.; Wang, S.; Chen, M.; Wang, Y., Systematic Study of Chinese Medicine Herb Pairs (IV)-Herb Pair of *Coptis Chinensis* and *Euodia Rutaecarpa*. *World Science and Technology/Modernization of Traditional Chinese Medicine and Mateira Medica* **2012**, 14, (2), 1334-1341.
31. Chen, R.; Shen, D.; Li, P.; Wang, S.; Hu, Y.; Chen, M.; Wang, Y., Systematic Study of Chinese Medicine Herb Pairs (V)-Herb Pair of *Salvia Miltiorrhiza* and *Panax Notoginseng*. *World Science and Technology/Modernization of Traditional Chinese Medicine and Mateira Medica* **2012**, 14, (2), 1342-1348.
32. Hu, Y.; Chen, R.; Wang, S.; Chen, M.; Wang, Y., Systematic Study of Chinese Medicine Herb Pairs (VI)-Herb Pair of *Radix Astragali* and *Angelica Sinensis*. *World Science and Technology/Modernization of Traditional Chinese Medicine and Mateira Medica* **2012**, 14, (2), 1349-1356.

33. Zeng, G.-F.; Xu, Q.; Xiao, H.-B.; Liang, X.-M., Influence of compatibility ratio of Fufang Danshen on the dissolution of Danshen compositions. *Chinese Journal of Chromatography* **2004**, 22, (2), 141-143.
34. Chabner, B. A.; Roberts, T. G., Jr., Timeline: Chemotherapy and the war on cancer. *Nat. Rev. Cancer* **2005**, 5, (1), 65-72.
35. Perelson, A. S.; Essunger, P.; Cao, Y.; Vesanen, M.; Hurley, A.; Saksela, K.; Markowitz, M.; Ho, D. D., Decay characteristics of HIV-1-infected compartments during combination therapy. *Nature* **1997**, 387, (6629), 188-91.
36. 2016 Alzheimer's disease facts and figures. *Alzheimer's & Dementia* **2016**, 12, (4), 459-509.
37. Prince, M.; Wimo, A.; Guerchet, M.; Ali, G.-C.; Wu, Y.-T.; Prina, M. *World Alzheimer Report 2015: The Global Impact of Dementia*; Alzheimer's Disease International: 2015; pp 1-92.
38. Alzheimer's Association. *Changing the Trajectory of Alzheimer's Disease: How a Treatment by 2025 Saves Lives and Dollars*; Alzheimer's Association: 2015.
39. Qian, X.; Hamad, B.; Dias-Lalcaca, G., The Alzheimer disease market. *Nature reviews. Drug discovery* **2015**, 14, (10), 675-6.
40. Carroll, J. Alzheimer's R&D suffers as trial failure rate hits an 'astounding' 99.6%. <http://www.fiercebiotech.com/r-d/alzheimer-s-r-d-suffers-as-trial-failure-rate-hits-an-astounding-99-6>
41. Tang, C.; Ye, Y.; Feng, Y.; Quinn, R. J., TCM, brain function and drug space. *Nat. Prod. Rep.* **2016**, 33, (1), 6-25.
42. Olin, J.; Schneider, L., Galantamine for Alzheimer's disease. *The Cochrane database of systematic reviews* **2002**, (3), Cd001747.
43. Lee, E.; Park, H. R.; Ji, S. T.; Lee, Y.; Lee, J., Baicalein attenuates astroglial activation in the 1-methyl-4-phenyl-1,2,3,4-tetrahydropyridine-induced Parkinson's disease model by downregulating the activations of nuclear factor- $\kappa$ B, ERK, and JNK. *J. Neurosci. Res.* **2014**, 92, (1), 130-139.
44. Yuan, T.; Ma, H.; Liu, W.; Niesen, D. B.; Shah, N.; Crews, R.; Rose, K. N.; Vatter, D. A.; Seeram, N. P., Pomegranate's Neuroprotective Effects against Alzheimer's Disease Are Mediated by Urolithins, Its Ellagitannin-Gut Microbial Derived Metabolites. *ACS Chem. Neurosci.* **2016**, 7, (1), 26-33.
45. Turner, R. S.; Thomas, R. G.; Craft, S.; van Dyck, C. H.; Mintzer, J.; Reynolds, B. A.; Brewer, J. B.; Rissman, R. A.; Raman, R.; Aisen, P. S., A randomized, double-blind, placebo-controlled trial of resveratrol for Alzheimer disease. *Neurology* **2015**, 85, (16), 1383-1391.

## **STATEMENT OF CONTRIBUTION TO CO-AUTHORED PUBLISHED PAPER**

This chapter includes a co-authored paper. The bibliographic details (if published or accepted for publication)/status (if prepared or submitted for publication) of the co-authored paper, including all authors, are:

### **TCM, brain function and drug space**

Chunping Tang,<sup>abc</sup> Yang Ye,<sup>bc</sup> Yunjiang Feng<sup>ac</sup> and Ronald J. Quinn<sup>\*ac</sup>

<sup>a</sup>Eskitis Institute for Drug Discovery, Griffith University, Brisbane, QLD 4111, Australia.

<sup>b</sup>State Key Laboratory of Drug Research, Shanghai Institute of Materia Medica, Chinese Academy of Sciences, Shanghai 201203, China

<sup>c</sup>Eskitis-SIMM Joint Laboratory for Drug Discovery, Australia

This paper has been published in *Natural Product Reports* (2016, **33**, 6-25).

My contribution to the paper involved:

Data collection and acquiring from literatures and database, data analysis, and paper writing.

(Signed) \_\_\_\_\_ (Date) \_\_\_\_\_  
Chunping Tang

(Countersigned) \_\_\_\_\_ (Date) \_\_\_\_\_  
Corresponding author of paper: Ronald J. Quinn

(Countersigned) \_\_\_\_\_ (Date) \_\_\_\_\_  
Supervisor: Ronald J. Quinn

## **CHAPTER 2 Selection of herbs and herb pairs and physicochemical analysis of major compounds from the selected herbs**

### **2.1 Selection of herbs and herb pairs targeting neurodegenerative disease**

#### **2.1.1 Selection of herbs frequently used to treat PD and AD**

In Traditional Chinese Medicine, there are no specific terms corresponding exactly to Parkinson's disease (PD), Alzheimer's disease (AD) or Huntington's disease (HD), which were introduced from western medicine. In principle, TCM is used to treat symptoms, rather than diseases. In the long history of TCM, a number of formulas have been recorded in a variety of medical books to treat symptoms like tremor, muscle rigidity, forgetfulness, insomnia, and dementia. These symptoms are commonly related to brain degeneration with aging, and these formulas are thereof considered as formulas with therapeutic effects to neurodegenerative diseases like PD and AD.

This research began by data mining. Some TCM formulas are known to treat symptoms related to PD and AD for hundreds or even thousands of years, and still are used clinically nowadays. By reviewing the academic theories in three important ancient books (about 100 BC-1600 AD), which were mentioned at the beginning of

Chapter 1, and searching related literature published in the last 40 years, the most commonly used formulas to treat PD and AD in current clinic were obtained by statistical processing and logical analysis. The top 10 of them are listed in a descending order in **Table 2.1**. It should be noted that some of them, e.g. Dihuang Yinzi, Liuwei Dihuang Wan, Renshen Yangrong Tang, and Tianma Gouteng Tang are used for both PD and AD, but others like Dingzhen Wan are used for PD, or Shenwu Jiaonang for AD only. It is rational since both PD and AD are diseases related to brain function and they show some symptoms in common, and therefore, some formulas used to treat these symptoms are overlapping. However, at the same time, each disease has its specific symptoms, e.g. tremor for PD, and Dingzhen Wan is a formula used to stop body shaking and so is only used for PD.

**Table 2.1** Commonly used formulas used clinically for PD and AD in descending order.

Formulas for PD (Chinese/Pinyin)	Formulas for AD (Chinese/Pinyin)
地黄饮子 Dihuang Yinzi	参乌胶囊 Shenwu Jiaonang
六味地黄丸 Liuwei Dihuang Wan	地黄饮子 Dihuang Yinzi
人参养荣汤 Renshen Yangrong Tang	六味地黄丸 Liuwei Dihuang Wan
十味温胆汤 Shiwei Wendan Tang	人参养荣汤 Renshen Yangrong Tang
天麻钩藤汤 Tianma Gouteng Tang	当归芍药散 Danggui Shaoyao San
羚角钩藤汤 Lingjiao Gouteng Tang	天麻钩藤饮加味 Tianma Gouteng Yin Jiawei
振肝熄风汤 Zhengan Xifeng Tang	补肾益智方 Bushen Yizhi Fang
定振丸 Dingzhen Wan	补肾益智方加味 Bushen Yizhi Fang Jiawei
桃红四物汤 Taohong Siwu Tang	脑灵汤 Nao Ling Tang
涤痰汤 Ditan Tang	天智颗粒 Tianzhi Keli

<sup>a</sup> Chinese name of formula is presented here because no English name is given in the Chinese Pharmacopoeia for formula.

<sup>b</sup> Generally speaking, a formula name gives information about the principal drugs and its preparation and formulation. For example, in 天麻钩藤汤 (Tianma Gouteng Tang), the first four Chinese characters tell us that two principal drugs are 天麻 (Tianma) and 钩藤 (Gouteng), and the last character 汤 (Tang) means it should be cooked with water to afford a decoction. The same material could be prepared in a different way in a different formula.

Some of these conventional formulas have been investigated using up-to-date technologies and methods, and their efficacies were proven further from the perspective of modern pharmacology. For example, Tianma Gouteng San (天麻钩藤散), a formula comprising 11 herbs, was firstly recorded in Xiaer Weisheng Zongwei Fanglun (小儿卫生总微论方), a medicinal book published in 1156.<sup>1</sup> He *et al* reported in 2010 that Tianma Gouteng Decoction significantly restrained apoptosis of dopaminergic neurons in rats with Parkinson's disease and its mechanism may be explained by increased expression of B-cell lymphoma 2 (Bcl-2) and restrained activation of Bax through anti-oxidative stress.<sup>2</sup> The results verified the potential of the formula for the treatment of Parkinson's disease.

Data mining the drugs in a formula, especially the monarch (principal) ones, some frequently used herbs could be identified, which are believed to be responsible for the formula's effects to a great degree.

The herbs used to treat Parkinson's disease in 202 publications published during 1987-2007 were reviewed, which included a total of 157 materials.<sup>3</sup> The frequency of the top 20 materials are listed as follows (**Table 2.2**). All English names are given according to the 2015 edition of the Chinese Pharmacopoeia.

**Table 2.2** Top 20 materials with frequency recorded in formulas used to treat PD during 1987-2007.

Chinese Name	Pinyin	English Name	Frequency*
白芍	Baishao	<u>Paeoniae Radix alba</u>	50
钩藤	Gouteng	<u>Uncariae Ramulus Cum Uncis</u>	44
天麻	Tianma	<u>Gastrodiae Rhizoma</u>	37
熟地黄	Shudihuang	<u>Rehmanniae Radix Praeparata</u>	33
甘草	Gancao	<u>Glycyrrhizae Radix et Rhizoma</u>	29
当归	Danggui	<u>Angelicae Sinensis Radix</u>	28
川芎	Chuanxiong	<u>Chuanxiong Rhizoma</u>	27
丹参	Danshen	<u>Salviae Miltiorrhizae Radix et Rhizoma</u>	27
生地黄	Shengdihuang	<u>Rehmanniae Radix</u>	26

全蝎	Quanxie	<u>Scorpio</u>	25
僵蚕	Jiangcan	<u>Bombyx Batryticatus</u>	22
龟板	Guiban	<u>Testudinis Carapax Plastrum</u>	21
黄芪	Huangqi	<u>Astragali Radix</u>	21
山萸肉	Shanyurou	<u>Corni Fructus</u>	20
枸杞子	Gouqizi	<u>Lycii Fructus</u>	18
蜈蚣	Wugong	<u>Scolopendra</u>	18
茯苓	Fuling	<u>Poria</u>	17
白术	Baizhu	<u>Atractylodis Macrocephalae Rhizoma</u>	15
人参	Renshen	<u>Ginseng Radix et Rhizoma</u>	15
石菖蒲	Shichangpu	<u>Acori Tatarinowii Rhizoma</u>	12

\* Times of usage in the formulas

Hu *et al* collected 132 prescriptions for treating senile dementia or AD. A total of 150 herbs were used in these prescriptions, and the top 10 most frequently used are listed in **Table 2.3**.<sup>4</sup>

**Table 2.3** Top 10 materials with frequency recorded in 132 prescriptions used to treat dementia or AD.

Chinese Name	Pinyin	English Name	Frequency*
石菖蒲	Shichangpu	<u>Acori Tatarinowii Rhizoma</u>	65
川芎	Chuanxiong	<u>Chuanxiong Rhizoma</u>	51
黄芪	Huangqi	<u>Astragali Radix</u>	47
何首乌	Heshouwu	<u>Polygoni Multiflori Radix</u>	46
人参	Renshen	<u>Ginseng Radix et Rhizoma</u>	40
丹参	Danshen	<u>Salviae Miltiorrhizae Radix et Rhizoma</u>	35
远志	Yuanzhi	<u>Polygalae Radix</u>	34
熟地黄	Shudihuang	<u>Rehmanniae Radix Praeparata</u>	28
茯苓	Fuling	<u>Poria</u>	26
枸杞子	Gouqizi	<u>Lycii Fructus</u>	25

\* Times of usage in the formulas

Another review reported the frequently used herbs in 100 prescriptions for the treatment of AD published during 1979-2006.<sup>5</sup> The top 12 herbs with the times used in the prescriptions are listed in **Table 2.4**.

**Table 2.4** Top 12 materials with frequency recorded in 100 prescriptions used to treat AD published during 1979-2006.

Chinese Name	Pinyin	English Name	Frequency*
--------------	--------	--------------	------------

石菖蒲	Shichangpu	<u>Acori Tatarinowii Rhizoma</u>	65
何首乌	Heshouwu	<u>Polygoni Multiflori Radix</u>	50
远志	Yuanzhi	<u>Polygalae Radix</u>	45
熟地黄	Shudihuang	<u>Rehmanniae Radix Praeparata</u>	35
丹参	Danshen	<u>Salviae Miltiorrhizae Radix et Rhizoma</u>	35
川芎	Chuanxiong	<u>Chuanxiong Rhizoma</u>	34
黄芪	Huangqi	<u>Astragali Radix</u>	33
茯苓	Fuling	<u>Poria</u>	29
枸杞子	Gouqizi	<u>Lycii Fructus</u>	28
当归	Danggui	<u>Angelicae Sinensis Radix</u>	26
益智仁	Yizhiren	<u>Alpinize Oxyphyllae Fructus</u>	23
人参	Renshen	<u>Ginseng Radix et Rhizoma</u>	22

\* Times of usage in the formulas

According to 141 conventional prescriptions used to treat dementia during the Ming dynasty and the Qing dynasty, Wang *et al* listed the top 14 herbs from a total of 167 materials used in the prescriptions in a descending order (**Table 2.5**).<sup>6</sup>

**Table 2.5** Top 14 materials recorded in 141 prescriptions used to treat dementia during the Ming dynasty and the Qing dynasty.

Order	Chinese Name	Pinyin	English Name
1	人参	Renshen	<u>Ginseng Radix et Rhizoma</u>
2	远志	Yuanzhi	<u>Polygalae Radix</u>
3	石菖蒲	Shichangpu	<u>Acori Tatarinowii Rhizoma</u>
4	甘草	Gancao	<u>Glycyrrhizae Radix et Rhizoma</u>
5	茯苓	Fuling	<u>Poria</u>
6	茯神	Fushen	*
7	麦冬	Maidong	<u>Ophiopogonis Radix</u>
8	当归	Danggui	<u>Angelicae Sinensis Radix</u>
9	酸枣仁	Suanzaoren	<u>Ziziphi Spinosae Semen</u>
10	熟地黄	Shudihuang	<u>Rehmanniae Radix Praeparata</u>
11	朱砂	Zhusha	<u>Cinnabaris</u>
12	白术	Baizhu	<u>Atractylodis Macrocephalae Rhizoma</u>
13	半夏	Banxia	<u>Pinelliae Rhizoma</u>
14	生地黄	Shengdihuang	<u>Rehmanniae Radix</u>

\* Not recorded in the Chinese Pharmacopoeia.

According to the formulas recorded in the literatures and the medicinal classics, 15 commonly used TCMs were selected. The criteria for the selection are as follows:

1. Frequently present in classical formulas to treat symptoms related to neurodegenerative diseases;
2. Well-known and thoroughly investigated;
3. Containing different types of chemical structures;
4. Easy-to-obtain in market, including herbal material and its major chemical constituents;
5. Containing chemicals proven to have potential against neurodegenerative diseases by modern pharmacology.

The detailed information about the selected 15 herbal medicines is shown in **Table 2.6**. Plants 1-14 were identified from the ancient literatures. Plant 15 was also a TCM but prioritized under criteria 5.

**Table 2.6** 15 selected TCMs commonly used to treat neurodegenerative diseases.

No	Chinese Name	Pinyin	English Name	Original Plant(s)
1	人参	Renshen	<u>Ginseng Radix et Rhizoma</u>	<i>Panax ginseng</i> C. A. Mey. <i>Codonopsis pilosula</i> (Franch.) Nannf.
2	党参	Dangshen	<u>Codonopsis Radix</u>	<i>Codonopsis pilosula</i> Nannf. var. <i>modesta</i> (Nannf.) L. T. Shen; <i>Codonopsis tangshen</i> Oliv.
3	白芍	Baishao	<u>Paeoniae Radix Alba</u>	<i>Paeonia lactiflora</i> Pall.
4	何首乌	Heshouwu	<u>Polygoni Multiflori Radix</u>	<i>Polygonum multiflorum</i> Thunb.
5	熟地黄	Shudihuang	<u>Rehmanniae Radix Praeparata</u>	<i>Rehmannia glutinosa</i> Libosch.
6	天麻	Tianma	<u>Gastrodiae Rhizoma</u>	<i>Gastrodia elata</i> Bl.
7	钩藤	Gouteng	<u>Ramulus Uncariae Cum Uncis</u>	<i>Uncaria rhynchophylla</i> (Miq.) Miq. ex Hail. <i>Uncaria macrophylla</i> Wall. <i>Uncaria hirsute</i> Havil. <i>Uncaria sinensis</i> (Oliv.) Havil.
8	川芎	Chuanxiong	<u>Chuanxiong Rhizoma</u>	<i>Ligusticum chuanxiong</i> Hort.
9	丹参	Danshen	<u>Salviae Miltiorrhizae Radix et Rhizoma</u>	<i>Salvia miltiorrhiza</i> Bge.
10	石菖蒲	Shichangpu	<u>Acori Tatarinowii Rhizoma</u>	<i>Acorus tatarinowii</i> Schott
11	远志	Yuanzhi	<u>Polygalae Radix</u>	<i>Polygala tenuifolia</i> Willd.

			<i>Polygala sibirica</i> L.
12	酸枣仁	Suanzaoren	<u>Ziziphi Spinosae Semen</u> <i>Ziziphus jujuba</i> Mill. var. <i>spinosa</i> (Bunge) Hu ex H. F. Chou.
13	柏子仁	Baiziren	<u>Platycladi Semen</u> <i>Platycladus orientalis</i> (L.) Franco
14	葛根	Gegen	<u>Puerariae Lobatae Radix</u> <i>Pueraria lobata</i> (Willd.) Ohwi
15	豆蔻	Doukou	<u>Amomi Fructus Rotundus</u> <i>Amomum kravanh</i> Pierre ex Gagnep <i>Amomum compactum</i> Soland ex Maton

All information is presented according to the Chinese Pharmacopoeia of the 2010 edition. The herbs are denoted by the underlined English name and Pinyin in the text, in order to be distinguished from the Latin names of the original plants.

### 2.1.2 Selection of herb pairs

In order to reflect the characteristics of the TCM theories, the herb pairs were prepared. As mentioned, herb pair is a combination of two herbs commonly used together in formulas. Looking into the 15 selected herbs, 5 herb pairs from 9 selected herbs were identified. The detailed information of the 5 herb pairs is shown in **Table 2.7**.

**Table 2.7** 5 Selected herb pairs used to treat neurodegenerative diseases.

Code	药对	Herb pairs	Ratio	Compatibility
6+7	天麻/钩藤	<u>Gastrodiae Rhizoma /</u> <u>Ramulus Uncariae Cum Uncis</u>	3:4	6 g / 8 g
6+8	天麻/川芎	<u>Gastrodiae Rhizoma /</u> <u>Chuanxiong Rhizoma</u>	1:4	3 g / 12 g
9+14	丹参/葛根	<u>Salviae Miltiorrhizae Radix et Rhizoma</u> <u>/Puerariae Lobatae Radix</u>	1:1	7 g / 7 g
10+11	石菖蒲/远志	<u>Acori Tatarinowii Rhizoma /</u> <u>Polygalae Radix</u>	1:1	7 g / 7 g
12+13	酸枣仁/柏子仁	<u>Ziziphi Spinosae Semen /</u> <u>Platycladi Semen</u>	1:1	7 g / 7 g

Herb pair 6+7 was recorded in many ancient medicinal books, such as Xiaoyer Weisheng Zongwei Fanglun (小儿卫生总微方论) and Zhongyi Neike Zabing Zhengzhi Xinyi (中医内科杂病证治新义), with traditional functions of calming liver wind, and used for the treatment of the symptoms caused by PD,<sup>2</sup> e.g. meliorating sleep disorders.

Ren *et al* reported the clinical efficacy of 43 cases, and 60% of PD patients showed obvious improvement in their sleeping quality.<sup>7</sup> The herb pair was also found to have good effects on stubborn insomnia in clinical research including 60 cases.<sup>8</sup>

Herb pair 6+8 was an herb pair used traditionally to treat headaches, particularly migraine. Current researches also proved its efficacy in clinic. Liu reported a clinical study of 100 patients treated with the herb pair 6+8 and the total effective rate was high as 97%.<sup>9</sup> Zhou *et al* found that the ratio of these two herbs in the prescription of Da Chuanxiong Wan (大川芎丸) has different effects on blood rheology indexes of rats with acute blood stasis syndrome and common carotid artery blood flow of rabbits. Gastrodiae Rhizoma did not show effects on the animal models on its own, but the herb pair 6+8 showed synergistic effects on improving the functions of Chuanxiong Rhizoma.<sup>10</sup>

Herb pair 10+11 was listed as the top 1 recipe in treating cognitive functions in history. It was recorded in the herbal remedy Yuanzhi Decotion (远志汤) in the medicinal books such as Shengji Zonglu (圣济总录), and Kongsheng Zhenzhong Dan (孔圣枕中丹) in Qianjin Yaofang (千金要方). The compatibility of these two herbs was believed to eliminate phlegm and clear the brain, and used to improve the cognition and memory of PD and AD patients.<sup>11</sup>

Herb pairs 9+14 and 12+13 were recorded as empirical prescriptions in Shijinmo Duiyao Linchuang Jinyan Ji (施今墨对药临床经验集), a collection of about 370 herb pairs used in the clinic.<sup>12</sup> The herb pair 9+14 was applied to promote blood circulation by removing blood stasis. The herb pair 12+13 had the functions of tranquilizing the mind and was used to treat palpitation, insomnia, and constipation.

## **2.2 Physicochemical analysis of major compounds from the 15 selected herbs**

### **2.2.1 Methods used for physicochemical analysis**

A thorough literature search of the selected herbs afforded a total of 84 major bioactive compounds reported previously. The review of these compounds and their bioactivities is presented in section 2.2.2. Considering the intrinsic relationship between the chemical structures and their biological activities, a series of analyses based on the physicochemical properties of the known structures were carried out through using the following methods.

#### ***2.2.1.1 Lipinski's rule of five***

Lipinski's rule of five, also known as the Rule of five (Ro5), is a rule of thumb to evaluate drug-likeness and predict if a chemical compound has physicochemical properties that would make it orally bioavailable in humans.<sup>13, 14</sup> Lipinski's rule states that, in general, an orally active drug has no more than one violation of the following criteria: a molecular weight (MW) less than 500 Daltons, no more than 5 hydrogen bond donors (HBDs), no more than 10 hydrogen bond acceptors (HBAs), and an octanol-water partition coefficient  $\log P$  not greater than 5. Although the rule cannot guarantee a molecule compliant with all criteria is drugable, it provides a guide for medicinal chemists for better design of compounds with satisfactory pharmacokinetics. So far, the criteria have spawned many extensions. In particular, compounds that meet the two criteria of 10 or fewer rotatable bonds (ROTB) and polar surface area (PSA) equal to or less than 140 Å<sup>2</sup> are predicted to have good oral bioavailability.<sup>15</sup>

The structures of compounds were converted into SMILES format and imported into Instant JChem16 to calculate the physicochemical parameters of each molecule including molecular weight (MW), hydrogen bond donor (HBD), hydrogen bond

acceptor (HBA), octanol-water partition coefficient  $\log P$ , rotatable bonds (ROTB) and polar surface area (PSA). Graphing and data analysis software Origin 8.0 was used to generate pie charts and histograms of the results.<sup>17</sup>

#### **2.2.1.2 ChemGPS-NP**

In contrast to Lipinski's parameters focusing on a restricted set of drug-like properties generated directly from the molecular structures, ChemGPS-NP is a tool tuned for identifying volumes of chemical space to allow correlation to biological activities.<sup>18</sup> ChemGPS-NP has been designed to handle the chemical diversity of natural products. It can discover physicochemical properties not directly discernible from structural data, and can chart biologically relevant chemical space and provide an efficient mapping device for prediction of properties and activities of groups of compounds.

The set of structures with calculated physicochemical data was exported from JChem and saved as a daylight smiles file. The extracted file from JChem was then uploaded through the ChemGPS-NP website (<http://chemgps.bmc.uu.se/batchelor/queue.php?show=submit>), and the result files given by the website were viewed and downloaded. The results were checked and the first three principle components were found to be able to explain 71% of the variance. Origin 8.0 was finally used to chart 3D physicochemical space on the basis of the first three principle components.<sup>17</sup>

#### **2.2.1.3 In silico prediction of the BBB permeability**

The ability to permeate across the blood brain barrier (BBB) is essential for drugs acting on the central nervous system. It is determined by their molecular size and physicochemical properties, as well as by complex binding and elimination processes occurring in the circulation, peripheral organs, at the BBB and in the brain parenchyma and its fluids.<sup>19</sup> A number of methods and models are available for examining BBB

permeation *in vivo*, *in vitro*, and *in silico*. A combination of techniques can give valuable information on ways to optimize permeation, and implications for drug discovery, delivery and toxicity.<sup>20, 21</sup>

*In silico* prediction of the BBB permeability of 84 TCM compounds was carried out. LigPrep (version 2.3, Schrödinger, LLC, New York, NY, 2009) was used to generate 3D structures of all TCM compounds, with the selected OPLS\_2005 force field, neutralized functional groups, retained specified chiralities, and other parameters default. The generated 3D structures and QikProp (version 3.2, Schrödinger, LLC, New York, NY, 2009) were then used to calculate three descriptors QPPCaco, QPlogBB and QPPMDCK, which can reflect directly the ability of a molecule to permeate the BBB.

### **2.2.2 Physicochemical analysis of major compounds from the selected herbs**

Research on the 15 selected herbs has been published.<sup>22</sup> The first part consisted of a review of 84 major compounds reported from the 15 selected herbs and their bioactivity associated with brain functions. The second part focused on an array of calculations and data analyses.

In order to compare the TCM compounds with current drugs, two sets of reference compounds, 38 anti-PD and 65 anti-AD small molecule drugs, were identified through searching the Thomson Reuters Cortellis. Lipinski's rule of five was used to evaluate drug-likeness of these major compounds so that molecular weight (MW), hydrogen bond donor (HBD), hydrogen bond acceptor (HBA), octanol-water partition coefficient log P, rotatable bonds (ROTB) and polar surface area (PSA) of the TCM compounds were calculated, along with those of anti-PD and anti-AD drugs. ChemGPS-NP was used for principle component analysis (PCA) of these three sets of compounds to compare their distribution in physicochemical space. *In silico* prediction of the blood brain barrier (BBB) permeability of 84 TCM compounds was also given.



Cite this: *Nat. Prod. Rep.*, 2016, 33, 6

## TCM, brain function and drug space

Chunping Tang,<sup>abc</sup> Yang Ye,<sup>bc</sup> Yunjiang Feng<sup>ac</sup> and Ronald J. Quinn<sup>\*ac</sup>

Covering: up to 2015

Traditional Chinese medicine has played a significant role in the mainstream healthcare system in China for thousands of years. Here, we summarize 84 major compounds from 15 selected herbal medicines targeting neurodegenerative diseases. We present a perspective based on the analysis of physicochemical properties of these TCM compounds, and comparison with current drugs and candidates for the treatment of Parkinson's and Alzheimer's disease. The results demonstrate that traditional Chinese medicines contain compounds possessing physicochemical properties that have excellent overlap with developed western medicines.

Received 1st May 2015

DOI: 10.1039/c5np00049a

[www.rsc.org/npr](http://www.rsc.org/npr)

- 1 Introduction
- 2 TCM herbs targeting neurodegenerative diseases and the major bioactive compounds
  - 2.1 TCM herbs targeting neurodegenerative diseases
  - 2.2 Major compounds from the selected TCM herbs
- 3 Physicochemical properties
  - 3.1 Physicochemical properties of anti-PD drugs, anti-AD drugs and TCM compounds
  - 3.2 Comparison of physicochemical space of anti-PD drugs, anti-AD drugs and TCM compounds
  - 3.3 Prediction of blood-brain barrier permeation of TCM compounds
- 4 Conclusions
- 5 Acknowledgments
- 6 Notes and references

## 1 Introduction

Traditional Chinese Medicine (TCM) has played a significant role in the mainstream healthcare system in China for thousands of years. It has its own theoretical basis and practical application. The comprehensive system of TCM features the use of large numbers of herbal medicines, which have been recorded scrupulously and precisely in a number of ancient texts. For example, the *Compendium of Materia Medica*, one of the most famous classics written in the Ming dynasty (~1590 AD), recorded 1892 drugs with 1095 of them being herbal medicines (58%). Herbal medicines, as well as animal and mineral medicines, have also been documented in the

Chinese Pharmacopeia since 1953, with the number increasing from 78 in the first version to 1146 in the 2005 version.

Based on such accumulated knowledge, the chance to identify biologically active small molecules from TCMs is higher in comparison with random collection and screening. One of the success stories is the discovery of artemisinin (qinghaosu) from *Artemisia annua* as an effective anti-malaria therapy that has saved millions of lives around the world. Youyou Tu, “for her discoveries concerning a novel therapy against Malaria” (nobelprize.org), shared the Nobel Prize in Physiology or Medicine 2015 with two other scientists. She narrated the story about the discovery of artemisinin and its development into a drug in *Nature Medicine*.<sup>1</sup> She said the medicinal herb Qinghao was one of the most frequently used herbs for the treatment of malaria after investigating more than 2000 Chinese herbal prescriptions. Artemisinin is “a true gift from old Chinese medicine”.<sup>1</sup> Another representative example is deposite salts from *Salvia miltiorrhiza*, a traditional herb known as “Danshen”. Deposite salts is a mixture in which magnesium lithospermate B and its 5 analogs are the active components.<sup>2</sup> China's State Food and Drug Administration (SFDA) granted a new drug license for this mixture and its injectable form in May 2005 for the treatment of angina and other cardiovascular diseases.

These two cases provide a glimpse of successful drugs derived from traditional medicines. Professor Zhibi Hu, a member of the Chinese Academy of Engineering, said in *Nature Biotechnology*, “This success means China's biopharmaceutical industry can develop innovative drugs by investigating the chemical ingredients of TCMs whose clinical effects have long been observed. Compared with developing new compounds from scratch, the approach is potentially more rapid and less expensive”.<sup>3</sup>

Although the successful stories have shown that therapeutic molecules can be derived from TCMs, the majority of the traditional medicines are still waiting to be studied. The chemicals

<sup>a</sup>Eskitis Institute for Drug Discovery, Griffith University, Brisbane, QLD 4111, Australia. E-mail: [r.quinn@griffith.edu.au](mailto:r.quinn@griffith.edu.au)

<sup>b</sup>State Key Laboratory of Drug Research, Shanghai Institute of Materia Medica, Chinese Academy of Sciences, Shanghai 201203, China

<sup>c</sup>Eskitis-SIMM Joint Laboratory for Drug Discovery, Australia

responsible for the therapeutic effects, that have the potential to be leads, need thorough and in-depth investigations from multiple perspectives. Herein, we review the literature and classical Chinese medicinal books to search for commonly used herbal medicines applied to neurodegenerative diseases. Major and bioactive compounds identified from these herbs are summarized. Their physicochemical properties are analyzed and compared with anti-Parkinson's and anti-Alzheimer's disease drugs launched and in clinical trial in order to assess the drug potential.

## 2 TCM herbs targeting neurodegenerative diseases and the major bioactive compounds

Neurodegenerative disease is an umbrella term for a range of conditions that primarily affect the neurons in the human brain such as Parkinson's (PD), Alzheimer's (AD), and Huntington's

disease (HD). The global prevalence of dementia in people aged over 60 years was estimated to be over 24 million in 2001 and is expected to double every 20 years.<sup>4</sup> With the increase in the aging population, neurodegenerative diseases are becoming a major social and economic burden worldwide. There is an urgent need to develop more effective therapeutic strategies for neurodegenerative disease.

In Traditional Chinese Medicine, there are no specific terms corresponding exactly to PD, AD or HD. However, many herbs are recorded to treat symptoms like tremor, muscle rigidity, forgetfulness, insomnia, and dementia. It is commonly believed that these symptoms are due to brain degeneration with aging, and therefore are directly related to neurodegenerative diseases.

Many TCM formulae have been used for hundreds or even thousands of years to treat these symptoms and continue to be used clinically. For example, *Tianma Gouteng Decoction*, a formula comprising 11 herbs, was firstly recorded in *Xiaoei Weisheng Zongwei Lunfang*, a medicinal book published in 1156.



*Chunping Tang obtained her master degree of natural products chemistry in Shanghai Institute of Materia Medica in 1998. After that, she worked there as a Research Assistant and then a Research Associate, focusing on seeking bioactive constituents from traditional Chinese medicines. Now she is a PhD student in Eskitis Institute for Drug Discovery. Her research program is discovering bioactive constituents from TCMs targeting neurodegenerative diseases.*



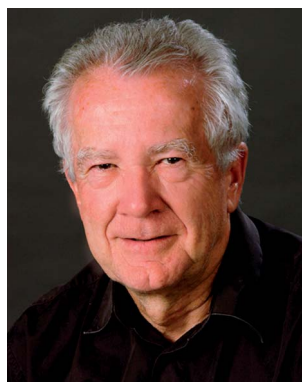
*Dr Yunjiang Feng graduated from Beijing Medical University (now Peking University). She was awarded a PhD in marine natural products from James Cook University, followed by postdoctoral research in fungal metabolites at University of Canterbury (NZ). In 2004, Dr Feng was appointed a research fellow by Griffith University conducting natural product lead discovery. In 2014, she joined*

*the School of Natural Sciences, Griffith University, as a senior lecturer. Her recent research focus has been Traditional Chinese Medicine (TCM) where she investigates whether single component responsible for the biological function, and the synergistic effects of different components.*



*Professor Yang Ye has his research focus in natural products chemistry, particularly the isolation and structural elucidation of secondary metabolites from plants. His major objective is to identify bioactive components from traditional Chinese medicine (TCM) that help to understand the effect of such plants in their traditional applications. Ye has published over 80 peer-reviewed publica-*

*tions and edited two books. He is in the editorial boards of *Planta Medica*, *Phytochemistry Letters*, *Progress in the Chemistry of Organic Natural Products*.*



*Ronald Quinn obtained his PhD in chemistry from the University of New South Wales, Australia in 1970. He joined Griffith University in 1982 and is Professor and Director of the Eskitis Institute for Drug Discovery. His research concentrates on the use of molecules as probes to understand interactions in biological systems, conducting research on bioactive natural products and bioaffinity mass spectrometry to*

*identify protein–ligand complexes. He is a Member of the Order of Australia (AM) for service to scientific research, in the field of chemistry and a Fellow of the Australian Academy of Technological Sciences and Engineering.*

He *et al.* reported in 2010 that *Tianma Gouteng Decoction* significantly restrained the apoptosis of dopaminergic neurons in rats with Parkinson's disease and its mechanism may be explained by increasing expression of B-cell lymphoma 2 (Bcl-2) and restraining activation of Bax through anti-oxidative stress.<sup>5</sup> The results suggested that the formula has potential in the treatment of Parkinson's disease.

## 2.1 TCM herbs targeting neurodegenerative diseases

Some herbal medicines are frequently used in these formulae, particularly as the monarch (principal) drug in a prescription. Hu *et al.* collected 132 prescriptions for treating senile dementia or AD. There were 150 herbs used in these prescriptions, and the top 10 most frequently used were Acori Tatarinowii Rhizoma, Chuanxiong Rhizoma, Astragali Radix, Polygoni Multiflori Radix, Ginseng Radix et Rhizoma, Salviae Miltiorrhizae Radix et Rhizoma, Polygalae Radix, Rehmanniae Radix Preparata, Poria, and Lycii Fructus.<sup>6</sup> Su *et al.* found 157 herbs used in prescriptions for the treatment of relevant symptoms of neurodegenerative diseases. The top 8 of the most frequently used herbs were Paeoniae Radix Alba, Ramulus Uncariae Cum Uncis, Gastrodiae Rhizoma, Rehmanniae Radix Preparata, Glycyrrhizae Radix et Rhizoma, Angelicae Sinensis Radix, Chuanxiong Rhizoma, and Salviae Miltiorrhizae Radix et Rhizoma.<sup>7</sup>

According to the literature and the formulae recorded in the medicinal classics, we selected 15 commonly used TCMs, which are frequently present in formulae to treat neurodegenerative diseases. The detailed information about the selected herbal medicines is shown in Table 1.

## 2.2 Major compounds from the selected TCM herbs

From the selected 15 herbal medicines, a variety of compounds have been reported. We list 84 compounds, which are either the major compounds existing in the plants or have relevant bioactivities to brain-related diseases including AD, PD.

Ginseng Radix et Rhizoma (Renshen) is one of the most famous Chinese medicines and has been used for thousands of years with significant functions of *strengthening the body resistance, consolidating the constitution, improving the cognitive functions, and prolonging life*.

Ginsenosides, a series of dammarane or oleanane type triterpenoid glycosides, are believed to be the pharmacologically active ingredients in ginseng.<sup>8</sup> The Ginseng Evaluation Program of the American Botanical Council recommended seven major components, Rb1, Rb2, Rc, Rd, Re, Rf and Rg1 (1–7), for quality control of Ginseng and its related species. In the Chinese Pharmacopeia, ginsenosides Rb1, Re, Rf and Rg1 are used as standard

**Table 1** 15 selected TCMs commonly used to treat neurodegenerative diseases<sup>a</sup>

No	Chinese name	Pinyin	English name	Original plant(s)
1	人参	Renshen	Ginseng Radix et Rhizoma	<i>Panax ginseng</i> C. A. Mey
2	党参	Dangshen	Codonopsis Radix	<i>Codonopsis pilosula</i> (Franch.) Nannf. <i>Codonopsis pilosula</i> Nannf. var. <i>modesta</i> (Nannf.) L. T. Shen; <i>Codonopsis tangshen</i> Oliv. <i>Paeonia lactiflora</i> Pall.
3	白芍	Baishao	Paeoniae Radix Alba	<i>Polygonum multiflorum</i> Thunb.
4	何首乌	Heshouw	Polygoni Multiflori Radix	<i>Rehmannia glutinosa</i> Libosch.
5	熟地黄	Shudihuang	Rehmanniae Radix Praeparata	<i>Gastrodia elata</i> Bl.
6	天麻	Tianma	Gastrodiae Rhizoma	<i>Uncaria rhynchophylla</i> (Miq.) Miq. ex Hail. <i>Uncaria macrophylla</i> Wall. <i>Uncaria hirsute</i> Havil. <i>Uncaria sinensis</i> (Oliv.) Havil. <i>Uncaria sessilifructus</i> Roxb. <i>Ligusticum chuanxiong</i> Hort.
7	钩藤	Gouteng	Ramulus Uncariae Cum Uncis	<i>Salvia miltiorrhiza</i> Bge.
8	川芎	Chuanxiong	Chuanxiong Rhizoma	<i>Acorus tatarinowii</i> Schott
9	丹参	Danshen	Salviae Miltiorrhizae Radix et Rhizoma	<i>Polygala tenuifolia</i> Willd. <i>Polygala sibirica</i> L.
10	石菖蒲	Shichangpu	Acori Tatarinowii Rhizoma	<i>Ziziphus jujuba</i> Mill. var. <i>spinosa</i> (Bunge) Hu ex H. F. Chou
11	远志	Yuanzhi	Polygalae Radix	<i>Platycladus orientalis</i> (L.) Franco
12	酸枣仁	Suanzaoren	Ziziphi Spinosae Semen	<i>Pueraria lobata</i> (Willd.) Ohwi
13	柏子仁	Baiziren	Platycladi Semen	<i>Amomum kravanh</i> Pierre ex Gagnep, <i>Amomum compactum</i> Soland ex Maton
14	葛根	Gegen	Puerariae Lobatae Radix	
15	豆蔻	Doukou	Amomi Fructus Rotundus	

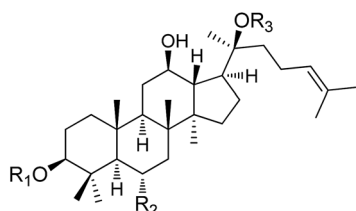
<sup>a</sup> All information is presented according to the Chinese Pharmacopoeia of the 2010 version. The herbs are denoted by the English name and Pinyin in the text, in order to be distinguished from the Latin names of the original plants.

compounds for identification and quality control of the raw material.

The effects of ginseng extracts and ginsenosides are relevant to a variety of diseases. Ginseng was reported to have potentially positive effects on heart disease through its various properties including antioxidation, reduced platelet adhesion, vasomotor regulation, improving lipid profiles, and influencing various ion channels.<sup>9–11</sup> Lü *et al.* reviewed the bioactive effects of ginsenosides on antioxidation, the vascular system, signal transduction pathways and interaction with receptors, and their therapeutic applications in animal models and humans as well as the pharmacokinetics and toxicity of ginsenosides.<sup>12</sup>

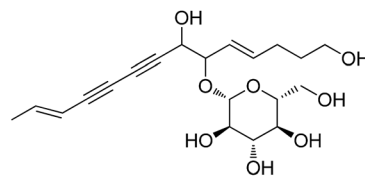
A number of publications reported the effects of ginsenosides on the central nervous system (CNS) and the peripheral nervous system by regulating various types of ion channels.<sup>13,14</sup> Ginsenoside Rg3 regulates voltage-gated ion channels such as Ca<sup>2+</sup>, K<sup>+</sup>, and Na<sup>+</sup> channels, and ligand-gated ion channels such as GABA<sub>A</sub>, 5-HT<sub>3</sub>, nicotinic acetylcholine, and *N*-methyl-D-aspartate (NMDA) receptors through interactions with various sites including channel blocker binding sites, toxin-binding sites, channel gating regions, and allosteric channel regulator binding sites with the respective ion channels or receptors.<sup>15</sup> Rg1 can increase proliferation and differentiation of neural progenitor cells in dentate gyrus of the hippocampus of normal adult mice and the global ischemia model in gerbils.<sup>16</sup> Ginsenoside Rh2 (8) was reported to reverse memory impairment caused by scopolamine in mice,<sup>17</sup> to increase pituitary adenylate cyclase-activating polypeptide (PACAP), to activate a PACAP selective receptor (PAC1), and to attenuate amyloid  $\beta$  (A $\beta$ )-induced toxicity.<sup>18</sup> In a vascular dementia (VD) rat model, ginsenoside Rg2 (9) was able to improve neurological performance and memory ability of VD rats through mechanisms related to anti-apoptosis.<sup>19</sup>

Pharmacokinetic studies by oral administration of Ginseng extract or ginsenosides indicated that the major metabolites detectable in plasma or in urine involved several compounds such as ginsenosides K, F1, Rb1, Rb3, Rd, Rg2, Rg3, Rh1, Rh2, protopanaxadiol, and protopanaxatriol. Compound K, for example, is a major metabolite of the ginsenosides present in *P. ginseng* extracts.<sup>20</sup>



	R <sub>1</sub>	R <sub>2</sub>	R <sub>3</sub>
1	glucose-2 → 1-glucose	2H	glucose-6 → 1-glucose
2	glucose-2 → 1-glucose	2H	glucose-6 → 1-arabinose (pyr)
3	glucose-2 → 1-glucose	2H	glucose-6 → 1-arabinose (fur)
4	glucose-2 → 1-glucose	2H	glucose
5	H	O-glucose-2 → 1-rhamnose	glucose
6	H	O-glucose-2 → 1-glucose	glucose
7	H	O-glucose	glucose
8	glucose	2H	H
9	H	O-glucose-2 → 1-rhamnose	H

Codonopsis Radix (Dangshen) has been traditionally used as a tonic and a substitute of Ginseng although its therapeutic efficacy is much lower than Ginseng. Its chemical constituents do not contain the ginsenosides, but mainly carbenes, atractylenolides, phenylpropanoids, alkaloids, triterpenoids, and polysaccharides. Lobetyolin (10) exists in all the original plants, and is documented in the Chinese Pharmacopeia to be a standard compound for the identification of the raw material. It was reported that lobetyolin was able to trigger the transcriptional activity of NF- $\kappa$ B, which is related to neuro cell growth.<sup>21</sup>

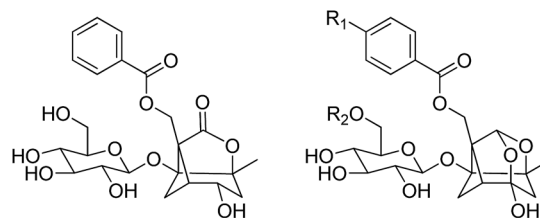


10

Monoterpene glucosides are an important class of bioactive compounds identified from *Paeoniae Radix Alba* (Baishao). Major compounds include paeoniflorin (11), albiflorin (12), oxypaeoniflorin (13), and benzoylpaeoniflorin (14).<sup>22</sup> The content of paeoniflorin (11) is greater than 70% of the total glucoside extract, and is used as a chemical marker for the identification and content determination of the raw material in the Chinese Pharmacopeia.

Paeoniflorin showed neuroprotective effects against glutamate (Glu)-induced neurotoxicity in PC12 cells through amelioration of the reduction of cell viability, nuclear and mitochondrial apoptotic alteration, reactive oxygen species (ROS) accumulation, and Bcl-2/Bax ratio.<sup>23,24</sup> Paeoniflorin could also protect PC12 cells against MPP<sup>+</sup>- or acid-induced injury associated with the up-regulation of LC3-II protein.<sup>25</sup> Wang *et al.* found that paeoniflorin could attenuate or restore the viability loss, apoptotic increase, and ROS production induced by A $\beta$ <sub>25–35</sub> in SH-SY5Y cells, and strikingly inhibit A $\beta$ <sub>25–35</sub>-induced mitochondrial dysfunction.<sup>26</sup>

Paeoniflorin (11) showed extremely poor absorption and low bioavailability when orally administrated, but it was found to be transformed to a major metabolite paeonimetabolin I in high percentage by intestinal bacteria and absorbed rapidly from the gastrointestinal tract. A high concentration of paeonimetabolin I rather than paeoniflorin was detected in the rat plasma.<sup>27</sup> Another investigation of oral administration to rats with the decoction of Baishao revealed that paeoniflorin was not absorbed *per se*, whereas its aglycone paeoniflorigenin was absorbed and circulating in the bloodstream.<sup>28</sup>



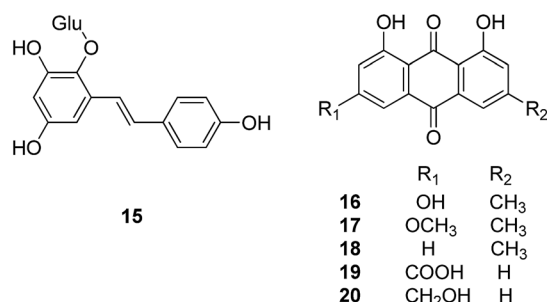
12

	R <sub>1</sub>	R <sub>2</sub>
11	H	H
13	OH	H
14	H	benzoyl

Stilbene glucosides, anthraquinones and phospholipids are three major classes of compounds isolated from *Polygoni Multiflori Radix* (Heshouwu). 2,3,5,4'-Tetrahydroxystilbene-2-O- $\beta$ -D-glucopyranoside (**15**), the main stilbene glucoside present in the plant material, is used in the Chinese Pharmacopeia as quality control of the raw material, together with two anthraquinones, emodin (**16**) and physcion (**17**). Chrysophanol (**18**), rhein (**19**) and aloemodin (**20**) are other major anthraquinones identified from this plant.

Compound **15** was reported to attenuate MPP<sup>+</sup>-induced apoptosis in PC12 cells by inhibiting ROS generation, modulating JNK activation, and improving mitochondrial function.<sup>29,30</sup> It could also reduce LPS-induced microglia-derived release of proinflammatory factors such as TNF- $\alpha$ , IL-1 $\beta$ , and NO.<sup>31</sup> The pharmacokinetic profile of **15** in rat plasma and tissues after oral administration showed that compound **15** was rapidly absorbed and widely distributed throughout the body, followed by quick elimination. The highest levels were detected in liver and lung whereas there was little in brain and testes, indicating **15** cannot readily penetrate the blood-brain and blood-testis barriers.<sup>32</sup>

As one major class of compounds widely existing in many plants, anthraquinones were found to inhibit insulin, amyloid and tau aggregations, which are linked directly to a number of neurodegenerative syndromes.<sup>33–35</sup>

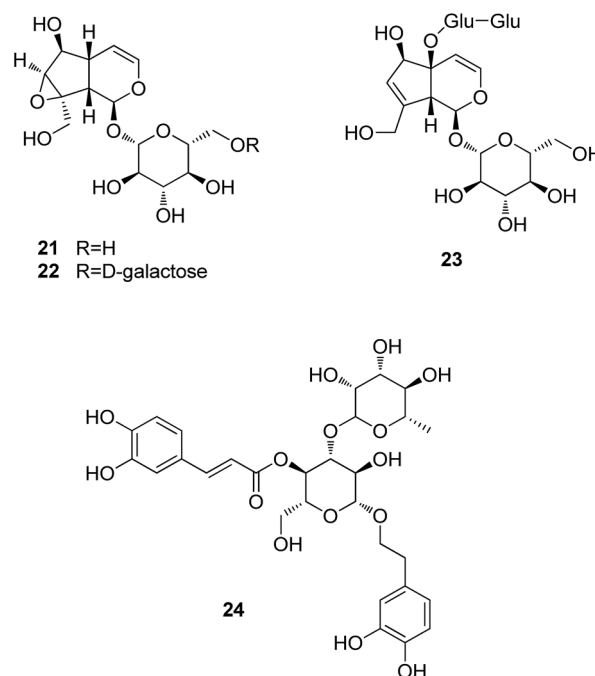


Glycosides are the most important constituents identified from *Rehmanniae Radix Praeparata* (Shudihuang), particularly iridoid glycosides. Catalpol (**21**), rehmannioside A (**22**), and rehmannioside D (**23**) are three major iridoid glycosides isolated from this plant. Verbascoside (**24**, also known as acteoside), the major phenolic glycoside, is used for the identification of the authentic material in the Chinese Pharmacopeia.

Pretreatment by catalpol (**21**) protected dopaminergic neurons against LPS-induced neurotoxicity,<sup>36</sup> and attenuated the A $\beta$ <sub>1–42</sub>-triggered neurotoxicity to neurons and inhibited glial activation.<sup>37</sup> Catalpol also showed neuroprotective effect against MPP<sup>+</sup>-induced oxidative stress in mesencephalic neurons.<sup>38</sup>

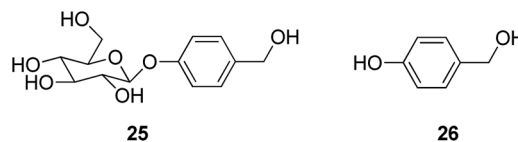
*p*-Hydroxybenzyl derivatives are the principle constituents identified from *Gastrodiae Rhizoma* (Tianma), represented by two major compounds, gastrodin (**25**) and gastrodigenin (*p*-hydroxybenzyl alcohol, **26**).

Dai *et al.* reported that gastrodin significantly attenuated levels of neurotoxic proinflammatory mediators and proinflammatory cytokines by inhibition of the NF- $\kappa$ B signaling pathway and phosphorylation of MAPKs in LPS-stimulated microglial cells.<sup>39</sup> Gastrodin also prevented glutamate-induced [Ca<sup>2+</sup>]<sub>i</sub> influx, blocked the activation of the calmodulin-



dependent kinase II (CaMKII) and the apoptosis signaling-regulating kinase-1 (ASK-1), and inhibited phosphorylation of p38 mitogen-activated kinase (MAPK).<sup>40</sup> Gastrodin showed neuroprotective effects in the subchronic MPTP mouse PD model by ameliorating bradykinesia and motor impairment in the pole and rotarod tests, respectively. Consistent with this finding, gastrodin prevented dopamine depletion and reduced reactive astrogliosis caused by MPTP in the substantia nigrae and striata of mice. Moreover, gastrodin was effective in preventing neuronal apoptosis by attenuating antioxidant and antiapoptotic activities in the brain.<sup>41</sup>

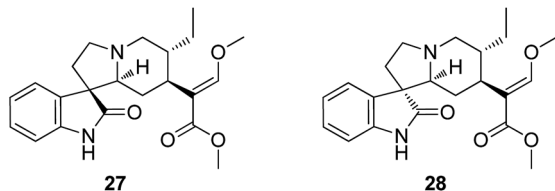
When gastrodin was administered *via* the femoral vein at a dose of 200 mg kg<sup>–1</sup>, its distribution in rat showed that levels of gastrodin declined rapidly after administration, and the entry of gastrodin into the brain was rapid. However, the ratios of AUC<sub>brain</sub>/AUC<sub>plasma</sub> were not high. The AUC in the cerebellum was significantly higher than that in other brain regions such as CSF, frontal cortex, hippocampus, and thalamus. The concentrations of *p*-hydroxybenzyl alcohol, the main metabolite of gastrodin, were very low both in the CSF and plasma.<sup>42</sup>



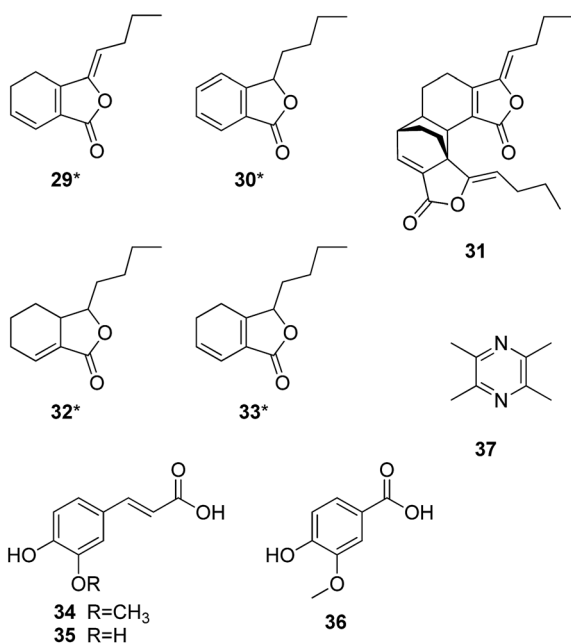
Indole alkaloids, which are believed to be responsible for its therapeutic effects, are the most important type of constituents identified from *Ramulus Uncariae Cum Uncis* (Gouteng). Rhynchophylline (**27**) and isorhynchophylline (**28**) are two alkaloids present abundantly in all the original plants of the herbal material.

Xian *et al.* reported that rhynchophylline and isorhynchophylline significantly decreased A $\beta$ <sub>25–35</sub>-induced cell

death, intracellular calcium overload, and tau protein hyperphosphorylation in PC12 cells.<sup>43</sup> These two compounds could also, concentration-dependently, attenuate LPS-induced production of pro-inflammatory cytokines such as TNF- $\alpha$  and IL-1 $\beta$  as well as NO in mouse N9 microglial cells through suppression of iNOS protein level, phosphorylation of ERK and p38 MAPKs, and degradation of I $\kappa$ B $\alpha$ .<sup>44,45</sup>

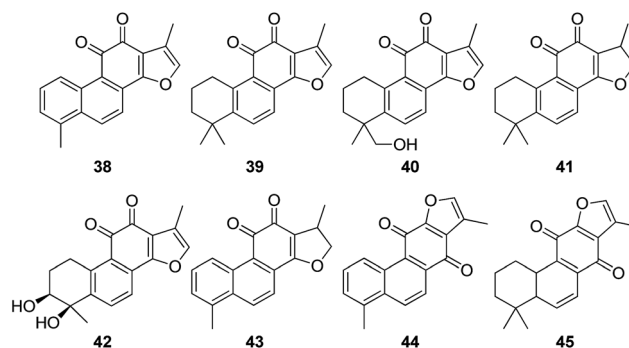


Chuanxiong Rhizoma (Chuanxiong) contains a high level of volatile oil, mainly lactone derivatives, including ligustilide (29 $\dagger$ ), butylphthalide (30), levistilide A (31), neocnidilide (32), and senkyunolide (33). The yield of ligustilide is more than 50%, but its structure is unstable. Levistilide A is therefore used in the Chinese Pharmacopeia as the chemical marker for the identification of the raw material. Phenolic acids are other major constituents responsible for its bioactivities. Ferulic acid (34), caffeic acid (35), and vanillic acid (36) are the major compounds of this type, and the level of ferulic acid in the raw material is used in the Chinese Pharmacopeia for its quality control. Ligustrazine (37) is the major alkaloid identified from the raw material.



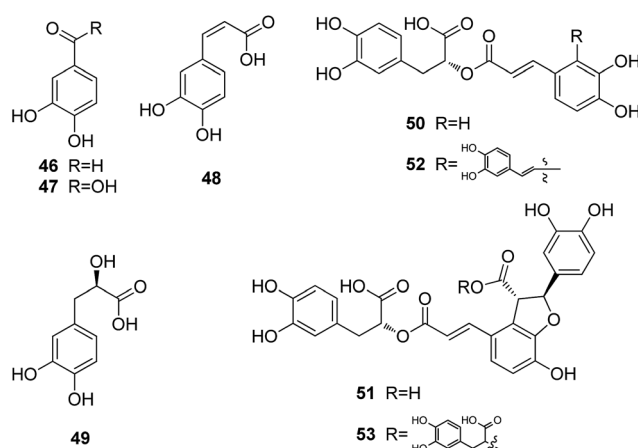
Ligustilide was reported to exert neuroprotective effects against ischemia/reperfusion (I/R) injury by promoting EPO transcription *via* an ERK signalling pathway and inhibition of RTP801 expression.<sup>46</sup> Ligustrazine and butylphthalide have been applied in practice in China to treat ischemic cerebrovascular

diseases like cerebral arterial thrombosis. Butylphthalide showed effects on improving cognitive impairment and reducing amyloid- $\beta$  proteins in a triple-transgenic AD mouse model.<sup>47</sup> The long-term treatment with butylphthalide might prevent age-related neurodegenerative changes by modulation of the cholinergic system, cause reduction of phosphorylated tau and maintain structure and morphology of neurons.<sup>48</sup> Phenolic acids are natural antioxidants with a wide range of therapeutic effects against various diseases including neurodegeneration. Ferulic acid was reported as a potent scavenger of ROS and reactive nitrogen species (RNS) and thereby reduced the chance of free radical attack on proteins and hence prevented their oxidative modification.<sup>49</sup>



Salviae Miltiorrhizae Radix et Rhizoma (Danshen) is one of the most famous Chinese traditional herbs with more than 1000 years of clinical application as a common hemorheologic agent to promote blood circulation, remove blood stasis, nourish the blood, and tranquilize the mind. Nowadays Danshen is mainly used for the treatment of cardiovascular and cerebrovascular diseases.<sup>50</sup> Pharmaceutical investigations revealed multiple bioactivities of Danshen and its constituents such as antioxidative stress, anti-platelet aggregation, anti-inflammation, anti-cancer, and *etc.*<sup>51,52</sup>

There are two groups of chemical constituents isolated from Danshen.<sup>53</sup> One is the fat-soluble diterpene quinones, such as tanshinone I (38), tanshinone IIA (39), tanshinone IIB (40), cryptotanshinone (41), tanshindiol C (42), dihydrotanshinone I (43), isotanshinone I (44), and isotanshinone II (45). The other group is the water-soluble phenolic acids, including protocatechuic aldehyde (46), protocatechuic acid (47), caffeic acid



$\dagger$  The structures with an asterisked number means their stereochemistry was unidentified or unclear in the publications.

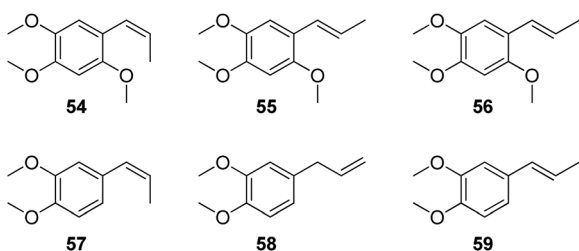
(48), danshensu (49), rosmarinic acid (50), lithospermic acid (51), salviandic acid A (52), and salviandic acid B (53).

Han *et al.* reported in a review that the water soluble fraction of *Salviae miltiorrhiza* root extract, as well as water-soluble compounds, protocatechuic aldehyde (46), danshensu (49) and salvianolic acid B (53) have an ability to scavenge peroxides and are able to inhibit the expression of adhesion molecules in vascular endothelium and leukocytes. Moreover, lipophilic compounds from *S. miltiorrhiza* root extract also prevent the development of vascular damage. NADPH oxidase and platelet aggregation are inhibited by tanshinone IIA (52) and tanshinone IIB (53), respectively, and mast cell degranulation is hindered by cryptotanshinone (41) and 15,16-dihydrotanshinone I. Thus, the water-soluble and lipophilic compounds appear to improve the I/R-induced vascular damage multifactorially and synergistically.<sup>54</sup>

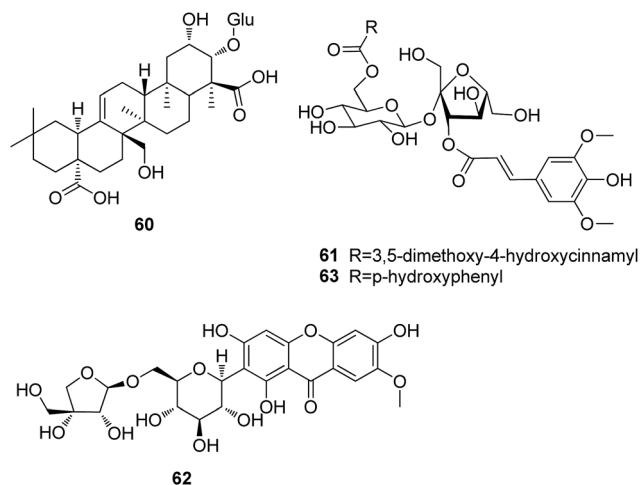
Depside salts from *S. miltiorrhiza* are an approved drug in China and its active components include magnesium lithospermate B and its analogues. A pharmacokinetic study of three major components, lithospermic acid B, rosmarinic acid, and lithospermic acid, showed that they are readily distributed to most tissues but cannot efficiently cross the blood–brain barrier. The elimination of the active components in blood is rapid and the major route of elimination of these compounds is excretion in the bile.<sup>2</sup> Another metabolism and pharmacokinetic studies of lithospermic acid B on rat showed that lithospermic acid B was rapidly and extensively metabolized to its methylated metabolites, and these metabolites were detected in rat bile, plasma and feces samples after intravenous administration of lithospermic acid B.<sup>55</sup>

Volatile oil is believed to be the active principles of *Acori Tatarinowii* Rhizoma (Shichangpu). The major constituents identified from the volatile oil were  $\beta$ -asarone (54),  $\alpha$ -asarone (55),  $\gamma$ -asarone (56), *cis*-methylisoeugenol (57), methyl eugenol (58), and *trans*-methylisoeugenol (59).<sup>56</sup>

$\beta$ -Asarone (54) and  $\alpha$ -asarone (55) were reported to be the chemical bases for its effects on sedation, convulsion, and depression. In asenescence-accelerated prone 8 (SAMP8) mice, which mimic many of the salient features of Alzheimer's disease,  $\beta$ -asarone prevented autophagy and synaptic loss by reducing ROCK expression, and improved cognitive function of the SAMP8 mice.<sup>57</sup> Mo *et al.* reported that  $\beta$ -asarone could protect PC12 cells against OGD/R-induced injury partly due to attenuating beclin-1-dependent autophagy caused by decreasing  $[Ca^{2+}]_i$  and increasing MMP.<sup>58</sup>  $\alpha$ -Asarone exhibited antioxidant property against noise-stress-induced changes in different brain regions of model rats.<sup>59</sup>



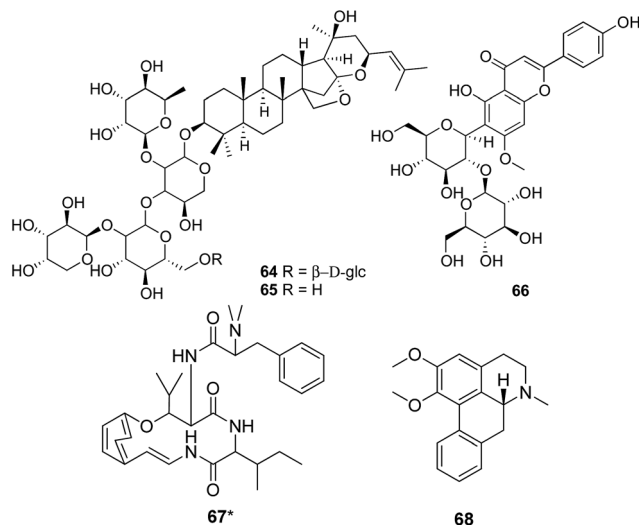
Polygalae Radix (Yuanzhi) is rich in triterpenoid saponins, oligosaccharide esters, and xanthenes. Taxifolin (60), 3,6'-disinapoyl sucrose (61), and polygalaxanthone III (62) are three compounds documented in the Chinese Pharmacopeia for identification and content determination of the original materials.



Chen *et al.* reported that oral administration of the crude saponins to rats could significantly improve learning and memory ability in the step-through test. The muscarinic receptor density and the activity of ChAT within rat brain were markedly enhanced, whereas the activity of AChE in rat brain was significantly inhibited.<sup>60</sup> Hu *et al.* reported that 3,6'-disinapoyl sucrose could have neuroprotective effects and anti-depressive activity in rats partially by increased expression of cyclic AMP response element (CRE)-binding protein (CREB) and its downstream target protein, brain-derived neurotrophic factor (BDNF). At concentrations above 30  $\mu$ M, 3,6'-disinapoyl sucrose could promote the neuron cell viability and protect the glutamate and  $H_2O_2$ -induced toxicity in the human neuroblastoma (SH-SY5Y) cell line.<sup>61,62</sup> Ikeya *et al.* pointed out that tenuifoliside B (63),<sup>63</sup> one of the acylated oligosaccharides in the roots of *P. tenuifolia*, showed cerebral protective effect on potassium cyanide (KCN)-induced anoxia in mice, and also had an ameliorative effect on the scopolamine-induced impairment of performance in passive avoidance task in rats.<sup>64</sup>

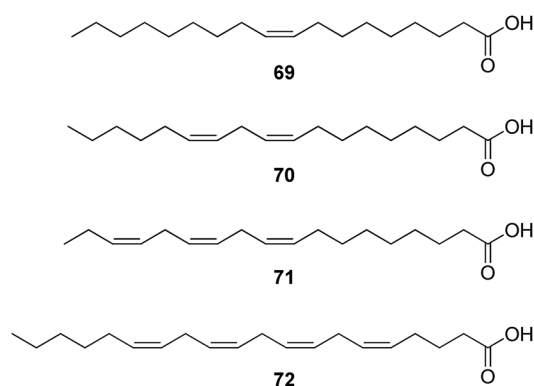
The chemical investigations of *Ziziphi Spinosae* Semen (Suanzaoren) revealed the presence of triterpenoid glycosides, flavonoid glycosides, alkaloids, and fatty oil. Jujubosides A (64) and B (65) are two major triterpenoids identified from the original plants and also documented in the Chinese Pharmacopeia as the chemical markers for the identification and content determination of the raw material. The flavonoid glycosides, spinosin (66) and its derivatives, are also used as chemical markers. The alkaloidal constituents include sanjoinine A (frangufoline, 67) and sanjoinine E (nuciferine, 68). More than 60% of the herbal material are fatty acids, of which 38.8% is oleic acid (69) and 37.1% is linoleic acid (70).<sup>65</sup>

Ziziphi Spinosa Semen has very unique effects on insomnia, which is directly associative with its sedative activity. The total triterpenoid glycoside,<sup>66</sup> the total flavonoid glycoside,<sup>67</sup> the total alkaloid,<sup>68</sup> and the fatty oil fraction,<sup>69</sup> all could significantly reduce spontaneous activity and increase sleeping time in mice. Jujuboside A was reported to have an inhibitory effect on the spontaneous activity in mice, and could regulate the transcription of Mark3 and Rpgrip1 in mouse hippocampus.<sup>70</sup>



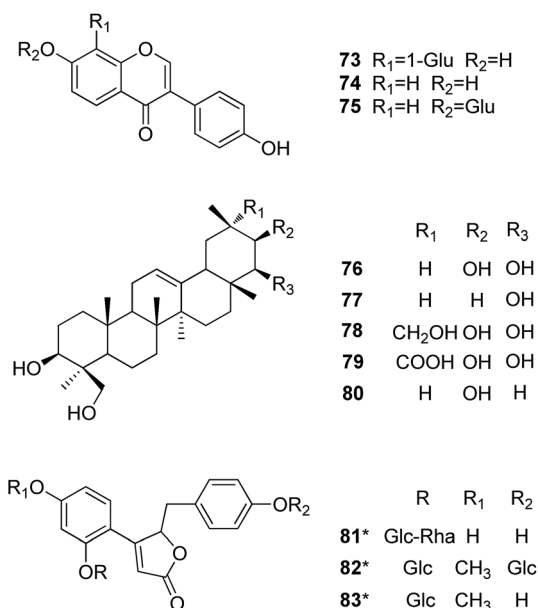
Platycladi Semen (Baiziren) was reported to contain about 60% of fatty oil with 62.39% being unsaturated fatty acids.<sup>71</sup> GC-MS analysis of the fatty oil further identified three major unsaturated fatty acids – linoleic acid (70), linolenic acid (71) and arachidonic acid (72).<sup>72</sup>

This herb was reported to ameliorate memory acquisition disorder induced by amygdala lesion in mice following oral administration.<sup>73</sup> Linoleic and linolenic acid are essential for normal cellular function, and act as precursors for the synthesis of longer chained polyunsaturated fatty acids such as arachidonic acid. Neurodegenerative disorders such as PD and AD appear to exhibit membrane loss of polyunsaturated fatty acids. Supplementary of these essential fatty acids may help to delay their onset or reduce the insult to brain functions which these diseases elicit.<sup>74</sup>



Puerariae Lobatae Radix (Gegen) is rich in isoflavones. Puerarin (73), daidzein (74), and daidzin (75) were identified in

high yields from this material. Triterpenoids, another major constituent, are characterized by an oleanane type nucleus such as soyasapogenols A and B (76–77), and kudzuapogenols A–C (78–80). Puerosides A–C (81–83) represent dihydrochalcones isolated from this material.<sup>75</sup>



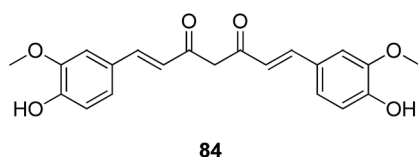
Puerarin (73) was reported to be a possible therapeutic agent in neurodegenerative diseases involving oxidative stress induced by ROS. Zhang *et al.* found that puerarin could inhibit oxidative-stress-induced apoptosis through down-regulation of Bax/Bcl-2 ratio.<sup>76</sup> It can also protect differentiated PC12 cells from H<sub>2</sub>O<sub>2</sub>-induced apoptosis through activation of the PI3K/Akt signalling pathway.<sup>77</sup> Wang *et al.* reported that puerarin protected PC12 cells against MPP<sup>+</sup>-induced neurotoxicity through the inhibition of the INK signalling pathways.<sup>78</sup> In addition, pretreatment of primary hippocampal neurons with puerarin significantly reduced Aβ<sub>25–35</sub>-induced oxidative stress characterized by scavenging of ROS and inhibiting lipid peroxidation.<sup>79</sup> Daidzein (74) was also reported to protect dopaminergic neurons against LPS-induced injury through inhibition of microglia activation and proinflammatory factors generation,<sup>80</sup> and exhibit neurocytoprotective effects against 6-hydroxydopamine (6-OHDA)-induced cytotoxicity in nerve growth factor (NGF)-differentiated PC12 cells.<sup>81</sup>

Prasain *et al.* reported that puerarin was hydrolyzed to daidzein by bacterial enzymes in the large intestine and subsequently reduced to dihydrodaidzein and equol. The persistence of puerarin in blood and urine as the principal metabolic form during the period of 4–72 h after oral administration suggested that puerarin was rapidly absorbed from the intestine without metabolism. Its presence in organs such as the brain suggested that puerarin might enter tissues by specific transport pathways.<sup>82</sup>

The investigations of the *Amomum* genus such as *A. kravanh* and *A. compactum* (Doukou) revealed the presence of diarylheptanoids, flavonoids, chalcones, and terpenoids.<sup>83</sup>

Curcumin (**84**) and its analogues diarylheptanoids are present in the family of Zingiberaceae in high yield. Ahmed and Gilani summarized the literature and found that the curcuminoid mixture, as well as the individual compounds including curcumin, bisdemethoxycurcumin, and demethoxycurcumin, shows an array of activities that can be helpful in ameliorating AD symptoms by acting on various target sites. These compounds were reported to be able to prevent the spread of plaque found in the brains of Alzheimer's patients, and are regarded as a potential treatment for Alzheimer's disease.<sup>84</sup>

The uptake and metabolism of curcumin has been reviewed.<sup>85</sup> The known *in vivo* metabolism of curcumin and other curcuminoids comprises stepwise reduction of the olefinic heptanoid chain and conjugation of the parent compound and the reductive metabolites with glucuronic acid and sulfate.<sup>85</sup>



### 3 Physicochemical properties

Lipinski's rule of five, also known as the rule of five (Ro5), is a rule of thumb to evaluate drug-likeness and predict if a chemical compound has physico-chemical properties that would make it orally bioavailable in humans.<sup>86,87</sup> Lipinski's rule states that, in general, an orally active drug has no more than one violation of the following criteria: a molecular weight (MW) less than 500 Daltons, no more than 5 hydrogen bond donors (HBDs), no more than 10 hydrogen bond acceptors (HBAs), and an octanol–water partition coefficient  $\log P$  not greater than 5. Although the rule cannot guarantee a molecule compliant with all criteria is druggable, it provides a guide for medicinal chemists for better design of compounds with satisfactory pharmacokinetics. So far, the criteria have spawned many extensions. In particular, compounds that meet the two criteria of 10 or fewer rotatable bonds (ROTB) and polar surface area (PSA) equal to or less than  $140 \text{ \AA}^2$  are predicted to have good oral bioavailability.<sup>88</sup>

Neurodegenerative diseases such as PD, AD, HD, and others share common features at cellular and subcellular levels as well as sharing common molecular signaling pathways that may lead to apoptosis, necroptosis, and inflammation.<sup>89</sup> Compounds with neuroprotective properties must possess certain physico-chemical properties to allow brain penetration and exposure.

Herein, we analyze the four Lipinski properties MW, HBD, HBA, and  $\log P$  along with ROTB and PSA of the above 84 TCM compounds, and those of current anti-PD and anti-AD drugs and candidates in clinical trials. We then compare these three sets to evaluate the likelihood of the TCM components being useful CNS active drugs.

#### 3.1 Physicochemical properties of anti-PD drugs, anti-AD drugs and TCM compounds

Searching Parkinson's disease and Parkinson's disease dementia in Thomson Reuters Cortellis identified a total of 38 small molecules. Similarly, searching Alzheimer's disease in Thomson Reuters Cortellis resulted in a total of 65 small molecules. Memantine and GM-600 are two drugs in Phase II clinical trial now with indications for both Parkinson's and Alzheimer's diseases.

The structures of the 38 anti-PD drugs, the 65 anti-AD drugs and the 84 TCM compounds were converted into SMILES format and imported into Instant JChem to calculate the physicochemical parameters of each molecule.<sup>90</sup> The calculated data for anti-PD and anti-AD drugs and candidates in clinical trials are shown in Tables 2 and 3, respectively, and those for 84 TCM compounds in Table 4. The percentages of anti-PD drugs, anti-AD drugs and TCM compounds compliant with Lipinski's rule of five are depicted in Fig. 1. The histograms for molecular weight, calculated  $\log P$ , and hydrogen bond acceptors and donors for three sets of compounds are shown in Fig. 2.

It was found that 92% of anti-PD drugs and 92% of anti-AD drugs had less than two violations of the Lipinski's parameters, with 82% and 77% having no violations, respectively. These values were decreased in the TCM data set, which had 71% and 57% in these categories, respectively.

The histogram of molecular weight (Fig. 2a) showed that about 84% of the anti-PD drugs, 88% of the anti-AD drugs and 69% of the TCM compounds were distributed between molecular weights of 100–500 Da, with the anti-PD drugs and TCM compounds peaking at 200–300 Da while the anti-AD drugs peaked at 300–400 Da. About 13% of the anti-PD drugs and 12% of the anti-AD drugs had molecular weights over 500 Da while 31% for the TCM compounds had molecular weights over 500.

The calculated  $\log P$  (Fig. 2b) of the majority of all sets (90% for anti-PD, 86% for anti-AD and 92% for TCM) fell into the same region from  $-2$  to  $6$  but the distribution maximum was at  $2$ – $3$  for the anti-PD and anti-AD drugs while at  $3$ – $4$  for the TCM compounds. The overall percentage of compounds satisfying the  $\log P$  criteria was enhanced for the TCM compounds (95%) as compared to the anti-PD (92%) and anti-AD (86%) drugs.

The histogram of hydrogen bond acceptors (HBA) (Fig. 2c) for the anti-PD and anti-AD drugs showed a narrower distribution compared with that of the TCM compounds. About 95% of the anti-PD drugs and 91% of the anti-AD drugs concentrated in a range of  $1$ – $7$  while only 60% of the TCM compounds fall into the same range. The HBA values of the TCM compounds fluctuated from  $1$  to more than  $16$ . The percentage of the TCM compounds with acceptable HBA (no more than  $10$ ) was 73% as compared to 95% for both anti-PD and anti-AD drugs.

The HBD histogram distribution showed a maximum at zero donors for the TCM compounds, in contrast to  $1$  for the anti-PD and anti-AD drugs. About 95% of the anti-PD and anti-AD drugs had no more than 5 hydrogen bond donors while the number of the TCM compounds compliant with Ro5 was 65%.

Table 2 Physicochemical property of 38 anti-PD drugs launched and in clinical trials<sup>a</sup>

Name	MW	log <i>P</i>	HBA	HBD	ROTB	PSA	Ro5	No. violations
Levodopa	197.19	−1.79	5	4	3	103.78	Pass	0
Melevodopa	211.21	0.62	4	3	4	92.78	Pass	0
Pergolide	314.49	4.23	1	1	4	19.03	Pass	0
Apomorphine	267.32	2.87	3	2	0	43.70	Pass	0
Bromocriptine	654.60	3.89	6	3	5	118.21	Pass	1
Ropinirole	260.37	3.06	2	1	7	32.34	Pass	0
Cabergoline	451.60	2.58	4	2	8	71.68	Pass	0
Aplindore	310.35	2.01	4	2	4	59.59	Pass	0
Pramipexole	211.33	1.76	3	2	3	50.94	Pass	0
Entacapone	305.29	1.63	6	2	5	127.70	Pass	0
Tolcapone	273.24	3.28	5	2	3	100.67	Pass	0
Opicapone	385.12	2.33	7	2	3	149.46	Pass	0
Rasagiline	171.24	2.30	1	1	2	12.03	Pass	0
Selegiline	223.74	2.85	1	0	4	3.24	Pass	0
Budipine	293.45	4.95	1	0	3	3.24	Pass	0
Carbidopa	226.23	−1.21	6	5	4	115.81	Pass	0
Altropane	429.27	3.95	2	0	5	29.54	Pass	0
123I-ioflupane	431.28	3.70	2	0	6	29.54	Pass	0
Aemantine	179.3	2.07	1	1	0	26.02	Pass	0
Amantadine	151.25	1.47	1	1	0	26.02	Pass	0
GM1 ganglioside	1602.93	3.76	31	20	56	540.58	Fail	3
Pardoprunox	233.27	1.29	4	1	1	44.81	Pass	0
Rotigotine	315.47	4.34	2	1	6	23.47	Pass	0
Istradefylline	384.43	2.42	5	0	6	76.90	Pass	0
Tozadenant	406.50	1.48	6	2	3	87.16	Pass	0
V-81444	321.34	2.22	6	2	3	121.67	Pass	0
123I-MNI-420	573.36	4.07	7	1	5	106.54	Pass	1
AAD-2004	325.28	2.56	4	3	6	69.56	Pass	0
IRX-4204	366.54	6.61	2	1	4	37.30	Pass	1
GM-600	798.89	−7.00	16	15	24	373.08	Fail	3
Talipexole	209.31	1.65	3	1	2	42.15	Pass	0
Baicalein	272.25	2.84	5	3	1	86.99	Pass	0
Mitoquinone	678.81	8.71	4	0	16	52.60	Fail	2
Nicotine	162.23	1.16	2	0	1	16.13	Pass	0
Monosodium alpha luminol	200.15	−0.06	3	3	0	84.22	Pass	0
Vatiquinone	440.66	7.81	3	1	12	54.37	Pass	1
Fampridine	94.11	−0.07	2	1	0	38.91	Pass	0
Zonisamide	212.23	0.11	3	1	2	86.19	Pass	0

<sup>a</sup> The physicochemical data of memantine and GM-600 are given in Table 2 and not duplicated in Table 3.

The histograms of the four Lipinski's parameters showed more similarities among these three datasets on the properties of MW and the calculated log *P* than the hydrogen bond acceptors and donors. This is probably due to the natural products having more O-containing functionalities and hydroxyl groups. The percentages of the TCM compounds were lower than those of the anti-PD and anti-AD drugs in all Ro5 parameters except for the calculated log *P*. The results for the TCM compounds are quite similar to the two previous analyses of natural products.<sup>91,92</sup>

Considering the structural aspects some conclusions are presented. For anti-PD drugs, GM1 ganglioside (85), GM-600 (86) and mitoquinone (87) have two or three violations of Lipinski's rules. GM1 ganglioside is now an approved drug while the other two are drug candidates in Phase II clinical trial. GM-600 is a peptide used in intravenous formulation. Mitoquinone, a mitochondria-targeted antioxidant, is used with mitoquinol as a redox mixture in the treatment of Parkinson's disease, liver

disease, *etc.* The anti-AD drugs, bryostatin-1 (88), davunetide (89) and SEMAX (90) violated three of the Lipinski's parameters, and TTP-488 (91) and rilapladib (92) had two violations. Bryostatin-1 is a natural product in Phase II clinical trial used in intravenous formulation. Davunetide and SEMAX are two peptides used as biological therapeutics. They are not drugs in oral formulation but in nasal or buccal systemic formulation.

With respect to the TCM set, 24 of 84 compounds had two or more violations of the Lipinski's parameters. The structural survey of these compounds further revealed that 22 of them contained at least one sugar moiety in the molecule, *e.g.* ginsenosides (1–9), rehmannioside A (22), rehmannioside D (23), and jujubosides A (64) and B (65). The existence of sugar moiety provides more O-containing functionalities and hydroxyl groups, which might account for the violations of HBA and HBD values, as well as molecular weights, rotatable bonds and polar surface area.

Table 3 Physicochemical property of 65 anti-AD drugs launched and in clinical trials

Name	MW	log <i>P</i>	HBA	HBD	ROTB	PSA	Ro5	No. violations
Huperzine A	242.32	0.62	2	2	0	55.12	Pass	0
Bryostatin-1	905.03	5.04	12	4	13	240.11	Fail	3
Galantamine	287.35	1.16	4	1	1	41.93	Pass	0
Rivastigmine	250.34	2.41	2	0	5	32.78	Pass	0
Posiphen	337.42	4.25	4	1	3	44.81	Pass	0
Pioglitazone	356.44	3.33	4	1	7	68.29	Pass	0
PRX-3140	384.51	1.23	4	2	7	69.64	Pass	0
ABT-126	313.42	2.71	4	0	3	38.25	Pass	0
TTP-488	532.12	8.22	3	0	14	39.52	Fail	2
Idalopirdine	394.41	5.17	2	2	9	37.05	Pass	1
Roflumilast	403.21	4.45	4	1	7	60.45	Pass	0
Encenicline	320.84	3.04	2	1	2	32.34	Pass	0
Ladostigil	272.34	2.38	2	1	5	41.57	Pass	0
ARC-100	869.99	4.65	10	3	17	211.68	Pass	1
Laquinimod	356.80	2.55	3	1	3	60.85	Pass	0
Risperidone	410.48	2.63	4	0	4	61.94	Pass	0
MK-8931	338.43	2.53	4	2	3	69.08	Pass	0
Circadin	232.28	1.15	2	2	4	54.12	Pass	0
IRX-4204	366.54	6.61	2	1	4	37.30	Pass	1
NSI-189	366.50	3.95	4	1	7	48.47	Pass	0
Donepezil	379.49	4.21	4	0	6	38.77	Pass	0
DSP-8658	417.50	5.86	4	1	9	68.53	Pass	1
AZD-3293	361.46	3.67	4	1	4	60.50	Pass	0
T-817MA	291.41	2.29	3	1	7	32.70	Pass	0
Shionogi	347.41	2.97	4	1	4	67.92	Pass	0
Zibotentan	424.43	1.01	8	1	5	132.99	Pass	0
Idebenone	338.44	3.57	5	1	12	72.83	Pass	0
ANAVEX-2-73	281.39	3.50	2	0	4	12.47	Pass	0
Velusetrag	504.64	−0.10	6	2	7	110.26	Pass	1
Masitinib	498.64	4.97	6	2	7	73.39	Pass	0
S-38093	449.59	2.88	6	1	9	65.37	Pass	0
Saracatinib	542.03	3.20	10	1	8	90.44	Pass	1
T3D-959	419.47	4.53	5	1	9	81.79	Pass	0
ELND-005	180.16	−3.78	6	6	0	121.38	Pass	1
Apabetalone	370.40	2.49	6	2	6	89.38	Pass	0
CHF-5074	325.16	5.24	2	1	3	37.30	Pass	1
SUVN-502	448.38	3.56	4	0	3	45.55	Pass	0
Pinocembrin	256.25	3.14	4	2	1	66.76	Pass	0
GLN-1062	391.46	3.66	4	0	4	48.00	Pass	0
TAK-070	385.54	6.64	2	0	7	12.47	Pass	1
Pozanicline	192.26	0.83	3	1	3	34.15	Pass	0
Davunetide	824.92	−7.48	13	10	22	355.85	Fail	3
MSDC-0160	370.42	3.15	5	1	7	85.36	Pass	0
Nimodipine	418.44	2.54	6	1	10	117.00	Pass	0
Clioquinol	305.50	3.36	2	1	0	33.12	Pass	0
Acetyl-L-carnitine	203.24	−4.45	3	0	6	66.43	Pass	0
Octahydroaminoacridine	202.30	2.58	2	1	0	38.91	Pass	0
AAD-2004	325.28	2.56	4	3	6	69.56	Pass	0
Moclobemide	268.74	1.45	3	1	4	41.57	Pass	0
ST-101	236.27	1.84	3	0	0	32.67	Pass	0
PU-H71	494.33	2.67	7	2	7	100.11	Pass	0
Nilvadipine	385.37	2.24	6	1	7	131.56	Pass	0
Bisnorcymserine	379.50	5.50	4	1	4	44.81	Pass	1
GTS-21	308.37	2.96	4	0	4	43.71	Pass	0
Cutamesine dihydrochloride	368.51	4.19	4	0	9	24.94	Pass	0
Piromelatine	312.32	1.59	4	2	5	80.42	Pass	0
HF-0220	306.44	2.46	3	2	0	57.53	Pass	0
(−)Clausenamide	297.35	1.47	3	2	3	60.77	Pass	0
Oxiracetam	158.16	−2.60	3	2	2	83.63	Pass	0
Tacrine	202.30	2.58	2	1	0	38.91	Pass	0
SEMAX	813.92	−6.65	12	8	21	286.32	Fail	3
Resveratrol	228.24	3.40	3	3	2	60.69	Pass	0
Rilapladib	735.81	8.08	5	0	13	53.09	Fail	2
Lovastatin	404.54	3.90	3	1	7	72.83	Pass	0
Minaprine	298.38	2.19	5	1	5	50.28	Pass	0

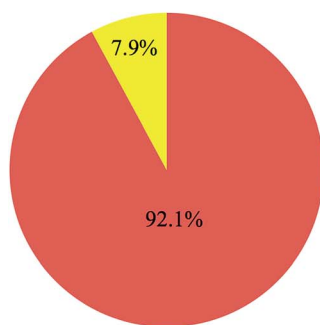
**Table 4** Physicochemical property of 84 TCM compounds from 15 selected plants. The right three columns indicate if this compound falls into the red rectangle area shown in Fig. 3c–e

No	MW	log <i>P</i>	HBA	HBD	ROTB	PSA	Ro5	No. violations	In Fig. 3c	In Fig. 3d	In Fig. 3e
1	1109.29	−1.55	23	15	16	377.29	Fail	3			
2	1079.27	−0.92	22	14	15	357.06	Fail	3			
3	1079.27	−0.92	22	14	16	357.06	Fail	3			
4	947.15	0.22	18	12	13	298.14	Fail	3			
5	947.15	−0.04	18	12	12	298.14	Fail	3			
6	801.01	0.68	14	10	10	239.22	Fail	3			
7	801.01	0.68	14	10	10	239.22	Fail	3			
8	622.87	3.76	8	6	7	139.84	Fail	2			
9	785.01	1.73	13	9	9	218.99	Fail	3			
10	396.43	−0.22	8	6	11	139.84	Pass	1	✓	✓	✓
11	480.46	−0.39	10	5	7	164.37	Pass	0	✓	✓	✓
12	480.46	−1.12	9	5	7	172.21	Pass	0	✓	✓	✓
13	496.46	−0.69	11	6	7	184.60	Fail	2	✓	✓	✓
14	584.57	2.11	10	4	10	170.44	Pass	1		✓	
15	406.38	0.83	9	7	5	160.07	Pass	1	✓	✓	✓
16	270.24	3.82	5	3	0	94.83	Pass	0	✓	✓	✓
17	284.26	3.97	5	2	1	83.83	Pass	0	✓	✓	✓
18	254.24	4.12	4	2	0	74.60	Pass	0	✓	✓	✓
19	284.22	3.27	6	3	1	111.90	Pass	0	✓	✓	✓
20	270.24	2.84	5	3	1	94.83	Pass	0	✓	✓	✓
21	362.33	−3.43	10	6	4	158.30	Pass	1	✓		
22	524.47	−5.20	15	9	7	237.45	Fail	3			
23	686.61	−7.39	20	13	10	327.60	Fail	3			
24	624.59	0.82	14	9	11	245.29	Fail	3			
25	286.28	−1.37	7	5	4	119.61	Pass	0	✓	✓	✓
26	124.14	0.90	2	2	1	40.46	Pass	0	✓	✓	✓
27	384.47	2.61	4	1	5	67.87	Pass	0	✓	✓	✓
28	384.47	2.61	4	1	5	67.87	Pass	0	✓	✓	✓
29	190.24	2.73	1	0	2	26.30	Pass	0	✓	✓	✓
30	190.24	3.36	1	0	3	26.30	Pass	0	✓	✓	✓
31	380.48	4.69	2	0	4	52.60	Pass	0	✓	✓	✓
32	194.27	3.39	1	0	3	26.30	Pass	0	✓	✓	✓
33	192.25	3.07	1	0	3	26.30	Pass	0	✓	✓	✓
34	194.18	1.67	4	2	3	66.76	Pass	0	✓	✓	✓
35	180.16	1.53	4	3	2	77.76	Pass	0	✓	✓	✓
36	168.15	1.17	4	2	2	66.76	Pass	0	✓	✓	✓
37	136.19	0.06	2	0	0	25.78	Pass	0	✓	✓	✓
38	276.29	4.00	2	0	0	47.28	Pass	0	✓	✓	✓
39	294.34	4.53	2	0	0	47.28	Pass	0	✓	✓	✓
40	310.34	3.25	3	1	1	67.51	Pass	0	✓	✓	✓
41	296.36	3.89	3	0	0	43.37	Pass	0	✓	✓	✓
42	312.32	1.92	4	2	0	87.74	Pass	0	✓	✓	✓
43	278.30	3.36	3	0	0	43.37	Pass	0	✓	✓	✓
44	276.29	4.00	2	0	0	47.28	Pass	0	✓	✓	✓
45	296.36	3.51	2	0	0	47.28	Pass	0	✓	✓	✓
46	138.12	1.08	3	2	1	57.53	Pass	0	✓	✓	✓
47	154.12	1.02	4	3	1	77.76	Pass	0	✓	✓	✓
48	180.16	1.53	4	3	2	77.76	Pass	0	✓	✓	✓
49	198.17	0.58	5	4	3	97.99	Pass	0	✓	✓	✓
50	360.31	3.00	7	5	7	144.52	Pass	0	✓	✓	✓
51	538.46	3.75	11	7	9	211.28	Fail	3		✓	
52	494.45	4.74	9	7	9	184.98	Pass	1		✓	
53	718.61	4.99	14	9	14	278.04	Fail	3		✓	
54	208.25	2.62	3	0	4	27.69	Pass	0	✓	✓	✓
55	208.25	2.62	3	0	4	27.69	Pass	0	✓	✓	✓
56	208.25	2.62	3	0	4	27.69	Pass	0	✓	✓	✓
57	178.23	2.78	2	0	3	18.46	Pass	0	✓	✓	✓
58	178.23	2.76	2	0	4	18.46	Pass	0	✓	✓	✓
59	178.23	2.78	2	0	3	18.46	Pass	0	✓	✓	✓
60	680.82	1.66	12	8	6	214.44	Fail	3			
61	754.69	0.30	17	8	17	279.05	Fail	3		✓	
62	568.48	−1.49	14	9	6	245.29	Fail	3			

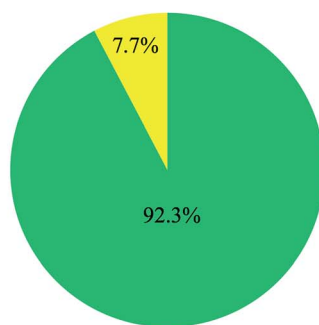
Table 4 (Contd.)

No	MW	log <i>P</i>	HBA	HBD	ROTB	PSA	Ro5	No. violations	In Fig. 3c	In Fig. 3d	In Fig. 3e
63	668.60	0.08	15	8	14	260.59	Fail	3		√	
64	1045.21	0.15	21	11	10	314.83	Fail	3			
65	1207.35	−1.63	26	14	13	393.98	Fail	3			
66	608.54	−1.68	15	9	7	245.29	Fail	3			
67	534.69	4.29	5	3	8	99.77	Pass	1	√	√	√
68	295.38	3.39	3	0	2	21.70	Pass	0	√	√	√
69	282.46	6.78	2	1	15	37.30	Pass	1	√	√	√
70	280.45	6.42	2	1	14	37.30	Pass	1	√	√	√
71	278.43	6.06	2	1	13	37.30	Pass	1	√	√	√
72	304.47	6.59	2	1	14	37.30	Pass	1	√	√	√
73	416.38	−0.03	9	6	3	156.91	Pass	1	√	√	√
74	254.24	2.73	4	2	1	66.76	Pass	0	√	√	√
75	416.38	0.46	9	5	4	145.91	Pass	0	√	√	√
76	460.69	3.59	4	4	1	80.92	Pass	0		√	√
77	444.69	4.59	3	3	1	60.69	Pass	0	√	√	√
78	490.72	2.69	5	5	2	101.15	Pass	0		√	√
79	504.70	3.16	6	5	2	118.22	Pass	1		√	√
80	444.69	4.51	3	3	1	60.69	Pass	0	√	√	√
81	636.60	−1.18	14	8	10	234.29	Fail	3		√	
82	474.46	1.09	9	5	7	155.14	Pass	0	√	√	√
83	606.57	0.22	13	8	8	225.06	Fail	3		√	
84	368.38	4.12	6	2	8	93.06	Pass	0	√	√	√

Anti-PD drugs/candidates



Anti-AD drugs/candidates



TCM compounds

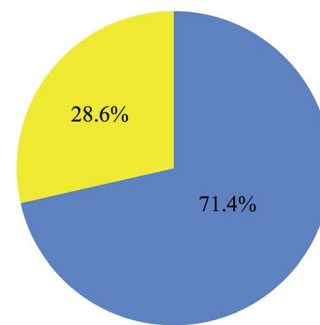


Fig. 1 Pie chart presentation of the percentage of anti-PD drugs (left), anti-AD drugs (middle) and TCM compounds (right) following or violating Lipinski's rule of five. Non-compliant (more than one violation) is shown in yellow and compliant (less than two violations) in red, olive and blue, respectively.

These analyses revealed one fact that nearly all launched drugs or candidates are compliant with the Ro5 or only have one violation. A majority of the TCM set follows this rule although the percentage is lower than for the drug sets. Those failing in the Ro5 are mostly compounds with one or more sugar moieties.

### 3.2 Comparison of physicochemical space of anti-PD drugs, anti-AD drugs and TCM compounds

In contrast to Lipinski's parameters focusing on a restricted set of drug-like properties generated directly from the molecular structures, ChemGPS-NP<sup>93</sup> is a tool tuned for identifying

volumes of chemical space to allow correlation to biological activities. ChemGPS-NP has been designed to handle the chemical diversity of natural products. It can discover physicochemical properties not directly discernible from structural data, and can chart biologically relevant chemical space and provide an efficient mapping device for prediction of properties and activities of groups of compounds. Therefore, ChemGPS-NP was used for principle component analysis (PCA) of anti-PD drugs, anti-AD drugs and TCM compounds to compare their distribution in physicochemical space. The first three principle components that explained 71% of the variance are plotted in Fig. 3a and b. Size, shape and polarizability were described in

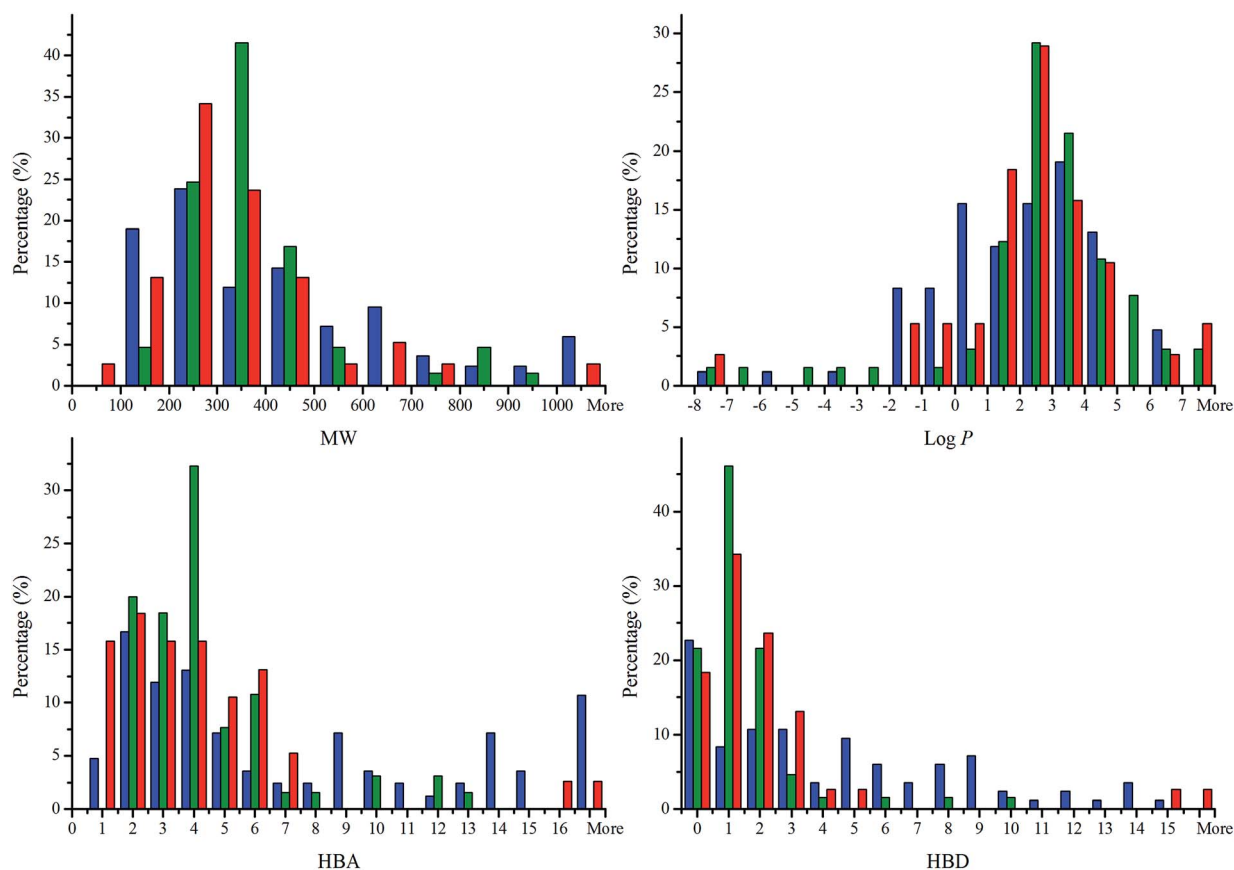


Fig. 2 Physicochemical property histograms of TCM compounds (blue), anti-AD drugs (olive) and anti-PD drugs (red): (a) molecular weight (MW), (b) calculated log *P*, (c) hydrogen bond acceptors (HBA), (d) hydrogen bond donors (HBD).

PC1, aromaticity- and conjugation-related properties of the compounds were explained in PC2, and lipophilicity, polarity and H-bond capacity were expressed in PC3.

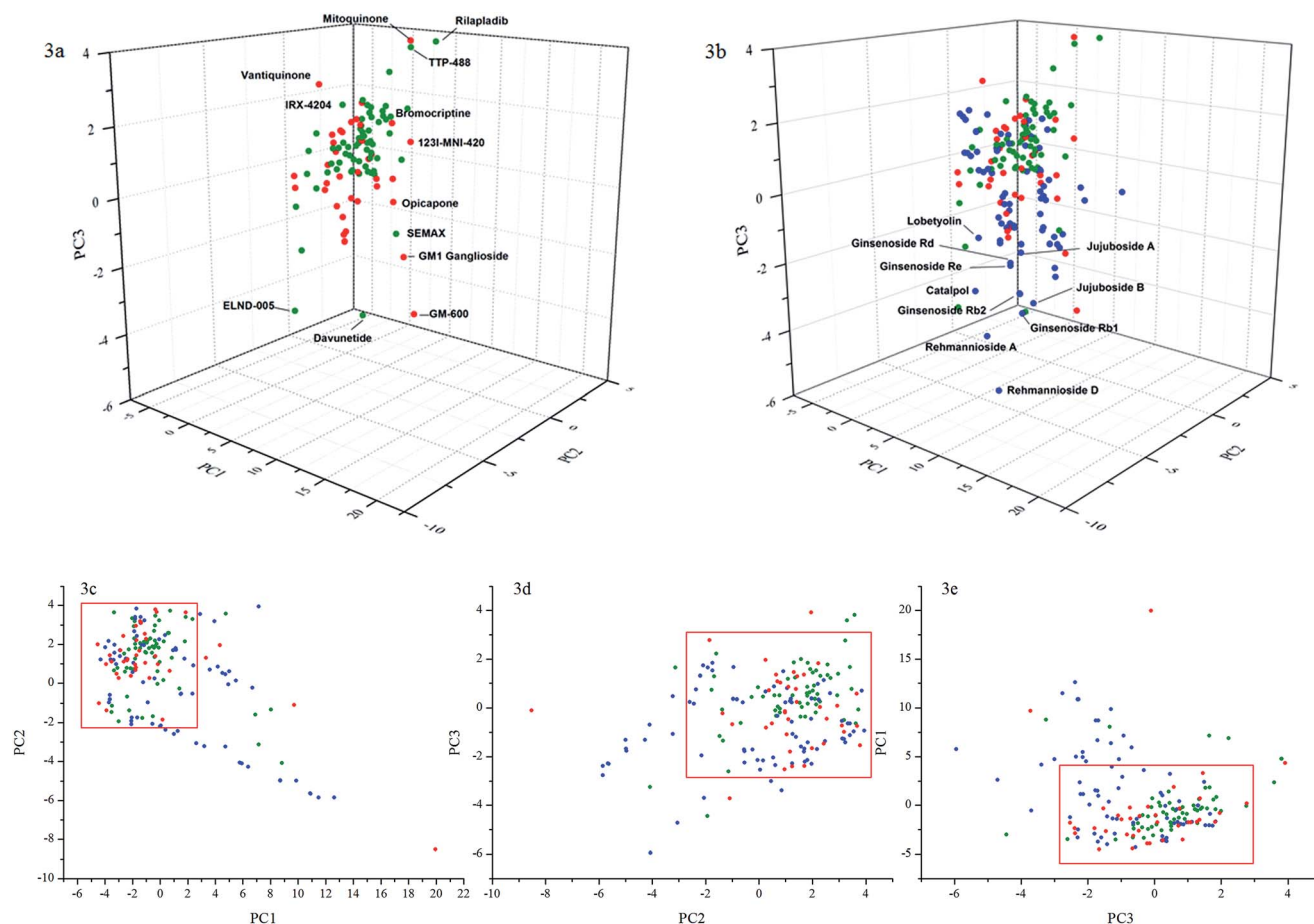
Fig. 3a demonstrates the score plot of 38 anti-PD drugs and 65 anti-AD drugs. The graph shows that the majority of these molecules concentrated in a relatively narrow area of physicochemical space, which means that these compounds shared similarities in the described parameters. GM1 ganglioside, GM-600, mitouquinone, devunetide, SEMAX, TTP-488 and rilapladib, violating more than two Lipinski's parameters, were found to be a relatively far distance from the core of the area. Bryostat-1 was also at such a distance but cannot be discerned from this perspective. Other compounds with one violation of the Lipinski's rules such as vatiquinone, bromocriptine, 123I-MNI-420, opicapone, and IRX-4204 were also observed in the skirt area of the space.

Fig. 3b displayed the score plot comparison of physicochemical spaces of the current drugs and the TCM compounds. The majority of the TCM compounds fall into the drug-like physicochemical space defined by anti-PD and anti-AD drugs. The cluster of the spots, which were found below the core space, represented ginsenosides Rb1, Rb2, Rd, and Re, jujubosides A and B, rehmanniosides A and D, catalpol, and *etc.* All these compounds, containing at least one sugar moiety, possesses

higher molecular weights than 500, and the HBA and HBD values exceed the Lipinski's rule of five while having a log *P* value within the range. They were quite close to GM1 ganglioside and peptides like GM-600, davunetide and SEMAX in physicochemical space.

It is noticeable that more than 30 compounds containing sugar moieties were identified as the major bioactive constituents from the 15 selected traditional herbal medicines. A large number of saponins including ginsenosides are biologically active and have favourable ADME/T properties (absorption, distribution, metabolism, excretion, and toxicology), despite the fact that they do not satisfy the proposed "drug-likeness" criteria like the Ro5. The launched anti-PD drug GM1 ganglioside is an example.

In summary, the majority of the current anti-PD and anti-AD drugs and candidates are compliant with the Lipinski's rules and concentrated in a narrow area of physicochemical space. The 2D plots identify a narrow area of physicochemical space for the anti-PD and anti-AD group (enclosed within the rectangles) that also contains many TCM derived compounds. The cluster of compounds containing sugar moieties is the exceptions and may constitute a special class. Details of the TCM spots in the red rectangles of three 2D plots are indicated also in Table 4.



**Fig. 3** 3D plots of anti-PD drugs, anti-AD drugs and TCM compounds. (a) Physicochemical space of 38 anti-PD drugs (red dots) and 65 anti-AD drugs (olive dots) launched and in clinical trial. (b) Comparison of the physicochemical space of 84 TCM compounds (blue dots) with physicochemical space of anti-PD (red dots) and anti-AD drugs (olive dots). (c–e) 2D plots of overlapped anti-PD drugs (red dots), anti-AD drugs (olive dots) and TCM compounds (blue dots). The red rectangle is defined as an area covering the majority of the overlapped plots with PC1 from –6 to 2.5, PC2 from –2 to 4 and PC3 from –2.5 to 3.

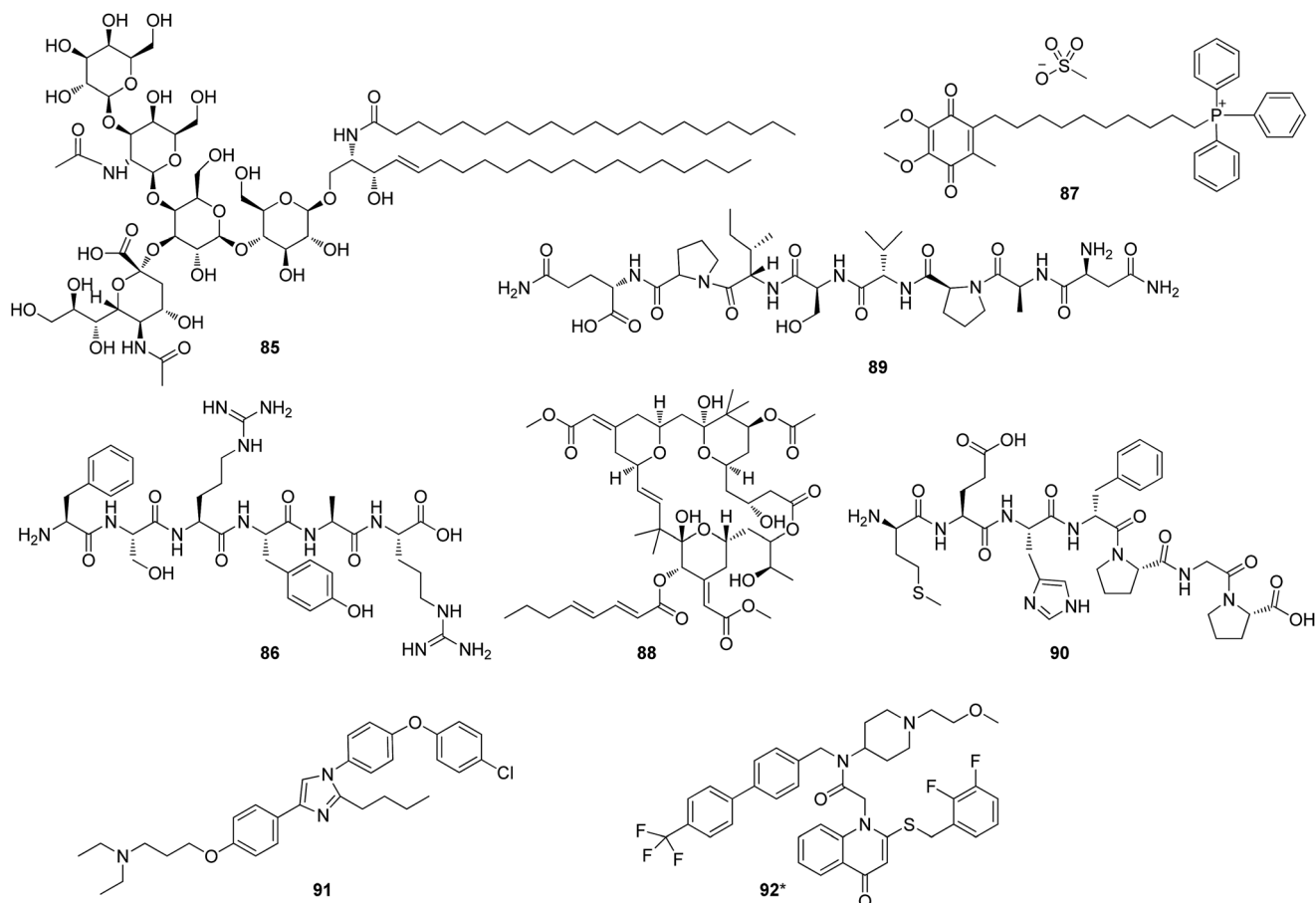
### 3.3 Prediction of blood–brain barrier permeation of TCM compounds

The ability to permeate across the blood brain barrier (BBB) is essential for drugs acting on the central nervous system. It is determined by their molecular size and physicochemical properties, as well as by complex binding and elimination processes occurring in the circulation, peripheral organs, at the BBB and in the brain parenchyma and its fluids.<sup>94</sup> A number of methods and models are available for examining BBB permeation *in vivo*, *in vitro*, and *in silico*. A combination of techniques can give valuable information on ways to optimize permeation, and implications for drug discovery, delivery and toxicity.<sup>95,96</sup>

*In silico* prediction of the BBB permeability of 84 TCM compounds was carried out. 3D structures of all TCM compounds were generated by LigPrep (version 2.3, Schrödinger, LLC, New York, NY, 2009) with the selected OPLS\_2005 force field, neutralized functional groups, retained specified chiralities, and other parameters default. The generated 3D structures and QikProp (version 3.2, Schrödinger, LLC, New York, NY, 2009) were then used to calculate three

descriptors QPPCaco, QPlogBB and QPPMDCK, which can reflect directly the ability of a molecule to permeate the BBB. Table 5 showed the recommended values of three descriptors for CNS drugs with good BBB permeability.

The calculation results of 84 TCM compounds are showed in Table 6. Up to 58 of 84 compounds (69%) had QPlogBB values falling into the recommended range, and 54 and 46 compounds had QPPCaco and QPPMDCK values greater than 25, respectively, while 24 and 20 had values greater than 500. Taking all three descriptors into consideration, 46 of 84 compounds (54.8%) gave both ideal QPlogBB values and reasonable QPPCaco and QPPMDCK values (greater than 25). Among them, 20 of 46 compounds had QPPCaco and QPPMDCK values greater than 500, that is, 23.8% of 84 TCM compounds showed good BBB permeability in the *in silico* model. Compared with the fact that more than 98% of all small molecule drugs do not cross the BBB,<sup>97</sup> the ratio of 23.8% of TCM compounds having good predicated BBB permeability is impressive. It might be ascribed to the fact that all these are bioactive compounds



coming from the selected herbs that had definite therapeutic effects on brain disorders.

An in-depth investigation into chemical structures revealed that most saponins with two or more sugar units such as ginsenosides (1–7) showed very bad BBB permeability. The small molecules with good BBB permeability included lactones (29–33) and ligustrazine (37) from Chuanxiong, diterpene quinones (38, 39, 41, 44, 45) and phenolic acid (46) from Danshen, and sesquiterpenes (54–59) from the volatile oil of Shichangpu. These results were consistent with those obtained on *in vitro* and *in vivo* models. Yuan *et al.* established a BBB model of ECV304/C6 cell co-culture, on which the Danshen extract was screened. The results indicated that 16 compounds could permeate over this model and four of them, tanshinone I (38), cryptotanshinone (41), danshensu (49) and protocatechuic acid (47) were identified.<sup>98</sup>  $\alpha$ -Asarone (55),  $\beta$ -asarone (54), and elemicin, the major compounds of the volatile oil of Shichangpu were found to pass through the blood brain barrier in pharmacokinetics investigations on rat.<sup>99,100</sup> Senkyunolide I was detectable in the cerebrospinal fluid in a study to find the absorbed constituents of the Chuanxiong active fraction of migraine following oral administration.<sup>101</sup>

A matching of the BBB permeability with the physicochemical properties of the TCM compounds revealed that the 23.8% of TCM compounds with good predicated BBB permeability also obeyed Lipinski's rules. Saponins, especially those with two or more sugar units are a special class, which had bad predicted BBB permeability and did not obey the Lipinski's rule of five, either. The saponins (11, 21, 25 and 73) with molecular weight less than 500 and only one sugar unit, however, showed ideal BBB permeability and physicochemical properties. Given metabolism in the body, the biological function of saponins might be ascribed to their metabolites. As a large portion of the TCM natural products, saponins require further investigation to become drug leads.

Table 5 The recommended values for QPPCaco, QPlogBB, and QPPMDCK

Descriptor	Description	Recommended values
QPPCaco	Predicting Caco-2 cell permeability in $\text{nm s}^{-1}$	<25 poor, >500 great
QPlogBB	Predicting brain/blood coefficient	–3.0 to 1.2
QPPMDCK	Predicting MDCK cell permeability in $\text{nm s}^{-1}$	<25 poor, >500 great

Table 6 Prediction of BBB permeation of 84 TCM compounds using the Schrödinger software

No	QPPCaco	QPlogBB	QPPMDCK	No	QPPCaco	QPlogBB	QPPMDCK
1	0.081	−7.756	0.019	43	1580.237	−0.183	811.233
2	0.154	−7.038	0.038	44	1624.592	−0.142	835.872
3	0.104	−7.455	0.024	45	1557.722	−0.159	798.746
4	1.704	−5.192	0.503	46	197.54	−1.002	85.711
5	1.561	−5.088	0.458	47	26.733	−1.237	12.549
6	6.096	−4.425	1.996	48	33.041	−1.359	15.778
7	4.468	−4.582	1.427	49	12.457	−1.823	5.497
8	209.676	−2.047	91.416	50	1.534	−3.62	0.571
9	31.67	−3.325	11.85	51	0.085	−4.249	0.032
10	11.159	−3.336	29.957	52	0.624	−4.083	0.216
11	73.028	−2.156	29.236	53	0.05	−4.76	0.018
12	16.988	−2.616	6.044	54	9906.038	−0.058	5899.293
13	19.024	−2.808	6.831	55	9906.038	−0.068	5899.293
14	35.924	−2.784	13.58	56	9906.038	−0.068	5899.293
15	16.523	−3.062	5.865	57	9906.038	0.102	5899.293
16	79.729	−1.532	32.146	58	9906.038	0.078	5899.293
17	263.149	−1.084	116.858	59	9906.038	0.108	5899.293
18	262.357	−0.979	116.477	60	0.589	−3.117	0.258
19	6.468	−1.969	2.707	61	3.432	−4.466	1.073
20	80.467	−1.586	32.468	62	4.102	−4.024	1.301
21	36.491	−2.155	13.812	63	5.792	−3.942	1.889
22	7.37	−3.417	2.451	64	6.108	−4.615	2.001
23	1.026	−4.855	0.291	65	0.355	−6.534	0.092
24	1.881	−5.141	0.56	66	2.508	−4.066	0.764
25	71.41	−2.057	28.536	67	142.653	−0.306	190.75
26	919.525	−0.463	451.821	68	2268.275	0.807	1326.462
27	276.504	−0.309	136.387	69	228.773	−1.609	127.756
28	182.992	−0.435	87.298	70	299.059	−1.165	170.664
29	2169.133	−0.244	1142.446	71	228.77	−1.287	127.754
30	2302.987	−0.176	1218.833	72	270.453	−1.191	153.09
31	1152.492	−0.814	576.731	73	17.867	−2.766	6.383
32	2367.728	−0.186	1255.91	74	391.215	−0.903	179.39
33	2334.953	−0.178	1237.129	75	36.51	−2.536	13.819
34	67.212	−1.139	33.994	76	510.616	−0.93	239.241
35	22.483	−1.537	10.407	77	928.264	−0.624	456.464
36	80.015	−0.862	41.044	78	270.196	−1.291	120.244
37	5483.01	0.344	3112.735	79	45.367	−1.356	22.227
38	1529.531	−0.195	783.133	80	1043.056	−0.578	517.772
39	1657.431	−0.164	854.149	81	6.021	−3.761	1.97
40	690.871	−0.628	331.709	82	31.585	−2.569	11.816
41	1713.375	−0.153	885.354	83	2.969	−3.78	0.917
42	328.906	−0.942	148.718	84	178.589	−2.159	76.859

## 4 Conclusions

Natural products have been a major resource of new drugs due to their highly diversified structures and specific biological activities. Traditional Chinese Medicines not only embrace these characteristics but also have thousands of years of clinical practice. Artemisinin from *Artemisia annua* and depside salts from *Salvia miltiorrhiza* are two successful examples of the use of compounds contained in TCMs. These constituents can explain, at least partially, the traditional therapeutic effects of the respective herbs.

Our investigation concentrated on TCMs which have long been used to treat neurodegenerative diseases. The biological activities of the main constituents from the selected TCMs were reviewed and the results showed that they have a close

relationship with brain disorders. The physico-chemical analyses of these TCM compounds showed that many TCM compounds obey Lipinski's rule of five, and fall into similar physico-chemical space, following PCA analysis, as occupied by current anti-PD and anti-AD drugs or candidates. In other words, these TCM compounds showed an excellent matching with the launched drugs or drug candidates from the physico-chemical perspective. On the other hand, the predicted BBB permeability showed that some TCM constituents had good BBB permeability. These results indicate that a high ratio of TCM compounds have the requisite physico-chemical properties and BBB permeability to have potential to be CNS drug leads.

The analysis reveals a remarkable convergence of thousands of years of traditional use and modern medicinal chemistry developments to front-lead physicochemical space in the design

of new therapeutics. While, the combination of molecules as practiced in TCM remains to be developed into western medicinal design, the convergence between TCM components and modern medicinal chemistry understanding of physico-chemical properties is amazing.

This convergence, which reveals a common physico-chemical base for TCM and western medicine, is pivotal to further development of ancient TCM in an understandable and generally acceptable way. Herbal materials with distinct chemical constitution, known mechanism of action and identified targets will contribute to the modernization, standardization and globalization of TCM. Screening TCMs for lead compounds taking into account the physico-chemical properties and predicted BBB properties is likely to be a productive method to discover new leads for neurodegenerative diseases, in particular.

Notwithstanding the above, TCM still confronts many challenges. Generally accepted regulations for raw materials are urgently required. More bioactive constituent(s) separated from TCMs need to have their mechanism of action and targets identified. Synergistic effects of combinations provide another area that needs to be addressed.

Our review provides evidence that supports the view of Dr Margaret Chan, WHO Director-General, given in her opening remarks at the International Forum on Traditional Medicine, held in Macao SAR on 19 August 2015, "Countries aiming to integrate the best from traditional and modern medicine would do well to look not at the many differences between the two approaches. Instead, they should look at those areas where both converge to help tackle the unique health challenge of the 21st century."

## 5 Acknowledgments

The work was financially supported by Griffith University International Postgraduate Research Scholarship (GUIPRS) and Griffith University Postgraduate Research Scholarship (GUPRS) to CT, and partially supported by the National Science and Technology Major Project "Key New Drug Creation and Manufacturing Program" (No. 2012ZX09301001-001) in China.

## 6 Notes and references

- 1 Y. Y. Tu, *Nat. Med.*, 2011, **17**, 1217–1220.
- 2 X. C. Li, C. Yu, Y. L. Lu, Y. L. Gu, J. Lu, W. Xu, L. J. Xuan and Y. P. Wang, *Drug Metab. Dispos.*, 2007, **35**, 234–239.
- 3 Hepeng Jia, *Nat. Biotechnol.*, 2005, **23**, 771–772.
- 4 J. D. Adams, *Traditional Chinese Medicine: Scientific Basis for Its Use*, RSC Publishing, 2013.
- 5 J. C. He and W. W. Wang, *J. Tradit. Chin. Med.*, 2010, **51**, 1024–1027.
- 6 Z. Y. Hu, Y. Huang, G. Liu, F. Liu, W. X. Zhou and Y. X. Zhang, *Pharmacol. Clin. Chin. Mater. Med.*, 2012, **28**, 252–256.
- 7 Q. Z. Su, Y. Z. Sun, L. Zeng and L. X. Fu, *Guangming Zhongyi*, 2008, **23**, 542–543.
- 8 W.-Z. Yang, Y. Hu, W.-y. Wu, M. Ye and D.-A. Guo, *Phytochemistry*, 2014, **106**, 7–24.
- 9 C. H. Lee and J.-H. Kim, *J. Ginseng Res.*, 2014, **38**, 161–166.
- 10 L. Peng, S. Sun, L.-H. Xie, S. M. Wicks and J.-T. Xie, *Cardiovasc. Ther.*, 2012, **30**, e183–e188.
- 11 J.-H. Kim, *J. Ginseng Res.*, 2012, **36**, 16–26.
- 12 J.-M. Lü, Q. Yao and C. Chen, *Curr. Vasc. Pharmacol.*, 2009, **7**, 293–302.
- 13 H. J. Kim, P. Kim and C. Y. Shin, *J. Ginseng Res.*, 2013, **37**, 8–29.
- 14 S.-Y. Nah, D.-H. Kim and H. Rhim, *CNS Drug Rev.*, 2007, **13**, 381–404.
- 15 S.-Y. Nah, *Front. Physiol.*, 2014, **5**, 1–13.
- 16 Y. Cheng, L. H. Shen and J. T. Zhang, *Acta Pharmacol. Sin.*, 2005, **26**, 143–149.
- 17 J. H. Yang, S. J. Han, J. H. Ryu, I. S. Jang and D. H. Kim, *Biol. Pharm. Bull.*, 2009, **32**, 1710–1715.
- 18 P. C. Shieh, C. W. Tsao, J. S. Li, H. T. Wu, Y. J. Wen, D. H. Kou and J. T. Cheng, *Neurosci. Lett.*, 2008, **434**, 1–5.
- 19 G. Z. Zhang, A. L. Liu, Y. B. Zhou, X. San, T. W. Jin and Y. Jin, *J. Ethnopharmacol.*, 2012, **142**, 754–761.
- 20 I. Smith, E. M. Williamson, S. Putnam, J. Farrimond and B. J. Whalley, *Nutr. Rev.*, 2014, **72**, 319–333.
- 21 H. Sungwon, Y. Yong, K. Kang, S. Y. Shin, Y. H. Lee and Y. Lim, *J. Microbiol. Biotechnol.*, 2009, **19**, 556–559.
- 22 S. Xu, L. Yang, Q. Lin, Z. Liu, Q. Feng, L. Ma and M. Liu, *Chromatographia*, 2008, **68**, 459–462.
- 23 D. Wang, Q.-R. Tan and Z.-J. Zhang, *J. Mol. Neurosci.*, 2013, **51**, 581–590.
- 24 R. Sun, K. Wang, D. Wu, X. Li and Y. Ou, *Folia Neuropathol.*, 2012, **50**, 270–276.
- 25 B.-Y. Cao, Y.-P. Yang, W.-F. Luo, C.-J. Mao, R. Han, X. Sun, J. Cheng and C.-F. Liu, *J. Ethnopharmacol.*, 2010, **131**, 122–129.
- 26 K. Wang, L. Zhu, X. Zhu, K. Zhang, B. Huang, J. Zhang, Y. Zhang, L. Zhu, B. Zhou and F. Zhou, *Cell. Mol. Neurobiol.*, 2014, **34**, 227–234.
- 27 O. A. Heikal, T. Akao, S. Takeda and M. Hattori, *Biol. Pharm. Bull.*, 1997, **20**, 517–521.
- 28 S. L. Hsiu, Y. T. Lin, K. C. Wen, Y. C. Hou and P. D. L. Chao, *Planta Med.*, 2003, **69**, 1113–1118.
- 29 X. Li, Y. Li, J. Chen, J. Sun, X. Li, X. Sun and X. Kang, *Neurosci. Lett.*, 2010, **483**, 1–5.
- 30 F.-L. Sun, L. Zhang, R.-Y. Zhang and L. Li, *Eur. J. Pharmacol.*, 2011, **660**, 283–290.
- 31 F. Zhang, Y.-Y. Wang, J. Yang, Y.-F. Lu, J. Liu and J.-S. Shi, *Oxid. Med. Cell. Longevity*, 2013, **2013**, 680545.
- 32 G. Y. Lv, Z. H. Lou, S. H. Chen, H. Gu and L. T. Shan, *J. Ethnopharmacol.*, 2011, **137**, 449–456.
- 33 H. Gong, Z. He, A. Peng, X. Zhang, B. Cheng, Y. Sun, L. Zheng and K. Huang, *Sci. Rep.*, 2014, **4**, 5648.
- 34 M. Convertino, R. Pellarin, M. Catto, A. Carotti and A. Caffisch, *Protein Sci.*, 2009, **18**, 792–800.
- 35 M. Pickhardt, Z. Gazova, M. von Bergen, I. Khlistunova, Y. P. Wang, A. Hascher, E. M. Mandelkow, J. Biernat and E. Mandelkow, *J. Biol. Chem.*, 2005, **280**, 3628–3635.
- 36 Y.-Y. Tian, L.-J. An, L. Jiang, Y.-L. Duan, J. Chen and B. Jiang, *Life Sci.*, 2006, **80**, 193–199.
- 37 B. Jiang, J. Du, L. Jian-hui, Y.-M. Bao and L.-J. An, *Brain Res.*, 2008, **1188**, 139–147.

- 38 Y.-Y. Tian, B. Jiang, L.-J. An and Y.-M. Bao, *Eur. J. Pharmacol.*, 2007, **568**, 142–148.
- 39 J.-N. Dai, Y. Zong, L.-M. Zhong, Y.-M. Li, W. Zhang, L.-G. Bian, Q.-L. Ai, Y.-D. Liu, J. Sun and D. Lu, *PLoS One*, 2011, **6**(7), e21891.
- 40 G. Jiang, H. Wu, Y. Hu, J. Li and Q. Li, *Cell. Mol. Neurobiol.*, 2014, **34**, 591–602.
- 41 H. Kumar, I. S. Kim, S. V. More, B. W. Kim, Y. Y. Bahk and D. K. Choi, *J. Evidence-Based Complementary Altern. Med.*, 2013, **2013**, 514095.
- 42 Q. Wang, G. Chen and S. Zeng, *J. Pharm. Biomed. Anal.*, 2008, **46**, 399–404.
- 43 Y.-F. Xian, Z.-X. Lin, Q.-Q. Mao, Z. Hu, M. Zhao, C.-T. Che and S.-P. Ip, *J. Evidence-Based Complementary Altern. Med.*, 2012, **2012**, 802625.
- 44 D. Yuan, B. Ma, J.-y. Yang, Y.-Y. Xie, L. Wang, L.-J. Zhang, Y. Kano and C.-F. Wu, *Int. Immunopharmacol.*, 2009, **9**, 1549–1554.
- 45 Y. Song, R. Qu, S. Zhu, R. Zhang and S. Ma, *Phytother. Res.*, 2012, **26**, 1528–1533.
- 46 X. M. Wu, Z. M. Qian, L. Zhu, F. Du, W. H. Yung, Q. Gong and Y. Ke, *Br. J. Pharmacol.*, 2011, **164**, 332–343.
- 47 Y. Peng, J. Sun, S. Hon, A. N. Nylander, W. Xia, Y. Feng, X. Wang and C. A. Lemere, *J. Neurosci.*, 2010, **30**, 8180–8189.
- 48 S. Ma, S. Xu, B. Liu, J. Li, N. Feng, L. Wang and X. Wang, *Naunyn-Schmiedeberg's Arch. Pharmacol.*, 2009, **379**, 565–574.
- 49 M. Srinivasan, A. R. Sudheer and V. P. Menon, *J. Clin. Biochem. Nutr.*, 2007, **40**, 92–100.
- 50 T. O. Cheng, *Int. J. Cardiol.*, 2007, **121**, 9–22.
- 51 L. M. Zhou, Z. Zuo and M. S. S. Chow, *J. Clin. Pharmacol.*, 2005, **45**, 1345–1359.
- 52 X. Chen, J. Guo, J. Bao, J. Lu and Y. Wang, *Med. Res. Rev.*, 2014, **34**, 768–794.
- 53 L. Chen, Y. Lu and S. Z. Zheng, *Chin. Tradit. Herb. Drugs*, 2009, **40**, 476–479.
- 54 J. Y. Han, J. Y. Fan, Y. Horie, S. Miura, D. H. Cui, H. Ishii, T. Hibi, H. Tsuneki and I. Kimura, *Pharmacol. Ther.*, 2008, **117**, 280–295.
- 55 L. Cui, W. Chan, J.-L. Wu, Z.-H. Jiang, K. Chan and Z. Cai, *Talanta*, 2008, **75**, 1002–1007.
- 56 C. H. Liu, X. J. Liu and H. S. Yang, *Chin. Arch. Tradit. Chin. Med.*, 2006, **24**, 1280–1281.
- 57 Y. Chen, G. Wei, H. Nie, Y. Lin, H. Tian, Y. Liu, X. Yu, S. Cheng, R. Yan, Q. Wang, D. H. Liu, W. Deng, Y. Lai, J. H. Zhou, S. X. Zhang, W. W. Lin and D. F. Chen, *Brain Res.*, 2014, **1552**, 41–54.
- 58 Z.-T. Mo, Y.-Q. Fang, Y.-P. He and S. Zhang, *Acta Pharmacol. Sin.*, 2012, **33**, 737–742.
- 59 S. Manikandan and R. S. Devi, *Pharmacol. Res.*, 2005, **52**, 467–474.
- 60 Q. Chen, Y. G. Cao and C. H. Zhang, *Acta Pharmacol. Sin.*, 2002, **37**, 913–917.
- 61 Y. Hu, J. Li, P. Liu, X. Chen, D.-H. Guo, Q.-S. Li and K. Rahman, *J. Biomed. Biotechnol.*, 2012, **2012**, 1–5.
- 62 Y. Hu, M.-Y. Liu, P. Liu, X. Dong and A. D. W. Boran, *J. Mol. Neurosci.*, 2014, **53**, 600–607.
- 63 Y. Ikeya, K. Sugama, M. Okada and H. Mitsuhashi, *Chem. Pharm. Bull.*, 1991, **39**, 6.
- 64 Y. Ikeya, S. Takeda, M. Tunakawa, H. Karakida, K. Toda and T. Yamaguchi, *Biol. Pharm. Bull.*, 2004, **27**, 1081–1085.
- 65 J. W. Zhang and Q. Zhao, *China J. Chin. Med.*, 2013, **28**, 550–553.
- 66 B. Q. Chen, G. J. Du and Q. T. Xu, *J. Chin. Med. Mater.*, 2002, **25**, 429–430.
- 67 S. M. Guo, X. W. Fan and J. W. He, *J. Chin. Med. Mater.*, 1998, **21**, 578.
- 68 J. W. Fu, W. Qiao and Z. H. Chen, *Journal of Tianjin Medical University*, 2005, **11**, 52–54.
- 69 B. L. Li, C. T. Xia and B. X. Yuan, *Journal of Xi'an Jiaotong University (Medical Sciences)*, 2008, **29**, 227–229.
- 70 C. Wang, Z. L. You, Q. Xia, T. Xiong, Y. Xia and D. Z. Yao, *Acta Pharmacol. Sin.*, 2007, **28**, 334–338.
- 71 S. Z. Li and X. P. Wang, *Chin. Tradit. Pat. Med.*, 1999, **21**, 88–89.
- 72 L. J. Sun, *J. Hebei Norm. Univ., Nat. Sci. Ed.*, 2001, **25**, 217–218.
- 73 N. Nishiyama, Y.-L. Wang, J. Y. Kaimori, A. Ishihara and H. Saito, *Phytother. Res.*, 2006, **6**, 289–293.
- 74 K. A. Youdim, A. Martin and J. A. Joseph, *Int. J. Dev. Neurosci.*, 2000, **18**, 383–399.
- 75 Y. Dong, B. Xu, L. Lin and Q. Za, *Food & Machinery*, 2005, **21**, 85–88.
- 76 H. Zhang, Y. Liu, M. Lao, Z. Ma and X. Yi, *Exp. Gerontol.*, 2011, **46**, 30–37.
- 77 Q. Zhang, W.-d. Huang, X.-y. Lv and Y.-m. Yang, *Cell Biol. Int.*, 2012, **36**, 419–426.
- 78 G. Wang, L. Zhou, Y. Zhang, M. Dong, X. Li, J. Liu and Y. Niu, *Neurosci. Lett.*, 2011, **487**, 88–93.
- 79 Y. Zou, B. Hong, L. Fan, L. Zhou, Y. Liu, Q. Wu, X. Zhang and M. Dong, *Free Radical Res.*, 2013, **47**, 55–63.
- 80 H.-Q. Chen, X.-J. Wang, Z.-Y. Jin, X.-M. Xu, J.-W. Zhao and Z.-J. Xie, *Neurosci. Res.*, 2008, **62**, 123–130.
- 81 C.-M. Lin, R.-D. Lin, S.-T. Chen, Y.-P. Lin, W.-T. Chiu, J.-W. Lin, F.-L. Hsu and M.-H. Lee, *Phytochemistry*, 2010, **71**, 2147–2156.
- 82 J. K. Prasain, K. Jones, N. Brissie, R. Moore, J. M. Wyss and S. Barnes, *J. Agric. Food Chem.*, 2004, **52**, 3708–3712.
- 83 O. Pancharoen, U. Prawat and P. Tuntieachwuttiul, in *Studies in Natural Products Chemistry*, ed. Atta-ur-Rahman, Elsevier Science B. V., The Netherlands, 2000, pp. 797–865.
- 84 T. Ahmed and A.-H. Gilani, *Phytother. Res.*, 2014, **28**, 517–525.
- 85 M. Metzler, E. Pfeiffer, S. I. Schulz and J. S. Dempe, *BioFactors*, 2013, **39**, 14–20.
- 86 C. A. Lipinski, F. Lombardo, B. W. Dominy and P. J. Feeney, *Adv. Drug Delivery Rev.*, 2001, **46**, 3–26.
- 87 C. A. Lipinski, *Drug Discovery Today: Technol.*, 2004, **1**, 337–341.
- 88 D. F. Veber, S. R. Johnson, H. Y. Cheng, B. R. Smith, K. W. Ward and K. D. Kopple, *J. Med. Chem.*, 2002, **45**, 2615–2623.
- 89 M. Rasool, A. Malik, M. S. Qureshi, A. Manan, P. N. Pushparaj, M. Asif, M. H. Qazi, A. M. Qazi,

- M. A. Kamal, S. H. Gan and I. A. Sheikh, *J. Evidence-Based Complementary Altern. Med.*, 2014, **2014**, 1–7.
- 90 *Instant JChem*, ChemAxon Ltd., 6.2.1. edn, 2014.
- 91 R. J. Quinn, A. R. Carroll, N. B. Pham, P. Baron, M. E. Palframan, L. Suraweera, G. K. Pierens and S. Muresan, *J. Nat. Prod.*, 2008, **71**, 464–468.
- 92 M. Feher and J. M. Schmidt, *J. Chem. Inf. Comput. Sci.*, 2003, **43**, 218–227.
- 93 J. Larsson, J. Gottfries, S. Muresan and A. Backlund, *J. Nat. Prod.*, 2007, **70**, 789–794.
- 94 G. F. Ecker and C. R. Noe, *Curr. Med. Chem.*, 2004, **11**, 1617–1628.
- 95 N. J. Abbott, *J. Inherited Metab. Dis.*, 2013, **36**, 437–449.
- 96 D. B. Stanimirovic, M. Bani-Yaghoub, M. Perkins and A. S. Haqqani, *Expert Opin. Drug Discovery*, 2014, **10**, 1–15.
- 97 W. M. Pardridge, *Neurotherapeutics*, 2005, **2**, 3–14.
- 98 J. Yuan, J. Cui, W. Shang, J. Liu and Z. Zhang, *Sci. Sin.: Chim.*, 2010, **40**, 717–724.
- 99 H. Wu and Y. Fang, *Acta Pharmacol. Sin.*, 2004, **39**, 836–838.
- 100 H. Tang and R. Li, *J. Tradit. Chin. Med.*, 2002, **18**, 40–41.
- 101 Y. Yuan, X. Lin, Y. Feng, D.-S. Xu and Y.-H. Wang, *Chin. Pharm. J.*, 2010, **45**, 694–697.

## 2.3 Conclusion

The physicochemical analysis of the selected herbs showed an amazing convergence between TCM components and modern medicinal chemistry, which, on the one hand, provides evidences to support the searching for bioactive single compounds from TCM, and on the other hand, indicates a feasible in-depth investigation of a mixture of compounds and their possible interactions, which might touch upon the synergistic effect, from the perspective of individual compound.

It should be pointed out that traditional Chinese medicines did not include intravenous drugs, and most of them were taken orally. 71.4% of the TCM compounds compliant with the Lipinski's rule and the high overlapping with those anti-PD and anti-AD drugs in a narrow area of physicochemical space suggested that these molecules would tend to have high oral bioavailability. It was also consistent with the results obtained from the *in silico* calculation of the BBB permeability, 69% having QPlogBB values within the recommended range. The physicochemical analysis revealed the high oral bioavailability of most TCM compounds, which could explain well the efficacy of TCM from the absorption point of view.

Moreover, this analysis provides a basis to further investigate the herb pairs using cell-based phenotypic analysis to examine the herb pair, the individual herb, and the reported compounds.

## 2.4 References

1. Anonymous, 小儿卫生总微论方. In Huaxia Press: Beijing, 1997.
2. He, J. C.; Wang, W. W., Effect of Tianma Gouteng Yin on Apoptosis of Dopaminergic Neurons in Parkinson's disease Model Rats *J. Tradit. Chin. Med.* **2010**, 51, (11), 1024-27.
3. Su, Q. Z.; Sun, Y. Z.; Zeng, L.; Fu, L. X., The current state of Traditional Chinese medicine in Treatng Parkinson's Disease. *Guangming Zhongyi* **2008**, 23, (4), 542-3.
4. Hu, Z. Y.; Huang, Y.; Liu, G.; Liu, F.; Zhou, W. X.; Zhang, Y. X., Analysis of medication law of Traditional Chinese Medicine in treating dementia. *Pharmacology and Clinics of Chinese Materia Medica* **2012**, 28, (5), 252-6.

5. Deng, J.-G.; Hao, E.-W.; Guo, H.-W.; Liu, J.-H., Analysis of drug law of compound prescription in treating
6. Alzheimer disease. *Shandong Zhongyi Zazhi* **2007**, 26, (6), 363-365.
7. Wang, X.-L.; Bahaer, H., 明清时期治疗老年性痴呆的用药规律. *Guangming Zhongyi* **2010**, 25, (5), 749-750.
8. 任浩; 方之勇; 余一明, 天麻钩藤饮加减治疗帕金森病睡眠障碍 43 例. *光明中医* **2013**, 28, (6), 1134-5.
9. Shao, Y.-F., 天麻钩藤饮合酸枣仁汤治疗顽固性失眠 60 例. *Zhejiang Zhongyi Zazhi* **2012**, 47, (4), 263.
10. Liu, H.-F., 川芎天麻散治疗偏头痛 100 例临床观察. *Modern Journal of Integrated Traditional Chinese and Western Medicine* **2005**, 14, (5), 607-608.
11. Zhou, M.-M.; Yang, K.; Wang, Y., 从血液流变学和血流速度评价大川芎丸方中川芎天麻治疗偏头痛的协同作用. *Pharmacology and Clinics of Chinese material Medica* **2008**, 24, (3), 6-8.
12. Xiao, S.-M.; Peng, Y.-K., 百家配伍用药经验采菁. China Press of Traditional Chinese Medicine: 2004.
13. Lu, J.-S., 施今墨对药临床经验集. People's Medicinal Publishing House Co. LTD.: 1982.
14. Lipinski, C. A.; Lombardo, F.; Dominy, B. W.; Feeney, P. J., Experimental and computational approaches to estimate solubility and permeability in drug discovery and development settings. *Adv Drug Deliver Rev* **2001**, 46, (1-3), 3-26.
15. Lipinski, C. A., Lead- and drug-like compounds: the rule-of-five revolution. *Drug discovery today. Technologies* **2004**, 1, (4), 337-41.
16. Veber, D. F.; Johnson, S. R.; Cheng, H. Y.; Smith, B. R.; Ward, K. W.; Kopple, K. D., Molecular properties that influence the oral bioavailability of drug candidates. *J. Med. Chem.* **2002**, 45, (12), 2615-2623.
17. JChem, I. 6.2.1. ; ChemAxon Ltd. : 2014.
18. Origin 8.0; OriginLab: 2007.
19. Larsson, J.; Gottfries, J.; Muresan, S.; Backlund, A., ChemGPS-NP: tuned for navigation in biologically relevant chemical space. *Journal of natural products* **2007**, 70, (5), 789-94.
20. Ecker, G. F.; Noe, C. R., *In silico* prediction models for blood-brain barrier permeation. *Curr. Med. Chem.* **2004**, 11, (12), 1617-28.
21. Abbott, N. J., Blood-brain barrier structure and function and the challenges for CNS drug delivery. *J. Inherit. Metab. Dis.* **2013**, 36, (3), 437-449.
22. Stanimirovic, D. B.; Bani-Yaghoub, M.; Perkins, M.; Haqqani, A. S., Blood-brain barrier models: in vitro to in vivo translation in preclinical development of CNS-targeting biotherapeutics. *Expert Opinion on Drug Discovery* **2015**, 10, (2), 141-155.
23. Tang, C.; Ye, Y.; Feng, Y.; Quinn, R. J., TCM, brain function and drug space. *Nat. Prod. Rep.* **2016**, 33, (1), 6-25.

CHAPTER 3 Sample preparation and chemical profiling







3.1 Preparation of TCM samples

3.1.1 Herb materials

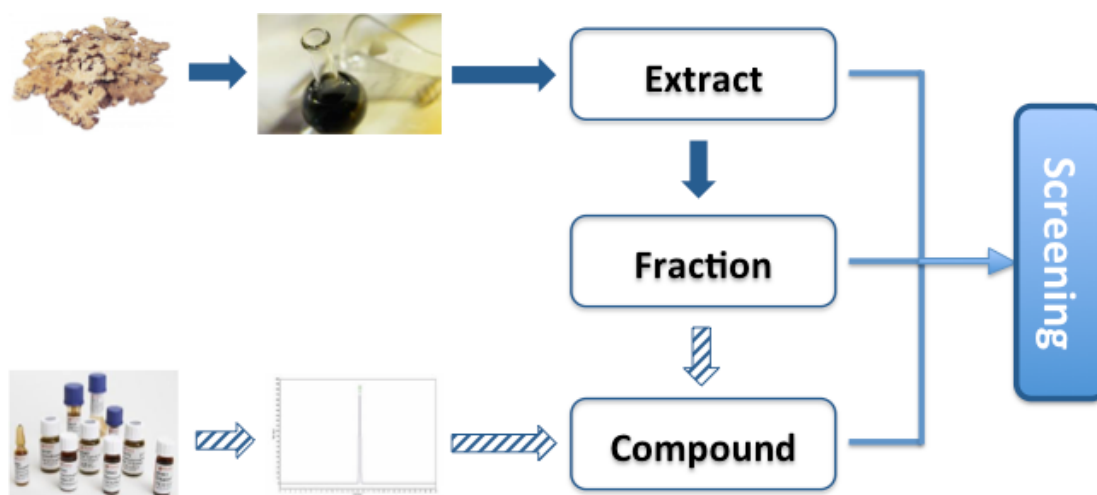
All herb materials were purchased from Pudong Sub-branch of Tong-Ren-Tang (同仁堂浦东分店), one of the biggest TCM manufacturers and retailers in China. The herb pairs were made in the lab according to the weight ratios shown in Table 2.7. The photos of all purchased materials were taken in March 2013 and are shown in Table 3.1.

Table 3.1 Photos of 15 selected TCM herb materials purchased from Tong-Ren-Tang. The herb numbers here are consistent with those in Table 2.6.

Photo			
	Herb No. 1	2	3
Photo			
	Herb No. 4	5	6

Photo			
Herb No.	7	8	9
Photo			
Herb No.	10	11	12
Photo			
Herb No.	13	14	15

### 3.1.2 Sample preparation



**Figure 3.1** Strategy of preparation of extracts, fractions and compounds for screening.

Three levels of samples were prepared – extract, fraction and compound. The total extract was prepared from the herb or herb pair, and then fractions from the extract. Compounds were obtained from two sources, either separated from fraction or extract, or purchased from market (**Fig. 3.1**).

### 3.1.2.1 Extracts and fractions

The flowchart from herb to extract and fraction is shown in **Fig. 3.2**. Extracted by 70% ethanol or water, the herb or herb pair afforded the total extract, which was then treated by column chromatograph over C18 to give two fractions, water-soluble fraction and fat-soluble fraction. Given decoction is one of the most popular formulations in TCM, some herbs/herb pairs were treated both with 70% ethanol and water. The results are shown in **Table 3.2**.

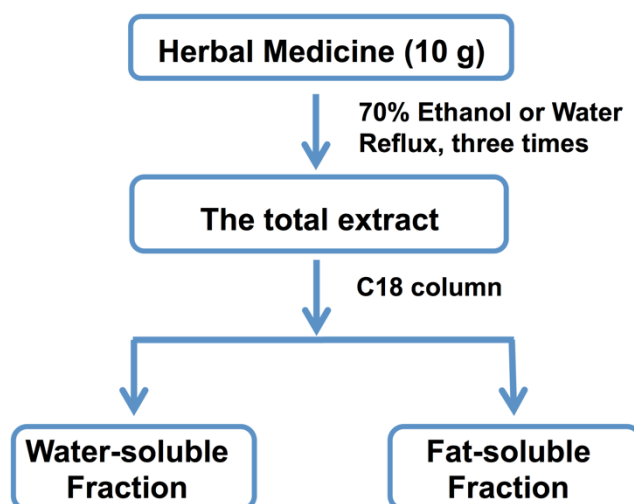


**Figure 3.2** Flowchart of preparation of extract and fraction.

**Table 3.2** Detailed information about preparation of extracts and fractions.

Herb/ Herb pair	Method <sup>a</sup>	Wt. (g) <sup>b</sup>	Total Extract Wt. (g)	Fractionation				
				Extract for Frac. (g)	W. Frac. (mg)	% of the extract	F. Frac. (mg)	% of the extract
1	E	10	2.34	1.00	~800	80%	149	15%
2 <sup>c</sup>	E	10	5.63	1.00	~900	90%	105	10%
3	E	10	1.58	1.00	738	74%	306	31%
4	E	10	1.31	1.00	554	55%	460	46%
5	E	10	6.37	1.02	806	86%	32	9%

6	E	10	1.70	1.10	~700	64%	256	23%
7	E	10	1.58	1.02	489	48%	514	50%
8	E	10	2.37	1.02	705	69%	257	25%
9	E	10	3.62	1.01	887	88%	132	13%
10	E	10	1.22	0.66	413	62%	185	28%
11	E	10	3.94	1.02	534	52%	425	42%
12	E	10	1.13	0.85	457	54%	299	35%
13	E	10	1.05	0.36	199	55%	121	34%
14	E	10	2.25	1.00	573	57%	403	40%
15	E	10	0.74	0.45	274	61%	97	22%
6+7	E	14	1.85	1.00	556	56%	413	41.3%
10+11	E	14	3.98	1.00	623	62%	252	25%
12+13	E	14	1.90	1.00	560	56%	250	25%
9+14	E	14	4.10	1.00	720	72%	267	27%
6+8	E	15	3.46	1.00	727	73%	220	22%
6	W	5	2.82	2.57	2290	89%	56	2%
8	W	5	1.69	1.62	674	42%	278	16%
6+8	W	5	2.14	1.90	1620	85%	110	6%

<sup>a</sup> E-ethanol extraction, W-water extraction

<sup>b</sup> The weight of the raw material used for extraction; for the ratios of the herb pairs see Table 2.7.

<sup>c</sup> The extraction of herb 2 was performed twice for the mistakes in weighting the material.

### 3.1.2.2 Compounds

Since the selected herbal medicines are frequently used and have been thoroughly investigated in China, some bioactive principals isolated from them, particularly those documented in the Chinese Pharmacopeia as standard substances, are available from the market. Thus, some compounds were purchased from the market, and checked by HPLC/MS or NMR before registered into the compound library for further screening.

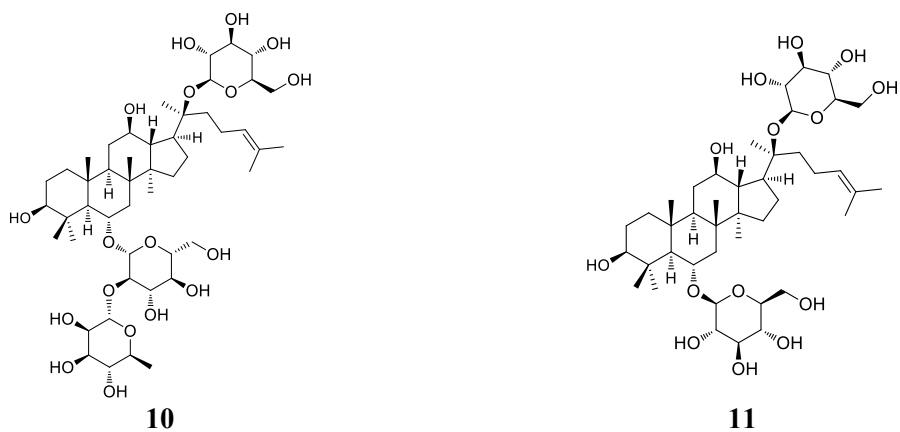
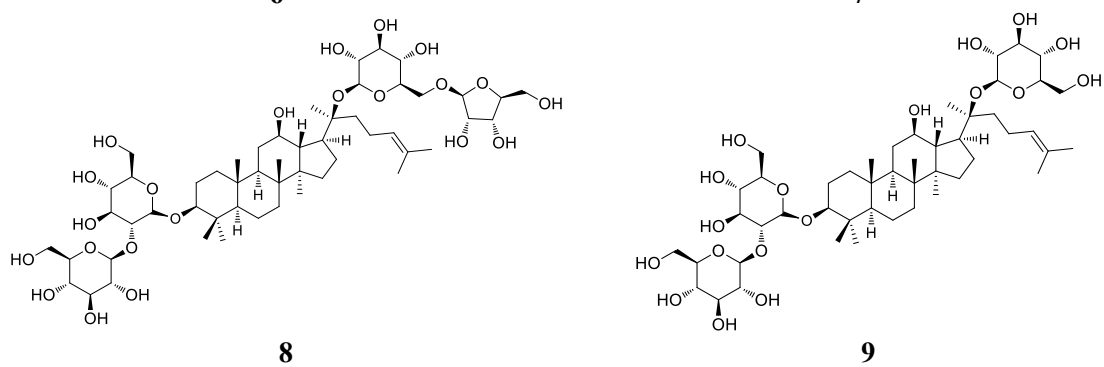
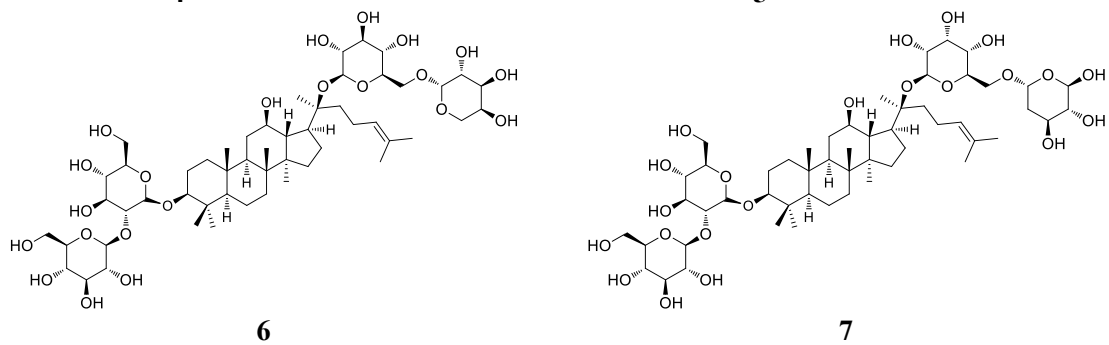
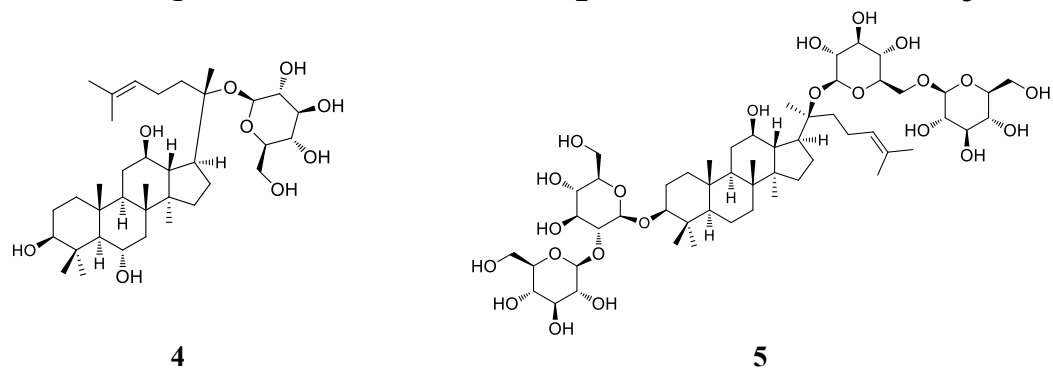
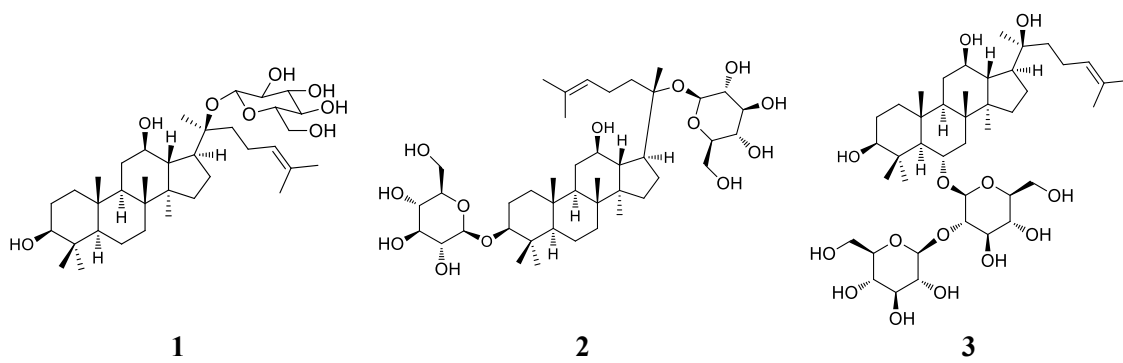
Some compounds that cannot be obtained from the market were separated from the extract or fraction by conventional methods such as column chromatography over silica gel, Sephadex LH-20, or preparative HPLC. For details see Supporting Information.

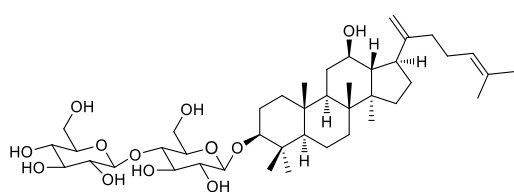
A total of 90 compounds from the 15 selected herbs were obtained (**Table 3.3**), and their structures are shown in **Fig. 3.3**.

**Table 3.3** Detailed information of 90 compounds from the selected herbs.

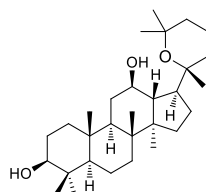
No	Compound Name	M.W.	From which herb
1	Ginsenoside CK	622.87	1
2	Ginsenoside F2	785.01	1
3	Ginsenoside Rf	801.01	1
4	Ginsenoside F1	638.87	1
5	Ginsenoside Rb1	1109.29	1
6	Ginsenoside Rb2	1079.27	1
7	Ginsenoside Rb3	1079.27	1
8	Ginsenoside Rc	1079.27	1
9	Ginsenoside Rd	947.15	1
10	Ginsenoside Re	947.15	1
11	Ginsenoside Rg1	801.01	1
12	Ginsenoside Rk1	767.00	1
13	Panaxadiol	460.73	1
14	Panaxatriol	476.73	1
15	Pseudoginsenoside F11	801.01	1
16	Pseudoginsenoside RT5	654.87	1
17	R-ginsenoside Rg3	785.01	1
18	R-ginsenoside Rh1	638.87	1
19	R-ginsenoside Rh2	622.87	1
20	Protopanaxatriol	476.73	1
21	S-ginsenoside Rh1	638.87	1
22	S-ginsenoside Rh2	622.87	1
23	S-protopanaxadiol	460.73	1
24	Ginsenoside Ro	957.11	1
25	Ginsenoside F3	770.99	1
26	Ginsenoside Rg6	767.00	1
27	Ginsenoside Rg2	785.01	1
28	R-ginsenoside Rg2	785.01	1
29	S-ginsenoside Rg3	785.01	1
30	R-protopanaxatriol	476.73	1
31	lobetyolin	396.18	2
32	paeoniflorin	480.16	3
33	albiflorin	480.16	3
34	aloe emodin	270.05	4
35	chrysophanol	254.06	4
36	physcion	284.07	4
37	emodin	270.05	4
38	2,3,5,4'-tetrahydroxystilbene- 2-O-β-D-glucopyranoside	406.13	4
39	catalpol	362.12	5
40	acetoside	624.21	5
41	5-hydroxymethyl-2-furaldehyde	126.03	5
42	gastrodin	286.11	6
43	parishin E	460.39	6
44	parishin B	728.65	6
45	parishin C	728.65	6
46	parishin	996.91	6
47	rhynchophylline	384.20	7
48	isorhynchophylline	384.20	7

49	ligustilide	190.10	8
50	ferulic acid	194.06	8
51	caffeic acid	180.04	8
52	levistilide A	380.20	8
53	senkyunolide A	192.12	8
54	butylphthalide	190.10	8
55	ligustrazine	136.10	8
56	senkyunolide I	224.25	8
57	cryptotanshinone	296.14	9
58	salviandic acid B	718.15	9
59	dihydrotanshinone I	278.09	9
60	rosmarinic acid	360.08	9
61	danshensu	198.05	9
62	tanshinone IIA	294.13	9
63	tanshinone I	276.08	9
64	salviandic acid A	494.12	9
65	3,4-dihydroxybenzaldehyde	138.03	9
66	3,4-dihydrobenzoic acid	154.03	9
67	lithospermic acid	538.11	9
68	eugenol	164.20	10
69	$\alpha$ -asarone	208.11	10
70	methyleugenol	178.10	10
71	methyl isoeugenol	178.10	10
72	senegenin	536.29	11
73	tenuifolin	680.38	11
74	onjisaponine B	1573.67	11
75	polygalaxanthone III	568.14	11
76	3,6'-disinapoyl sucrose	754.23	11
77	nuciferine	295.16	12
78	jujuboside A	1207.60	12
79	spinosin	608.17	12
80	jujuboside B	1044.55	12
81	arachidonic acid	304.24	13
82	oleic acid	282.26	13
83	linoleic acid	280.24	13
84	linolenic acid	278.22	13
85	daidzin	416.11	14
86	puerarin	416.11	14
87	daidzein	254.06	14
88	curcumin	368.13	15
89	bisdemethoxycurcumin	308.10	15
90	cardamonin	270.28	15

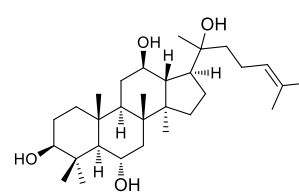




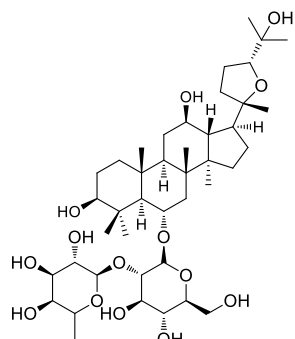
**12**



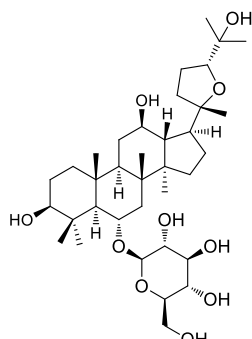
**13**



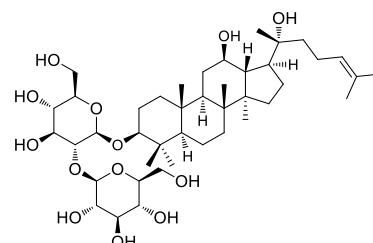
**14**



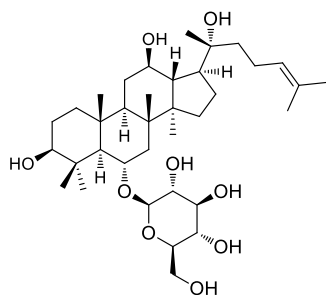
**15**



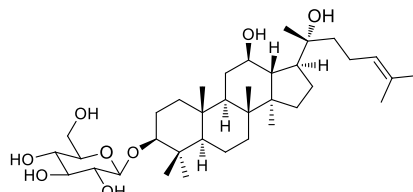
**16**



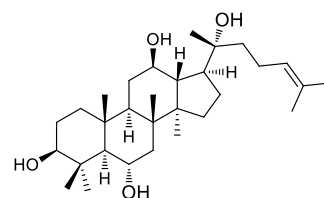
**17**



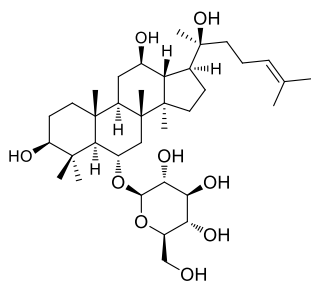
**18**



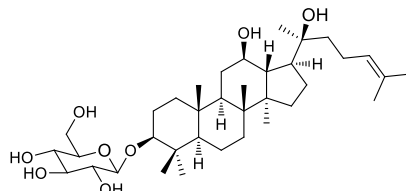
**19**



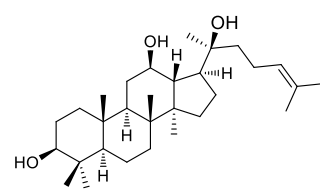
**20**



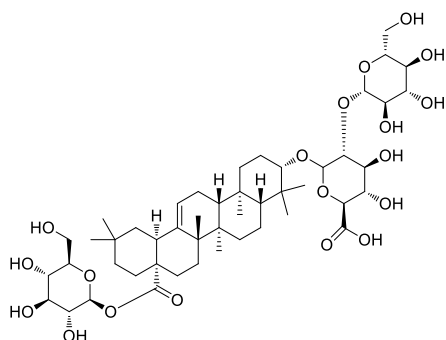
**21**



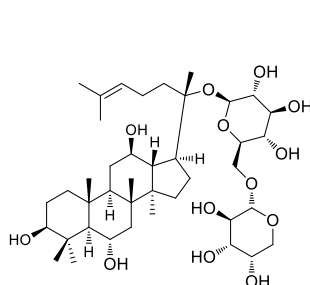
**22**



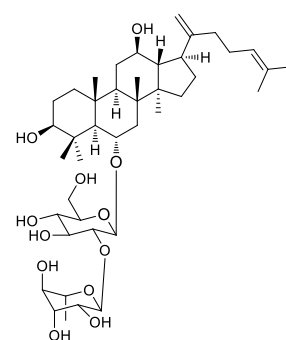
**23**



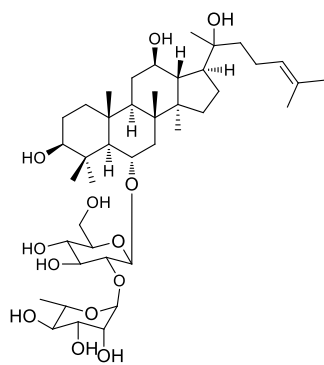
**24**



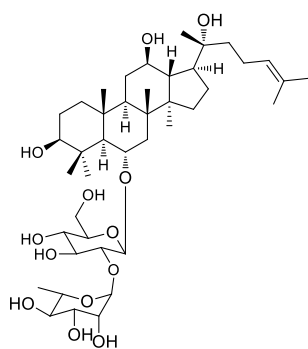
**25**



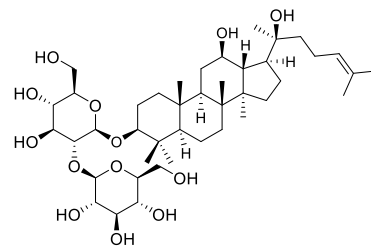
**26**



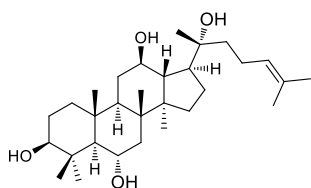
27



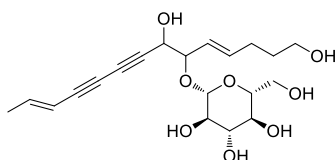
28



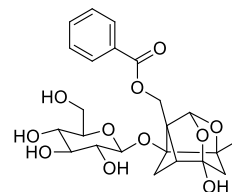
29



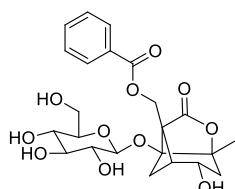
30



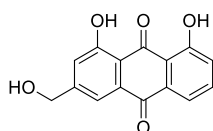
31



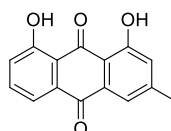
32



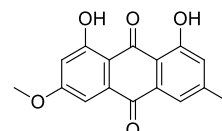
33



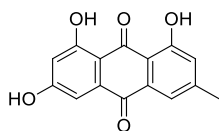
34



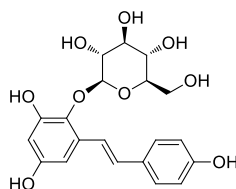
35



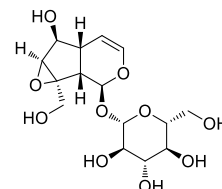
36



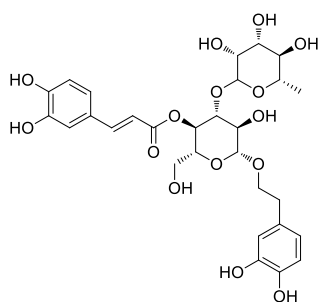
37



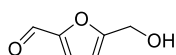
38



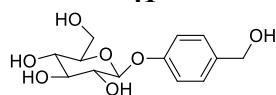
39



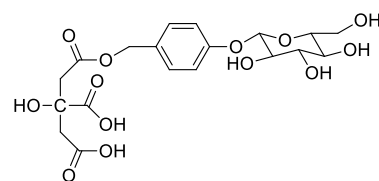
40



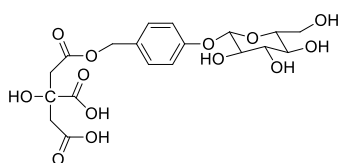
41



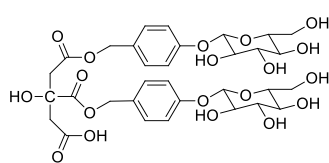
42



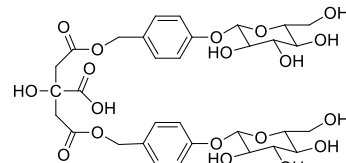
43



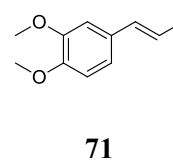
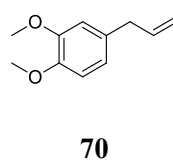
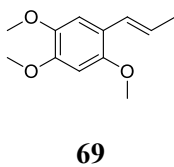
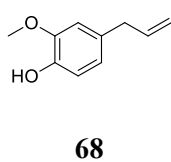
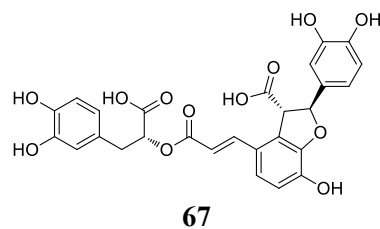
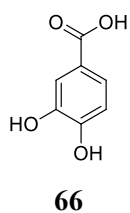
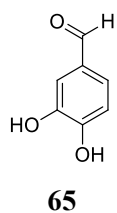
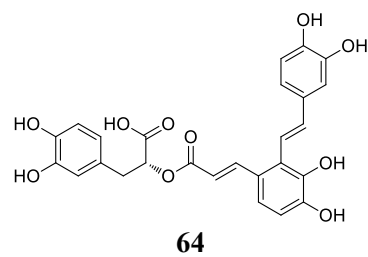
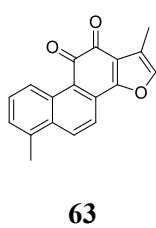
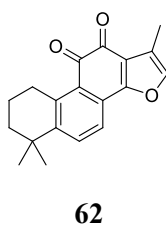
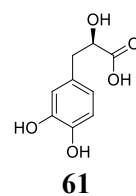
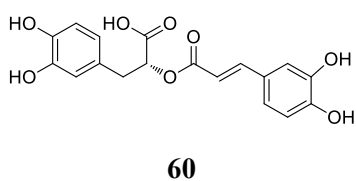
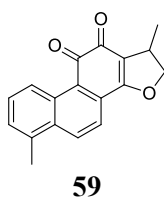
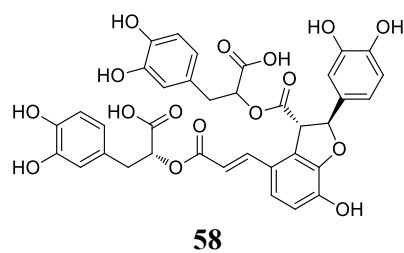
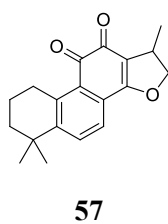
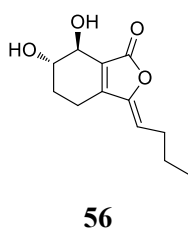
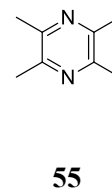
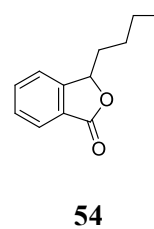
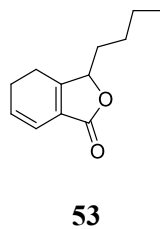
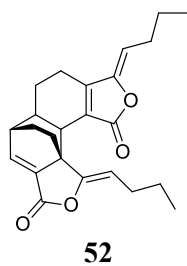
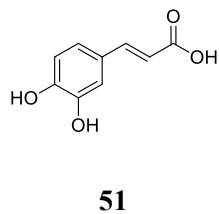
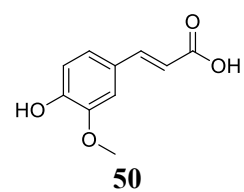
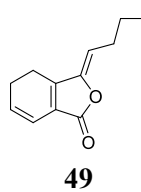
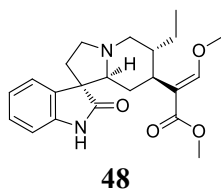
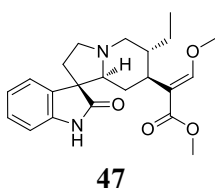
44



45



46



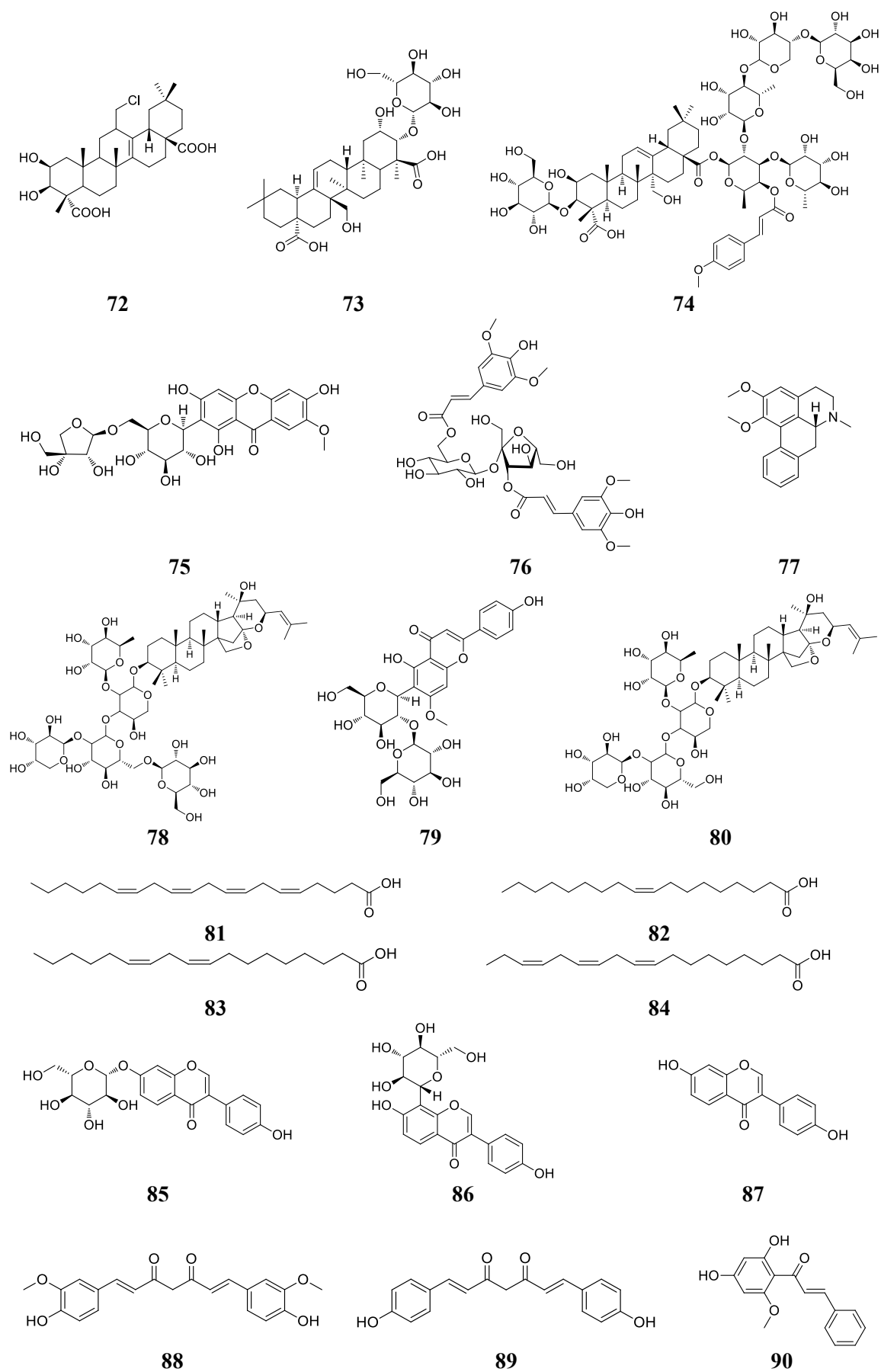


**Figure 3.3** Chemical structures of 90 compounds.

## 3.2 HPLC analysis of TCM samples

HPLC analysis was performed for all samples in order to:

1. Get information about the chemicals composition of each sample;
2. Disclose the chemical correlations among compound, fraction and extract obtained from the same herb or herb pair.
3. Reveal the chemical difference between samples obtained using different extraction method.

The chemical profiling aims to provide information for explanation of their biological behaviors in the following screening.

### 3.2.1 Extracts and fractions

The protocol to prepare two fractions from the total extract aims to separate the water-soluble constituents from the fat-soluble ones. In this program, we focus more on small molecules rather than big molecules with high polarity such as polysaccharide and peptide, which are prone to concentrate in the water-soluble fraction.

All extracts and fractions were run on HPLC under a SOP used for analysis. The comparison of the extract and its two fraction from one herb/herb pair were carried out. The results showed that the protocol could separate the water-soluble from the fat-soluble well.

The HPLC analysis of the total extract, the water-soluble and fat-soluble fractions of Ginseng are shown in **Fig. 3.4**. The results showed clearly that the small molecules could not be observed in the above chromatogram, but they showed as the predominant chemical constituents in the bottom chromatogram. The constituents in the water-soluble fraction were quite different from those in the fat-soluble fraction.

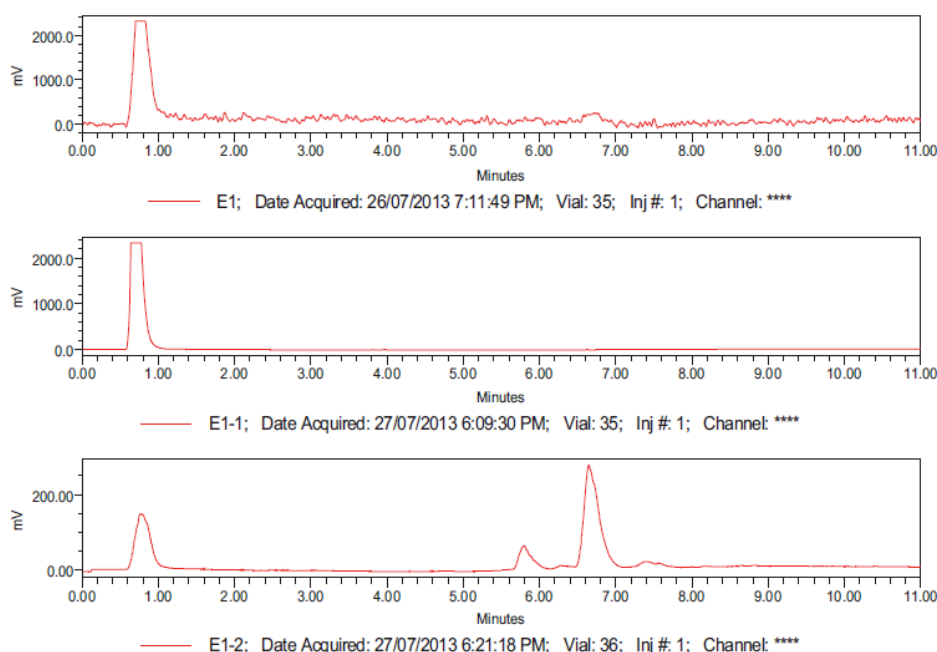


**Figure 3.4** The overlay report of E1 (total extract), E1-1 (water-soluble fraction) and E1-2 (fat-soluble fraction) from Ginseng Radix (herb 1).

We further compared the fat-soluble fraction with 30 ginsenosides, the major bioactive components of Ginseng, which were purchased from Tianjin IMAM Biotech Co. Ltd. The overlaid HPLC chromatograms indicated that all ginsenosides are right in the range of retention time from 5.5 to 8.0 min (**Fig. 3.5**), matching the peaks during this period observed for the fat-soluble fraction.

The similar phenomena were observed for other herbs/herb pairs. Most of the major components could be found concentrating in the fat-soluble fraction.

The comparison of the fat-soluble fraction of Polygoni Multiflori Radix and its five major bioactive components is shown in **Fig. 3.6**. The peaks that could be observed in the chromatogram of the fat-soluble fraction matched well with the peaks of five major compounds.

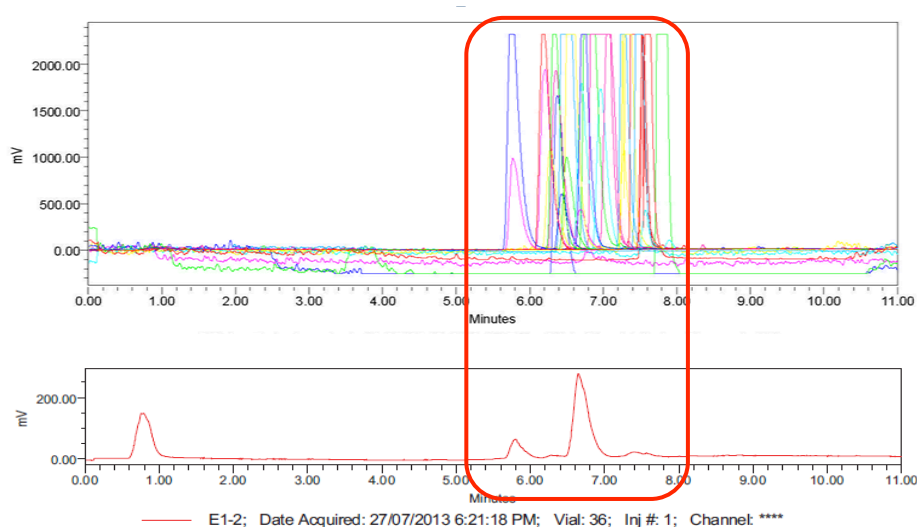


**Figure 3.5** The overlay report of 30 Ginsenosides purchased from market and comparison with the fat-soluble fraction E1-2 of herb 1.

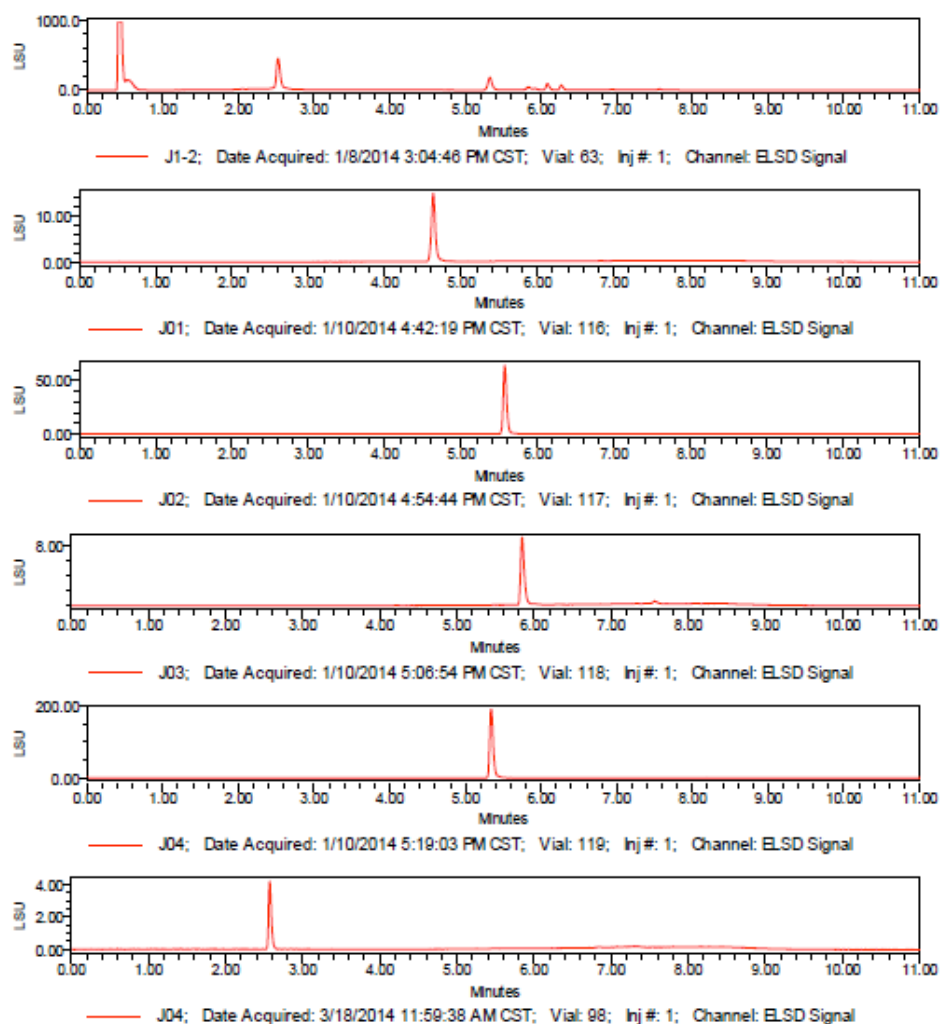


**Figure 3.6** Overlaid report for the fat-soluble fraction of *Polygoni Multiflori Radix* (herb 4) and five major components purchase from market: J01: aloe emodin, J02: chrysophanol, J03: physcion, J04: emodin, J05: 2,3,5,4'-tetrahydrosystillene-2-*O*- $\beta$ -D-glucopyranoside.

### 3.2.2 Pure compounds

The purity and molecular weights of all compounds were checked by LC-MS coupled with ELSD and UV detectors or NMR spectra.

Puerarin (**86**), for example, is the major bioactive compound isolated from *Puerariae Lobatae Radix*. The results (**Fig. 3.7**) showed that the purity of puerarin was above 95%, and the molecular weight gave by LC-MS was 416.

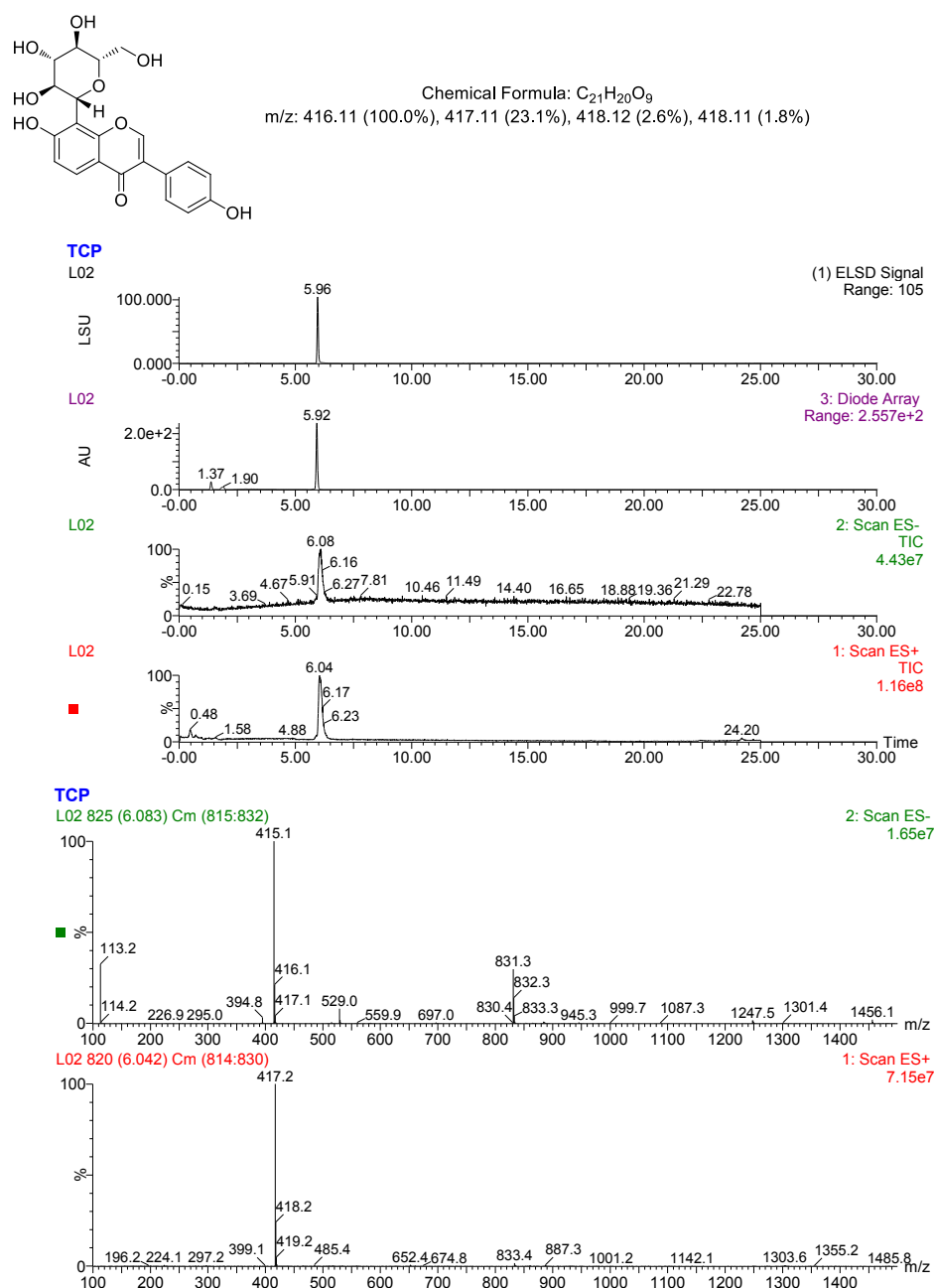


**Figure 3.7** Above: HPLC chromatograms: ELSD, UV, negative total ion, positive total ion; Below: negative and positive ion chromatograms of peak at retention time around 6.06 min.

### 3.2.3 Herbs and herb pairs

In order to find the chemical correlation between a herb pair and its constitutive herb, the extracts and fractions of herb pairs were run on HPLC under the same SOP used for the individual herbs. Their HPLC chromatograms were then compared, especially those of the fat-soluble fractions.

The result for the herb pair 9+14 is shown in **Fig. 3.8**. The herb pair consists of two herbs Puerariae Lobatae Radix and Salviae Miltiorrhizae Radix et Rhizoma in a ratio of 1:1. The HPLC-ELSD analysis showed that each herb contained one major compound, which were identified by LC-MS and comparison with the authentic samples as puerarin (**86**) and salviandic acid B (**58**), respectively. In the chromatogram of the herb pair, these two compounds were also clearly observed as two major compounds with a rough ratio of 4:1.

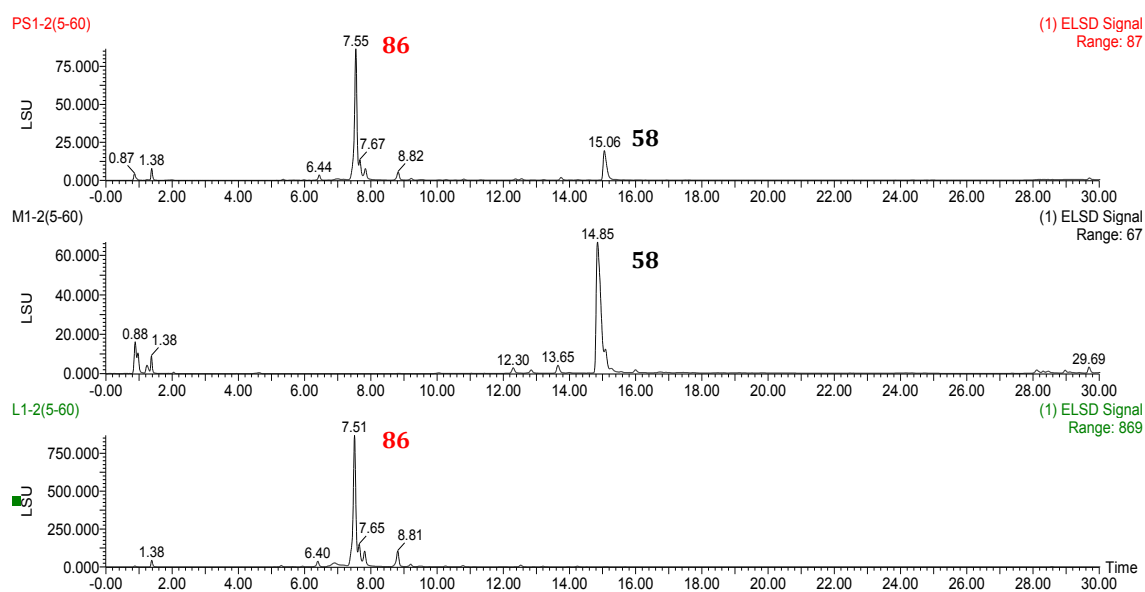


**Figure 3.8** Above: ELSD chromatogram of the herb pair 9+14 (1:1); Middle: ELSD chromatogram of the herb Puerariae Lobatae Radix; Below: ELSD chromatogram of the herb Salviae Miltiorrhizae Radix et Rhizoma.

The herb pair 6+8 consists of two herbs Gastrodiae Rhizoma and Chuanxiong Rhizoma in a ratio of 1:4. The HPLC analysis result is shown in **Fig. 3.9**. Four parishine derivatives (**43-46**) were identified as the major compounds of the fat-soluble fraction

of Gastrodiae Rhizoma, while ferulic acid (**50**) and senkyonolide I (**56**) were major compounds of Chuanxiong Rhizoma. All these six compounds were also observed in the chromatogram of the herb pair, indicating an addition of major compounds from two individual herbs.

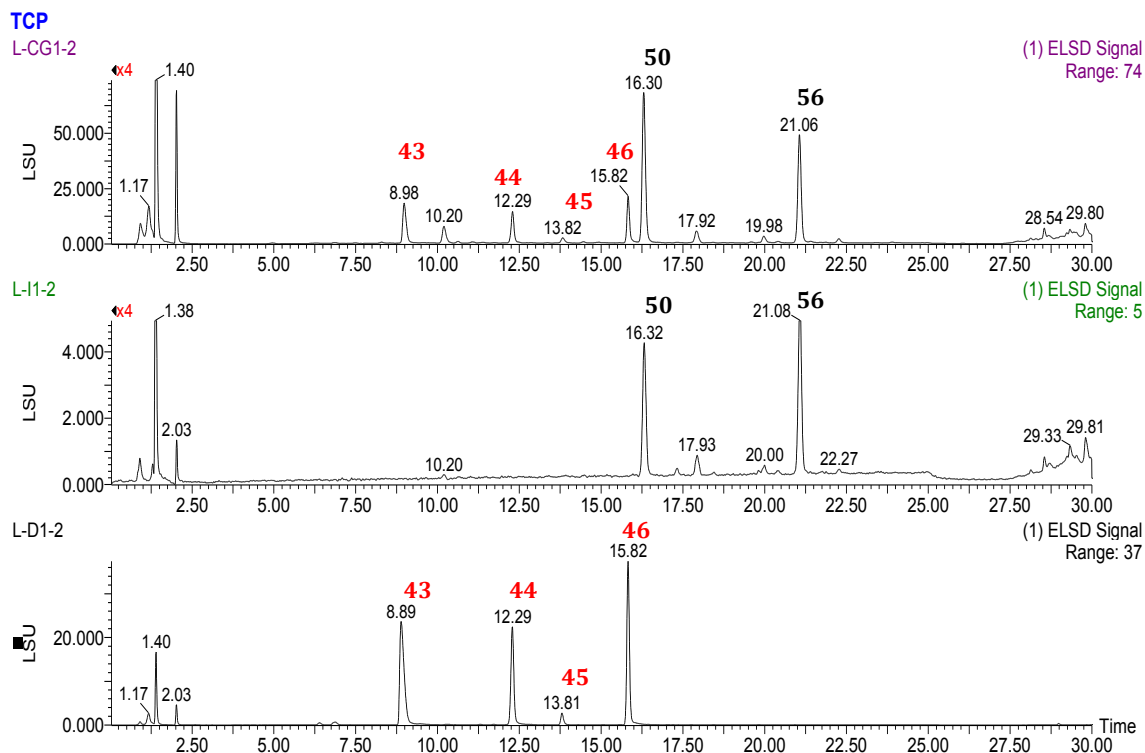


**Figure 3.9** Above: ELSD chromatogram of the herb pair 6+8 (1:4); Middle: ELSD chromatogram of the herb Chuanxiong Rhizoma; Below: ELSD chromatogram of the herb Gastrodiae Rhizoma.

The herb pair 12+13 was composed of Ziziphi Spinosae Semen and Platycladi Semen. Four unsaturated fatty acids, arachidonic acid (**81**), oleic acid (**82**), linoleic acid (**83**), and linolenic acid (**84**), are the major constituents of the fat-soluble fractions of these two herbs. The herb pair also showed the same four peaks but with different ratios (**Fig. 3.10**).

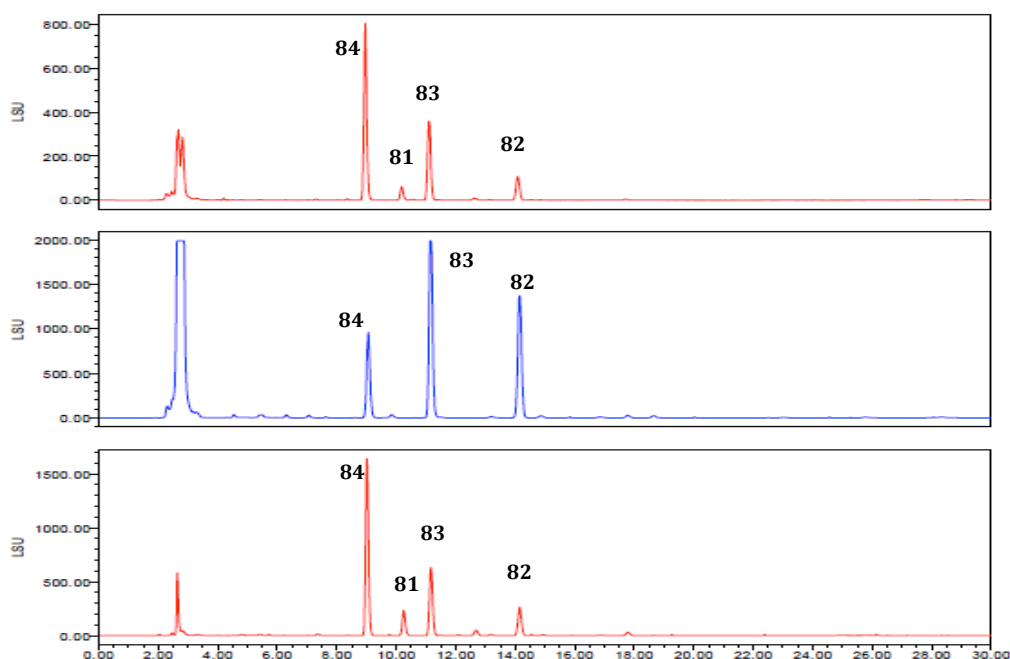


**Figure 3.10** Above: ELSD chromatogram of the herb pair 12+13 (1:1); Middle: ELSD chromatogram of the herb Ziziphi Spinosae Semen; Below: ELSD chromatogram of the herb Platycladi Semen.

The results for two other herb pairs 6+7 and 10+11 are shown in **Fig. 3.11** and **Fig. 3.12**, respectively.

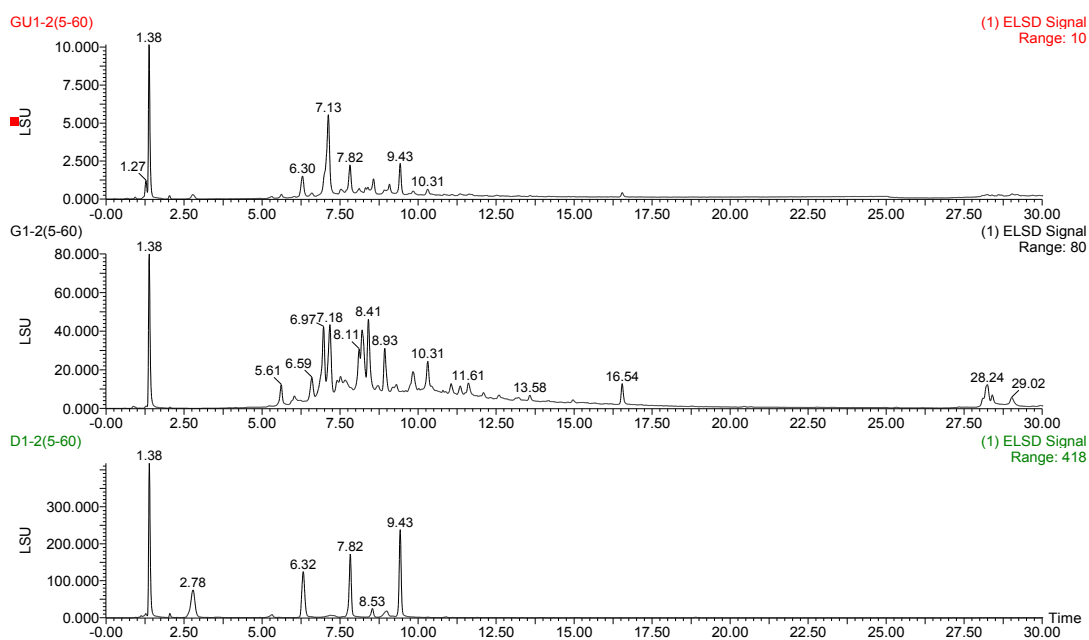


**Figure 3.11** Above: ELSD chromatogram of the herb pair 6+7 (3:4); Middle: ELSD chromatogram of the herb Ramulus Uncariae Cum Uncis; Below: ELSD chromatogram of the herb Gastrodiae Rhizoma.

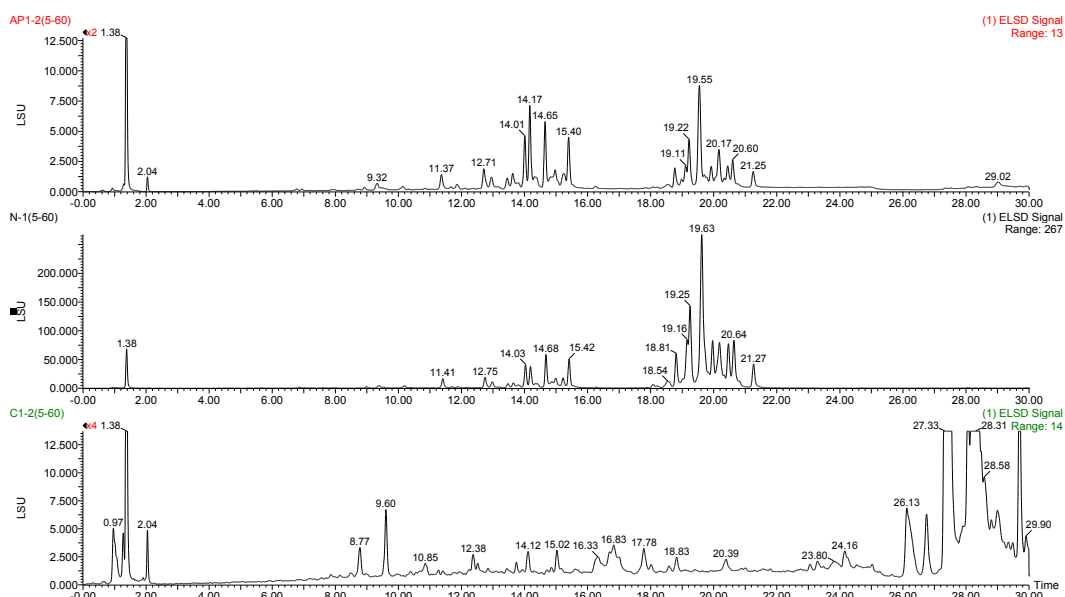


**Figure 3.12** Above: ELSD chromatogram of the herb pair 10+11 (1:1); Middle: ELSD chromatogram of the herb Polygalae Radix; Below: ELSD chromatogram of the herb Acori Tatarinowii Rhizoma.

These two results looked more complicated. In the herb pair 10+11, Polygalae Radix played a predominant role compared with Acori Tatarinowii Rhizoma. The constituents with low polarity in Acori Tatarinowii Rhizoma seemed to disappear in the herb pair. In the chromatogram of the herb pair 6+7, four peaks of Gastrodiae Rhizoma could be easily identified while the peaks of Ramulus Uncariae Cum Uncis were hard to be picked out. These two herb pairs exhibit another pattern, different from that for the herb pairs 9+14, 6+8, and 12+13, in which one herb seemed predominant compared to the other, from the chemical point of view.

Our qualitative analysis of the major compounds of five herb pairs suggested that there could be an addition correlation between the major compounds of the herb pair and its constitutive herbs. They might have changed in quantity due to interactions among different chemicals, or the changes of pH value of the mixture when they put together. This type of change has been reported in the compatibility of some herbs.<sup>1</sup>

### 3.2.4 Herbs and herb pairs treated with different extraction methods

As mentioned, we used 70% ethanol and water extractions for some herbs and herb pairs at the same time in order to compare the chemical differences caused by different extraction methods.

Gastrodiae Rhizoma (herb 6), Chuanxiong Rhizoma (herb 8) and their herb pair 6+8 were treated with 70% ethanol and water in extraction (**Table 3.4**). The results showed that using water could afford more extract than using ethanol. Compared with using the ethanol method, the percentage of the total extract of the raw material increased 39.4%, 10.1%, and 19.7%, respectively, for herb 6, herb 8 and the herb pair 6+8, while the percentage of the fat-soluble fraction obtained from the extract decreased 21.1%, 9.3%, and 16.2%. When using the ethanol extraction, the percentages of the fat-soluble fraction from three extracts were very close (about 22% to 25%), while the data varied a lot when using the water extraction.

**Table 3.4** Plant 6, plant 8 and the herb pair 6+8 treated by different extraction methods.

Materials	Method	Weight (g)	Extract Weight (g)	% in material	Fat-soluble fraction weight (mg) <sup>b</sup>	% in extract
<b>Herb 6</b>	1 <sup>a</sup>	10	1.70	17.0	256 /1.1	23.3
	2 <sup>a</sup>	5	2.82	56.4	56 /2.6	2.2
<b>Herb 8</b>	1	10	2.37	23.7	257/1.0	25.7
	2	5	1.69	33.8	278/1.6	16.4
<b>Herb pair 6+8</b>	1	15	3.46	23.1	220/1.0	22.0
	2	5	2.14	42.8	110/1.9	5.8

<sup>a</sup> 1-Extraction with 70% ethanol; 2-Extraction with water

<sup>b</sup> p/q means p mg of fat-soluble fraction obtained from q g of the extract used for fractionation

The data could be explained by the results obtained from the HPLC analysis. The ELSD chromatogram comparison of the total extracts obtained by two different methods (**Fig. 3.13**) showed that the major difference was the peaks in the blue square, which represent the chemicals with low polarity such as the volatile oil. The low-polarity chemical constituents were observed clearly in the ethanol extracts but

almost invisible in the water extracts. It is obvious that the ethanol extraction could afford more low-polarity chemicals while the water extraction yield more high-polarity ones. Herb 6 contains an array of high-polarity chemicals such as gastrodin and parishines, so the water extraction could produce much more extract, and accordingly the percentage of the fat-soluble fraction dropped a lot.

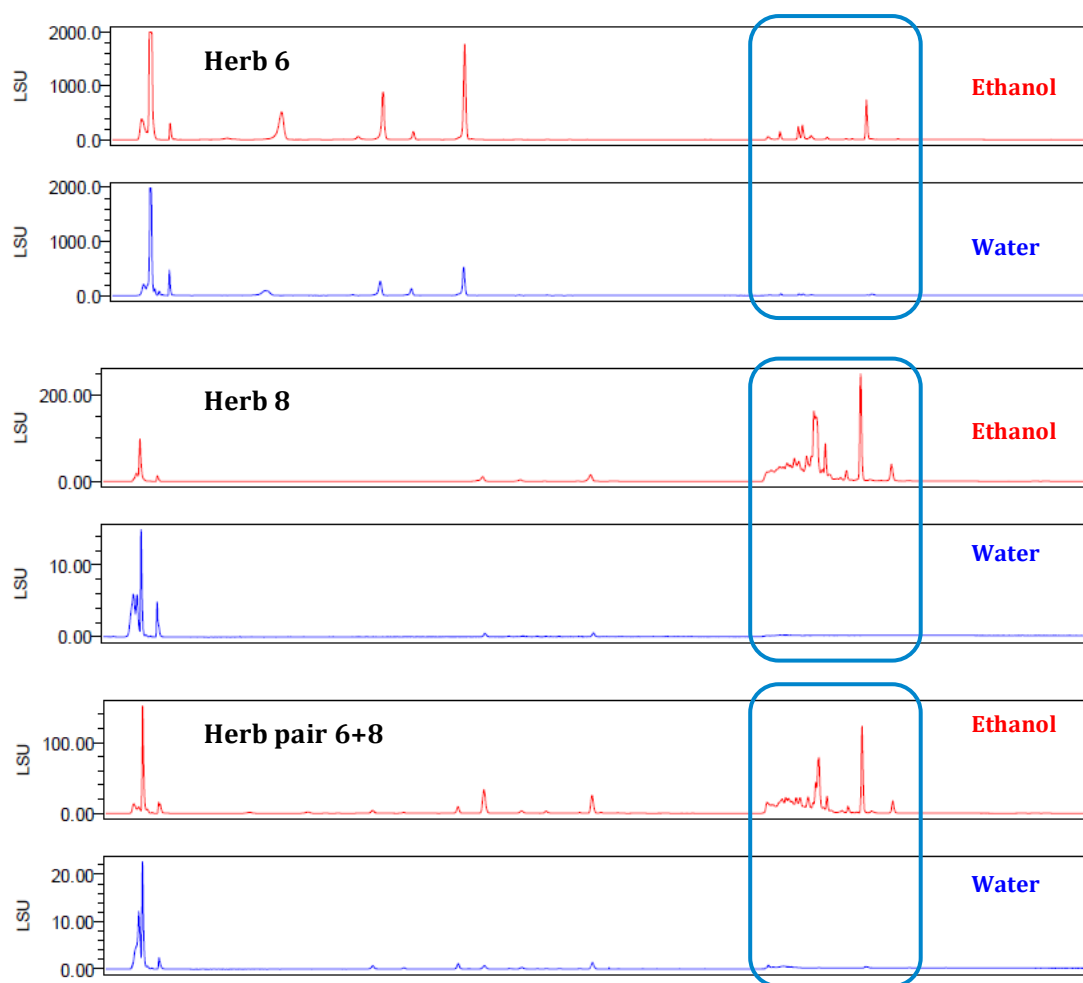


**Figure 3.13** ELSD chromatogram comparison of the ethanol and water extracts for herb 6 (above), herb 8 (middle), and herb pair 6+8 (below).

Our results showed that the extraction method has a big impact on the chemicals of the total extract, and of course the fractions obtained from the extract. These findings are consistent with those reported in literature.<sup>2, 3</sup>

### 3.2.5 Artificial mixtures

The HPLC chromatograms of extracts and fractions of different herb and herb pairs showed that, in some of them, one or several compounds exist as the predominant components. Considering the possible synergistic effects among compounds, combinations of several compounds were prepared according to their ratio in the herb or herb pairs.

**Fig. 3.8** shows that pueratin (**86**) and salviandic acid B (**58**) are two major compounds, which exist in the fat-soluble fraction of the herb pair 9+14 with a rough ratio of 4:1 according to the integrated areas of two peaks. An artificial mixture of pueratin and salviandic acid B (4:1) was then prepared.

Similarly, the mixtures of compounds **43-46** for herb 6, compounds **50** and **56** for herb 8, and compounds **43-46**, **50**, and **56** for herb pair 6+8 were also prepared, respectively, according to the ratio of the constitutive compounds in different samples as shown in **Fig. 3.9**.

According to the ratio shown in **Fig. 3.10**, combinations of four compounds (**81-84**) for the herb Ziziphi Spinosae Semen, Platycladi Semen and the herb pair 12+13 were prepared, respectively.

A total of 9 artificial mixtures were prepared (**Table 3.5**), which mimic the patterns of major compounds in herb 6, herb 8, herb pair 6+8, herb pair 9+14, herb 12, herb 13, and herb pair 12+13, respectively.

**Table 3.5** Nine artificial mixtures generated from the herbs and herb pairs

AM <sup>a</sup> No	Composition <sup>b</sup>	Ratio %	From which herb or herb pair
1	43:44:46:42	21.7:14.5:20.3:43.5	Herb 6
2	43:44:46	38.5:25.6:35.9	Herb 6 without gastrodin <sup>c</sup>
3	50:56	43.5:56.5	Herb 8
4	43:44:46:42:50:56	9.4:6.2:8.1:18.8:33.1:24.4	Herb pair 6+8
5	43:44:46:50:56	11.5:7.7:10.0:40.8:30.0	Herb pair 6+8 without gastrodin
6	86:58	80:20	Herb pair 9+14

<b>7</b>	<b>84:83:82</b>	20.8:45.8:33.3	Herb 12
<b>8</b>	<b>84:81:83:82</b>	56.8:8.5:23.7:11.0	Herb 13
<b>9</b>	<b>84:81:83:82</b>	56.5:4.6:29.2:9.7	Herb pair 12+13

<sup>a</sup> AM-artificial mixture; <sup>b</sup> For compound No see Table 3.3; <sup>c</sup> Gastrodin is the major chemical of Herb 6, and its content can reach to 0.6% of the dry material. In order to evaluate its effect on the herb, two samples, with and without gastrodin, of the artificial mixtures for herb 6 and herb pair 6+8 were prepared.

### 3.3 TCM samples for screening

According to the above-mentioned protocols, a total of 171 samples were prepared for further analysis. The detailed information is shown as follows.

Sample	Extract	Fraction	Compound	Artificial Mixture	TOTAL
<b>Number</b>	24	48	90	9	<b>171</b>

All samples were dissolved in DMSO before being registered at Compounds Australia. The concentrations for different types of samples are listed as follows.

Sample	Extract	Fraction	Compound/Mixture
<b>Concentration*</b>	10 mg/mL	5 mg/mL	5 mM

\* The average molecular weights of the extract and fraction were assumed to be 500, the apparent molecular weights of the artificial mixtures were calculated according to the percentage of the constitutive compound in the mixture.

### 3.4 Experimentals

#### 3.4.1 Preparation of extracts and fractions

10 grams of dry materials (for the weights of herb pairs see **Table 2.2**) were ground and then refluxed with 70% ethanol three times, one hour for the first time and half an hour for the second and third time. The ethanol solutions were combined and concentrated under reduced pressure, affording the total extract. 250 mg of the total extract was suspended in 2 mL of water, and then subjected to the pre-treated C18 column (20 g of C18 silica gel, dissolved in MeOH, and then washed with 50% MeOH,

10% MeOH, and water). The loaded column was eluted with water to afford the water-soluble fraction, and then 90% MeOH to afford the fat-soluble fraction.

### 3.4.2 HPLC SOP for extracts and fractions

Analytical HPLC for extracts and fractions of herbs and herb pairs was performed on a Waters 2690 instrument with a 996 PAD (photodiode array detector) and coupled with an Alltech 3300 ELSD detector. Chromatographic separations were carried out on an Onyx Monolithic C18, 5  $\mu$ , 4.6  $\times$ 100 mm column. The gradient table is shown as follows.

	Time (min)	Flow (mL/min)	%A	%B	Curve
1	0.01	4.00	10.0	90.0	6
2	3.00	4.00	50.0	50.0	6
3	3.01	3.00	50.0	50.0	6
4	6.50	3.00	100.0	0.0	6
5	7.00	3.00	100.0	0.0	6
6	7.01	4.00	100.0	0.0	6
7	8.00	4.00	100.0	0.0	6
8	9.00	4.00	10.0	90.0	6
9	11.00	4.00	10.0	90.0	6

A = 0.1% TFA in MeOH; B = 0.1% TFA in Water

### 3.4.3 LC-MS check for compounds

All samples were run on a Waters 2695 LC instrument coupled with a Waters 2998 PAD, a Waters 2424 ELSD, and a Waters 3100 SQDMS detector. Chromatographic separations were carried out on a Waters SunFire<sup>TM</sup> C18, 3.5  $\mu$ , 4.6  $\times$ 150 mm column. The gradient table is shown as follows.

	Time (min)	Flow (mL/min)	%A	%B	Curve
1	0.00	1.00	95.00	5.0	6
2	25.00	1.00	5.00	95.0	6

3	30.00	1.00	5.00	95.0	6
4	31.00	1.00	95.00	5.0	6
5	35.00	1.00	95.00	5.0	6

A = 0.1% TFA in Water; B = 0.1% TFA in CH<sub>3</sub>CN

#### 3.4.4 LC-MS analysis for herb pair and its constitutive herbs

LC-MS analysis for comparison of herb pair and its constitutive herbs, except for the Herb pair 12+13, was performed on the same instruments and column as described in 3.4.3, but with the different gradient tables.

Gradient Table for herb pair 6+8

	Time (min)	Flow (mL/min)	%A	%B	Curve
1	0.00	1.00	95.00	5.0	1
2	25.00	1.00	70.00	30.0	6
3	26.00	1.00	5.00	95.0	6
4	30.00	1.00	5.00	95.0	6
5	31.00	1.00	95.00	5.0	6

A = 0.1% TFA in Water; B = 0.1% TFA in CH<sub>3</sub>CN

Gradient Table for herb pairs 9+14, 6+7, and 10+11

	Time (min)	Flow (mL/min)	%A	%B	Curve
1	0.00	1.00	95.00	5.0	1
2	25.00	1.00	40.00	60.0	6
3	26.00	1.00	5.00	95.0	6
4	30.00	1.00	5.00	95.0	6
5	31.00	1.00	95.00	5.0	6

A = 0.1% TFA in Water; B = 0.1% TFA in CH<sub>3</sub>CN

LC-MS analysis for the Herb pair 12+13 was performed on a Waters 2690 instrument coupled with a Waters 996 and an Alltech 2000 ELSD detector. Chromatographic separations were carried out on a Cosmosil<sup>TM</sup> 5C8-MS, 5  $\mu$ , 4.6  $\times$  250 mm column. The gradient table is shown as follows.

	Time (min)	Flow (mL/min)	%A	%B	Curve
1	0.00	1.00	80.00	20.0	1
2	25.00	1.00	95.00	5.0	6
3	26.00	1.00	95.00	5.0	6
4	30.00	1.00	95.00	5.0	6

A = 0.1% TFA in CH<sub>3</sub>CN; B = 0.1% TFA in Water

### 3.5 References

1. Gao, W.-B.; Mi, J.; WU, W.; Wang, S.-M.; Liu, S.-Y., 高分离快速液相色谱法分析五味子与人参配伍化学成分变化. *Journal of China Traditional Chinese Medicine Information* **2011**, 3, (3), 1-3.
2. Cheng, S. H.; Khoo, H. E.; Ismail, A.; Abdul-Hamid, A.; Barakatun-Nisak, M. Y., Influence of Extraction Solvents on *Cosmos caudatus* Leaf Antioxidant Properties. *Iranian Journal of Science and Technology, Transactions A: Science* **2016**, 40, (1), 51-58.
3. Dent, M.; Dragovic-Uzelac, V.; Penic, M.; Brncic, M.; Bosiljkov, T.; Levaj, B., The Effect of Extraction Solvents, Temperature and Time on the Composition and Mass Fraction of Polyphenols in Dalmatian Wild Sage (*Salvia officinalis* L.) Extracts. *Food Technol Biotech* **2013**, 51, (1), 84-91.

## **CHAPTER 4 Image-Based Phenotypic Profiling**

### **4.1 Introduction**

#### **4.1.1 Phenotypic profiling**

The cellular phenotype is complex, as it is the summation of the activity state of many pathways. When biologically active compounds are used to treat cells, they can induce phenotypic changes in target cells. In this approach, broad and quantitative molecular and physiological measurements of cellular responses to the compound can be used to provide information on the compound activity and its underlying target mechanisms.<sup>1</sup>

Phenotypic profiling technologies are yet to be recognized as a new method of drug discovery, and newly modified phenotypic screens such as high-throughput, high-content imaging-driven, and omics-based screens have been developed as the initial step in the discovery of small molecule probes and drugs.<sup>2</sup> Multi-parameter phenotypic profiling of small molecules provides important insights into their mechanisms of action (MOA), as well as systematic understanding of biological pathways and their responses to small molecule treatments.<sup>3</sup>

In most cases, the information contained in each measurement of the phenotypic profiling, which describes a complex biological observation often caused by several mechanisms, is difficult to interpret. Target or mechanism of action predictions can be made by comparing the phenotypic profiles of new compounds with reference bioactive

compounds, which have known target or mechanisms of action and serve as landmarks in the multidimensional space.<sup>3</sup>

In recent years, with the evolution of automated microscopes, imaging technology and bioinformatics, image-based screening has been used to develop a number of unbiased whole cell phenotypic screening platforms.<sup>1, 4</sup> Osada *et al* reported a chemical-genetic phenotype profiling system based on the high-content cell morphology database Morphobase. This database compiled the phenotypes of cancer cell lines induced by hundreds of reference compounds, wherein those of well-characterized anticancer drugs are classified by mode of action. The applicability of this system was demonstrated by the identification of three compounds as tubulin inhibitors.<sup>2</sup> Linington *et al* extended a high-content image-based screening technology to the mechanistic characterization of unknown natural products libraries for the direct prediction of MOAs at the primary screening stage, and successfully annotated extracts based on MOA, dereplicated known compounds based on biological similarity to the training set, and identified and predicted the MOA of a unique family of iron siderophores by analyzing a training set of commercial compounds of known mechanism and comparing these profiles to those obtained from natural product library members.<sup>5</sup>

Obviously, the phenotypic screening approach takes a global view of biological attributes of compounds by determining the overall effect of small molecules on cell morphology, rather than examining specific molecular targets or pathways, as is common in target-based screening.<sup>6</sup> So far, this strategy is mainly applied for assessing small molecules associated with diseases with relatively distinct targets or pathways such as cancer. For those diseases with unclear targets or pathways, e.g. Parkinson's disease, phenotypic assay is expected to unveil unique phenotypic fingerprints that can reflect the underlying mechanism.

#### 4.1.2 A multidimensional image-based phenotypic screening on a PD patient derived cell model

An unbiased multidimensional image-based profiling method to examine the cytological responses of natural products on a PD patient derived cell model has been successfully established in house.<sup>7</sup> The general strategy of the method is presented in **Fig. 4.1**.

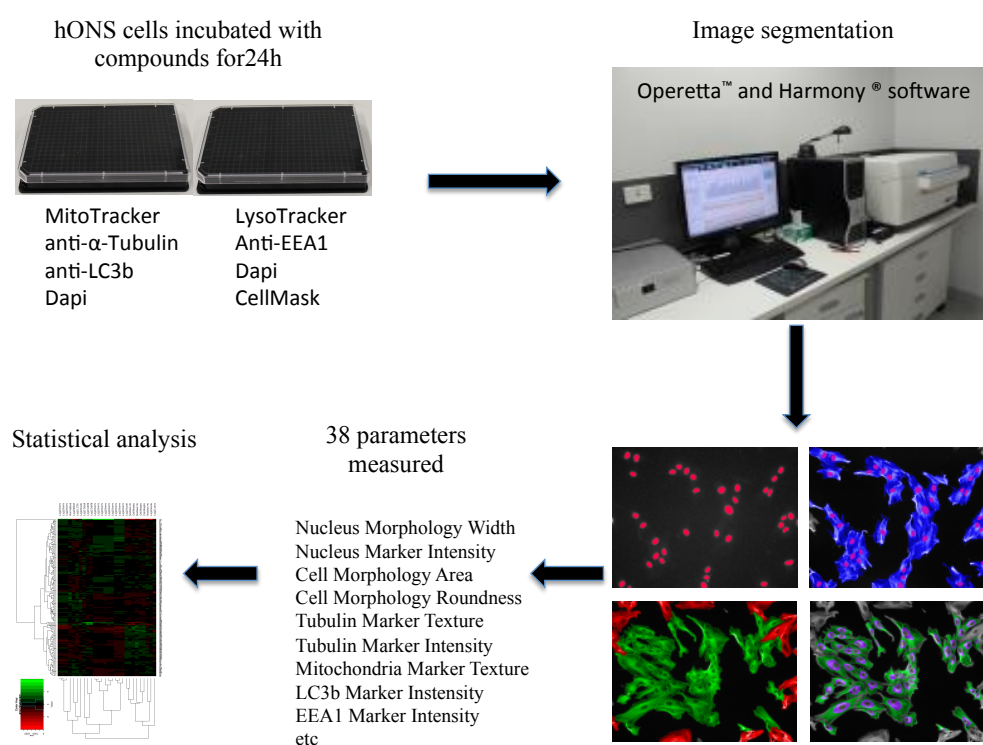


**Figure 4.1** General strategy of the established multidimensional profiling method.

In this method, non-transformed and non-immortalized human olfactory neurosphere-derived (hONS) cells, with a normal karyotype, derived from a PD patient were used. Cells were seeded in clear bottom CellCarrie 384-well plates, and incubated with compounds for 24 hours. The cellular markers including Dapi (nucleus), MitoTracker® (mitochondria), LysoTracker® (lysosomes), anti  $\alpha$ -tubulin antibody (microtubule cytoskeleton), anti EEA1 antibody (early endosomes) and anti LC3b antibody (autophagosomes) were selected to treat the cells. After cell staining, the plates were imaged automatically using Operetta, a high content imaging system. Individual

cell segmentation was done using Harmony® software. From the different fluorescent channels, a total of 38 parameters were generated from 6 dyes (**Table 4.1**). The parameters used for profiling were selected by investigating known cellular pathways and organelles implicated in PD such as mitochondria, lysosomes, endosomes, apoptosis, and autophagy. Subsequent informatics analysis was finally carried out through statistical software.

Of 38 parameters, nuclear marker intensity gave information about the total amount of dye in the nucleus, associated with the DNA content. Nuclear marker texture reflected nuclear fragmentation. Nucleus area provided information about nuclear swelling or shrinkage. The roundness, width, length, and the width to length ratio of nucleus were used to reflect an accurate quantification of the nuclear shape.

Similarly, cellular area was used to detect cellular swelling or shrinking. The cell roundness, the cell width, the cell length, and the width to length ratio characterized a precise quantification of the cellular shape.

The texture properties of different stains were used to provide information about cytoskeleton, mitochondria, lysosome, autophagosome and early endosome structures.  $\alpha$ -Tubulin, LC3b, EEA1, lysosome and mitochondria marker intensities throughout the cell and in different sub-cellular regions provided valuable information on distribution and re-arrangement of  $\alpha$ -tubulin, autophagosome, early endosomes, lysosome, and mitochondria, respectively.<sup>7</sup>

**Table 4.1** 38 parameter used in the multi-parameter phenotypic profiling.

Cell parameters	Dyes/antibodies
Nucleus Marker Intensity (mm <sup>2</sup> )	Dapi
Nucleus Marker Texture Index	
Nucleus Morphology Area (mm <sup>2</sup> )	
Nucleus Morphology Roundness Index	
Nucleus Morphology Width (mm)	
Nucleus Morphology Length (mm)	
Nucleus Morphology Ratio Width to Length	
Cell Morphology Area (mm <sup>2</sup> )	Anti- $\alpha$ -tubulin antibody
Cell Morphology Roundness Index	

Cell Morphology Width (mm)	
Cell Morphology Length (mm)	
Cell Morphology Ratio Width to Length	
Tubulin Marker Texture Index	
Tubulin Marker Intensity Cytoplasm Region (mm <sup>2</sup> )	
Tubulin Marker Intensity Outer Region (mm <sup>2</sup> )	
Tubulin Marker Intensity Inner Region (mm <sup>2</sup> )	
Mitochondria Marker Texture Index	
Mitochondria Marker Intensity Cytoplasm Region (mm <sup>2</sup> )	MitoTracker®
Mitochondria Marker Intensity Outer Region (mm <sup>2</sup> )	Orange CMTMRos
Mitochondria Marker Intensity Inner Region (mm <sup>2</sup> )	
LC3b Marker Texture Index	
LC3b Marker Intensity Cytoplasm Region (mm <sup>2</sup> )	
LC3b Marker Intensity Outer Region (mm <sup>2</sup> )	Anti-LC3b antibody
LC3b Marker Intensity Inner Region (mm <sup>2</sup> )	
Lysosomes Marker Texture Index	
Lysosomes Marker Intensity Cytoplasm Region (mm <sup>2</sup> )	LysoTracker® Red
Lysosomes Marker Intensity Outer Region (mm <sup>2</sup> )	DND-99
Lysosomes Marker Intensity Inner Region (mm <sup>2</sup> )	
EEA1 Marker Texture Index	
EEA1 Marker Intensity Cytoplasm Region (mm <sup>2</sup> )	
EEA1 Marker Intensity Outer Region (mm <sup>2</sup> )	
EEA1 Marker Intensity Outer Region (mm <sup>2</sup> )	
EEA1 Marker Intensity Inner Region (mm <sup>2</sup> )	
Number of EEA1 Marker Spots Cytoplasm Region	Anti-EEA1
Number of EEA1 Marker Spots per area of Cytoplasm	antibody
Number of EEA1 Marker Spots Outer Region	
Number of EEA1 Marker Spots per area of Outer Region	
Number of EEA1 Marker Spots Inner Region	
Number of EEA1 Marker Spots per area of Inner Region	

Based on the established platform, the TCM samples obtained from the selected herbs and herb pairs were profiled with multidimensional biological changes. These phenotypic signatures were analyzed further from different perspectives. In the following, we report the experimental details, results, data analysis, and conclusions from the phenotypic analysis.

## 4.2 Experimental

### 4.2.1 Materials and reagents

CellCarrier 384-well microplates (#6007550, Perkin Elmer, Waltham, MA) were used for the cell-based assay. Sterile, filtered Foetal Bovine Serum (Bovogen FBS,

#1107A), non-heat inactivated, was supplied by Interpath (Heidelberg West, VIC). Stock FBS was heat inactivated (HI) at 56°C in a water bath for 30 min to destroy heat-labile complement proteins prior to use in cell growth medium and then stored as frozen aliquots at -20°C. Dulbecco's Modified Eagle Medium/Nutrient Mixture F-12 (DMEM/F-12), Hank's Balanced Salt Solution (HBSS) with glucose and without calcium, magnesium or phenol red, and TrypLE™ Express Enzyme (1X), no phenol red were purchased from Life Technologies (Carlsbad, CA). Phosphate buffered saline (PBS), paraformaldehyde (PFA), normal goat serum and Triton X-100 were purchased from Sigma Aldrich (St. Louis, MO). Dimethyl sulfoxide (DMSO) was purchased from Ajax Finechem (Taren Point, NSW) as a negative control.

Antibodies and dyes used were as follows: MitoTracker® Orange CMTMRos, LysoTracker® Red DND-99, goat anti-mouse Alexa-647, goat anti-rabbit Alexa-488, goat anti-mouse Alexa-488, CellMask™ Deep Red, CellMask™ orange, and 4',6'-diamidino-2-phenylindole (Dapi) were purchased from Life Technologies (Carlsbad, CA). Monoclonal anti- $\alpha$ -Tubulin antibody produced in mouse, monoclonal anti-EEA1 antibody produced in mouse, and anti-LC3B antibody produced in rabbit were purchased from Sigma Aldrich (St. Louis, MO). All antibodies and dyes were stored in aliquots at -20°C.

#### **4.2.2 Cell line and cell culture**

The hONS cells used in the experiment were derived from PD cell line C1 200 08 0013 and stored in liquid nitrogen with 90% FBS and 10% DMSO. PD hONS cells passage 8 from cell line C1 200 08 013 were maintained in complete media (DMEM/F12 supplemented with 10% HI-FBS) under standard conditions in two 75 cm<sup>2</sup> tissue culture flask and incubated in a humidified incubator at 37°C and 5% CO<sub>2</sub>. When 70-90% confluence was reached, the cells were washed with 10 mL HBSS, and then

disassociated from the flask with 5 mL TrypLE™ Express Enzyme (5 min at 37°C). Cells were then transferred into a 10 mL tube with 5 mL complete media and centrifuged at  $0.3 \times 1000$  rcf for 5 min. The pellet was re-suspended in 4 mL of complete media. Cells were manually counted with a haemocytometer using trypan blue stain. hONS cells were added to each well at a density of 1350 cells per well in 50  $\mu$ L of growth medium (DMEM/F12, 10% FBS) leading to a final concentration of 10  $\mu$ M (0.6% DMSO) for each compound. DMSO (0.6%) was used as a negative control. The cells were incubated for 24 h at 37°C under 5% CO<sub>2</sub>.

#### **4.2.3 Sample transfer for biological assay**

A total of 171 samples including extracts, fractions, and pure compounds as described in Chapter 2 were transferred into two optically clear bottom CellCarrie 384-well plates with 98 samples for one plate and 73 samples for the other plate. Each sample was made in triplicate and with one concentration (100 nL filled up to 300 nL with DMSO). The blank wells were filled with 300 nL of DMSO as a negative control. A total of four plates (two copies) were prepared.

#### **4.2.4 Cell staining**

After 24 h of incubation, the medium was aspirated and two 384-well plates were treated with MitoTracker Orange CMTMRos (Invitrogen) (400 nM) for 30 min at 37°C under 5% CO<sub>2</sub>. Cells were fixed in 4% paraformaldehyde for 5 min at room temperature. Cells were washed twice with phosphate-buffered saline (PBS, Sigma-Aldrich) and treated with 3% goat serum (Sigma-Aldrich) and 0.2% Triton X-100 (Sigma-Aldrich) in PBS for 45 min at room temperature. Primary antibodies mouse anti- $\alpha$ -tubulin 1/4000 (Sigma-Aldrich) and rabbit anti-LC3b 1/335 (Sigma-Aldrich) were added to the plates. Plates were incubated at room temperature for 1 h, and then washed twice with PBS.

Secondary antibodies goat anti-mouse Alexa-647 1/500 (Invitrogen) and goat anti-rabbit Alexa-488 1/500 (Invitrogen) were added to the plates. Plates were incubated at room temperature for 30 minutes. Cells were washed twice with PBS and stained with 4',6'-diamidino-2-phenylindole 1/5000 (Dapi, Invitrogen). Plates were incubated for 10 min at room temperature. Cells were washed twice with PBS and plates were stored in the dark at 4°C with 25 µL of PBS per well.

The other two 384-well plates were treated with LysoTracker Red DND-99 (Invitrogen) (100 nM) for 1 h at 37°C under 5% CO<sub>2</sub>. Cells were fixed in 4% paraformaldehyde for 5 min at room temperature. Cells were washed twice with phosphate-buffered saline (PBS, Sigma-Aldrich) and treated with 3% goat serum (Sigma-Aldrich) and 0.2% Triton X-100 (Sigma-Aldrich) in PBS for 45 min at room temperature. Primary antibody, mouse anti-EEA1 1/200 (Sigma-Aldrich), was added to the plates. Plates were incubated at room temperature for 1 h, and then washed twice with PBS. Secondary antibody goat anti-mouse Alexa-488 1/500 (Invitrogen) was added to the plates. Plates were incubated for 30 min at room temperature. Cells were washed twice with PBS and stained with 4',6'-diamidino-2-phenylindole 1/5000 (Dapi, Invitrogen) and CellMask Deep Red 1/5000 (Invitrogen). Plates were incubated for 10 min at room temperature. Cells were washed twice with PBS and plates were stored in the dark at 4°C with 25 µL of PBS per well.

#### **4.2.5 Imaging and image analysis**

Plates were imaged automatically using Operetta (PerkinElmer), a high content imaging system using a 20× high numerical aperture objective lens. Six images per well for each wavelength were collected. Individual cell segmentation was done using the Harmony software and measurements for each cell were performed generating 38

parameters from six dyes: Dapi,  $\alpha$ -tubulin staining, MitoTracker Orange CMTMRos, LC3b staining, LysoTracker Red DND-99 and EEA1 staining.

The normality of the data was checked for each parameter and a log<sub>2</sub> transform was made when required in order to perform a *t*-test to identify significant changes when compared to DMSO. The log<sub>2</sub> compound/DMSO ratio was clustered using Cluster 3.0 software (uncentered correlation and centroid linkage) and analyzed using Java TreeView.

## **4.3 Results and discussion**

### **4.3.1 Clustering of TCM samples based on phenotypic responses**

The 171 TCM samples as described in Chapter 2 were assessed on the established multidimensional phenotypic assay on hONS cells. 38 phenotypic changes across the individual cell lines were examined. Unfortunately, the anti-EEA1 antibody did not work well, and thus ten parameters generated from the anti-EEA1 antibody were not included in the following analysis.

The profiling and clustering analysis performed on the 171 samples with one concentration generated a 171  $\times$  28 matrix of data. Based on the similarity of their biological profiles (uncentered correlation coefficient > 0.7), 7 bioclusters, containing 156 samples, were obtained (**Fig. 4.2**). Fifteen samples did not fall into any biocluster.

The *t*-test analysis showed that all samples profiled showed at least one phenotypic response that differs from DMSO-treated cells on the PD cell model. The clustering analysis exhibited that most samples have organelle effects that may arise from modulating human proteins or interactions with DNA or RNA.

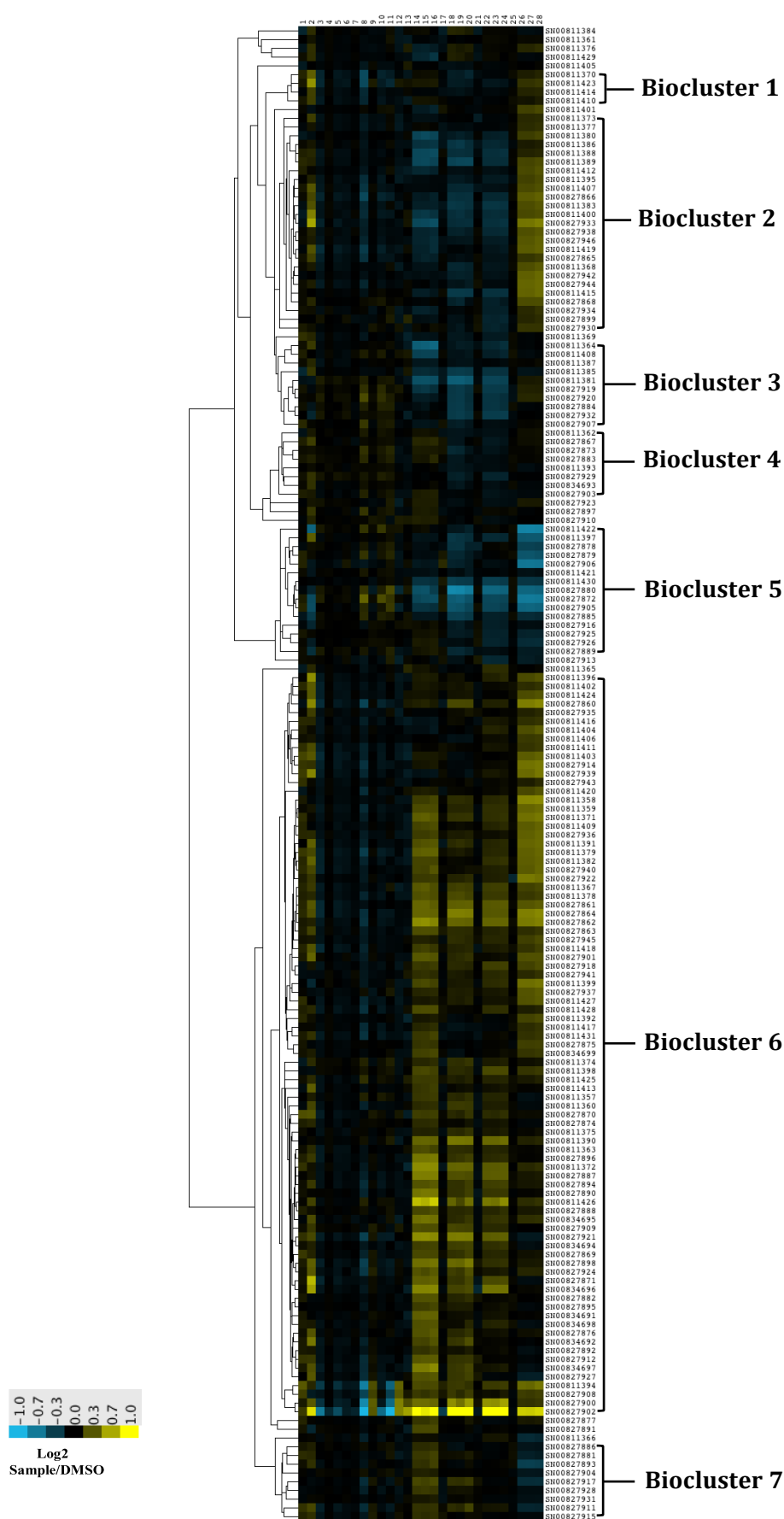


**Figure 4.2** Heatmap depicting the cytological profiles of 171 TCM samples. Based on the log2 compound/DMSO ratio, with pertinent clusters highlighted. Samples were hierarchically clustered based on their pairwise Pearson coefficients and 7 clusters with an uncentered correlation superior to 0.7 were defined from the dendrogram. Uncentered correlation

coefficient/cluster: 0.845/1, 0.727/2, 0.714/3, 0.718/4, 0.738/5, 0.736/6, and 0.761/7. Individual compounds are presented on the y-axis with 28 cytological parameters on the x-axis. Cytological parameters: 1- nucleus marker texture, 2- nucleus marker intensity, 3-nucleus area, 4- nucleus roundness, 5- nucleus width ( $\mu\text{m}$ ), 6- nucleus length ( $\mu\text{m}$ ), 7- nucleus ratio width to length, 8- cell area ( $\mu\text{m}^2$ ), 9- cell roundness, 10- cell width ( $\mu\text{m}$ ), 11- cell length ( $\mu\text{m}$ ), 12- cell ratio width to length, 13- tubulin marker texture, 14- tubulin marker intensity in cytoplasm, 15- tubulin marker intensity in outer region of cytoplasm, 16- tubulin marker intensity in inner region of cytoplasm, 17- mitochondria marker texture, 18- mitochondria marker intensity in cytoplasm, 19- mitochondria marker intensity in outer region of cytoplasm, 20- mitochondria marker intensity in inner region of cytoplasm, 21- LC3b marker texture, 22- LC3b marker intensity in cytoplasm, 23- LC3b marker intensity in outer region of cytoplasm, 24- LC3b marker intensity in inner region of cytoplasm, 25- lysosomes marker texture, 26- lysosome marker intensity in cytoplasm, 27- lysosome marker intensity in outer region of cytoplasm, 28- lysosome marker intensity in inner region of cytoplasm. Yellow represents positive effect. Blue represents negative effects. The data were the average of triplicate measurements.

The general view of the heatmap (**Fig. 4.2**) revealed that the majority of samples showed small effects on parameters associated with nucleus and cell features except for deviations on nucleus marker and cell area. Notably, these samples exhibited significant deviations on parameters of marker intensity of tubulin, mitochondria, LC3b, and lysosome while no obvious changes were observed for their texture properties. That means most TCM samples have weak influence on the cell and nucleus shapes, but strong effects on the cellular organelles without changing their structures.

For details about the samples, the SN number, and the bioclusters see **Appendix I**.

#### 4.3.2 Phenotypic descriptions of seven bioclusters

Seven bioclusters were afforded according to the uncentered correlation coefficient ( $> 0.7$ ) during clustering. A detailed examination of the samples in each cluster showed that almost every cluster contained extract, fraction and pure compound at the same time, and every cluster had its own characteristics of phenotypic responses.

##### 4.3.2.1 Biocluster 1

Biocluster 1 consisted of 4 samples including one fraction and three compounds from herb 1. The cluster did not exhibit obvious deviations of all parameters except for an increase in nucleus marker intensity and a decrease in cell area (**Fig. 4.3**).

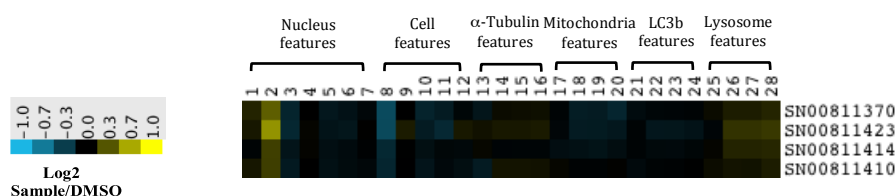


**Figure 4.3** Heatmap depicting the cytological profile of samples in biocluster 1, based on the log2 compound/DMSO ratio. Individual compounds are presented on the y-axis with individual features on the x-axis. The parameters are the same as described fully in Figure 4.2.

#### 4.3.2.2 Biocluster 2

Bioclusters 2 were composed of 25 samples which included two extracts from herb pairs 9+14 and 10+11, 15 fractions from herbs 3, 4, 5 (2)<sup>1</sup>, 6, 7, 8, 9, 13, 15, herb pairs 6+8 (3), 9+14, and 12+13, and eight compounds from herbs 1 (4), 10 (3), and 14. All these samples showed a positive deviation of lysosome marker intensity and negative deviations of tubulin, mitochondria, and LC3b marker intensity. The deviations of nucleus marker intensity and cell area, the same with those of biocluster 1, were also observed for biocluster 2 (**Fig. 4.4**).

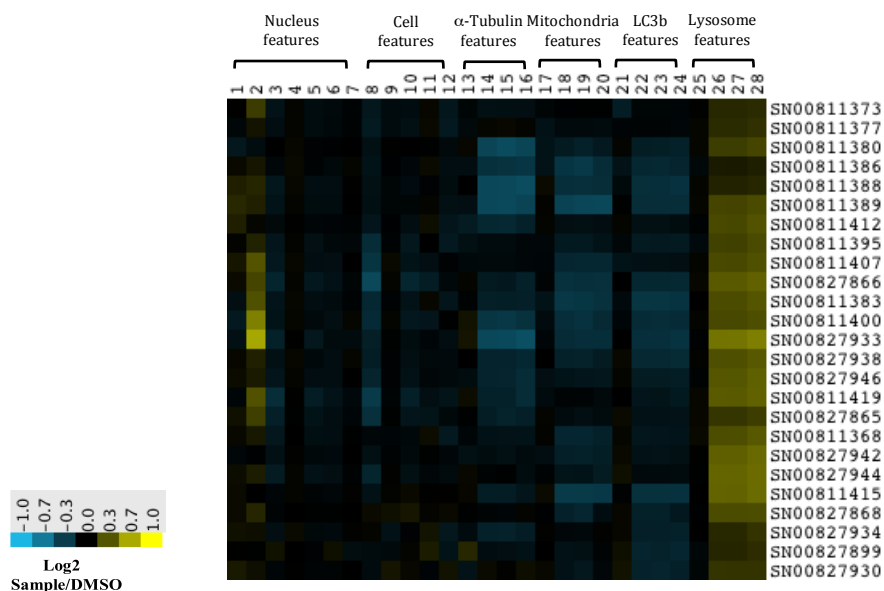


**Figure 4.4** Heatmap depicting the cytological profile of samples in biocluster 2, based on the log2 compound/DMSO ratio. Individual compounds are presented on the y-axis with individual features on the x-axis. The parameters are the same as described fully in Figure 4.2.

<sup>1</sup> The figure in the parenthesis refers to the number of samples belonging to the herb or herb pair, and only the number more than 1 is indicated.

#### 4.3.2.3 Biocluster 3

Ten samples were clustered into biocluster 3, including four extracts from herbs 2, 5, 8, and herb pair 6+8, two fractions from herbs 4 and 10, and four compounds from herbs 1, 8, 9 and 13. The biocluster 3 showed positive deviations of nucleus marker intensity and cell area, and negative ones of tubulin, mitochondria, and LC3b marker intensity. Little effect on lysosome features was observed (**Fig. 4.5**).

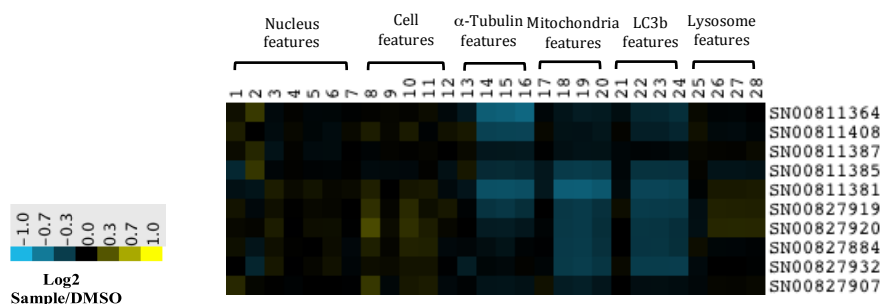


**Figure 4.5** Heatmap depicting the cytological profile of samples in biocluster 3, based on the log2 compound/DMSO ratio. Individual compounds are presented on the y-axis with individual features on the x-axis. The parameters are the same as described fully in Figure 4.2.

#### 4.3.2.4 Biocluster 4

Eight samples, containing two extracts from herb 9 and herb pair 6+8, one fraction from herb 12, four compounds from herbs 6, 8, 9, and 10, and one artificial mixture from herb 13, were clustered into biocluster 4. They did not show obvious changes on all parameters except for very weak positive deviations of nucleus marker intensity, cell area, and tubulin marker intensity, and weak negative deviations of mitochondria, and LC3b marker intensity (**Fig. 4.6**).

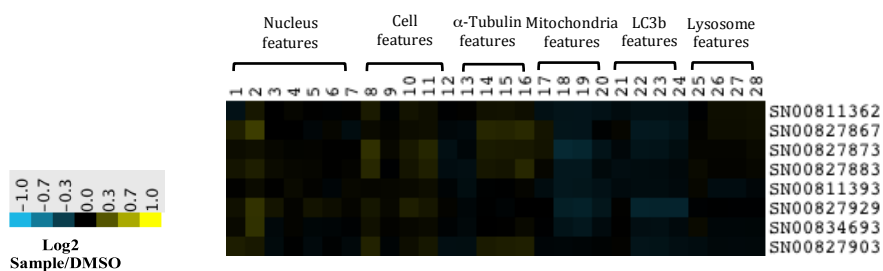


**Figure 4.6** Heatmap depicting the cytological profile of samples in biocluster 4, based on the log2 compound/DMSO ratio. Individual compounds are presented on the y-axis with individual features on the x-axis. The parameters are the same as described fully in Figure 4.2.

#### 4.3.2.5 Biocluster 5

Biocluster 5 was composed of 15 samples including one extract from herb 8, two fractions from herbs 6 and 11, and 12 compounds from herbs 1 (3), 4, 6, 8, 9 (2), 13, and 15 (3). The biocluster was characteristic with obvious decreases in the intensity of tubulin, mitochondria, LC3b, and lysosome makers associated with slight increases in parameters associated with cell shapes (Fig. 4.7).

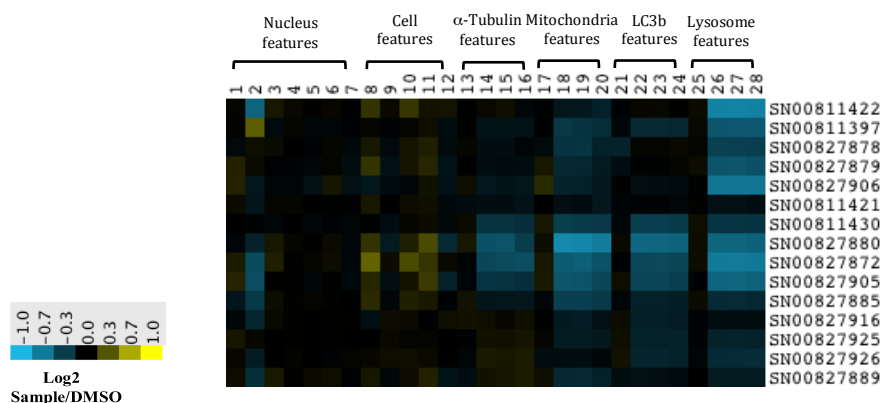


**Figure 4.7** Heatmap depicting the cytological profile of samples in biocluster 5, based on the log2 compound/DMSO ratio. Individual compounds are presented on the y-axis with individual features on the x-axis. The parameters are the same as described fully in Figure 4.2.

#### 4.3.2.6 Biocluster 6

Biocluster 6, the biggest cluster consisting of 85 samples, contained 11 extracts from herbs 2, 3, 7, 10-15, herb pairs 6+7, and 12+13, 21 fractions from herbs 1, 2 (4), 3, 6 (2), 8 (2), 9, 11, 14 (2), and 15, herb pairs 6+7 (2), 9+14, 10+11 (2), and 12+13, 45 compounds from herbs 1 (17), 2, 3 (2), 4 (2), 5 (3), 6 (3), 7, 8 (3), 9 (5), 11 (2), 12 (4), 13, and 14, and eight artificial mixtures from herbs 6 (2), 8, and 12, herb pairs 6+8 (2), 9+14, and 12+13. The biocluster featured the strong positive deviations of tubulin, mitochondria, LC3b, and lysosome marker intensity. An increase in nucleus marker intensity and a decrease in cell area were also observed (Fig. 4.8).

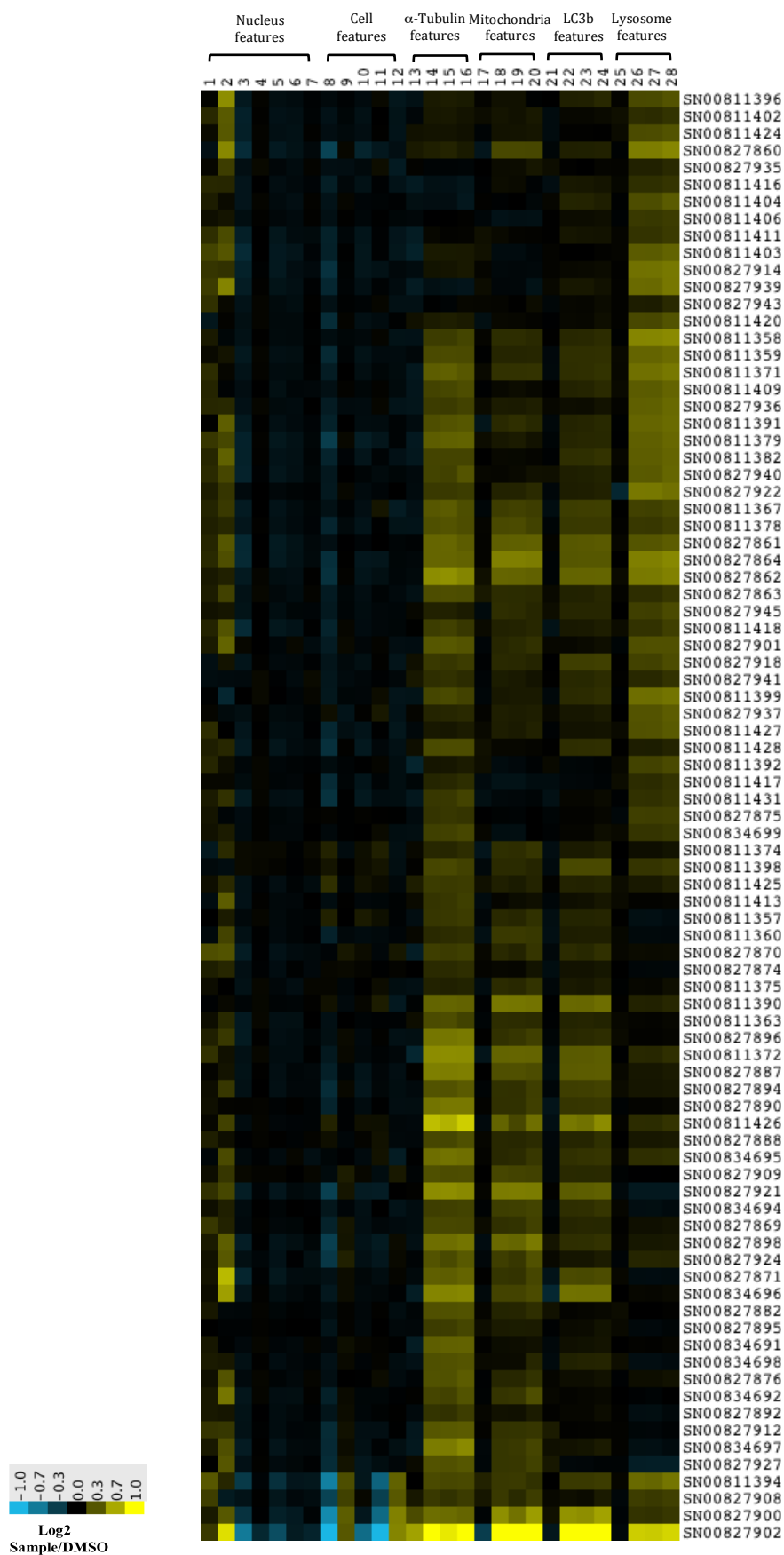


**Figure 4.8** Heatmap depicting the cytological profile of samples in biocluster 6, based on the log2 compound/DMSO ratio. Individual compounds are presented on the y-axis with individual features on the x-axis. The parameters are the same as described fully in Figure 4.2.

#### 4.3.2.7 Biocluster 7

Biocluster 7 contained 9 samples including two fractions from herb 8 and herb pair 6+8, and seven compounds from herbs 4 (1), 8 (2), 9 (1), 11 (2), and 13 (1). It did not show obvious changes on LC3b features. Positive deviations of tubulin and mitochondria marker intensity and negative deviations of lysosome marker intensity were observed (**Fig. 4.9**).

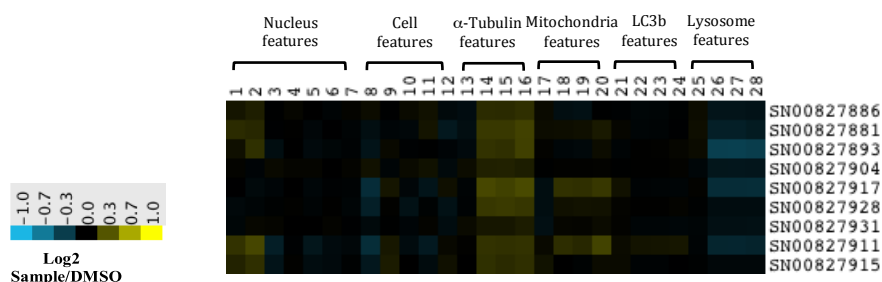


**Figure 4.9** Heatmap depicting the cytological profile of samples in biocluster 7, based on the log2 compound/DMSO ratio. Individual compounds are presented on the y-axis with individual features on the x-axis. The parameters are the same as described fully in Figure 4.2.

The clustering of all samples showed that nearly half of the samples (49.7%) could be grouped into biocluster 6, suggesting that these samples might have the same targets or the same pathway. It is reasonable given that all samples were obtained from the selected herbs targeting the brain disorders. The mechanism behind the profiling of the biocluster 6 might be common for drugs used to treat this type of diseases.

The pattern of deviations of intensity of tubulin, mitochondria, LC3b and lysosome were distinctly different from biocluster to biocluster. It is suggested that the mechanisms behind the bioclusters might be different but all associated with the effects on the subcellular organelles.

#### 4.3.3 Analysis of biological signatures from different respective

In order to explore the correlations among samples of different levels and between the individual herbs and the herb pair, comparison of phenotypic signatures were carried out.

#### 4.3.3.1 An overview

**Fig. 4.10** shows the phenotypic signatures of all samples, five groups of samples from every herb pair, 90 pure compounds, compounds from five herb pairs, and all extracts of herbs and herb pairs.

All samples showed effects on at least several parameters, especially on the intensity of tubulin, mitochondria, LC3b and lysosome, no matter they are extracts, fractions or pure compounds. The positive and negative deviations could be observed in every group of phenotypic signatures. Their biological signatures did not show the ability to discriminate extract, fraction or pure compound.

Comparison of five groups of phenotypic signatures from the five herb pairs (**Fig. 4.10B-F**) indicated that every herb pair had its own pattern, which depended on the properties of the constitutive herbs. For example, more negative deviations were observed for the group of herb pair 6+8 (**Fig. 4.10C**) when compared with that of herb pair 6+7 (**Fig. 4.10B**). The differences between these two herb pairs could be due to the fact that the samples from herb 8 showed more negative derivations than those from herb 7.

The group of phenotypic signatures from all extracts (**Fig. 4.10I**), the top level of samples, showed an average distribution of all samples. Of the eleven of the 24 extracts (45.8%) concentrated in the biocluster 6, eight were distributed in the biocluster 2 (2), biocluster 3 (4), biocluster 4 (2), and biocluster 5 (1), respectively, and four did not fall into any biocluster (**Table 4.2**). It is consistent with the fact that 49.7% of all samples were classified into the biocluster 6. In this view, the phenotypic signatures of all samples could be seen as an expansion from the 24 extracts to the fractions and pure compounds.

**Table 4.2** Extracts of 15 herbs and 5 herb pairs and their biocluster.

Extracts	Biocluster
Herb 1	*
Herb 2	6
Herb 2 <sup>a</sup>	3
Herb 3	6
Herb 4	*
Herb 5	3
Herb 6	*
Herb 6 <sup>a</sup>	*
Herb 7	6
Herb 8	3
Herb 8 <sup>a</sup>	5
Herb 9	4
Herb 10	6
Herb 11	6
Herb 12	6
Herb 13	6
Herb 14	6
Herb 15	6
Herb pair 6+7	6
Herb pair 6+8	3
Herb pair 6+8 <sup>a</sup>	4
Herb pair 9+14	2
Herb pair 10+11	2
Herb pair 12+13	6

\* Not fall into any biocluster; <sup>a</sup> Water extract.

The phenotypic overview of different groups of samples indicated the complexity of TCM. An in-depth exploration into the relationship between extracts, fractions and pure compounds were carried out.

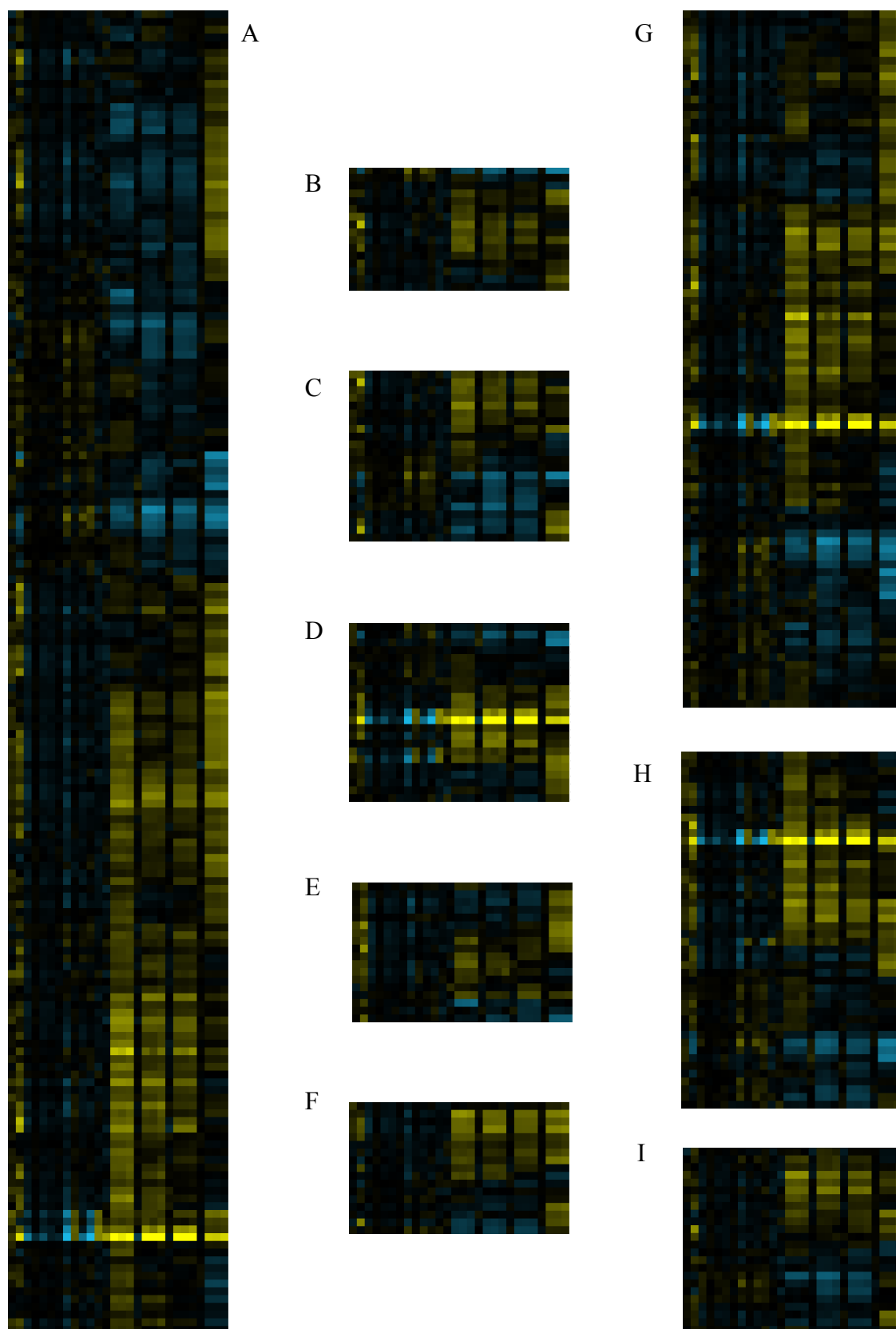
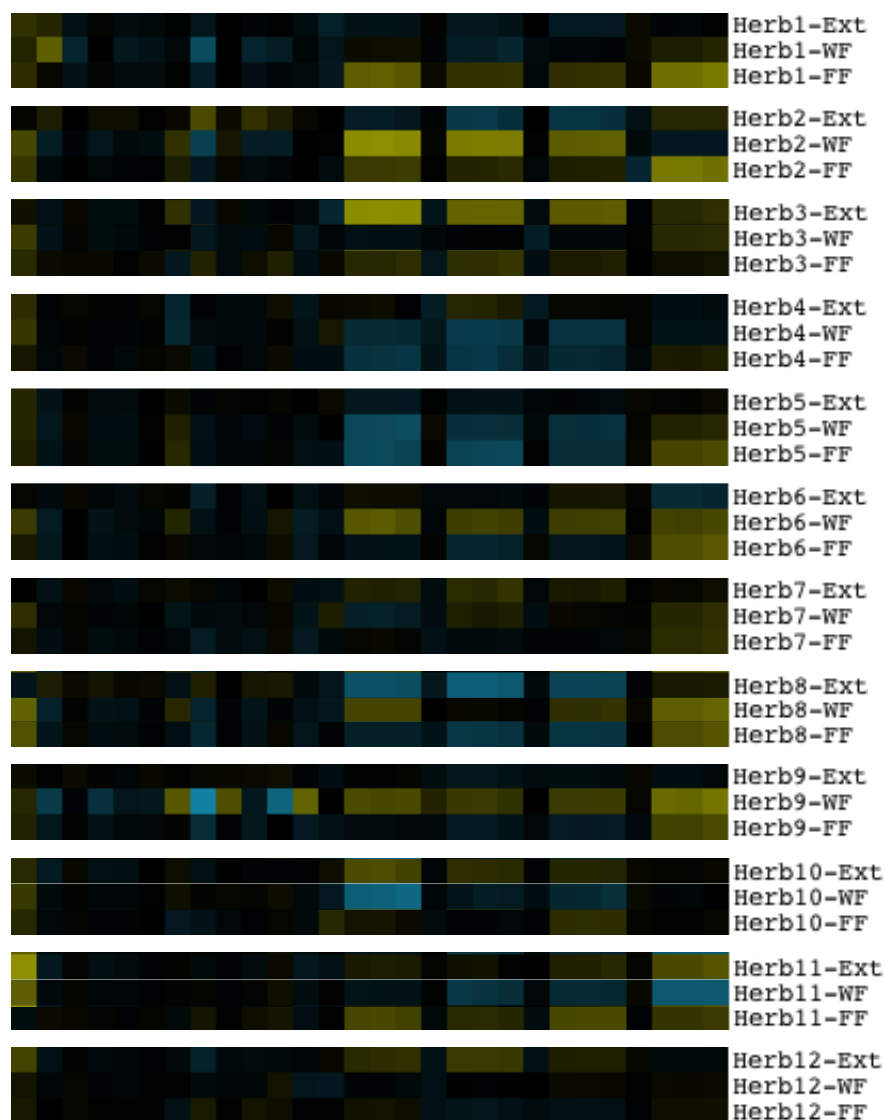


**Figure 4.10** Heatmap depicting the cytological profiles of 171 TCM samples (A), samples from five herb pairs 6+7 (B), 6+8 (C), 9+14 (D), 10+11 (E), and 12+13 (F), and 90 pure compounds (G), 46 compounds from 5 herb pairs (H), and the extracts of 15 herbs and 5 herb pairs (I).

#### 4.3.3.2 Extract VS fraction

The flowchart (**Fig. 3.2**) indicated that an extract was separated into one water-soluble fraction and one fat-soluble fraction through column chromatograph over C18. Such fractionation guarantees that the overwhelming majority of chemicals in the extract could be kept in these two fractions with the minimum loss. From the perspective of the chemical composition there was a correlation of addition between the extract and its two fractions. However, their biological signatures did not show such a correlation.

Phenotypic signatures of the extract and its two fractions were extracted from **Fig. 4.2** and sorted in **Fig. 4.11** according to the herb and the herb pair.



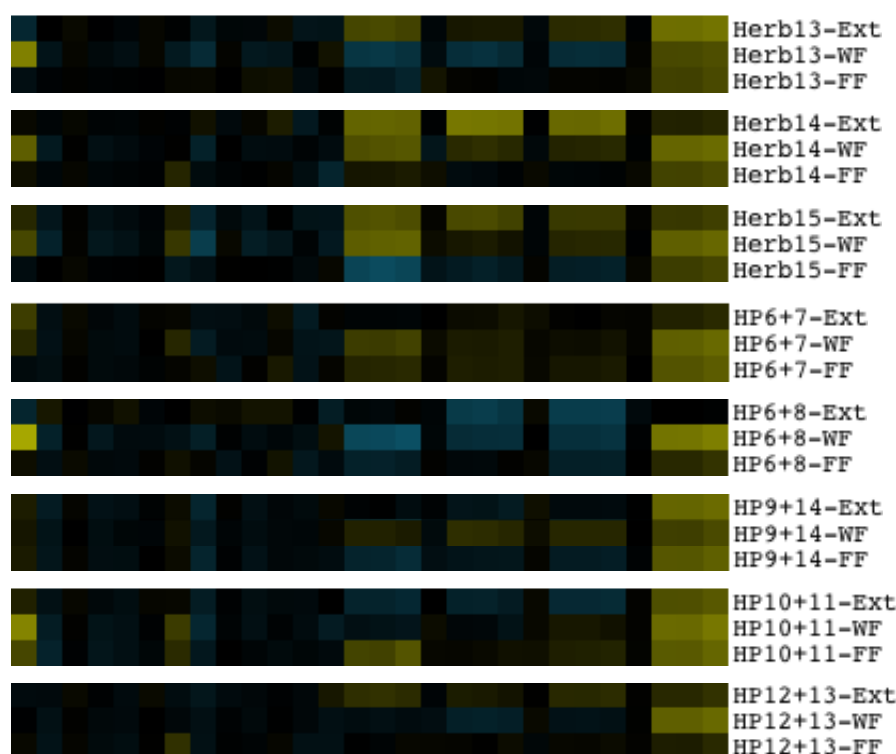


**Figure 4.11** Phenotypic signatures of the extract and its fractions obtained from 15 herbs and 5 herb pairs. HP–herb pair; Ext–extract; WF–water-soluble fraction; FF–fat-soluble fraction.

The results revealed that all the extracts and the fractions showed obvious deviations except for the extracts of herb 1 and herb 9, which suggested that the concentration of the extract and fraction (10 mg/mL and 5 mg/mL) we used were appropriate for most samples to give the biological responses. The extracts with small responses might be due to the concentration of the sample or the antagonistic effect caused by the combination of two fractions.

In addition, the biological correlations between an extract and its fractions were quite complicated. Take herb 2 as an example, the water-soluble fraction showed strong positive effects on the tubulin, mitochondria and LC3b intensity, the fat-soluble fraction exhibited strong positive effects on the lysosome parameters, while the extract showed negative deviations of mitochondria and LC3b makers and small positive deviations of tubulin and lysosome markers. It is obvious that there was not a simple additive or synergistic effect for the extract, and the effect on different subcellular organelle might be different.

#### 4.3.3.3 Fraction VS compound

The correlations between the fraction and the compounds of the same herb or the same herb pair were also complicated. In some cases, the major compounds seemed to play a predominant role in the biological signature of the fraction, e.g. herb 1, herb 2, and herb 3.

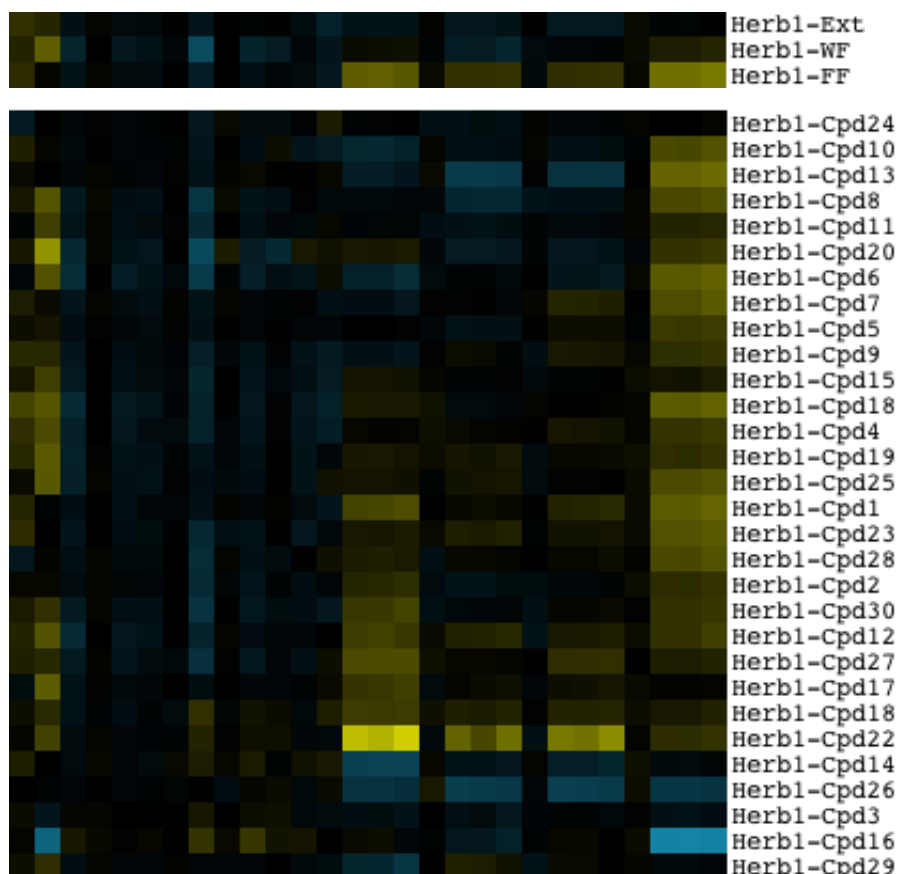


**Figure 4.12** Phenotypic signatures of the extract, fractions and 30 compounds obtained from herb 1. Ext–extract; WF–water-soluble fraction; FF–fat-soluble fraction; Cpd–compound. The numbers after Cpd are consistent with those in Table 3.3.

In terms of 30 compounds from herb 1, 17 of them were distributed in the biocluster 6, and the rest were in other bioclusters: 3 in the biocluster 1, 4 in the biocluster 2, 1 in the biocluster 3, and 3 in the biocluster 5 (**Fig. 4.12**). The ELSD-HPLC analysis showed that the ginsenosides were all included in the fat-soluble fraction (**Fig 3.5**). Taking all the above information into consideration, the phenotypic signature of the fat-soluble fraction was reasonable to show the characteristic features of the biocluster 6. In fact, the fat-soluble fraction fell into the biocluster 6 while the

water-soluble fraction was in the biocluster 1.

Additionally, ginsenosides Rf (**3**), Rb1 (**5**), Re (**10**) and Rg1 (**11**) are the major compounds but they showed weaker phenotypic responses compared with the minor ones such as pseudoginsenoside RT15 (**16**) and *S*-ginsenoside Rh2 (**22**). The same phenomena could also be observed in other herbs. Dihedrotanshinone I (**59**) was a minor compound of herb 9 but exhibit the strongest responses of all 171 samples. The results suggested that we could find the minor component from a plant with significant bioactivities, and that is what we did in the past looking for drug leads. At the same concentration, the minor compounds showed stronger effects than the major ones, which was also the results we got from the phenotypic screening. In the screening, the concentration of 10  $\mu$ M was used for every compound, and the results revealed that the minor compounds like compounds **16**, **22** and **59** showed the strong responses and the major one only exhibited the mild activity. However, it does not mean the minor compounds rather than the major ones contribute more to the bioactivity of an herb. In many cases, the content of the minor compounds in an herb is so low that they, even with strong effects, contribute little to the overall bioactivity when compared with the major ones.

Lobetyolin (**31**) is the characteristic component of herb 2, and it showed very similar phenotypic signatures to that of the fat-soluble fraction, having positive deviations of tubulin, mitochondria, LC3b, and lysosome marker intensity, especially the strong effects on the lysosome markers (**Fig. 4.13A**).

Paeoniflorin (**32**) is the major compound of herb 3, and it showed weak positive deviations of tubulin, mitochondria, and LC3b marker intensity, very similar with those of the fat-soluble fraction (**Fig. 4.13B**).

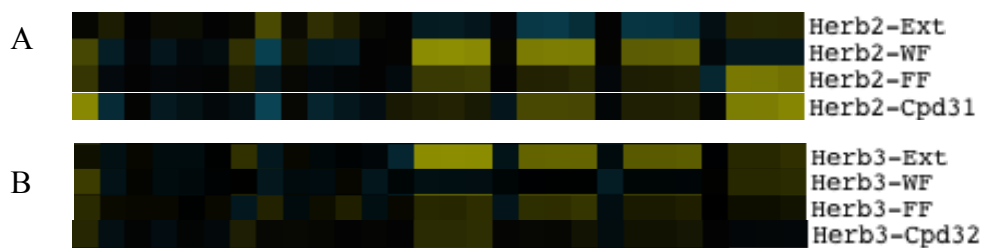


**Figure 4.13** Phenotypic signatures of the extract, fractions and characteristic compounds obtained from herb 2 (A) and herb 3 (B). Ext–extract; WF–water-soluble fraction; FF–fat-soluble fraction; Cpd–compound. The numbers after Cpd are consistent with those in Table 3.3.

It should be pointed out that ginsenosides, lobetyolin and paeoniflorin are characteristic compounds of herb 1, herb 2, and herb 3, respectively, and in Chinese Pharmacopoeia they are used for identification and quality control of the respective raw material.<sup>8</sup> Our results showed that a single compound or a group of compounds exhibited the similar biological behaviors on multiple parameters with those of the extract or fraction, which provided evidences to support the usage of these compounds to reflect the biological effects of the raw material.

Controversial signatures were also found in some other cases. Compounds **39-41** are three major compounds obtained from herb 5 (**Fig. 4.14**). All these three compounds showed obvious positive effects on tubulin, mitochondria, and LC3b parameters while the water-soluble and fat-soluble fractions exhibited strong negative deviations of these parameters. It might to be due to the existence of other compounds with strong negative deviations or the interactive effects caused by the combination of these major compounds.

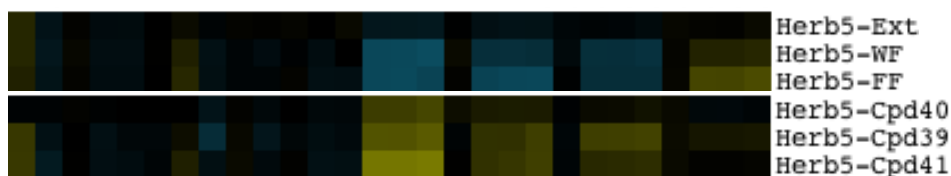


**Figure 4.14** Phenotypic signatures of the extract, fractions and characteristic compounds obtained from herb 5. Ext–extract; WF–water-soluble fraction; FF–fat-soluble fraction; Cpd–compound. The numbers after Cpd are consistent with those in Table 3.3.

#### 4.3.3.4 Impact of stereochemistry

The phenotypic signatures of the ginsenosides also revealed the impact of

stereochemistry on the biological behaviors. Compounds **18** and **21**, **17** and **29**, and **19** and **22** are three pairs of *R/S* stereoisomeric compounds, which share the same planar structure and are isomerized only at C-20, respectively (for structures see **Fig. 3.3**), but their phenotypic signatures indicated big differences (**Fig. 4.15**). Compound **18** with the 20*R*-configuration displayed obvious positive deviations of tubulin marker intensity while compound **21** with the 20*S*-configuration showed strong positive deviations of lysosome marker intensity. Compound **22** (20*S*) showed strong effects on tubulin, mitochondria, and LC3b parameters while compound **19** (20*R*) showed little effect on the same parameters. Compound **17** (20*R*) exhibited positive deviations of tubulin marker intensity, and compound **29** (20*S*), in contrast, showed negative ones.

In addition, the racemic mixture showed different biological responses with the non-racemic compound. Compounds **20** and **27** are racemic protopanaxatriol and ginsenoside Rg2, respectively, and their biological signatures showed obvious differences from those of *R*-protopanaxatriol (**30**) and *R*-ginsenoside Rg2 (**28**) (**Fig 4.15**). The racemic **20** showed an increase in the intensity of nucleus and lysosome marker while 20*R*-configured **30** showed an increase in the intensity of lysosome and tubulin marker. The racemic **27** exhibited positive deviations of tubulin and LC3b marker intensity while the 20*R*-configured **28** only showed obvious positive deviations of lysosome marker.

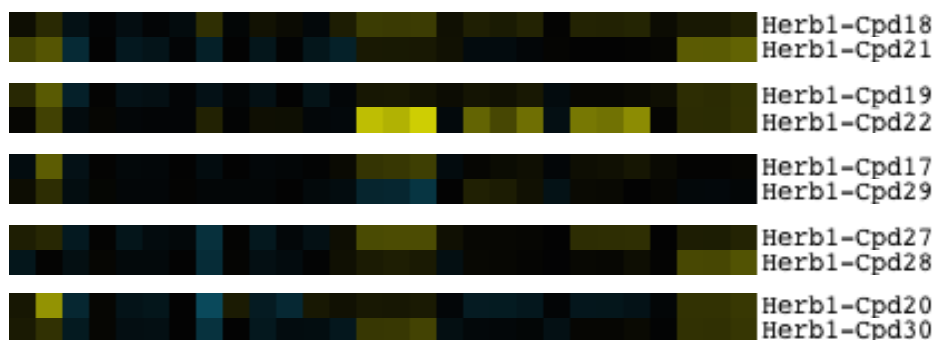


**Figure 4.15** Phenotypic signatures of three pairs of stereoisomeric compounds and two pairs of racemic and non-racemic compounds obtained from herb 1. Cpd-compound. The numbers after Cpd are consistent with those in Table 3.3.

The results provide evidence for the known fact that the stereochemistry of a compound is crucial for its bioactivities. The chiral carbon or the racemization could impact a lot on the biological behaviors of a molecule.

#### 4.3.3.5 Impact of extract method

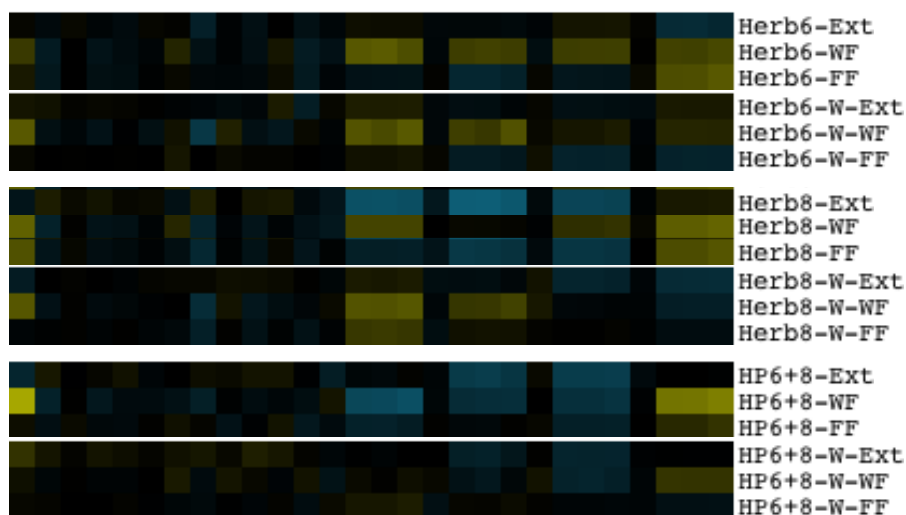


**Figure 4.16** Phenotypic signatures of the extract and fractions obtained from herb 6, herb 8 and herb 6+8 using ethanol and water extraction. Ext–extract; WF–water-soluble fraction; FF–fat-soluble fraction; W–water extraction method.

Considering the chemical differences caused by the different extraction methods (section 3.2.4), the phenotypic signatures of the extract and fractions of herb 6, herb 8 and herb pair 6+8 were compared (Fig. 4.16). A detailed comparison of the log<sub>2</sub> ratio values of the extracts is depicted in Fig. 4.17.

The results showed that there were obvious phenotypic differences observed for samples prepared from two extraction methods. The biggest differences were observed on herb 8. The two extracts exhibited opposite deviations of the intensity of tubulin and lysosome markers. Compared with the water extract, the ethanol extract showed stronger effects on almost all parameter except for those on lysosome markers. The log<sub>2</sub> ratio values of the tubulin, mitochondria and LC3b parameters of the ethanol extract were 2-5 fold than those of the water extract but the lysosome values of the ethanol extract were about half of those of the water extract.

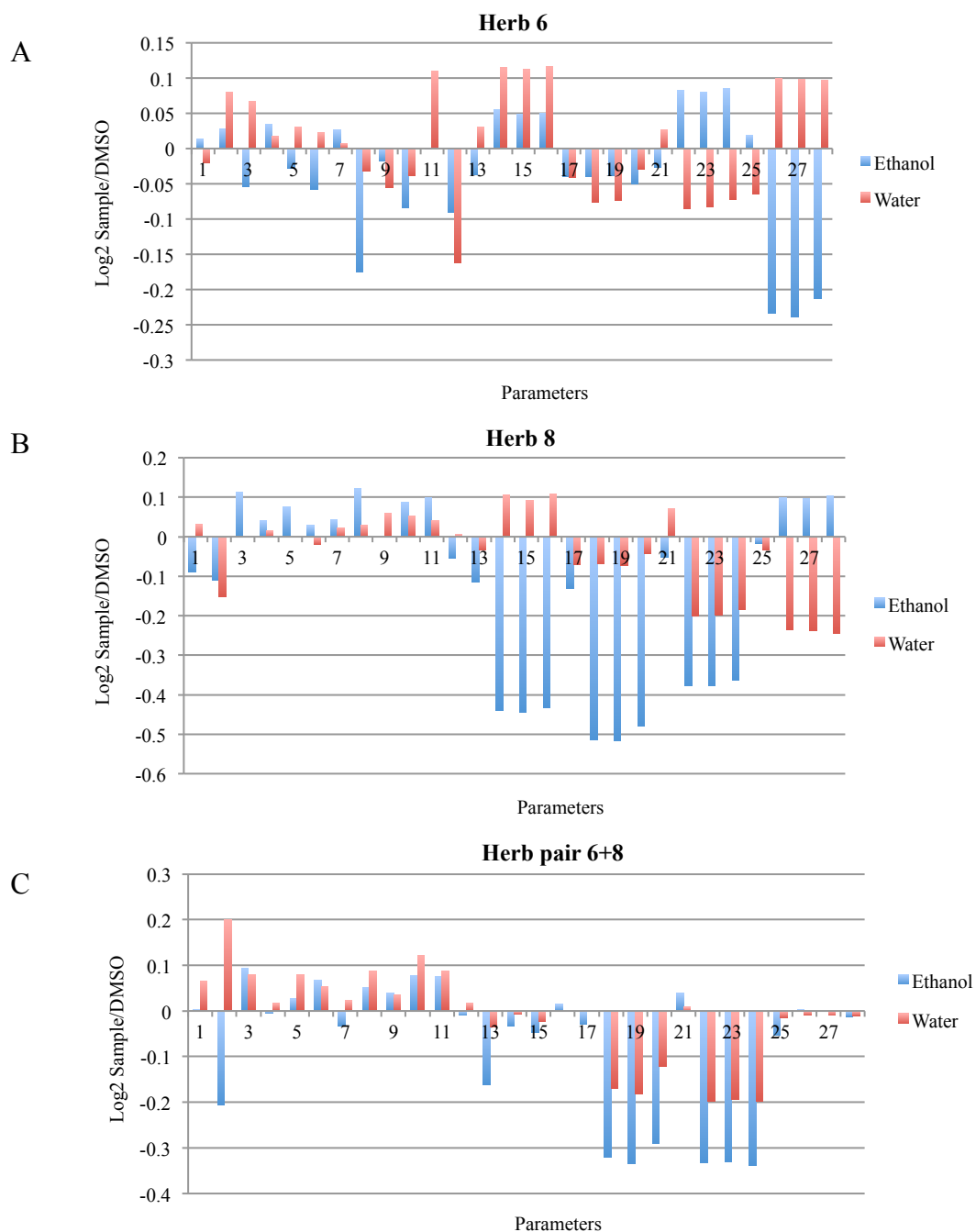


**Figure 4.17** Bar charts of log2 ratio values of the extracts of herb 6 (A), herb 8 (B), and herb pair 6+8 (C) using ethanol (Blue) and water (Red) extraction methods. The parameters are the same as described fully in Figure 4.2.

The impact of extraction method was also observe for herb 6, but not as strong as that on herb 8. The ethanol and water extracts of herb 6 showed opposite deviations of nucleus texture, area, width and length, tubulin texture, and especially the LC3b and lysosome parameters. The negative effect on the lysosome marker intensity of the ethanol extract was two-fold stronger than that of the water extract from the perspective

of the log<sub>2</sub> ratio value.

The differences were also observed for the herb pair 6+8. They showed consistent deviations on all parameter except for the significant opposite deviations of the nucleus marker intensity. Compared with herb 6 and herb 8, the herb pair showed small deviations of the tubulin and lysosome marker intensity, which might be ascribed to the opposite effects of that caused by herb 6 and herb 8 on the same parameters. In addition, the intensity of the deviations between the two methods for the herb pair was much closer when compared with those of the individual herbs. That means, when two herbs were combined, the impact of the extraction method on the bioactivities could decrease. The biological behavior of the herb pair might be more stable than that of the individual herb.

An examination of the biological responses and the chemical composition (see **Section 3.2.4**) revealed that there was a direct correlations between the samples prepared with different methods. The ethanol method could afford more low-polarity chemical constituents while the water method could provide more high-polarity chemicals (**Table 3.4**). The ethanol extract had the biggest impact on herb 8 because it was rich in volatile oil, a group of small molecules with low polarity.<sup>9</sup> The HPLC-ELSD analysis (**Fig. 3.13**) clearly shows that these low-polarity constituents were predominant in the ethanol extract while they were almost invisible in the water extract. Comparison of the phenotypic signatures of these two extracts implied that these constituents might be responsible for the significant negative deviations observed (**Fig. 4.17B**). The stronger negative deviations observed for the herb pair sample prepared from the ethanol method rather than the water method also supported such an elucidation. The low-polarity constituents from herb 8 were also observed as the predominant components in the ethanol extract of the herb pair (**Fig. 3.13**), although the content of the low-polarity constituents in the herb pair was lower than that in herb 8

(Table 3.4).

The results suggested that the extraction method had an impact on the chemical and biological behaviors of the herb and the herb pair, but its intensity was related to the properties of the material. Compared with the individual herbs, the extraction method had less effect on the herb pair. The biological phenotypes of herb pair 6+8, with major changes only related to intensity, were much more stable than those of herb 6 and herb 8, when comparing the biological signatures of extracts from different methods.

4.3.4 Analysis of herb and herb pair

As mentioned, herb pair is the simplest form of a formula, and also a starting point to explore the essence of TCM. The biological effects of the herb pair depend on the properties of the individual herbs and the interactive effects caused by the combination of two herbs.

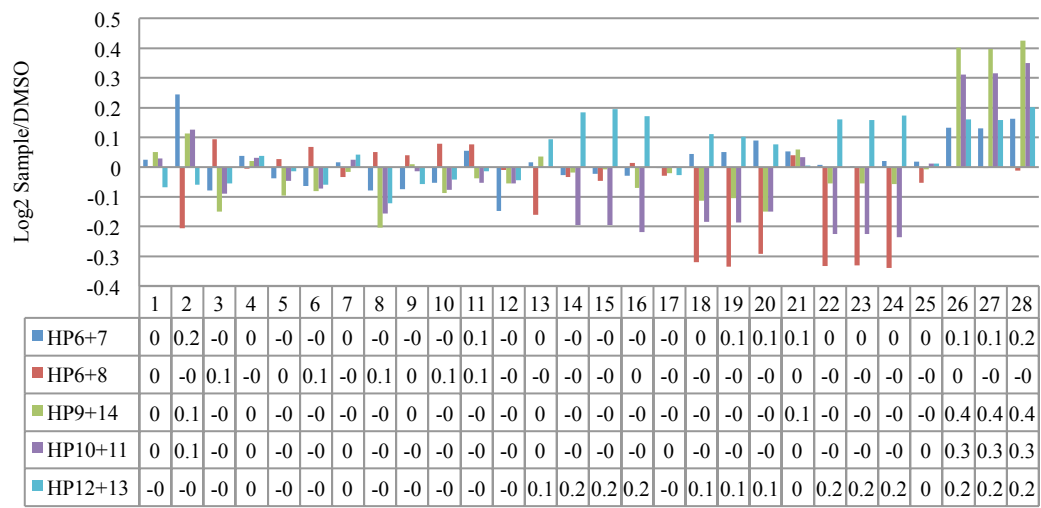


Figure 4.18 Bar charts of log2 ratio values of the extracts of five herb pairs. The parameters are the same as described fully in Figure 4.2.

The bar chart based on the log2 ratio values of five herb pairs are depicted in Fig. 4.18. Since all herb pairs were used to treat the diseases related to brain disorders, their extracts exhibited phenotypic signatures of different patterns. The common feature was observed for the lysosome marker intensity (parameters 25-28), almost all having positive deviations. In a general view, the five extracts showed relatively big effects on

the intensity of nucleus, tubulin, mitochondria, LC3b, and lysosome marker and small effects on their texture, indicating all of them had effects on DNA and the cellular organelles but with few changes on their structures.

In the following, the phenotypic signatures generated by every herb pair and its constitutive herbs were analyzed in detail.

#### 4.3.4.1 Herb pair 6+7

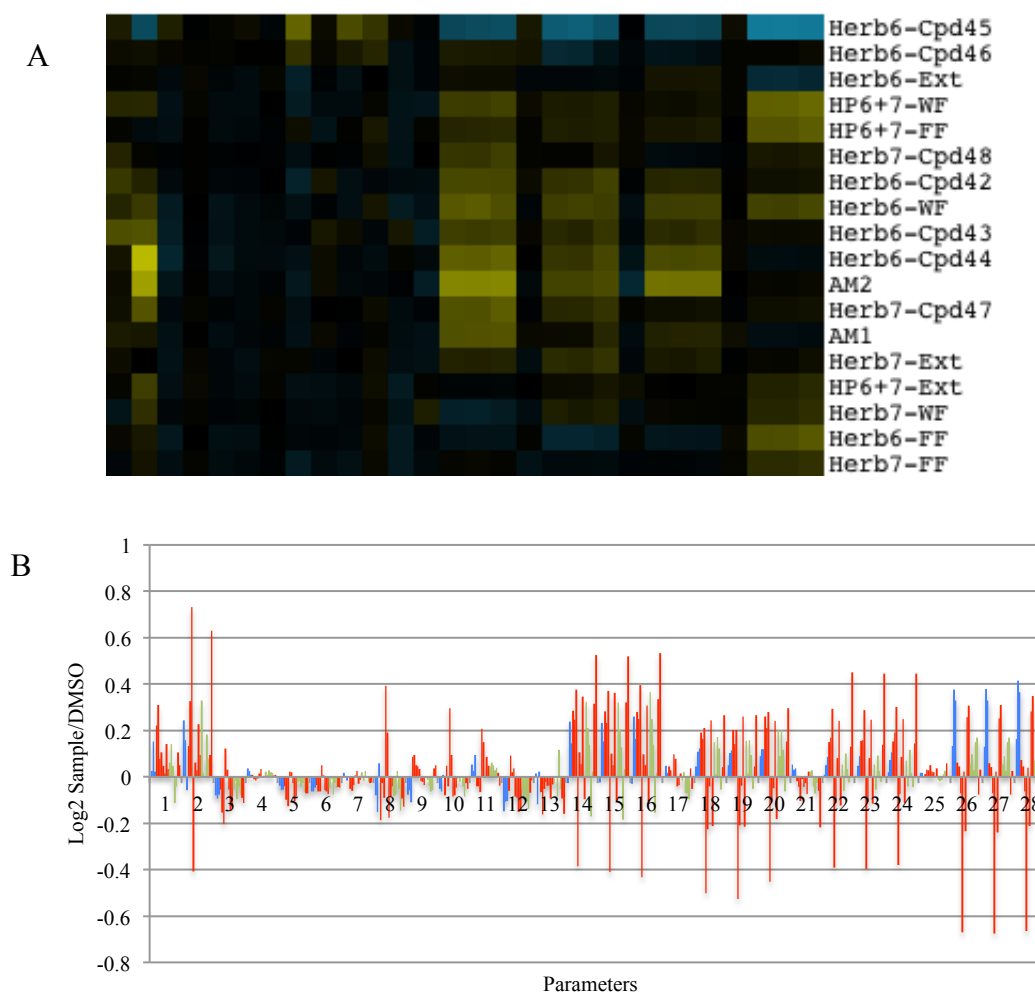


**Figure 4.19** Phenotypic signatures of all samples from herb 6, herb 7 and herb pair 6+7 (A), and bar chart of log2 ratio values of samples from herb 6 (red), herb 7 (green) and herb pair 6+7 (blue) (B). The parameters are the same as described fully in Figure 4.2.

Herb pair 6+7 consists of herb 6, Gastrodiae Rhizoma, and herb 7, Ramulus Uncariae Cum Uncis, in a ratio of 3:4. A total of 18 samples were obtained from herb 6, herb 7 and the herb pair 6+7, including three extracts, six fractions, seven compounds, and two artificial mixtures. Eleven of them were grouped in biocluster 6, two in biocluster 2, one in biocluster 4 and one in biocluster 5. Their phenotypic signatures and

bar chart of log2 ratio values are shown in **Fig. 4.19**.

The bar chart of all samples (**Fig. 4.19B**) shows the deviations of most samples ranged from -0.6 to 0.6. The deviations with  $|\log_2 \text{ ratio value}|$  more than 0.2 concentrated on the marker intensity of nucleus, tubulin, mitochondria, LC3b, and lysosome. The big negative changes came from the effects of compound **45**, the extract, and the fat-soluble fraction obtained from herb 6. The effects on the parameters associated with textures of nucleus, tubulin, mitochondria, LC3b, and lysosome, as well as those related to the nucleus and cell shapes, were much smaller, especially those of the herb pair.

A detailed examination of the extracts of herb 6, herb 7 and herb pair 6+7 indicated that they showed effects with the log2 ratio values ranging from -0.2 to 0.2 (**Fig. 4.20**). At the level of extract, the herb pair did not show a clear correlation with its individual herbs. On tubulin and LC3b intensity, both herb 6 and herb 7 showed positive effects, but the herb pair had minimal influence on these parameters. The changes observed for the herb pair on the lysosome intensity was opposite to that for herb 6. The herb pair showed an obvious increase on the nucleus intensity while herb 6 and herb 7 did not. It was obvious that the effect pattern of the herb pair were quite different from that of the individual herb.

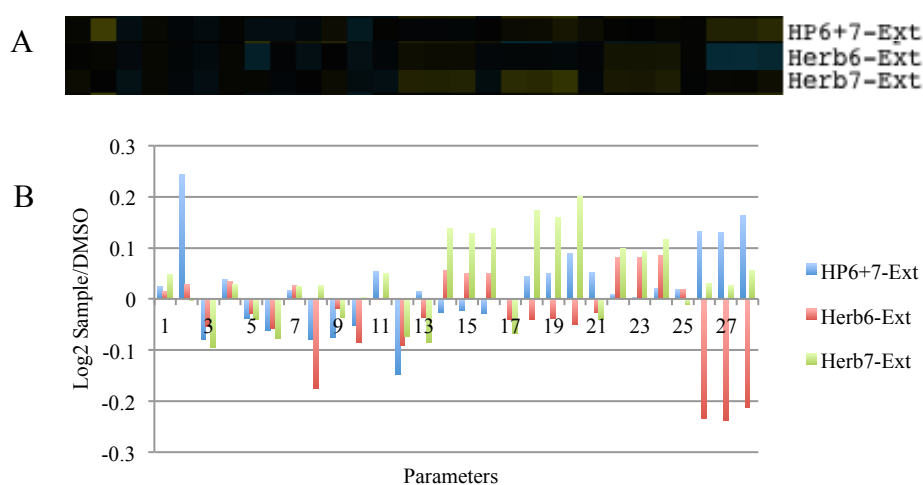


**Figure 4.20** Phenotypic signatures of extracts of herb 6, herb 7 and herb pair 6+7 (A), and bar chart of log2 ratio values of the extracts of herb 6, herb 7 and herb pair 6+7. The parameters are the same as described fully in Figure 4.2.

An in-depth investigation was done on the major compounds of herb 6. Gastrodin (**42**) is a major compound isolated from herb 6, and used as the standard compound for the identification and quality control of the raw material.<sup>10</sup> Parishine derivatives (**43-46**) are also obtained from herb 6 and shown as four main peaks in the HPLC-ELSD chromatogram of the fat-soluble fraction of herb 6 (**Fig. 3.9**). The comparison of gastrodin (**42**) and the extract of herb 6 revealed that they did fit well except for the decreases on the parameter of cell area (**Fig. 4.21A**). Compound **42** showed increases on nucleus texture and intensity, and the intensity of tubulin, mitochondria and LC3b markers ( $\log_2$  ratio  $> 0.1$ ) while the extract exhibited a big decrease ( $\log_2$  ratio  $< -0.2$ ) on the lysosome intensity.

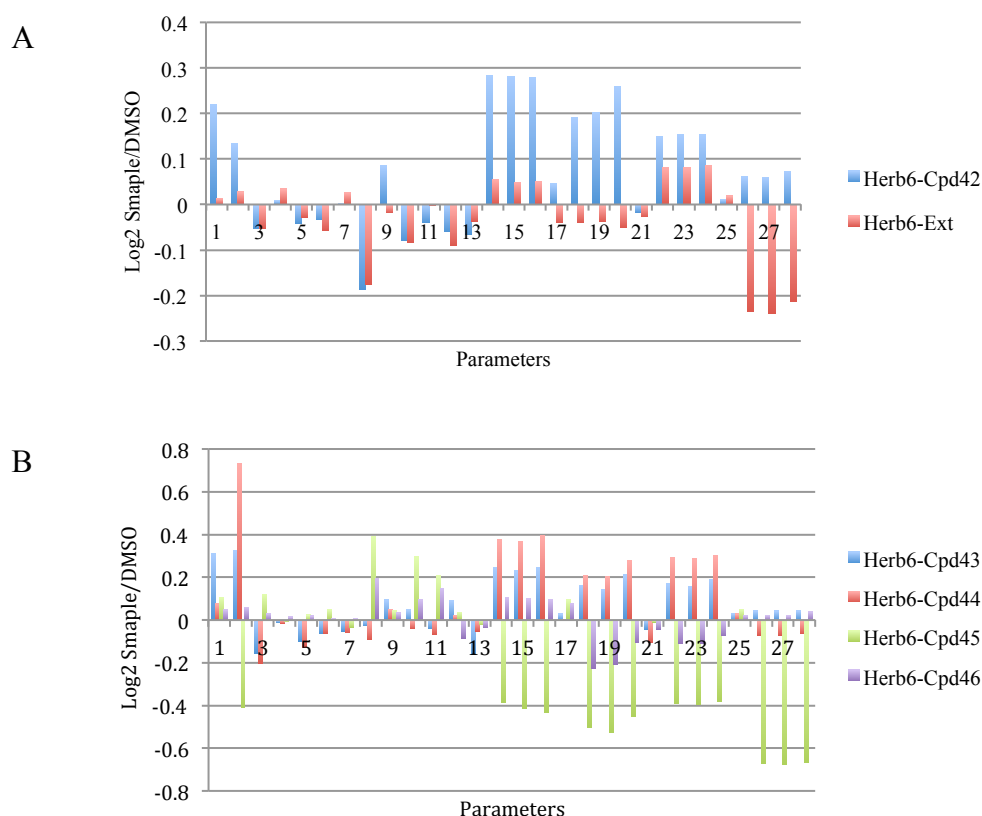


**Figure 4.21** Bar chart of  $\log_2$  ratio values of gastrodin (**42**) and the extract of herb 6 (A), and bar chart of  $\log_2$  ratio values of compounds **43-46**. The parameters are the same as described fully in Figure 4.2.

The phenotypic data of other major compounds (**Fig. 4.21B**) indicated that compounds **43** and **44** presented a quite similar pattern with that of compound **42**. The

effects of compound **46** on all parameters were comparatively small. Compound **45**, different from other parishines, showed strong negative deviations ( $\log_2$  ratio  $< -0.4$ ) of intensity of nucleus, tubulin, mitochondria, LC3b and lysosome markers.

In terms of the lysosome marker intensity, compounds **42-44** and **46** showed small deviations ( $|\log_2$  ratio|  $< 0.1$ ) while compound **45** had strong negative deviations ( $\log_2$  ratio  $< -0.6$ ), suggesting that the negative effects of the extract of herb 6 might come from compound **45**. Furthermore, the positive deviations of tubulin, mitochondria and LC3b intensity from compounds **42**, **43**, and **44** and corresponding negative deviations from compound **45** might contribute to the small deviations of the extract of herb 6 on these parameters.

The phenotypic signatures of the artificial mixtures AM1 and AM2 could support such an assumption. AM1 and AM2 were prepared according to the ratio of major compounds **42**, **43**, **44**, and **46** in the fat-soluble fraction of herb 6 (**Fig. 3.9** and **Table 3.5**). The AM2 mixture was deprived of gastrodin (**42**) in order to examine its influence on the bioactivity. Both were designed to mimic the chemical composition of herb 6 in order to reflect the impact of the major compounds on the biological behaviors of the mixture. Due to the low content of compound **45** as shown in the HPLC-ELSD chromatogram (**Fig. 3.9**), compound **45** was not included in the artificial mixtures when preparing AM1 and AM2.

**Fig. 4.22** illustrates that both AM1 and AM2 showed big increases on the tubulin, mitochondria and LC3b intensity and very small ones on the lysosome intensity, which proved that compound **45** rather than other compounds provided the negative effects on the lysosome intensity to herb 6. In addition, their phenotypic signatures of AM1 and AM2 indicated that the effects of AM2 were much stronger than those of AM1 on most parameters, implying that the presence of gastrodin countered the effects of the mixture.

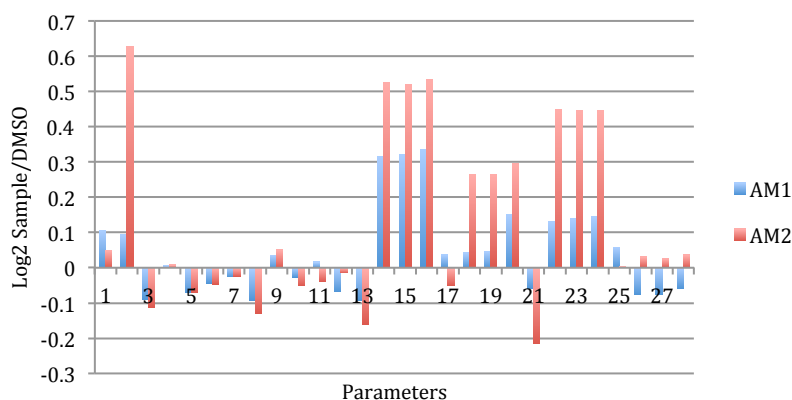


**Figure 4.22** Bar chart of log2 ratio values of artificial mixtures AM1 and AM2. The parameters are the same as described fully in Figure 4.2.

In order to explore the correlation between the artificial mixture and the pure compounds, we assumed a virtual artificial mixture that mimics exactly the chemical composition of the actual artificial mixture but its biological activity shows a simple addition of the phenotypic values of the individual compounds. On the basis of the log2 ratio values of individual compound and the ratio in the mixture, the values of the mimic artificial mixture on different parameters could be calculated.

For example, the mean values of the nucleus marker texture of compounds **42**, **43**, **44** and **46** were 0.01812, 0.01928, 0.01641 and 0.01609, respectively. AM1 consisted of 43.5% of **42**, 21.7% of **43**, 14.5% of **44**, and 20.3% of **46** (**Table 3.5**). Then, the values of the nucleus marker texture of the mimic AM1 should be  $0.01812 \times 43.5\% + 0.01928 \times 21.7\% + 0.01641 \times 14.5\% + 0.01609 \times 20.3\% = 0.01771$ , and its log2 sample/DMSO value is  $\text{Log}_2 0.01771/0.01556 = 0.18726$ . Similarly, AM2 was composed of 38.5% of **43**, 25.6% of **44**, and 35.9% of **46** (**Table 3.5**). The values of the nucleus marker texture of the mimic AM2 should be  $0.01928 \times 38.5\% + 0.01641 \times 25.6\% + 0.01609 \times 35.9\% = 0.01740$ , and its log2 sample/DMSO value is  $\text{Log}_2 0.01740/0.01556 = 0.16150$ . The log2 ratio values of other parameters for the mimics were calculated using the same method.

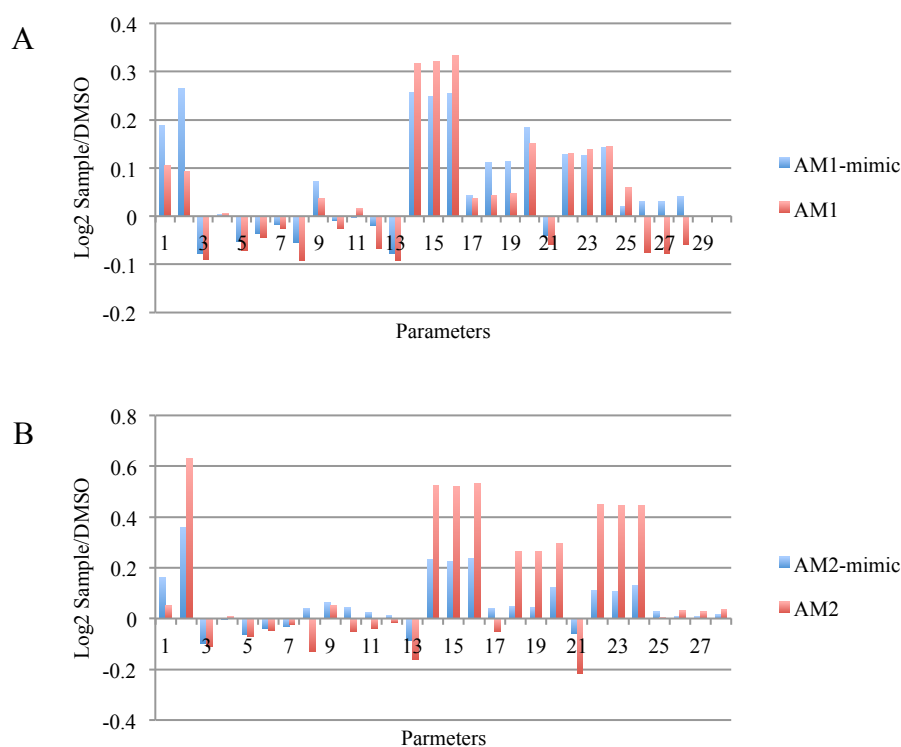


**Figure 4.23** Bar chart of log<sub>2</sub> ratio values of AM1 and its mimic (A), and AM2 and its mimic (B). The parameters are the same as described fully in Figure 4.2.

Comparison of AM1 and its mimic (**Fig. 4.23A**) and AM2 and its mimic (**Fig. 4.23B**) were carried out. AM1 and its mimic showed accordant positive and negative effects on most parameters. For the LC3b parameters, the calculated data were in line with the experimental data of AM1. At the same time, compared with its mimic, AM1 showed a stronger effect on the tubulin parameters, and weaker effect on the parameters of texture and intensity of nucleus and mitochondria, indicating that its effect was synergistic on the former, and antagonistic on the latter. In contrast, AM2 showed a different pattern when compared with its mimic. The absence of gastrodin increased the effects of AM1 on intensity of nucleus, tubulin, mitochondria, and LC3b makers. The obvious synergistic effects could be observed on these parameters.

The results demonstrated that the combination of several compounds could result in complicated biological responses when compared with the individual compounds. On different parameters, the mixture might exhibit synergistic effect, antagonistic effect, or additive effect. The presence of gastrodin played a tricky role in the overall effect

pattern of the mixture. Without gastrodin, the combination showed the synergistic effect on almost all parameters, while with gastrodin, the combination showed discriminative effects on different parameters.

Rhynchophylline (**47**) and isorhynchophylline (**48**) are two characteristic constituents isolated from herb 7, and isorhynchophylline (**48**) is used as the standard compound for the identification of the raw material.<sup>11</sup> Both compounds (**Fig. 4.24**) showed obvious positive deviations of the tubulin intensity ( $\log_2$  ratio  $> 0.1$ ), but only compound **47** exhibited positive deviations of the mitochondria intensity. Compound **47** had a positive effect on the nucleus texture while **48** showed a significant increase on the nucleus intensity. Again, the stereochemistry exhibited influences on the biological behaviors.

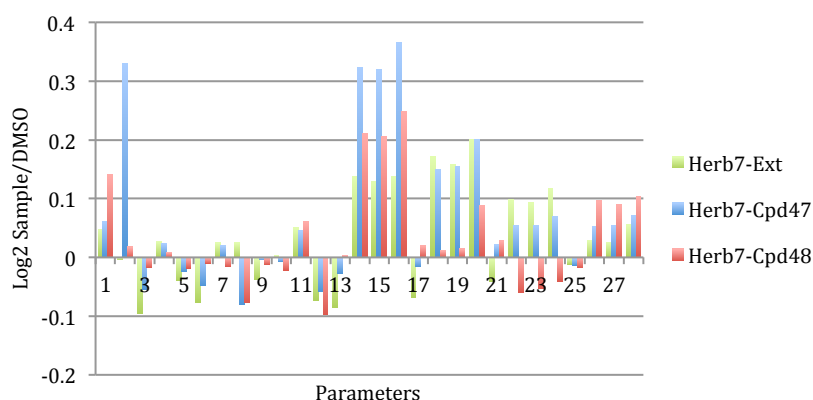


**Figure 4.24** Bar chart of  $\log_2$  ratio values of the extract of herb7 and compounds **47** and **48** isolated from herb 7. The parameters are the same as described fully in Figure 4.2.

When compared with the extract, the similar increases on the tubulin intensity was observed for both compound **48** and the extract, but on the other parameters, these two did not show a big similarity. On the other hand, compound **47** showed similar effect with the extract on the intensity of mitochondria and LC3b. The results did not support that compound **47** was used alone as a chemical standard for the quality control of herb 7. The combination of effects of both **47** and **48** showed a high likelihood with that of the extract.

#### 4.3.4.2 Herb pair 6+8

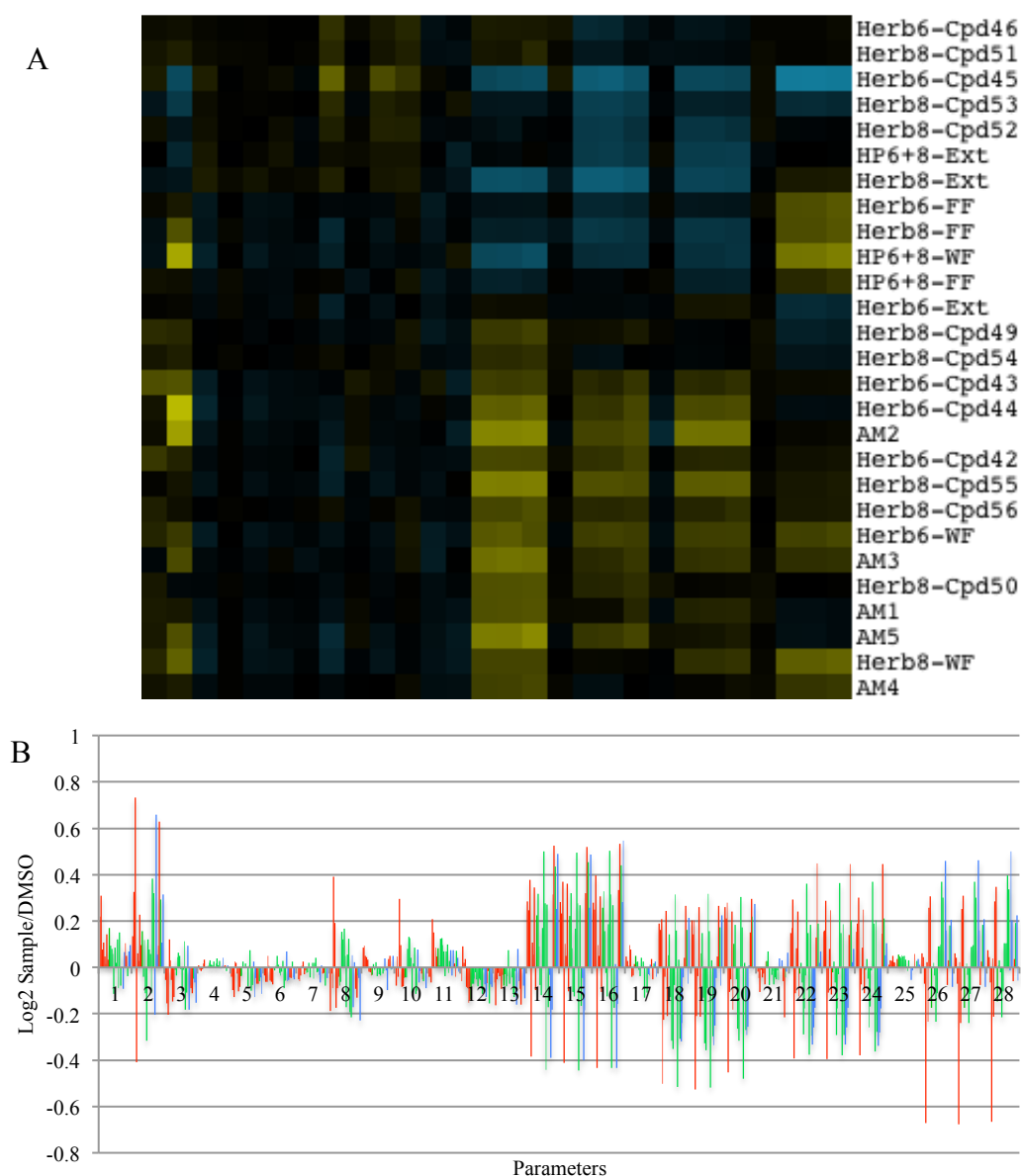


**Figure 4.25** Phenotypic signatures of all samples from herb 6, herb 8 and herb pair 6+8 (A), and bar chart of log2 ratio values of samples from herb 6 (red), herb 8 (green) and herb pair 6+8 (blue) (B). The parameters are the same as described fully in Figure 4.2.

Herb pair 6+8 is composed of herb 6 and herb 8, Chuanxiong Rhizoma, in a ratio of 1:4. A total of 27 samples were obtained including three extracts, six fractions, 13 compounds, and five artificial mixtures. Thirteen of them were grouped in biocluster 6, four in biocluster 2, three in biocluster 3, two in biocluster 4, two in biocluster 5, and two in biocluster 7. Their phenotypic signatures and bar chart of log2 ratio values are shown in **Fig. 4.25**.

The bar chart (**Fig. 4.25B**) indicates that the deviations of most samples fall into the

range of -0.6 to 0.6. The big changes caused by all samples also concentrated on the marker intensity of nucleus, tubulin, mitochondria, LC3b, and lysosome. Small effects were observed for parameters associated with texture and nucleus and cell shapes.

The biological signatures of herb pair 6+8, as shown in **Fig. 4.26**, featured the significant negative deviations ( $\log_2$  ratio  $< -0.3$ ) of the intensity of mitochondria and LC3b markers, which was most likely to come from the effects of herb 8. Herb 8 showed strong effects on the tubulin, mitochondria, and LC3b marker intensity with  $\log_2$  ratio values ranging from -0.4 to -0.3, but little effect on the tubulin and lysosome intensity.

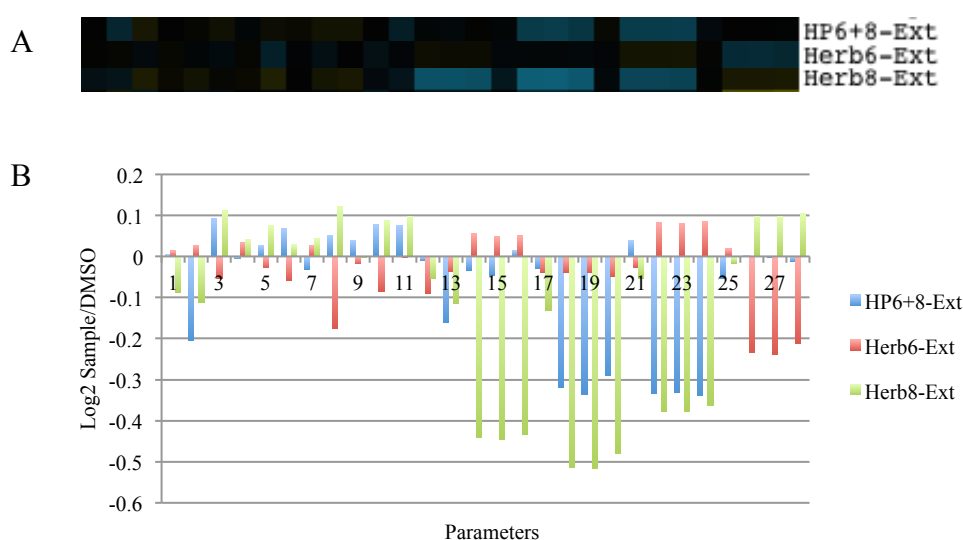


**Figure 4.26** Phenotypic signatures of extracts of herb 6, herb 8 and herb pair 6+8 (A), and bar chart of  $\log_2$  ratio values of the extracts of herb 6, herb 8 and herb pair 6+8 (B). The parameters are the same as described fully in Figure 4.2.

A comparison of phenotypic signatures of the extracts of herb pair 6+7 (**Fig. 4.20**) and herb pair 6+8 revealed that, although both herb pairs contained the same herb 6, their biological behaviors are quite different. In terms of the deviations with the  $|\log_2$  ratio| above 0.1, the herb pair 6+7 showed increases on nucleus and lysosome intensity and decrease on cell ratio width to length while herb pair 6+8 exhibit decreases on the intensity of nucleus, mitochondria, and LC3b marker, as well as tubulin texture.

Take the lysosome intensity as an example. Herb 6 showed big negative deviations ( $\log_2$  ratio  $< -0.2$ ), and both individual herb 7 and herb 8 showed small increases ( $\log_2$

ratio < 0.1) on the parameter. However, when they were used in the herb pairs, herb pair 6+7 showed positive deviations with log2 ratio > 0.1 while herb pair 6+8 still showed nearly nothing. The results suggested that the same herb in the different herb pair might make different contributions to the biological activity.

In terms of herb 8, the extract showed accordant changes with the fat-soluble fraction on the intensity of tubulin, mitochondria, LC3b, and lysosome, but opposite ones with two fractions on most nucleus and cell parameters (**Fig. 4.27A**). Ferulic acid (**50**) and senkyunolide I (**56**) are two major compounds observed in the ELSD-HPLC chromatogram of the fat-soluble fraction of herb 8 (**Fig. 3.9**). The content of ferulic acid is used to control the quality of the raw material in the Chinese Pharmacopeia.<sup>12</sup> An examination of compounds **50** and **56** showed that they had opposite effects on the intensity of tubulin, mitochondria and LC3b marker when compared with the fat-soluble fraction (**Fig. 4.27B**). It was obvious that the negative deviations of the extract and the fat-soluble fraction did not come from these two major compounds, and there might be other chemical constituents contributing to the negative effects.

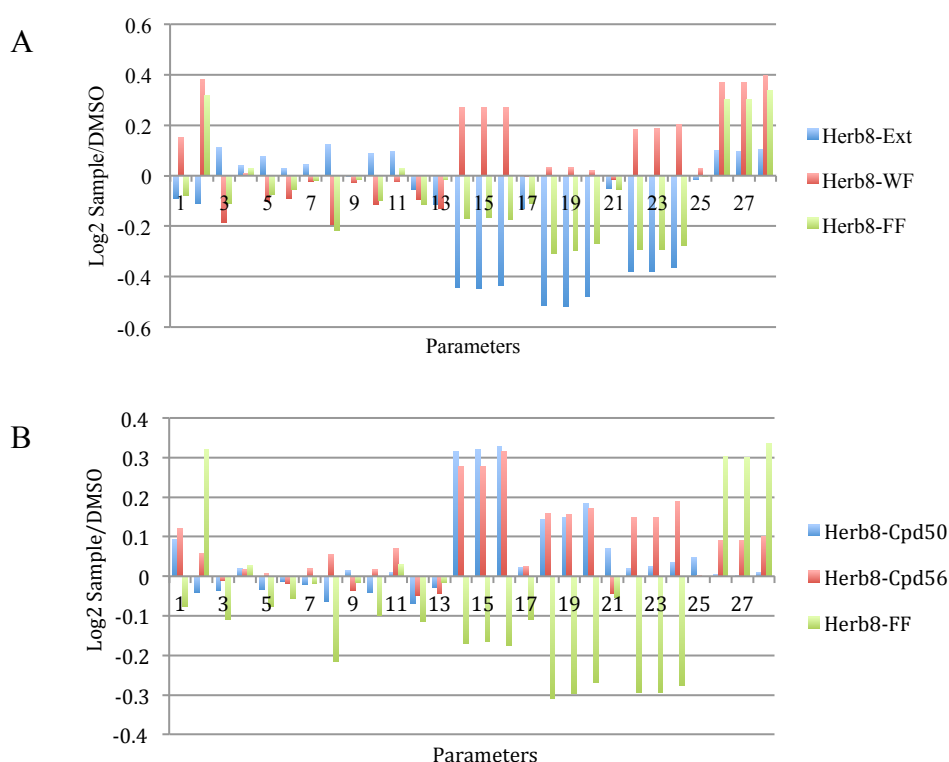


**Figure 4.27** Bar chart of log<sub>2</sub> ratio values of the extract and fractions obtained from herb 8 (A), and bar chart of log<sub>2</sub> ratio values of compounds **50** and **56** and the fat-soluble fraction of herb 8. The parameters are the same as described fully in Figure 4.2.

A detailed examination of phenotypic signatures of eight major compounds from herb 8 was carried out (**Fig. 4.28A**). The strong negative deviations were clearly observed mainly coming from compounds **52** and **53**. Comparison of phenotypic data of the extract of herb 8 and compounds **52** and **53** (**Fig. 4.28B**) indicated that these two compounds largely contributed to the biological activity of herb 8, especially to the characteristic negative deviations of mitochondria and LC3b intensity. In fact, compound **52**, known as levistilide A, is also used in the Chinese Pharmacopeia as the standard compound to identify the raw material of herb 8.<sup>12</sup>

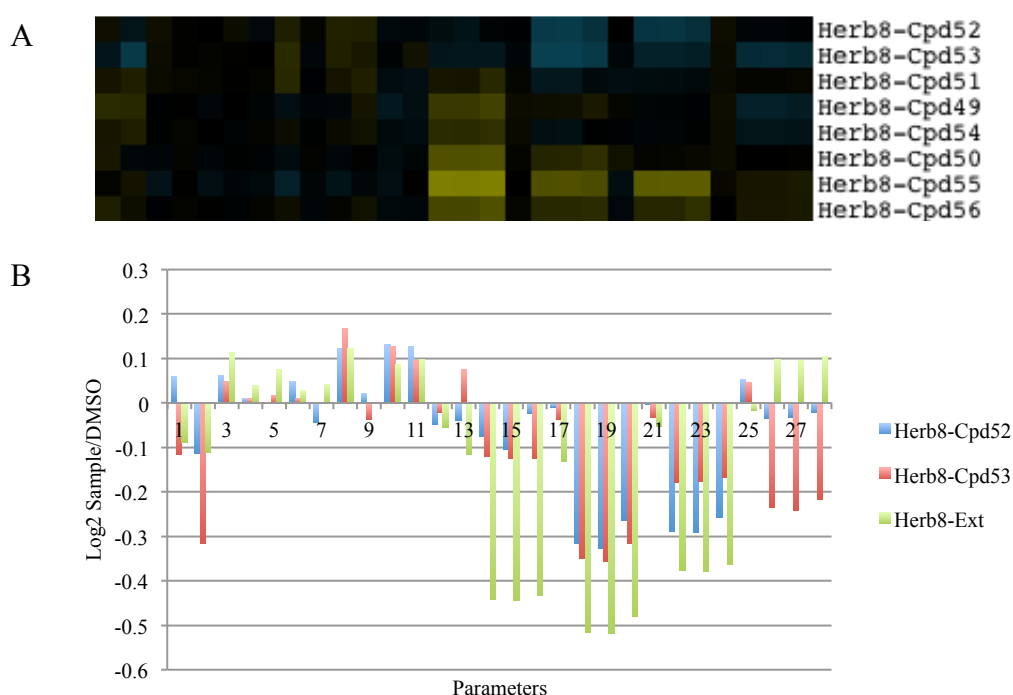


**Figure 4.28** Phenotypic signatures of compounds **49-56** from herb 8 (A), and bar chart of log<sub>2</sub> ratio values of compounds **52-53** and the extract of herb 8 (B). The parameters are the same as described fully in Figure 4.2.

In addition, compound **55**, ligustrazine, showed significant effects on the intensity of tubulin, mitochondria, and LC3b markers with log<sub>2</sub> ratio value above 0.3 (**Fig. 4.29**). In fact, ligustrazine products such as ligustrazine hydrochloride for injection and ligustrazine phosphate for injection have been approved in China for the treatment of cerebrovascular diseases. The result indicated that the established phenotypic screening

could reflect the therapeutic effects of the samples and could be used as a tool for the discovery of lead compounds.

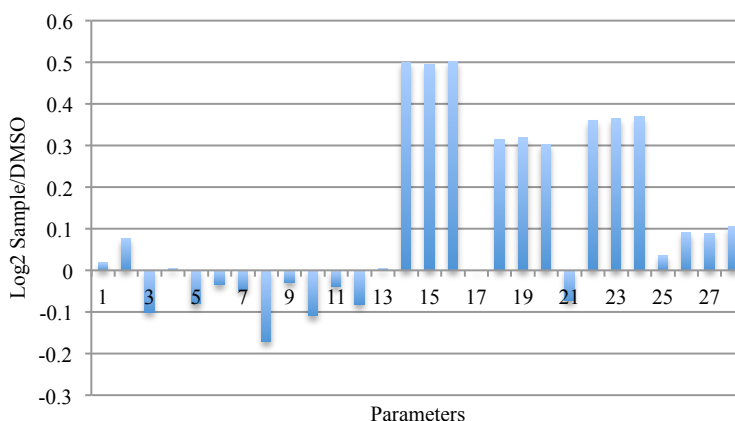


**Figure 4.29** Bar chart of log2 ratio values of compound **55**. The parameters are the same as described fully in Figure 4.2.

The artificial mixture AM3 was designed as a mimic to the fat-soluble fraction of herb 8, and it was composed of compounds **50** and **56** in a ratio of 1:1.3 (**Fig. 3.9** and **Table 3.5**). Comparison of the phenotypic data of AM3 and the individual compounds **50** and **56** showed accordant positive effects on the parameters of tubulin, mitochondria, LC3b, and lysosome intensity (**Fig. 4.30A**).

In order to explore further the correlation, the log2 ratio values of the virtual AM3, AM3-mimic, were calculated using the same method described for AM1 and AM2. The bar chart (**Fig. 4.30B**) shows clearly that the experimental data of AM3 were much stronger than the calculated data of the mimic AM3 on most parameters. The results suggested that when compounds **50** and **56** were put together, the biological activity of the mixture was greater than the sum of the effects of the individual compounds. The synergistic effect was observed for the AM3 when comparing the virtual and experimental data.

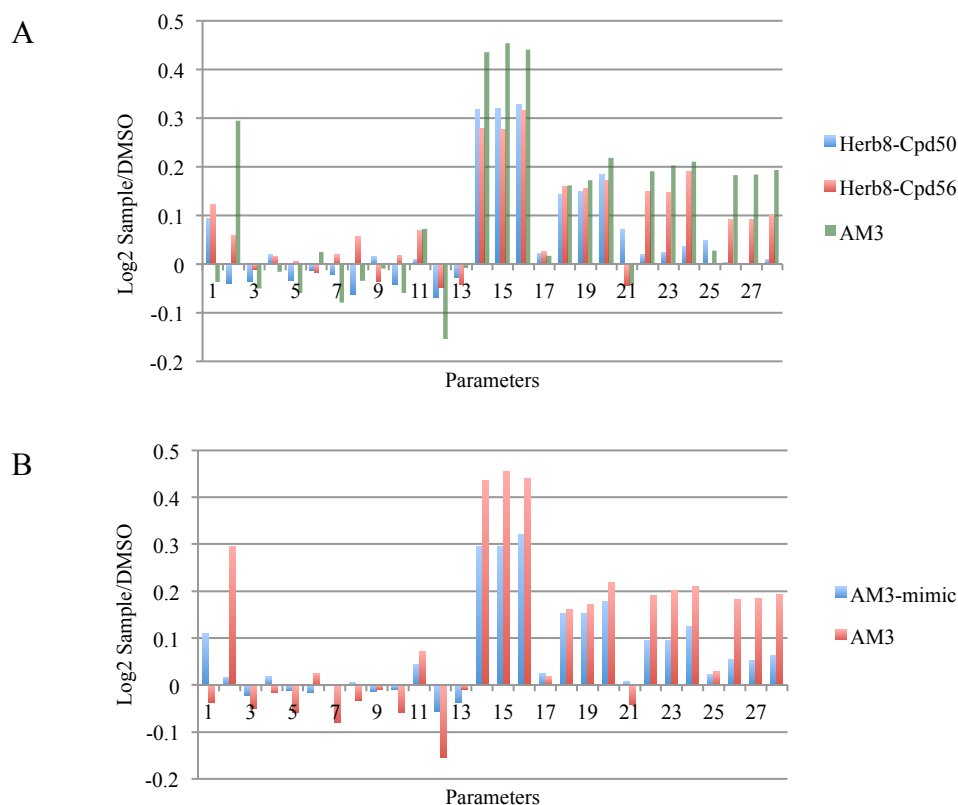


**Figure 4.30** Bar chart of phenotypic signatures of compounds **50** and **56**, and the artificial mixture of AM3 (A), and the mimic AM3 (B). The parameters are the same as described fully in Figure 4.2.

AM4 and AM5 were two artificial mixtures mimic to the chemical composition of the fat-soluble fraction of herb pair 6+8 (**Fig. 3.9** and **Table 3.5**). Compared with AM4, AM5 was deprived of gastrodin (**42**) in order to examine its influence on the biological responses. In the same way, the log<sub>2</sub> ratio values of the virtual AM4 and AM5 mimics based on the assumed additive effect of the individual compounds were calculated.

**Fig. 4.31** shows that the effects of AM5 looked stronger than those of AM4 on most parameters except for the lysosome. It was consistent with what we observed from the comparison of AM1 and AM2 (**Fig. 4.22**). The presence of gastrodin could decrease the effect of the mixture. The opposite deviations of the lysosome intensity further suggested that gastrodin might have an impact on the lysosome parameters in this mixture.

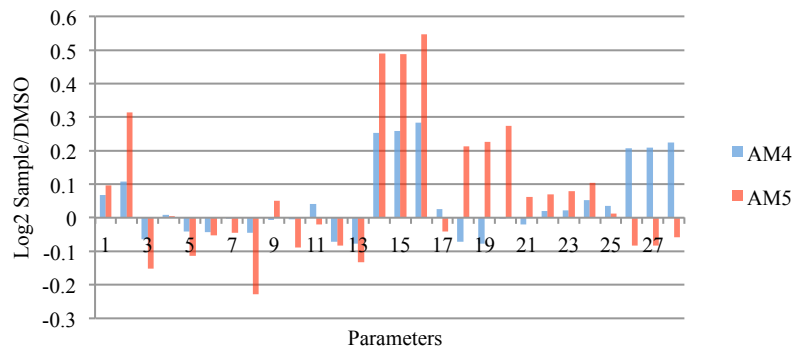


**Figure 4.31** Bar chart of log<sub>2</sub> ratio values of artificial mixtures AM4 and AM5. The parameters are the same as described fully in Figure 4.2.

Comparison of AM4 and its mimic (**Fig. 4.32A**) showed that there was a synergistic effect on the parameters of lysosome intensity, an approximate additive effect on the tubulin and nucleus intensity, and an obvious antagonistic effect on intensity of mitochondria and LC3b marker. Different from AM4, AM5 showed synergistic effects on most parameters except for an additive effect on the LC3b marker intensity (**Fig. 4.32B**).

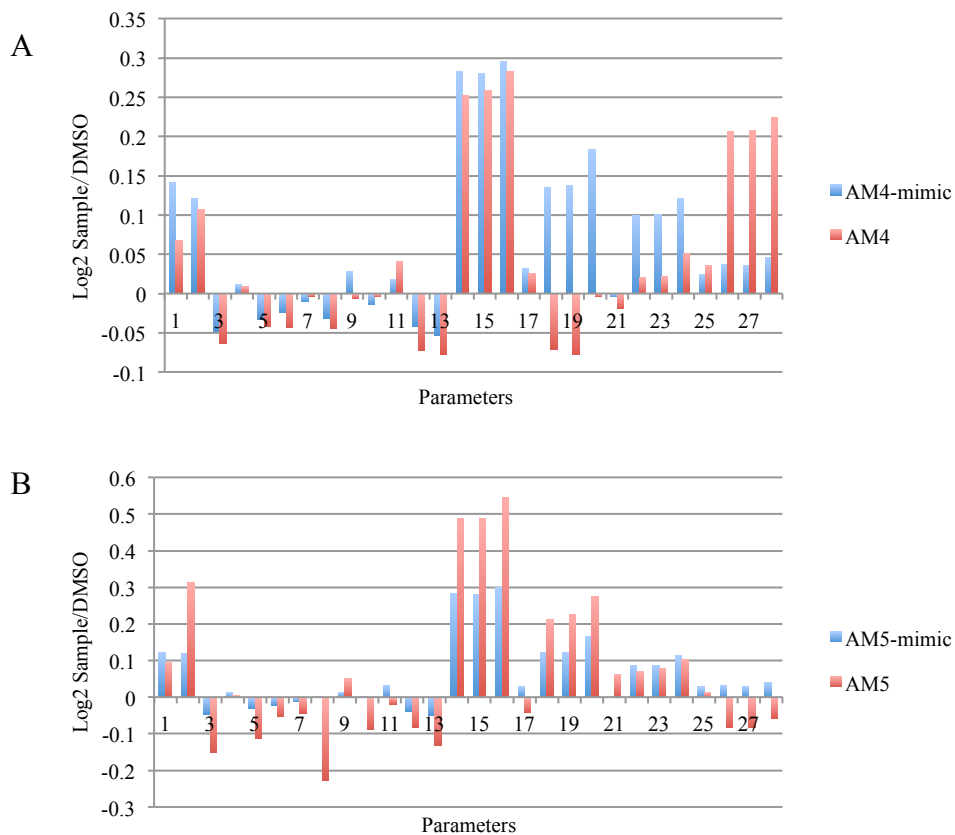


**Figure 4.32** Bar chart of log<sub>2</sub> ratio values of artificial mixtures AM4 and its mimic (A), and AM5 and its mimic (B). The parameters are the same as described fully in Figure 4.2.

#### 4.3.4.3 Herb pair 9+14

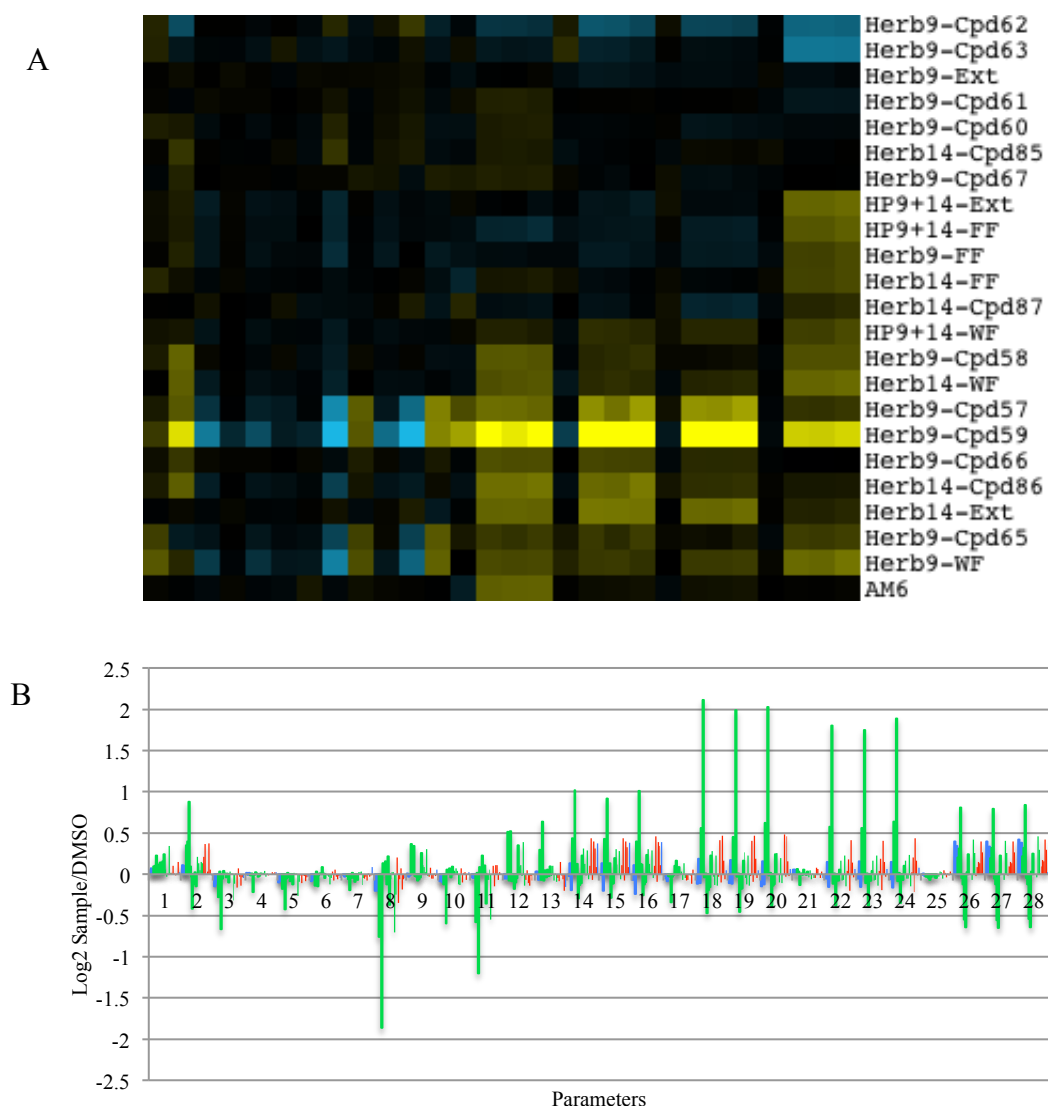


**Figure 4.33** Phenotypic signatures of all samples from herb 9, herb 14 and herb pair 9+14 (A), and bar chart of log2 ratio values of samples from herb 9 (green), herb 14 (red) and herb pair 9+14 (blue) (B). The parameters are the same as described fully in Figure 4.2.

Herb pair 9+14 consists of herb 9, Salviae Miltiorrhizae Radix et Rhizoma, and herb 14, Puerariae Lobatae Radix, in a ratio of 1:1. A total of 24 samples were obtained from herb 9, herb 14 and herb pair 9+14, including three extracts, six fractions, 14 compounds and one artificial mixture. Half of these samples (12) fall into biocluster 6, four into biocluster 2, one into biocluster 3, two into biocluster 4, two into biocluster 5, and one into biocluster 7. Their phenotypic signatures and bar chart of log2 ratio values are shown in **Fig. 4.33**.

The bar chart (**Fig. 4.33B**) shows extraordinary strong deviations with the |log2

ratio| reaching to 2.0. A detailed examination revealed that those strong effects were caused by one compound, dihydrotanshinone I (**59**). Except for those of **59**, the deviations of most samples still fall into the range of -0.6 to 0.6. The effects of all samples showed a similar overall pattern with those described for herb pair 6+7 and 6+8. The negative deviations were derived from compounds **62** and **63**, and the fat-soluble fraction of herb 9 as well.

Comparison of the phenotypic signatures of the extracts of herb pair 9+14, herb 9 and herb 14 (**Fig. 4.34**) revealed that the herb pair was characteristic of significant positive deviations (log2 ratio around 0.4) of the lysosome intensity, herb 14 featured strong positive deviations (log2 ratio around 0.4) of the tubulin, mitochondria, and LC3b intensity, and herb 9 showed small effects on all parameters (|log2 ratio| less than or around 0.1). The biological behaviors of herb pair 9+14 were completely different from those of the individual herbs.

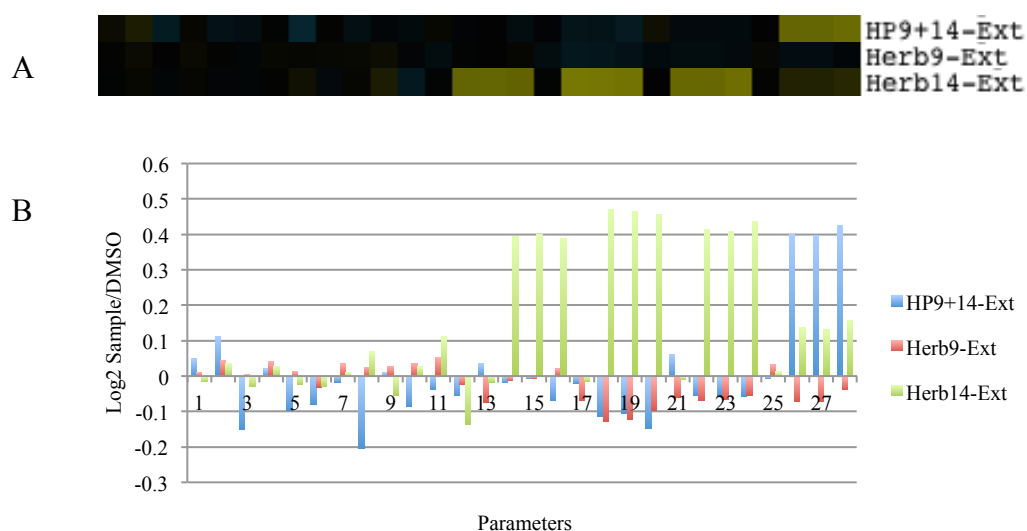


**Figure 4.34** Phenotypic signatures of extracts of herb 9, herb 14 and herb pair 9+14 (A), and bar chart of log2 ratio values of the extracts of herb 9, herb 14 and herb pair 9+14 (B). The parameters are the same as described fully in Figure 4.2.

An in-depth investigation was performed on 11 compounds obtained from herb 9. These compounds could be classified into two groups, one group of the fat-soluble diterpene quinones including compounds **57**, **59**, **62** and **63**, and the other group of the water-soluble phenolic acids containing compounds **58**, **60**, **61** and **64-67**. In Chinese

Pharmacopoeia, cryptotoanshinone (**57**), salviandic acid B (**58**), tanshinone IIA (**62**) and tanshinone I (**63**) are four major compounds and used for the identification and quality control of the raw material.<sup>13</sup> The bar charts of log<sub>2</sub> ratio values of these two groups of compounds are shown in **Fig. 4.35**, respectively.

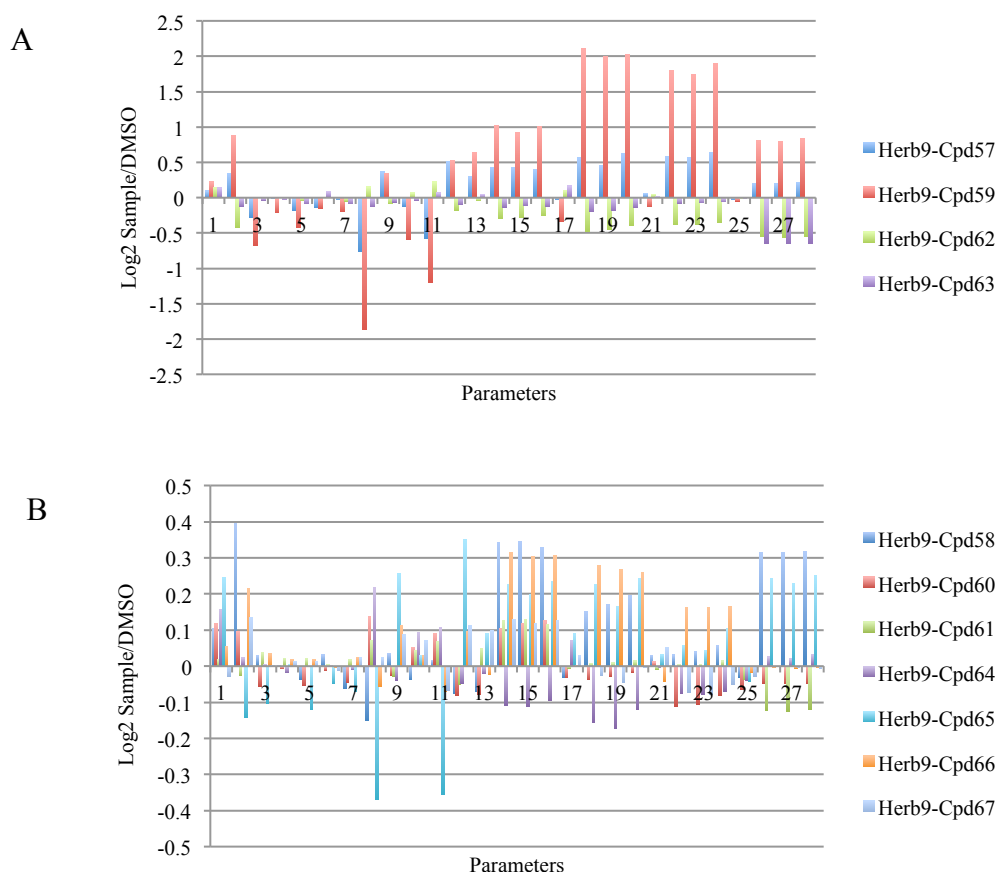


**Figure 4.35** Bar chart of log<sub>2</sub> ratio values of compounds of the fat-soluble group (A), and compounds of the water-soluble group (B). The parameters are the same as described fully in Figure 4.2.

All fat-soluble compounds showed significant effects on most parameters ( $|\log_2 \text{ratio}| > 0.2$ ), and the strongest effects of all 171 samples were observed for compounds **59**, dihydrotanshinone I, on intensity of nucleus, tubulin, mitochondria, LC3b, and lysosome markers, tubulin marker texture, and cell shape, with the  $|\log_2 \text{ratio}|$  values ranging from 0.5 to 2.0.

The phenotypic signatures of the water-soluble compounds (**Fig. 4.35B**) looked similar to those of the fat-soluble compounds, showing the strong positive deviations on the tubulin marker texture, intensity of nucleus, tubulin, mitochondria, LC3b, and

lysosome markers, as well as negative deviations of cell area and cell length. Compounds **58**, **65** and **66** significantly contributed to these changes.

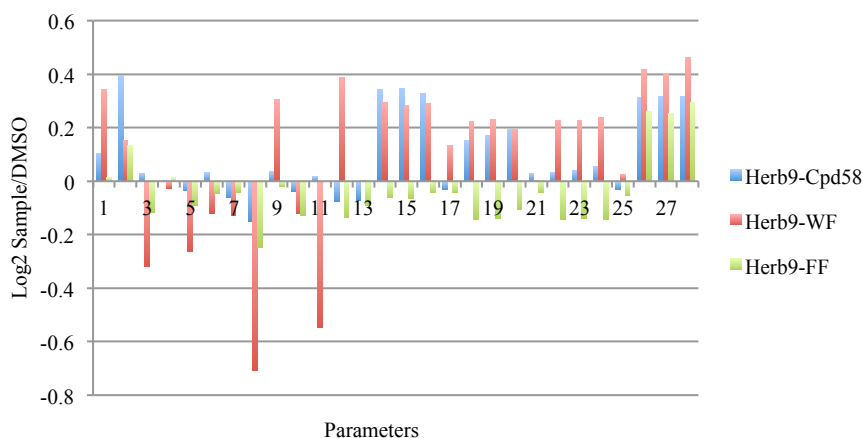


**Figure 4.36** Bar chart of log2 ratio values of compound **58** and water-soluble and fat-soluble fractions of herb 9. The parameters are the same as described fully in Figure 4.2.

Although the extract of herb 9 showed small effects (**Fig. 4.34**), its water-soluble fraction exhibited the strong effects similar to those described for the group of water-soluble compounds. Salviandic acid B (**58**) is the predominant constituent of the water-soluble compounds, and according to the Chinese Pharmacopoeia, its content should not be less than 3% of the dry material.<sup>13</sup> Comparison of the phenotypic signatures of compound **58** with two fractions of herb 9 indicated that **58** contributed a lot to the characteristic deviations of the intensity of nucleus, tubulin, mitochondria, and lysosome markers of the water-soluble fraction of herb 9 (**Fig. 4.36**). The positive deviations of the LC3b intensity might derive from compound **66**, while the strong increases on the nucleus texture, cell roundness, and cell ratio width to length, as well as the strong decreases on nucleus area, nucleus width, cell area, and cell length, could come from compound **65**.

In terms of herb 14, daidzin (**85**), puerarin (**86**), and daidzein (**87**) are three major compounds and puerarin is used for the identification and quality control of the raw material. The content of puerarin should not be less than 2.4% of the dry material.<sup>14</sup> The phenotypic signatures of both puerarin and the extract of herb 14 were grouped in the

same biocluster 6, and showed big similarities on the intensity of tubulin, mitochondria, LC3b, and lysosome markers (**Fig. 4.37**), which might be due to the high content of puerarin in the extract.

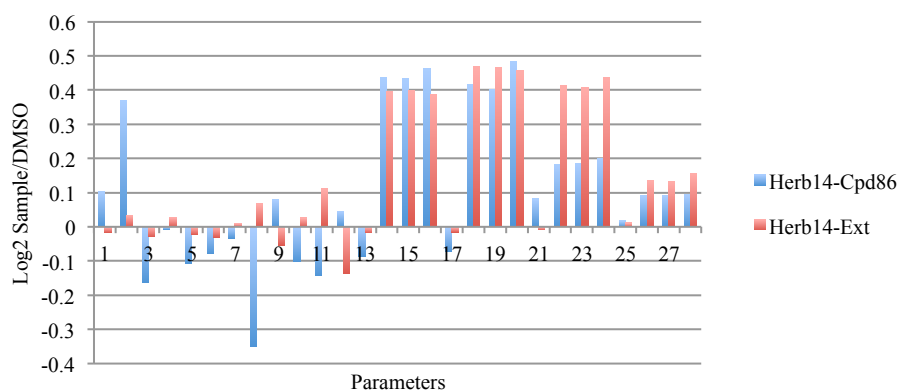


**Figure 4.37** Bar chart of log2 ratio values of compound **86** and the extract of herb 9. The parameters are the same as described fully in Figure 4.2.

An artificial mixture AM6 was prepared, consisting puerarin (**86**) and salviandic acid B (**58**) in a ratio of 4:1 (**Table 3.5** and **Fig. 3.8**). A virtual AM6 mimic was also produced using the method described before. Comparing their phenotypic values, AM6 and its mimic showed a good matching on the parameters of tubulin, but on the other parameters, the effects of AM6 were much weaker than those of its mimic (**Fig. 4.38**). The results suggested that when these two major compounds were applied together, the mixture showed an additive effect on tubulin parameters and an antagonistic effect on nucleus and cell shapes, and other cellular organelles as well.

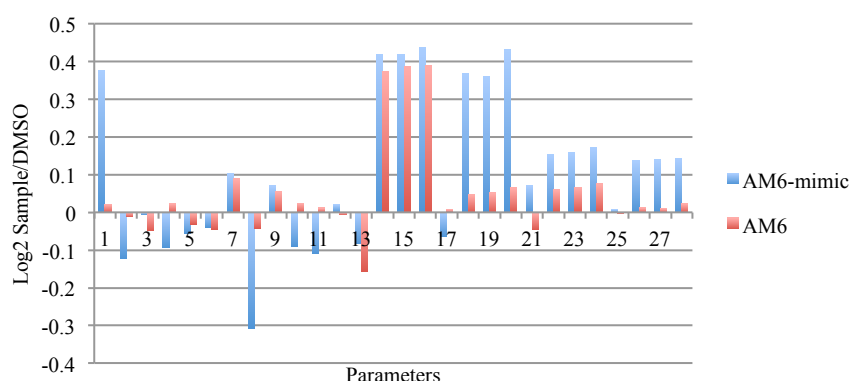


**Figure 4.38** Bar chart of log2 ratio values of AM6 and its mimic. The parameters are the same as described fully in Figure 4.2.

#### 4.3.4.4 Herb pair 10+11

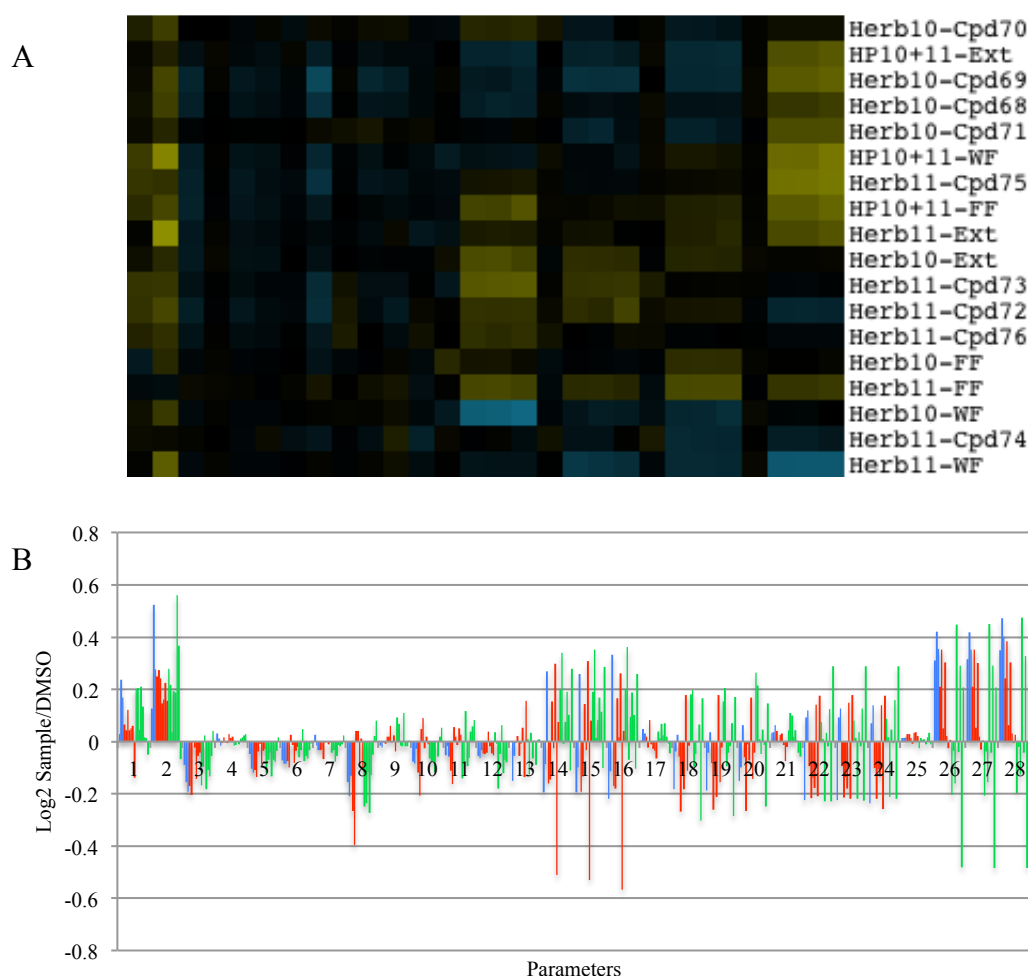


**Figure 4.39** Phenotypic signatures of all samples from herb 10, herb 11 and herb pair 10+11 (A), and bar chart of log<sub>2</sub> ratio values of samples from herb 10 (red), herb 11 (green) and herb pair 10+11 (blue) (B). The parameters are the same as described fully in Figure 4.2.

Herb pair 10+11 is composed of herb 10, *Acori Tatarinowii Rhizoma*, and herb 11, *Polygalae Radix*, in a ratio of 1:1. A total of 18 samples were obtained including three extracts, six fractions, and nine compounds. Seven samples were grouped in biocluster 6, and the rest fell into biocluster 2 (4), biocluster 3 (1), biocluster 4 (1), biocluster 5 (1), and biocluster 7 (2), respectively. Their phenotypic signatures and bar chart of log<sub>2</sub> ratio values are shown in **Fig. 4.39**.

The bar chart (**Fig. 4.39B**) shows that the deviations of all samples mainly fell into a range of -0.4 to 0.4. The effects of all samples showed a similar overall pattern with those described for the above-mentioned herb pairs. Almost every sample contributed to the negative effects on one or several parameters.

The phenotypic signatures of three extracts are depicted in **Fig. 4.40**. The herb pair featured negative deviations ( $\log_2$  ratio  $< -0.15$ ) of tubulin, mitochondria, and LC3b intensity, which were opposite to the changes caused by individual herb 10 and herb 11. On the parameters of lysosome intensity, the herb pair and herb 11 showed similar positive effects ( $\log_2$  ratio  $> 0.2$ ) while herb 10 exhibited little influence. An extraordinary increase on the nucleus intensity with  $\log_2$  ratio above 0.5 was observed for the extract of herb 11.

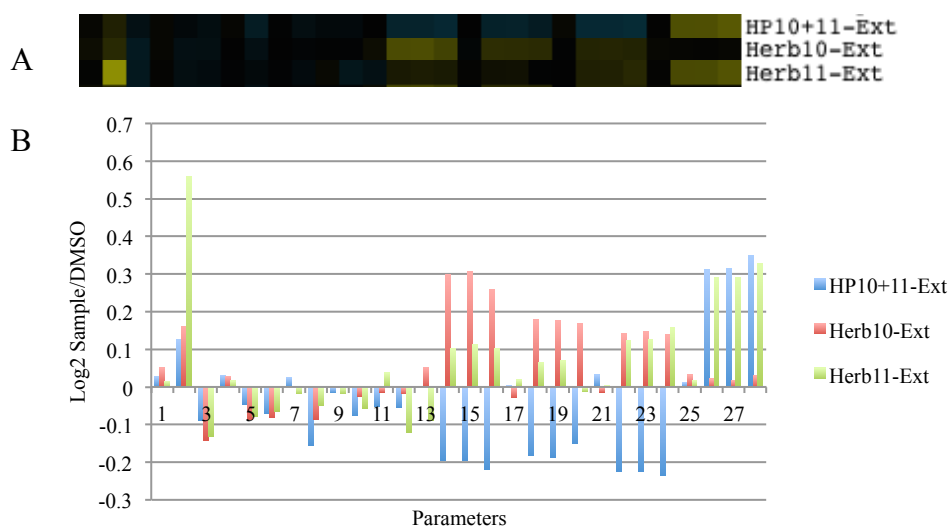


**Figure 4.40** Phenotypic signatures of extracts of herb 10, herb 11 and herb pair 10+11 (A), and bar chart of  $\log_2$  ratio values of the extracts of herb 10, herb 11 and herb pair 10+11 (B). The parameters are the same as described fully in Figure 4.2.

The extract and two fractions of herb 10 showed very weak influence on the lysosome parameters (**Fig. 4.41A**). A further examination of the biological signatures of compounds **68-71**, which were isolated from herb 10, showed that all four compounds had positive deviations of the lysosome parameters (**Fig. 4.41B**). Since compounds **68-71** are the major constituents of the volatile oil, the content of which is used in the Chinese Pharmacopoeia for the quality control of the raw material,<sup>15</sup> they should contribute a lot to the overall biological effect of the fraction or the extract of herb 10. However, the negative effects could not reflect in the biological signatures of the extract and fractions. Either the antagonistic effect of the mixture or the cancellation by the opposite effects caused by other components could explain the vanished effects on the

lysosome parameters.

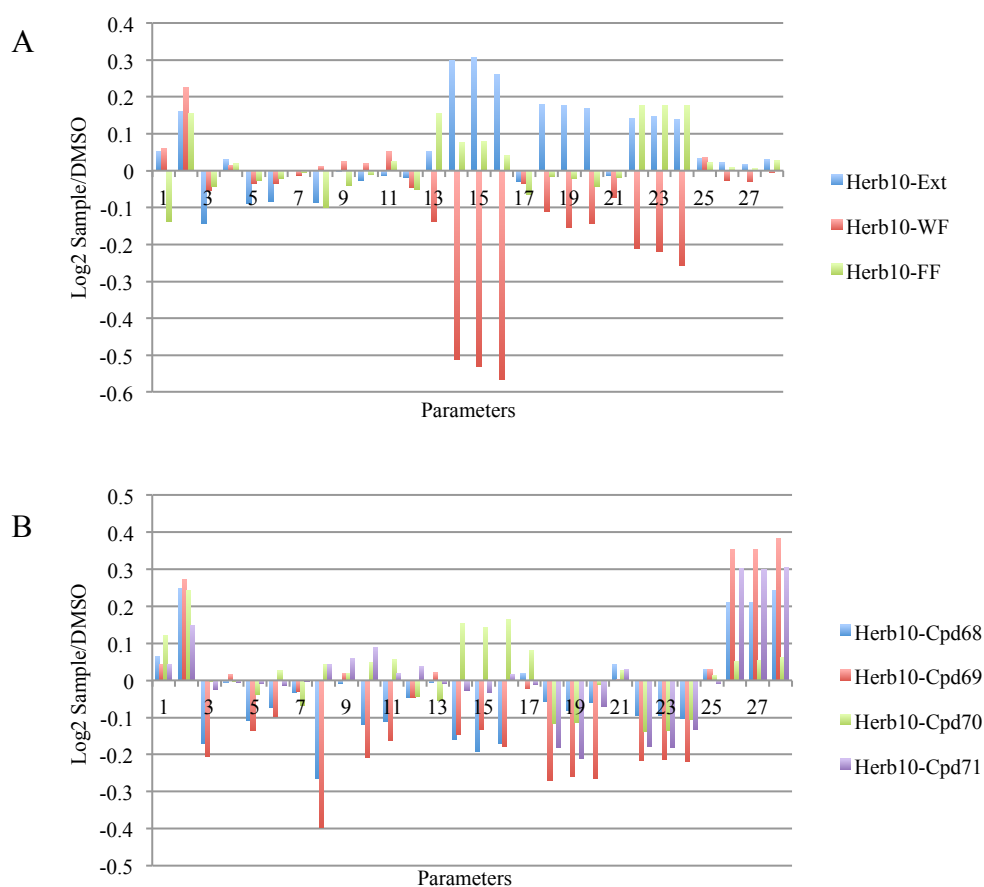


**Figure 4.41** Bar chart of log<sub>2</sub> ratio values of the extract and fractions of herb 10 (A), and compounds **68-71** (B). The parameters are the same as described fully in Figure 4.2.

Compounds **72-76** were obtained from herb 11, and among them, compounds **73**, **75**, and **76** are used in the Chinese Pharmacopoeia for the identification and quality control of the raw material.<sup>16</sup> Their phenotypic signatures (**Fig. 4.42**) were quite different. Compared with the extract and fractions, the individual compounds showed bigger changes on the structure and shape of nucleus and cell. However, it is hard to find a clear correlation in the biological behaviors between these compounds and the extract and fractions. This could be explained by the ELSD-HPLC chromatogram (**Fig. 3.12**), which showed that the chemical composition of the herb pair and the individual herbs were very complicated. Although compounds **68-72** were major and characteristic components, they were not as predominant as puerarin of herb 14, and the overall biological activity were affected also by other chemical constituents.

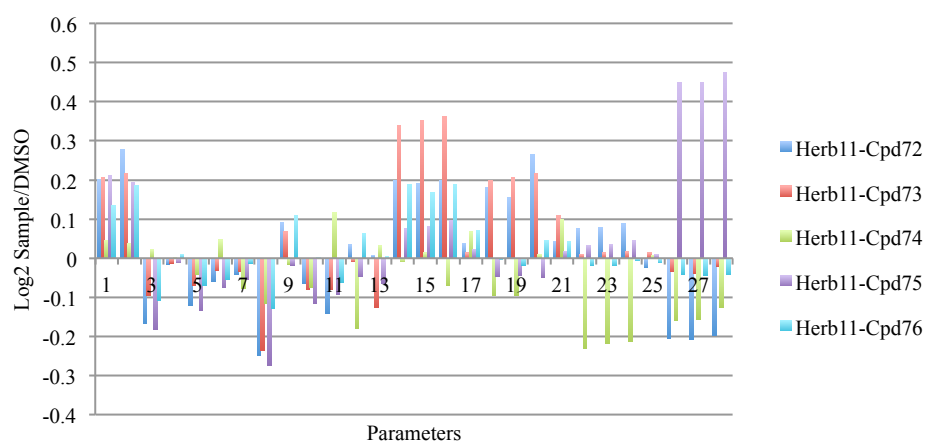


**Figure 4.42** Bar chart of log<sub>2</sub> ratio values of compounds **72-76** from herb 11. The parameters are the same as described fully in Figure 4.2.

#### 4.3.4.5 Herb pair 12+13

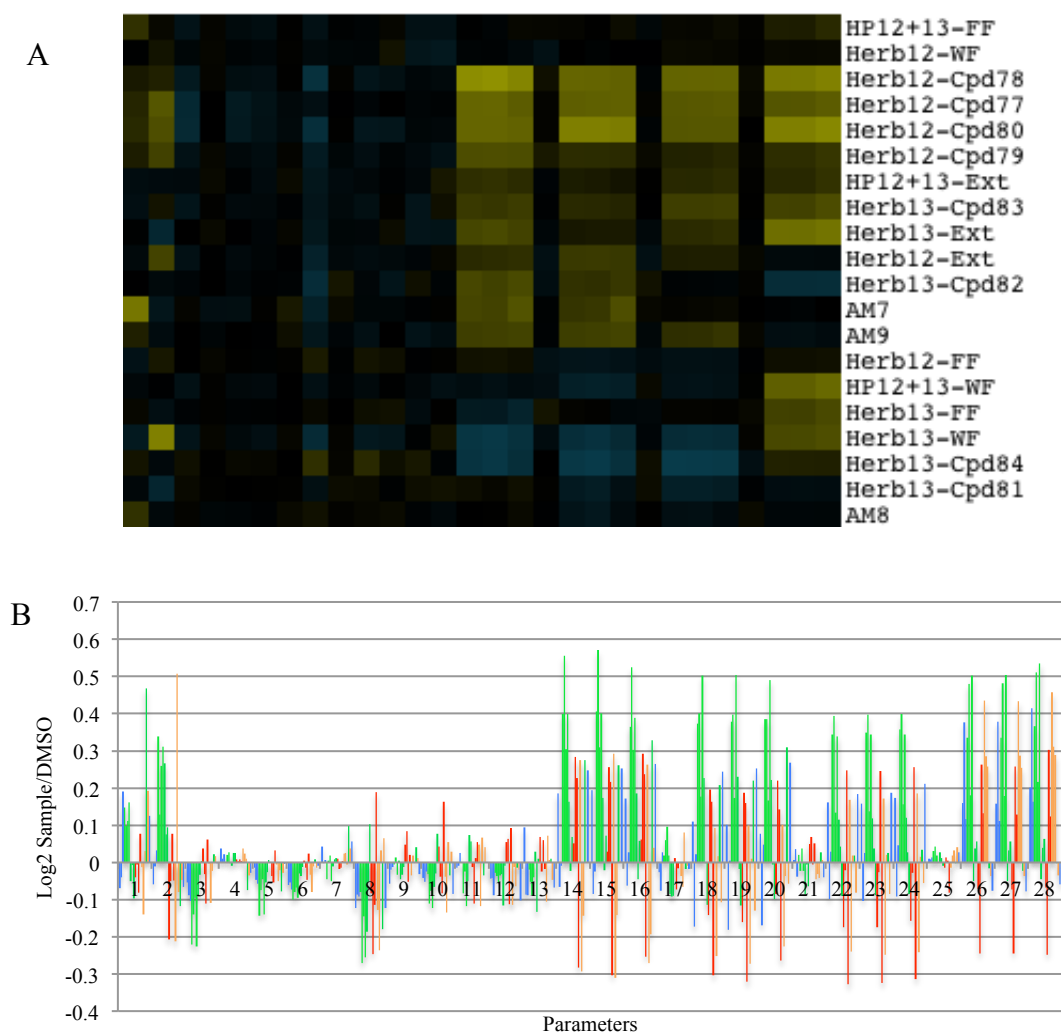


**Figure 4.43** Phenotypic signatures of all samples from herb 12, herb 13 and herb pair 12+13 (A), and bar chart of log<sub>2</sub> ratio values of common compounds **81-84** of herbs 12 and 13 (red), and samples from herb 12 (green), herb 13 (orange) and herb pair 12+13 (blue) (B). The parameters are the same as described fully in Figure 4.2.

Herb pair 12+13 consists of herb 12, Ziziphi Spinosae Semen, and herb 13, Platycladi Semen. A total of 20 samples were obtained including three extracts and six fractions, eight compounds, and three artificial mixtures. Eleven samples were grouped in the biocluster 6, and the rest fell into biocluster 2 (2), biocluster 3 (1), biocluster 4 (2), biocluster 5 (1), and biocluster 7 (1), respectively. Their phenotypic signatures and bar chart of log2 ratio values are shown in **Fig. 4.43**.

The bar chart (**Fig. 4.43B**) shows that the deviations of all samples mainly fell into a range of -0.4 to 0.4. The big changes concentrated on the intensity of nucleus, tubulin, mitochondria, LC3b, and lysosome, as well as nucleus and cell area. The major negative deviations were derived from the compounds **82**, **84**, and the water-soluble fraction from herb 13.

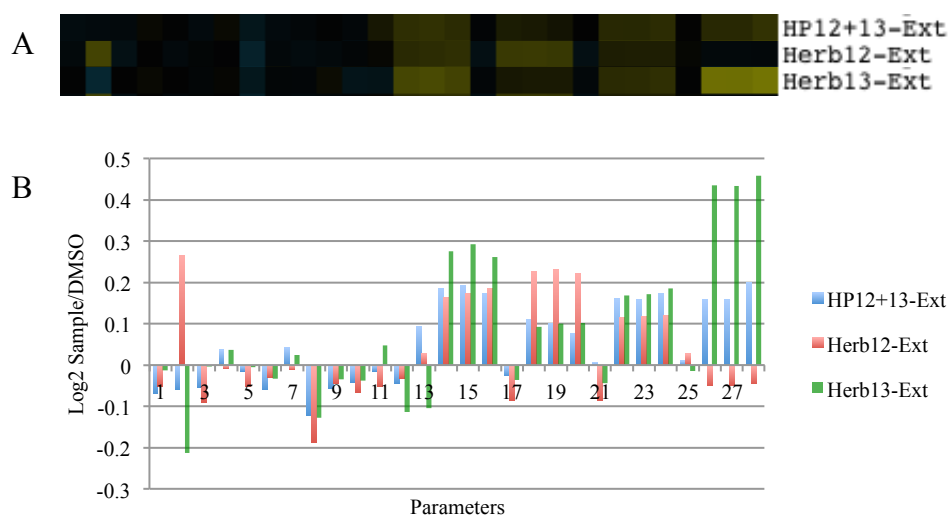


**Figure 4.44** Phenotypic signatures of extracts of the extracts of herb 12, herb 13 and herb pair 12+13 (A), and bar chart of log2 ratio values of the extracts of herb 12, herb 13 and herb pair 12+13 (B). The parameters are the same as described fully in Figure 4.2.

A detailed comparison of the log2 ratio values of three extracts (**Fig. 4.44**) revealed that these three extracts showed similar pattern of deviations. The herb pair exhibited positive deviations of the intensity of tubulin, mitochondria, LC3b, and lysosome, with log2 ratio values ranging from 0.1 to 0.2. Herb 13 also showed the similar deviations on these parameters but with stronger intensity. Especially, its log2 ratio values of the lysosome marker intensity were more than two fold of the herb pair. Herb 12 showed

similar positive deviations of the intensity of tubulin, mitochondria and LC3b marker but weak negative deviations of the lysosome marker intensity. In addition, the opposite deviations of the nucleus marker intensity were observed for herb 12 (log2 ratio 0.27) and herb 13 (log2 ratio -0.21), while the deviation was very weak for the herb pair (log2 ratio -0.06). In this case, the properties of herb 12 and herb 13 were quite similar, and the herb pair also showed relatively consistent biological behaviors with those of the individual herbs.

Compounds **77-80** were isolated from herb 12, and their phenotypic signatures were characteristic with positive deviations of tubulin, mitochondria, LC3b, and lysosome marker intensity (**Fig. 4.45**). Their phenotypic signatures, all grouped into the biocluster 6, showed accordant deviations on most parameters with those of the extract of herb 12. It should be noted that compounds **78**, **79** and **80** are used in the Chinese pharmacopeia for the identification of the raw material of herb 12.<sup>17</sup> Our results proved that these compounds, to great extent, could reflect the biological activities of the herb.

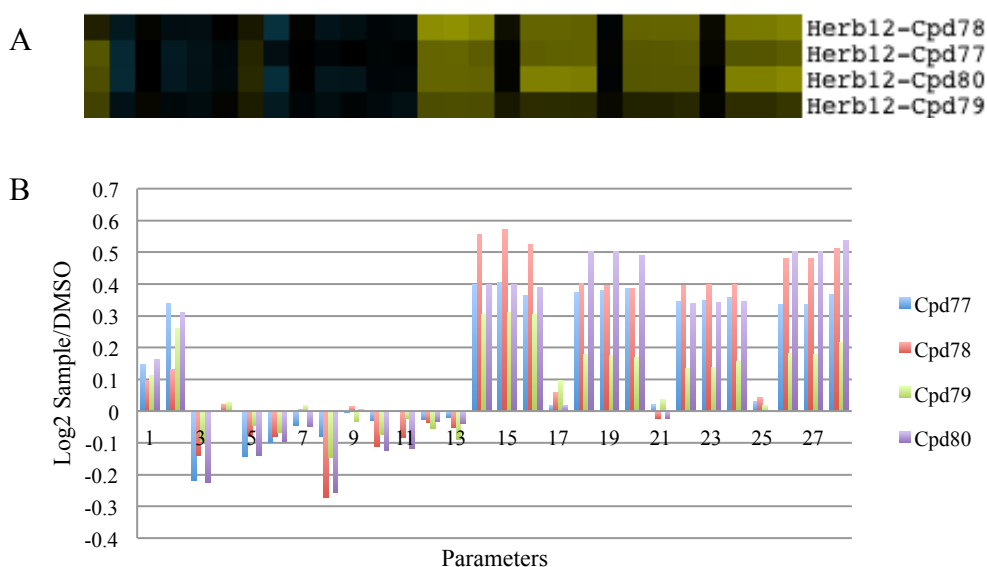
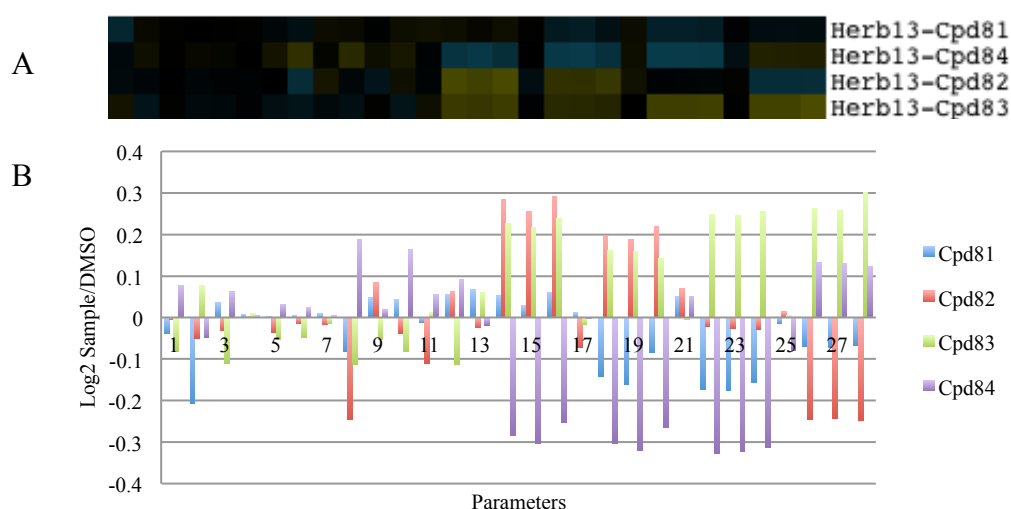


**Figure 4.45** Phenotypic signatures of extracts of compounds **77-80** (A), and bar chart of log2 ratio values of compounds **77-80** (B). The parameters are the same as described fully in Figure 4.2.

As stated in **2.2.2**, fatty acids are the major components of herb 12 and herb 13. More than 60% of herb 12 are fatty acids, of which 38.8% is oleic acid (**82**) and 37.1% is linoleic acid (**83**).<sup>18</sup> Herb 13 contains about 60% of fatty oil with 62.39% being

unsaturated fatty acids.<sup>19</sup> GC-MS analysis of the fatty oil further disclosed that the three major unsaturated fatty acids are linoleic acid (**83**), linolenic acid (**84**) and arachidonic acid (**81**).<sup>20</sup> Our ELSD-HPLC analysis result (**Fig. 3.10**) also revealed that arachidonic acid (**81**), oleic acid (**82**), linoleic acid (**83**), and linolenic acid (**84**) were four major compounds existing in the extracts and fat-soluble fractions of herb 12, herb 13 and the herb pair.

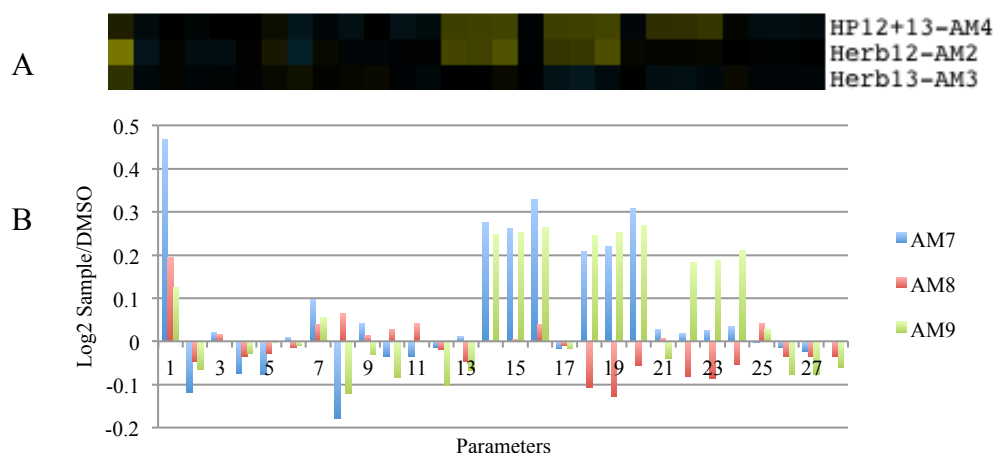
Although compounds **81-84** possess similar structures, their phenotypic patterns are quite different. **Fig. 4.46** depicts the phenotypic signatures and bar chart of compounds **81-84**, revealing that the negative deviations came mainly from the effects of compound **84** on the tubulin, mitochondria and LC3b marker intensity, and the effects of compound **82** on the lysosome marker intensity.



**Figure 4.46** Phenotypic signatures of extracts of compounds **81-84** (A), and bar chart of log2 ratio values of compounds **81-84** (B). The parameters are the same as described fully in Figure 4.2.

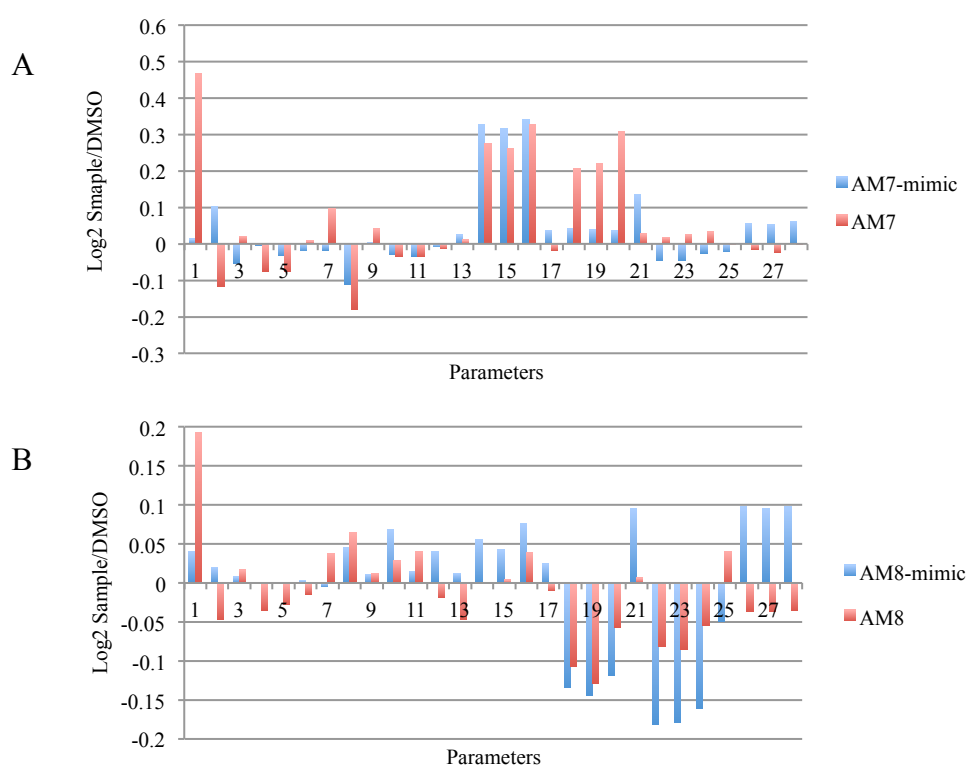
According to the ratio of different compounds as indicated in **Fig. 3.10**, three artificial mixtures, AM7, AM8, and AM9, were prepared (**Table 3.5**). Their phenotypic signatures and bar chart of the log2 ratio values are indicated in **Fig. 4.47**. The results showed that the artificial mixture of herb 13 (AM8) showed small deviations on most parameters. Both artificial mixtures of herb 12 (AM7) and the herb pair (AM9) had strong effects on the tubulin and mitochondria intensity. AM9 also showed big positive deviations of the LC3b intensity while AM7 displayed a significant increase in the

nucleus texture (**Fig. 4.47B**). The common feature of these three mixtures was small effect on the lysosome parameters.



**Figure 4.47** Phenotypic signatures of extracts of artificial mixtures AM7, AM8 and AM9 (A), and bar chart of log2 ratio values of artificial mixtures AM7, AM8 and AM9 (B). The parameters are the same as described fully in Figure 4.2.

In order to explore the correlation between the artificial mixture and the pure compounds, the virtual mimics of these three artificial mixtures based on an assumed additive correlation were calculated using the method described before. The data of the mimic AM7, AM8, and AM9 were compared with those of the experimental ones, respectively (**Fig 4.48**).



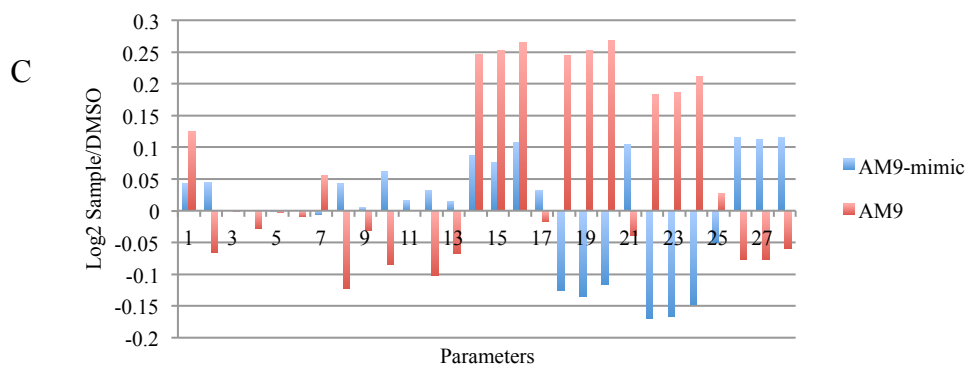


**Figure 4.48** Bar chart of log2 ratio values of AM7 and its mimic (A), AM8 and its mimic (B), and AM9 and its mimic (C). The parameters are the same as described fully in Figure 4.2.

The results indicated that AM7 and its mimic matched well on the tubulin marker intensity and cell shape parameters, but showed a big synergistic effect on the parameters of mitochondria intensity and nucleus texture. AM8 displayed a reasonable matching on the mitochondria marker intensity, a synergistic effect on the nuclear texture, and an antagonistic effect on the LC3b intensity. Notably, AM9 showed opposite deviations of almost all parameters to its mimic mixture except for the accordant deviations of the tubulin intensity, on which a significant synergistic effect was disclosed when compared with the mimic mixture.

It should be pointed out that the artificial mixtures AM7, AM8 and AM9 were composed of the same compounds but in different ratio. These mixtures showed quite different biological signatures, which demonstrated that the ratio of individuals in a mixture was essential to its biological activity. Different from the individual compound, a mixture not only has its chemical composition but also a specific ratio of individual chemicals, both of which eventually determine the biological activities.

#### 4.3.5 A summary

The major findings are summarised here.

1. The biological relationship between extract and fraction, mixture and compound, and herb pair and individual herb was very complicated. It depends on the properties of the sample to great extent. No common pattern was observed.

2. Biological behaviors of a mixture lie in the composition of the chemicals and their ratio in the mixture. Different ratios of the same constitutive components could afford different biological activity. That could explain to some extent why compatibility is so vital to the therapeutic effect of a formula.

3. A mixture could show synergistic effect, antagonistic effect, or additive effect on different cellular organelles, compared with the individual compounds. It was suggested that a mixture could affect different pathway with different mode of action.

4. An artificial mixture that mimicked the chemical composition of major compounds in an extract or fraction could not reflect the biological activity of the extract or fraction in most cases. The overall effect of an extract or fraction depends a lot on the compounds with high contents, especially the predominant ones, but the contributions from the minor constituents could not be overlooked. Some minor constituents showed significant bioactivity in the assay, although their contribution to the overall effect is not as big as the major one due to the low yield.

5. The different extraction method had an impact on the biological responses on the herb and the herb pair due to the changes in chemical composition caused by the extraction method. The extraction method influenced the individual herb more than the herb pair. From this point of view, the biological effect of the herb pair was more stable than that of the individual herb.

6. Some major compounds, in most cases, showed the similar biological responses to the whole herb, which supported the usage of these compounds in the Chinese Pharmacopoeia for the identification or quality control of the raw material.

#### **4.4 Conclusions from phenotypic analysis**

The analysis of phenotypic signatures of all samples from the herbs and the herb pairs targeting the neurodegenerative diseases demonstrates the complexity of TCM

from different perspectives, and more importantly, discovers common features of the proposed underlying mechanisms.

#### 4.4.1 Common features of TCM samples behind clustering

By clustering, we found that nearly half of the samples (49.7%) could be grouped into biocluster 6, which features the positive deviations of marker intensity of tubulin, mitochondria, LC3b, and lysosome. An examination from the perspective of extract, which reflect the overall effect of the herb or the herb pair, revealed that 11 of 24 extracts (45.8%) also fall into the biocluster 6 (**Table 4.2**). Another in-depth exploration on samples from five herb pairs exhibited the similar results (**Table 4.3**). In each herb pair, about half or more samples were clustered in biocluster 6, except for the samples from the herb pair 10+11.

**Table 4.3** Statistical data of clustering of samples from five herb pairs.

Herb pairs	6+7	6+8	9+14	10+11	12+13
Total samples	18	27	24	18	20
Samples in biocluster 6	11	13	12	7	11
% of biocluster 6	61.1%	48.1%	50%	38.7%	55%
Samples in biocluster 2	2	4	4	4	2
% of biocluster 2	11.1%	14.8%	16.7%	22.2%	10%
% of bioclusters 6 and 2	72.2%	62.9%	66.7%	61.1%	65%

Analysis of the clustering at the overview level showed an indication that a majority of the samples produced similar biological effects. This result was consistent with the fact that selected samples have been long used for the treatment of brain disorders, and they were likely to take effects on the same targets or through the same biological pathways.

Furthermore, biocluster 2, the second biggest cluster, contained 25 samples, 14.6 % of all samples. The biocluster 2 was characteristic of positive deviation of lysosome marker intensity and negative deviations of tubulin, mitochondria, and LC3b marker intensity. The samples from biocluster 6 and biocluster 2 accounted for 64.3% of all

samples tested. In terms of five herb pairs, biocluster 2 was also the second largest cluster, and the percentage of the samples in this biocluster varied from one herb pair to another with a range of 10% to 22% (**Table 4.3**). More than 60% of samples were found in these two clusters for each herb pair (**Fig. 4.49**).

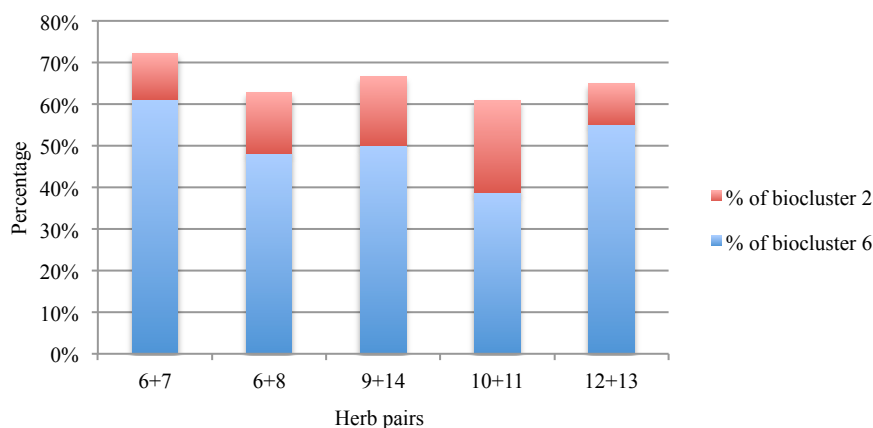


**Figure 4.49** Stacking chart of percentages of samples in biocluster 6 and biocluster 2.

Comparing the biological signatures of biocluster 6 and biocluster 2, a common feature, a positive effect on the lysosome marker intensity, was observed. This finding was consistent with what we found for five herb pairs at the extract level. All the extracts of five herb pairs showed the positive effects on the lysosome intensity, although individual herbs or compounds showed strong negative deviations. These results suggested that lysosome could play an important role in investigating the molecular mechanisms or the functional proteins underlying neurodegenerative diseases.

In addition, the opposite deviations of marker intensity of tubulin, mitochondria, and LC3b shown by biocluster 6 and biocluster 2 also implied that there might be more than one pathway related to the same therapeutic effect. If the biological signatures of biocluster 6 represented a mainstream pathway, those of biocluster 2 might reflect an alternative one with lysosome function as a common feature.

#### 4.4.2 Biological responses related with cell toxicity

Although every sample had its own pattern of phenotypic signatures, all samples disclosed strong effects on the intensity of nucleus, tubulin, mitochondria, LC3b, and lysosome, and weak effects on their texture properties, and the parameters associated with nucleus and cell shapes. To assess the magnitude of the effect of all samples on one parameter, the absolute values of log2 ratio of all samples on this parameter were added up to give a total sum, which was then divided by 171 to yield a mean value. This mean value was used to reflect the average effect of all samples on a specific parameter.

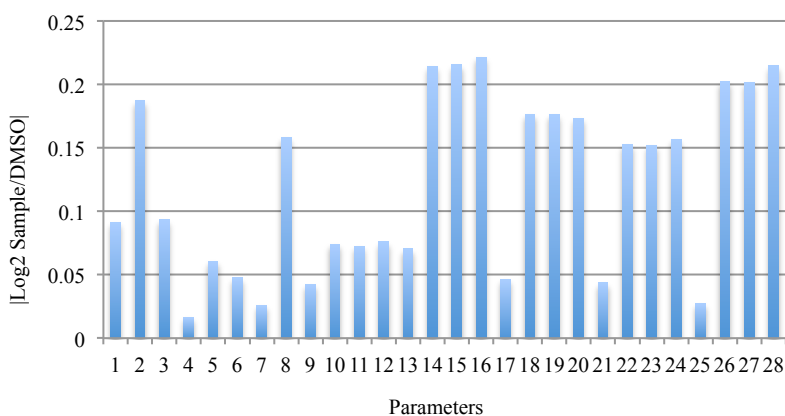


**Figure 4.50** Bar chart of mean values of  $|\log_2 \text{ratio}|$  of all samples on 28 parameters. The parameters are the same as described fully in Figure 4.2.

A total of 28 mean values were calculated and these data are charted in **Fig. 4.50**. The bar chart illustrates that the changes on all intensity parameters and the cell area were above 0.15 while on other parameters, the mean values were less than 0.1, especially those associated with nucleus shape, marker textures of mitochondria, LC3b, and lysosome ( $<0.05$ ). Except for the cell size, the samples slightly affected the nucleus and cell shape, as well as the structures of the cellular organelles, which implied that they had small toxicity to the cells. These results were consistent with the fact that all herbs selected here have historically been used to treat neurodegenerative diseases, and their efficacy and safety have been proven in the long-term practice. All of the selected herbs, except for herb 7 and herb 10, are granted official permission to be used as both food and drugs, or food supplements, by National Health and Family Planning

Commission of the People's Republic of China.

#### 4.4.3 Unique features of TCM samples

The established multidimensional image-based phenotypic screening had been successfully applied to profile natural products from Australian marine sponges *Iotrochota* sp.<sup>21</sup> and *Jaspis splendens*<sup>22</sup>, the bryozoan *Amathia tortusa*<sup>23</sup>, and a natural product library<sup>24</sup>. To unveil the differences among the compounds from different origins, we compared the general phenotypic features of the TCM samples with those of two groups of compounds.

Wang *et al* reported the phenotypic profiles of 22 metabolites isolated from *Jaspis splendens*, a marine sponge collected in Australia.<sup>22</sup> These compounds were assayed and analyzed using the same method described before. The results revealed that six of them (27.3%) showed increased changes on the parameters associated with tubulin, mitochondria LC3b, and lysosome intensity, a similar phenotypic pattern with that of biocluster 6. The other 12 compounds (54.5%), similar to our samples in biocluster 5, showed negative deviations of tubulin, mitochondria LC3b, and lysosome intensity.

Vial *et al* described the biological signature of 482 natural products from Nature Bank, a natural product library, which includes biologically active small molecules isolated from plant and marine sources.<sup>25</sup> In this paper, z score rather than the log2 ratio was used to cluster the samples. Although the analysis method was different and four concentrations were used for one compound, an increase in the lysosome intensity was observed in bioclusters 7, 8, 9, 10, and 11, which covered about 30% of the tested samples (different concentrations of the same compound were counted as different sample). Among them, only biocluster 8 also showed positive deviations in the tubulin, mitochondria, and LC3b maker intensity, namely, about 4% of the tested samples showed the similar biological signatures of our biocluster 6.

**Table 4.4** Percentage of samples with positive deviations of lysosome or similar biological signatures with biocluster 6 from TCM, marine and nature bank.

Sample set	TCM	Marine	Nature bank
Samples with similar biological signatures with biocluster 6 (%)	49.7	27.3	~ 4
Samples with positive deviations of lysosome (%)	64.3	27.3	~ 31

We focused on the differences between three sets of samples from the perspective of lysosome. The data (**Table 4.4**) indicated that up to 64.3% of the TCM samples had positive effects on the lysosome marker intensity, and 49.7% of them not only showed the increases on the lysosome parameters but also on the intensity of tubulin, mitochondria, and LC3b, the similar biological signatures of biocluster 6. The data for the compounds derived from nature bank were about 30% and 4%, respectively. The marine set was relatively small, but 27.3% of them showed positive effects on the lysosome intensity and at the same time on the other parameters associated with intensity.

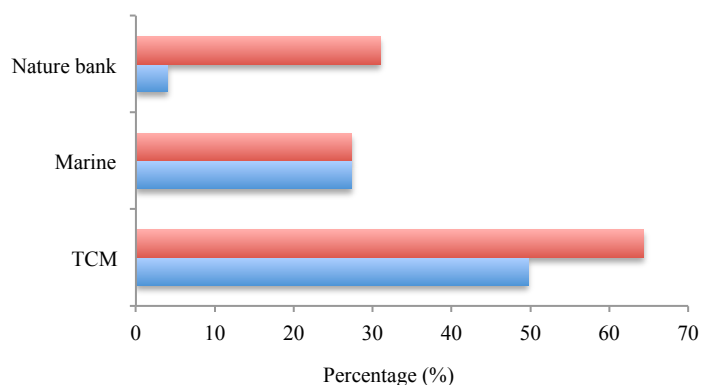


**Figure 4.51** Bar chart of samples with similar signatures of biocluster 6 (blue), and samples with positive deviations of lysosome (red) from TCM, marine, and nature bank.

**Fig. 4.51** clearly illustrates the differences among the three sets of samples. The percentages of samples with positive deviations of lysosome in the latter two sets were close, both being around 30%. This could be regarded as an average ratio of natural products that may show such a positive effect on lysosome, given the samples in these two sets were obtained without purpose on the brain disorders. In contrast, the TCM samples were prepared from the selected herb and herb pairs with known therapeutic

effect, and the samples with the positive effect on the lysosome parameters accounted for almost 2/3 of the total. These facts fully vindicate that lysosome is highly correlated with brain perturbations, and worthy of in-depth investigations to unlock the mechanism and functional proteins underlying the neurodegenerative diseases.

## 4.5 References

1. Fetz, V.; Prochnow, H.; Bronstrup, M.; Sasse, F., Target identification by image analysis. *Nat. Prod. Rep.* **2016**, 33, (5), 655-667.
2. Futamura, Y.; Kawatani, M.; Kazami, S.; Tanaka, K.; Muroi, M.; Shimizu, T.; Tomita, K.; Watanabe, N.; Osada, H., Morphobase, an Encyclopedic Cell Morphology Database, and Its Use for Drug Target Identification. *Chem. Biol.* **2012**, 19, (12), 1620-1630.
3. Feng, Y.; Mitchison, T. J.; Bender, A.; Young, D. W.; Tallarico, J. A., Multi-parameter phenotypic profiling: using cellular effects to characterize small-molecule compounds. *Nat. Rev. Drug Discov.* **2009**, 8, (7), 567-578.
4. Kurita, K. L.; Linington, R. G., Connecting Phenotype and Chemotype: High-Content Discovery Strategies for Natural Products Research. *J. Nat. Prod.* **2015**, 78, (3), 587-596.
5. Schulze, C. J.; Bray, W. M.; Woerhmann, M. H.; Stuart, J.; Lokey, R. S.; Linington, R. G., "Function-First" Lead Discovery: Mode of Action Profiling of Natural Product Libraries Using Image-Based Screening. *Chem. Biol.* **2013**, 20, (2), 285-295.
6. Ochoa, J. L.; Bray, W. M.; Lokey, R. S.; Linington, R. G., Phenotype-Guided Natural Products Discovery Using Cytological Profiling. *J. Nat. Prod.* **2015**, 78, (9), 2242-8.
7. Vial, M.-L. Chemical biology of natural products on Parkinson's disease. PhD dissertation, Griffith University, Australia, 2015.
8. Pharmacopoeia of Peoples Republic of China. In 2005 ed.; National Commission of Chinese Pharmacopoeia, Ed. Chemical Industry Press: Beijing, 2005.
9. 阮琴; 张颖; 胡燕月; 何新霞, 不同制备方法对川芎挥发油化学成分的影响. *中国中药杂志* **2003**, 28, (6), 572-574.
10. Pharmacopoeia of Peoples Republic of China. In 2015 ed.; National Commission of Chinese Pharmacopoeia, Ed. 中国医药科技出版社: Beijing, 2015; pp 58-59.
11. Pharmacopoeia of Peoples Republic of China. In 2015 ed.; National Commission of Chinese Pharmacopoeia, Ed. 中国医药科技出版社: Beijing, p 257.
12. Pharmacopoeia of Peoples Republic of China. In 2015 ed.; National Commission of Chinese Pharmacopoeia, Ed. 中国医药科技出版社: Beijing, 2015; pp 40-41.
13. Pharmacopoeia of Peoples Republic of China. In 2015 ed.; National Commission of Chinese Pharmacopoeia, Ed. 中国医药科技出版社: Beijing, 2015; pp 76-77.
14. Pharmacopoeia of Peoples Republic of China. In 2015 ed.; National Commission of Chinese Pharmacopoeia, Ed. 中国医药科技出版社: Beijing, 2015; p 333.
15. Pharmacopoeia of Peoples Republic of China. In 2015 ed.; National Commission of Chinese Pharmacopoeia, Ed. 中国医药科技出版社: Beijing, 2015; pp 91-92.
16. Pharmacopoeia of Peoples Republic of China. In 2015 ed.; National Commission of Chinese Pharmacopoeia, Ed. 中国医药科技出版社: Beijing, 2015; pp 155-156.
17. Pharmacopoeia of Peoples Republic of China. In 2015 ed.; National Commission of Chinese Pharmacopoeia, Ed. 中国医药科技出版社: Beijing, 2015; pp 366-367.
18. Zhang, J. W.; Zhao, Q., Research Progress of Biology Characteristics and Chemical Constituents of Semen Ziziphi Spinosae. *China Journal of Chinese Medicine* **2013**, 28, (4),

550-553.

19. Li, S. Z.; Wang, X. P., Chemical investigation of *Platyclus orientalis*. *Chinese Traditional Patent Medicine* **1999**, 21, (2), 88-89.
20. Sun, L. J., Composition analysis of fat-soluble substances in seed of Oriental Arborvitae. *Journal of Hebei Normal University (Natural Science Edition)* **2001**, 25, (2), 217-218.
21. Grkovic, T.; Pouwer, R. H.; Vial, M. L.; Gambini, L.; Noel, A.; Hooper, J. N.; Wood, S. A.; Mellick, G. D.; Quinn, R. J., NMR fingerprints of the drug-like natural-product space identify iotrochotazine A: a chemical probe to study Parkinson's disease. *Angew. Chem. Int. Ed. Engl.* **2014**, 53, (24), 6070-4.
22. Wang, D.; Feng, Y.; Murtaza, M.; Wood, S.; Mellick, G.; Hooper, J. N. A.; Quinn, R. J., A Grand Challenge: Unbiased Phenotypic Function of Metabolites from *Jaspis splendens* against Parkinson's Disease. *J. Nat. Prod.* **2016**, 79, (2), 353-361.
23. Dashti, Y.; Vial, M.-L.; Wood, S. A.; Mellick, G. D.; Roullier, C.; Quinn, R. J., Kororamide B, a brominated alkaloid from the bryozoan *Amathia tortuosa* and its effects on Parkinson's disease cells. *Tetrahedron* **2015**, 71, (41), 7879-7884.
24. Vial, M.-L.; Zencak, D.; Grkovic, T.; Gorse, A.-D.; Mackay-Sim, A.; Mellick, G. D.; Wood, S. A.; Quinn, R. J., A Grand Challenge. 2. Phenotypic Profiling of a Natural Product Library on Parkinson's Patient-Derived Cells. *J. Nat. Prod.* **2016**, 79, (8), 1982-1989.
25. Camp, D.; Davis, R. A.; Campitelli, M.; Ebdon, J.; Quinn, R. J., Drug-like properties: guiding principles for the design of natural product libraries. *J. Nat. Prod.* **2012**, 75, (1), 72-81.

## CHAPTER 5 Mass-based target identification

### 5.1 Introduction

#### 5.1.1 Target identification

Phenotype-based screening directly evaluates the holistic effect of small molecules or mixture samples in actual biological systems, and has become an important discovery modality for modern pharmaceuticals. It provides valuable and important information for the mechanism of action underlying the diseases, and facilitates the further step to identify the targets. Target identification is an essential step to reveal the interaction between bioactive small molecules and their interacting targets, and to further identify the underlying mechanism responsible for the induced phenotype (**Fig. 5.1**)<sup>1</sup>.

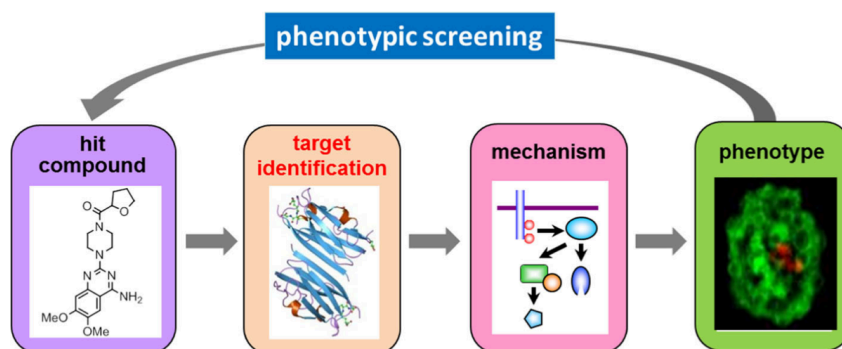


**Figure 5.1** Target identification connects bioactive small molecules with the biological phenotypes they induce and can facilitate the elucidation of the underlying molecular mechanisms of their biological activities.

*With reuse permission from Springer.*

Most drugs show therapeutic effects by forming a noncovalent complex with their biological targets.<sup>2</sup> Target identification remains one of the most challenging tasks in drug discovery. There are many strategies developed for target identification, especially the protein-ligand interactions, during the past several decades, such as X-ray crystallography, nuclear magnetic resonance, surface plasmon resonance, and isothermal titration calorimetry. Affinity purification is one of the most important and powerful approaches and can directly reveal the interactions between small molecules and their biological targets. Among them, electrospray ionization mass spectrometry (ESI-MS) provides a mass-based method with advantages of high sensitivity, selectivity, simplicity, and speed.<sup>3, 4</sup> As a soft-ionization ion method, ESI-MS can detect fragile noncovalent complexes. It can also distinguish whether a protein exists as its native folded state or remains in a denatured state in liquid phase.<sup>5</sup>

#### **5.1.2 ESI-FTICR-MS in study of noncovalent complex**

Electrospray ionization Fourier transform ion cyclotron resonance mass spectrometer (ESI-FTICR-MS, or ESI-FT-MS) is a coupling of ESI and FTICR-MS, which has been developed in the screening of synthetic combinatorial libraries<sup>6, 7</sup> and natural product extracts<sup>8, 9</sup>.

ESI-FT-MS has been proven a powerful tool for studying the noncovalent complexes, and has been applied to a variety of types of complexes.<sup>9-12</sup> RNA was used as a target in an affinity screening to search for the noncovalent interactions with the components from a bacterial natural product library.<sup>9</sup> In a natural product-based fragment library, seven securinine-related compounds were found to bind to *Plasmodium falciparum* 2'-deoxyuridine 5'-triphosphate nucleotidohydrolase (PfδUTPase).<sup>12</sup>

ESI-FT-MS provides a direct and simple method to observe the noncovalent protein-ligand complexes. So far, the general strategy is to use the identified protein to incubate with compounds or to screen in a mixture, identify the protein-ligand complex, and then acquire the binding ligand. This strategy is applicable for searching for small molecules having affinity with specific, identified therapeutic target. For example, *PfdUTPase* in the abovementioned fragment-based screening is a potential drug target used as a platform for antimalarial drug design.<sup>13</sup> However, this strategy does not work for diseases without a clear mechanism or identified validated proteins.

### 5.1.3 Identify direct protein-ligand interactions from cell lysate

The mechanisms of most neurodegenerative diseases such as PD and AD are unclear. It is impractical to apply the conventional method in search for ligand-protein complexes due to the lack of potential drug targets. In contrast, our phenotypic screening of TCM demonstrated that there might be a common lysosome-related mechanism or the same biological targets underlying the neurodegenerative disease. A majority of samples with similar phenotypic signatures might have a common target or pathway perturbation. Therefore, in contrast to using a target protein to identify a ligand, we describe here an attempt to identify the protein by using a bait molecule with a specific phenotypic effect.

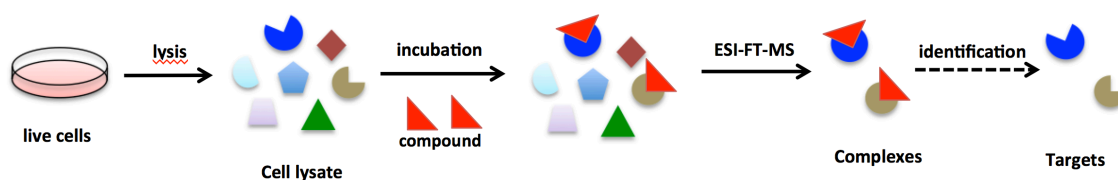


**Figure 5.2** General strategy of using a molecule as a bait to identify the protein binder.

The feasibility of using a molecule as a bait to identify the protein binder depends highly on the high resolving power and high mass accuracy of ESI-FT-MS. In this chapter, hONS cells will be grown and lysed to provide the proteome under native

conditions. ESI-FTMS is then used to screen the cell lysate incubated with a selected molecule. Our goal is to detect the noncovalent complexes in the background of the highly complex cell lysate using native mass spectrometry. Preliminary data will be generated to support the feasibility from molecule to protein (**Fig. 5.2**).

Dihydrotanshinone I (**59**, DSI) from Salviae Miltiorrhizae Radix et Rhizoma is selected as the molecular bait according to the phenotypic screening results. DSI showed the strongest effects on most phenotypic parameters, and was also one of the samples in biocluster 6.

## 5.2 Experimental

### 5.2.1 Materials and reagents

Sterile, filtered Foetal Bovine Serum (Bovogen FBS, #1107A), non-heat inactivated, was supplied by Interpath (Heidelberg West, VIC). Stock FBS was heat inactivated (HI) at 56°C in a water bath for 30 min to destroy heat-labile complement proteins prior to use in cell growth medium and then stored as frozen aliquots at -20°C. Dulbecco's Modified Eagle Medium/Nutrient Mixture F-12 (DMEM/F-12), Hank's Balanced Salt Solution (HBSS) with glucose and without calcium, magnesium or phenol red, and TrypLE™ Express Enzyme (1X), no phenol red, and Dulbecco's phosphate-buffered saline (DPBS) formulations without calcium and magnesium were purchased from Life Technologies (Carlsbad, CA). RIPA (Radio-Immunoprecipitation Assay) buffer was purchased from Sigma-Aldrich (Missouri, USA). M-PER® Mammalian Protein Extraction Reagent was purchased from Thermo Scientific (Rockford, USA). Illustra™ NAP-5 columns were purchased from GE Healthcare (Buckinghamshire, UK). Amicon® Ultra-0.5 10K Centrifugal Filter Devices were purchased from Millipore Corporation (Ireland). Bio-Rad® DC™ Protein Assay Kit was purchased from Bio-Rad Laboratories Pty Ltd (Australia). Ammonium acetate was purchased from SPI Supplier

(West Chester, USA).

### **5.2.2 Cell line and cell culture**

The hONS cells used in the experiment were derived from PD cell line C1 200 08 0013 and stored in liquid nitrogen with 90% FBS and 10% DMSO. PD hONS cells passage 8 from cell line C1 200 08 013 were maintained in complete media (DMEM/F12 supplemented with 10% HI-FBS) under standard conditions in a 150 cm<sup>2</sup> tissue culture flask and incubated in a humidified incubator at 37°C and 5% CO<sub>2</sub>.

### **5.2.3 Cell lysis**

When 90% confluence was reached, the culture medium was removed carefully. The adherent cells were washed with 30 mL cold DPBS for two times. 2 mL of M-PER Reagent with 80 µL of protease inhibitor cocktail was added to the flask, and the flask was then shaken on ice gently for 5 minutes. The lysate was collected using a cell scraper and transferred into a microcentrifuge tube. The lysate was centrifuged at 14,000 × g for 10 minutes to pellet the cell debris. The supernatant was transferred to a new tube for analysis.

### **5.2.4 Protein quantification in the cell lysate**

The protein quantification in the cell lysate was accomplished using the Bio-Rad protein assay kit in a 96-well microplate. 5 µL of the standard bovine serum albumin solution (2.0, 1.0, 0.5, 0.25, 0.125, 0 mg/mL) was added to duplicate wells to create a 0-10 µg calibration curve. In different well, 5 µL of the lysate solution was added in duplicates. 25 µL of Reagent A and then 200 µL of Reagent B were added to all wells. The plate was incubated in the dark at room temperature for 15 minutes and then the absorbance at 590 nm of every well was measured using a Bio-Teck® Synergy 2 plate

reader. The concentration of the lysate was calculated based on the linear equation of the calibration curve.

#### **5.2.5 Buffer exchange and lysate concentration**

The exchange of buffer of the lysate was accomplished in an Amicon<sup>®</sup> Ultra-0.5 10K device by concentrating the sample. An Amicon<sup>®</sup> Ultra-0.5 device was inserted into a microcentrifuge tube. 500  $\mu$ L of the lysate was added into the filter device. The device was capped and then spun at  $14,000 \times \text{rcf}$  for 10 minutes. The filtrate was discarded and the concentrate was reconstituted to the original 500  $\mu$ L volume with 158  $\mu$ L of 10 mM ammonium acetate. The device was spun again at  $14,000 \times \text{rcf}$  for 10 minutes, and discard the filtrate. Repeat the process of “washing out” for 5 times until the concentration of the M-PER Reagent was sufficiently reduced. The filter device was placed upside down in a clean microcentrifuge tube and spun at  $1,000 \times \text{rcf}$  for 2 minutes. The concentrated lysate was recovered in the centrifuge tube.

#### **5.2.6 Sample preparation**

The concentrated lysate in the centrifuge tube was diluted with 10 mM ammonium acetate to make 200  $\mu$ L of a lysate solution. The final concentration of proteins in the lysate was 0.5 mg/mL.

Dihydrodanhsinone I (0.7 mg) was dissolved in 0.5 mL of methanol to make a 5 mM solution. 20  $\mu$ L of the methanol solution was added into 200  $\mu$ L of the lysate solution to incubate together and afforded a lysate solution spiked with DSI.

#### **5.2.7 ESI-FTICR analysis**

All experiments were performed on a Bruker Solarix ESI ETD 12 Tesla FT-ICR mass spectrometer equipped with an external Apollo ESI source. All samples were

injected manually by a syringe pump with a flow rate of 120  $\mu\text{L}/\text{h}$ . A nebulizing  $\text{N}_2$  gas with a pressure of 2.0 bar and a counter-current drying  $\text{N}_2$  gas with a flow of 4.0 L per minute were employed. The drying gas temperature was maintained at 200°C for direct infusion ESI-FTICR-MS. The capillary exit voltage was tuned at 220 V. Ions were accumulated in an external ion reservoir comprised of an octopole. The accumulation time was set at 1.0 ms. The range of mass-to-charge ratio is scanned from 200 to 8,000.

The data were acquired in Bruker fimsControl 2.1.0 software. All spectra were recorded in positive ion mode, with a sum of 1024 or 2048 scans per acquisition and 4 M data points per transient. The obtained spectra were analyzed in Bruker Compass DataAnalysis 4.4 software under Windows operating system.

## 5.3 Results and discussion

### 5.3.1 Cell lysis and buffer exchange

The choice of detergent for native cell lysis is very important. RIPA is a popular choice for lysis and protein extraction of mammalian cells. The M-PER reagent extracts cytoplasmic and nuclear protein from cultured mammalian cells, and provides a rapid, mild and efficient lysis. RIPA buffer and M-PER reagent were used to lyse the living cells, respectively.

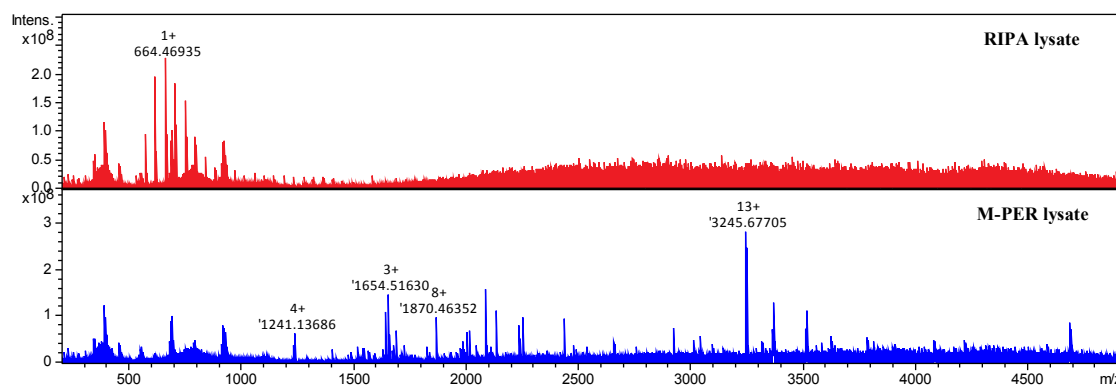
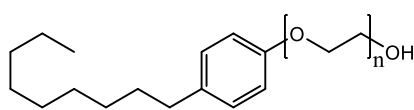


**Figure 5.3** Spectra of the lysates obtained from the treatment with RIPA buffer (red), and M-PER reagent (blue).

**Fig. 5.3** illustrates that, under the same condition, no protein could be observed for

the lysate obtained from the treatment with RIPA reagent, while some native proteins, as well as small peptides, were detected from the lysate obtained from the treatment with M-PER reagent. The peaks of native proteins detected were distributed in the range from  $m/z$  1,000 to 5,000.

There were some intense peaks in mass around  $m/z$  664 with a repeating unit of 44 in the spectrum of the RIPA lysate. The repeating unit of 44 ( $C_2H_4O$ ) suggested that these peaks could be ascribed to the presence of NP-40 (for structure see below), a detergent with  $n = 7-28$  used in the RIPA buffer.



NP-40

Illustra NAP-5 columns and Amicon centrifugal filter devices were used for buffer exchange of the lysate, respectively. Neither could remove the detergent of NP-40 from the RIPA lysate. It was found that cell lysis using detergents resulted in contamination by the detergent. In the case of RIPA, the detergent could not be removed and completely interfered with native protein detection. M-PER resulted in less residual detergent and allowed detection of some native proteins.

Therefore, the M-PER reagent was selected for native cell lysis, which was followed by buffer exchange and concentration using the Amicon centrifugal filter devices.

### 5.3.2 ESI-MS conditions optimization

To preserve the proposed weak noncovalent protein-ligand complexes, the ESI-MS conditions needed to be optimised. Many parameters impact on the signal intensity of protein and protein-ligand complex, including flow rate, temperature, nebulizing gas, drying gas, end plate voltage, capillary voltage, capillary exit voltage, skimmer 1, and skimmer 2.<sup>14</sup> Some investigations of the optimization of ESI-MS conditions have been

reported, but all focused on purified protein and tuning the conditions to maximize the relative ionization efficiency of the protein-ligand complex and minimize the complex dissociation during the ESI process.<sup>12, 15</sup> Different from pure protein, the cell lysate is a pool of native proteins. In this study, ESI-FT-MS is used to screen the cell lysate with the molecular weights of proteins ranging from several kDa to several hundred kDa. To minimize the parameters needing to be handled, three factors, time of flight, skimmer 1, and incubation time of the lysate with the molecule, were investigated first.

### 5.3.2.1 Time of flight

The parameter time of flight is a time measurement related to an ion's mass-to-charge ratio. The bigger the parameter is, the more ions with high mass-to-charge ratio can be detected. Two values of 3.0 and 2.0 ms were tried in the experiment.

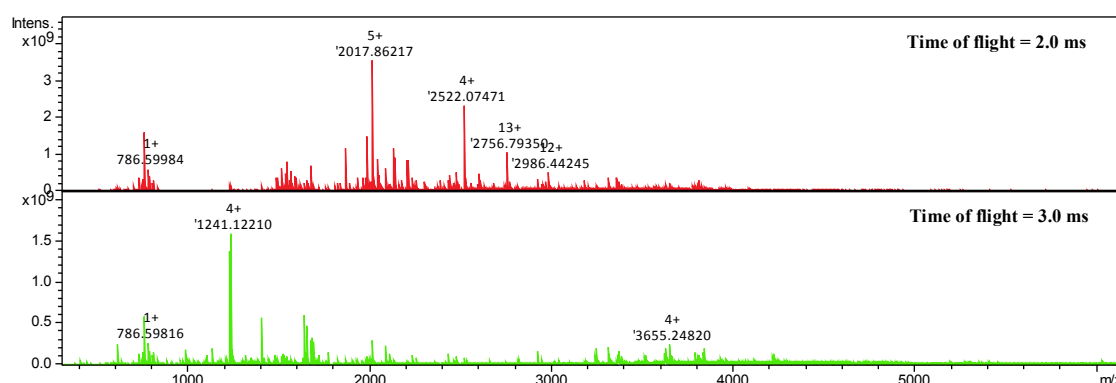


**Figure 5.4** Spectra of the M-PER lysates measured using different values of time of flight (skimmer 1=130 V)

**Fig. 5.4** illustrates that the time of flight made a big impact on the spectrum of the lysate. When time of flight was 2.0 ms, the protein peaks were distributed from  $m/z$  1,500 to 4,000, and some peaks with high intensity (above  $1 \times 10^9$ ) were observed around  $m/z$  2017, 2522, and 1756. When it was 3.0 ms, the peaks had a boarder distribution from  $m/z$  1,000 to 4,500, but except for the big peak with a charge state 4+, the rest showed the intensity less than  $1 \times 10^9$ . At same time, at the range from  $m/z$  3,500 to 4,500, the latter showed more peaks than the former.

The results suggested that due to the complexity of proteins in the lysate, different

times of flight could impact a lot on the spectrum. The longer time of flight could detect more peaks with high mass-to-charge ratio, but at the expense of the peaks in the lower  $m/z$  range.

### 5.3.2.2 Skimmer 1

The parameter of skimmer 1 is associated with the energy for solvent evaporation along the path from the atmospheric region to the high vacuum region. The higher the  $m/z$  complex ion value is, the bigger skimmer 1 voltage should be.<sup>16</sup> However, at the same time, the high voltage of skimmer 1 might cause complex dissociation. Given the molecular weights of proteins in the lysate reached up to several hundred kDa, the skimmer 1 voltages at 100, 115, 130 and 145 V were used to look for a value that can meet the controversial requirements for complete desolvation and preservation of complex ions.

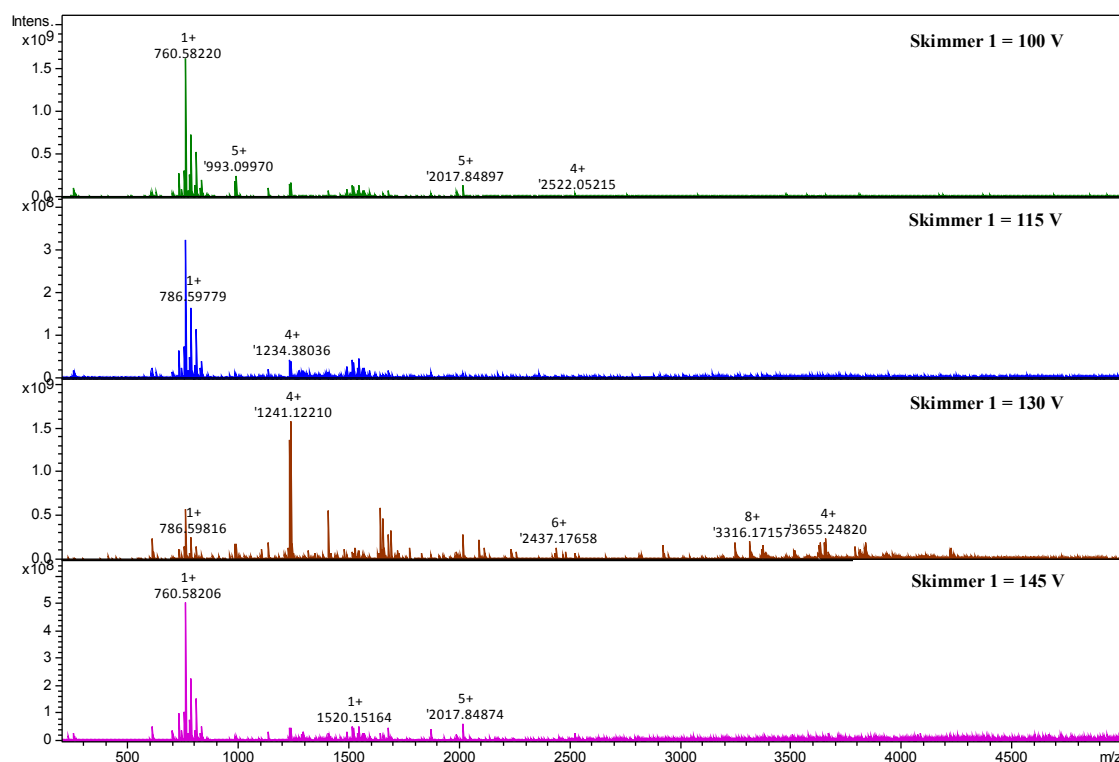


**Figure 5.5** Spectra of the M-PER lysates measured using different values of skimmer 1 (time of flight = 3.0).

**Fig. 5.5** shows that when skimmer 1 was 130 V, the detected peaks of native proteins and their intensity reached to optimum values. Less or more than 130 V both

decreased the number of the peaks that could be detected, as well as their intensity. However, the skimmer 1 voltage used in this study is much bigger than those reported in the literatures, which were usually less than 30 V.<sup>11, 15, 17</sup> It might be due to the fact that the proteins used in the literatures were pure while the cell lysate contained an array of different proteins.

### 5.3.2.3 Incubation time

The binding affinity between the molecule and the protein determines the incubation time. The weaker the binding affinity is, the longer incubation time requires. Considering a variety of proteins in the cell lysate, the binding affinity between the molecule and different proteins varies greatly. In order to maximize the chance to find the noncovalent complex from the lysate, 1, 6, and 24 hours of incubation time were performed.

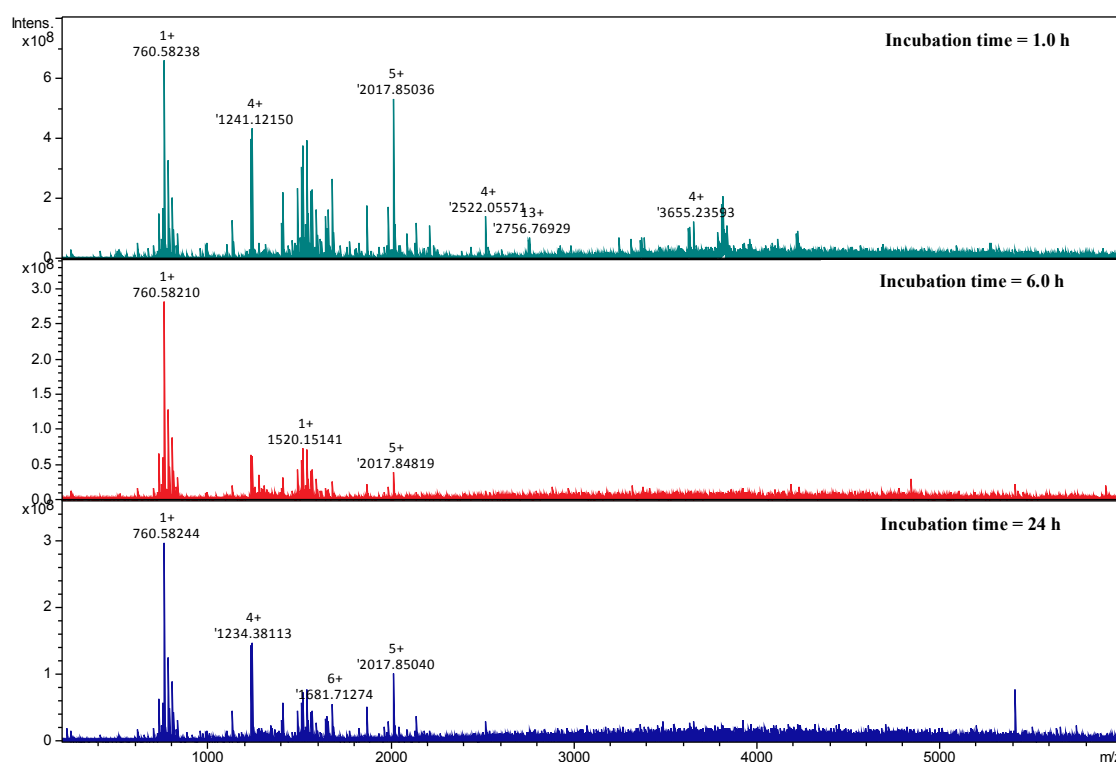


**Figure 5.6** Spectra of the M-PER lysates incubated with DSI in different times (skimmer 1 = 130 V, time of flight = 3.0 ms).

**Fig. 5.6** shows that the spectra recorded at 6 and 24 h lost the protein peaks in the range from  $m/z$  3,000-6,000 compared with that at 1.0 h. This might be due to the resolution of the FT-MS spectrometry. The expanded spectra at the range of  $m/z$

1,500-2,500 were examined carefully (**Fig. 5.7**). Except for intensity changes of some peaks, these three spectra were very similar, suggesting that the incubation time did not impact a lot at the detected primary proteins of the lysate.

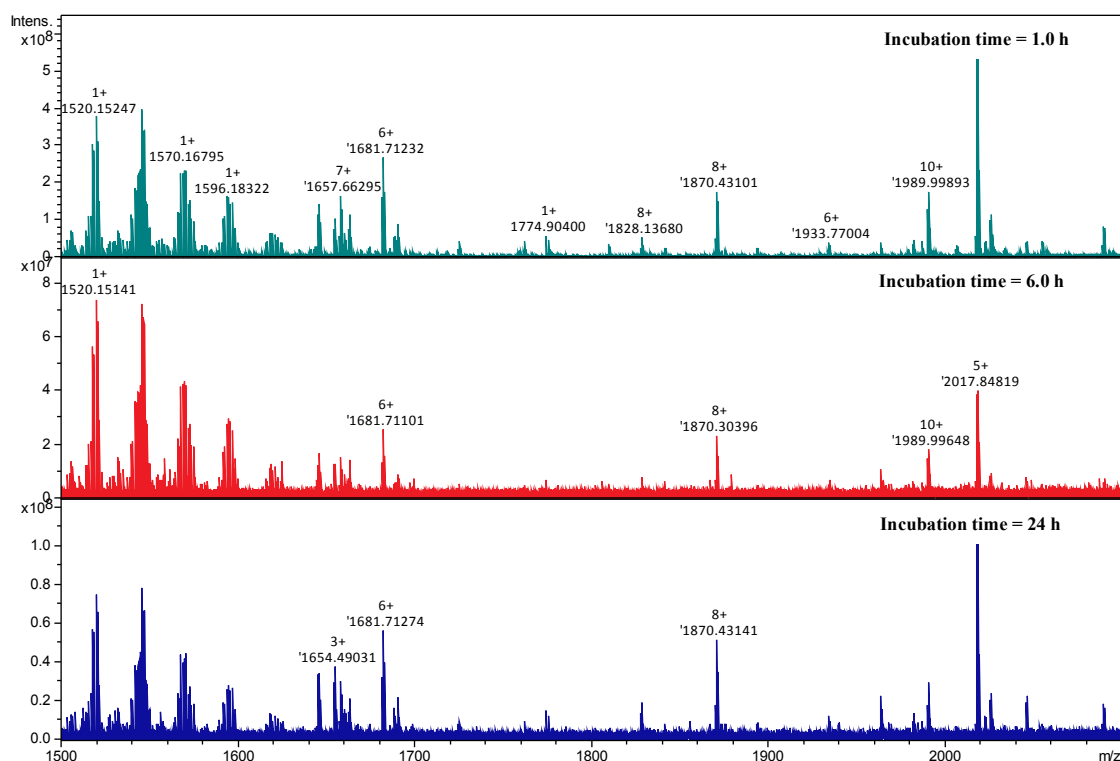


**Figure 5.7** Expanded spectra ( $m/z$  1,500-2,500) of the M-PER lysates incubated with DSI in different times (skimmer 1 = 130 V, time of flight = 3.0 ms).

### 5.3.3 Search for protein-ligand complexes

According to the above results, the optimised conditions were set as skimmer 1 voltage being 130 V, time of flight being 2.0 ms, and incubation time being 24 h. Two samples, the lysate and the lysate incubated with DSI, were run on the FT-MS, respectively, under the same conditions.

The strategy to search the possible complexes is to compare the two mass spectra and look for the native protein peaks only detected in the spectrum of the incubated lysate. These “extra” peaks correspond to putative complexes. Then from the protein-ligand peaks, the protein peaks can be found. A complex peak and its protein peak should have the same charge state, and the  $m/z$  relationship between them is:

$$m/z_{\text{protein}} = m/z_{\text{complex}} - MW_{\text{ligand}}/\text{charge state}$$

The FT-MS results for these two samples are shown in **Fig. 5.8**. A detailed analysis of these two spectra was therefore carried out.

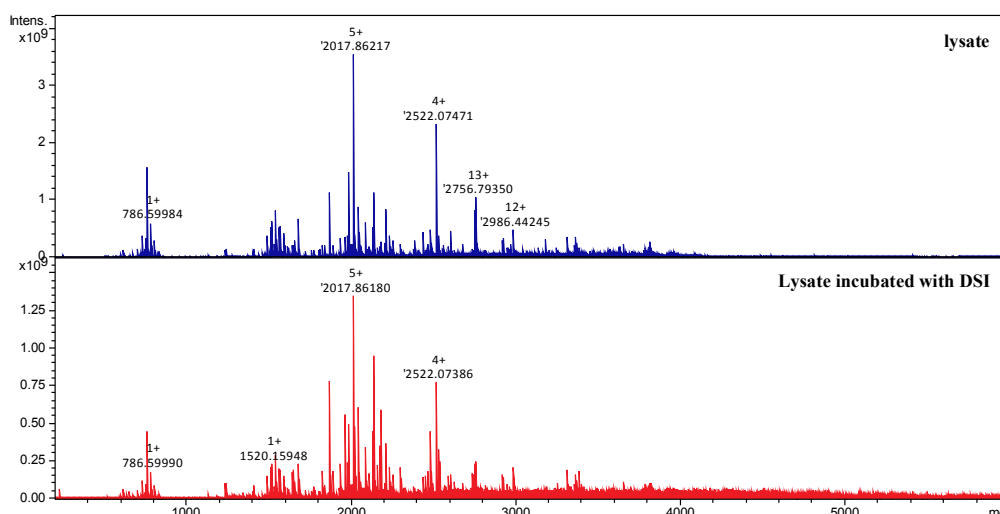


**Figure 5.8** Spectra ( $m/z$  200-6,000) of the M-PER lysate and the lysate incubated with DSI in different times (skimmer 1 = 130 V, time of flight = 2.0 ms, incubation time = 24 h).

Native proteins and peptides were two major species found in the spectrum. Native protein usually shows a broad and low charge state mass spectrum (high  $m/z$ ), which can be distinguished from the denatured protein because the unfolded protein has a narrow and high charge state spectrum (low  $m/z$ ).<sup>5</sup> Peptides might be degraded from the protein during the lysis, and always have a broader mass spectrum with a charge state +1. Some native proteins and the major peptides found in the lysate are shown in **Fig. 5.9**.

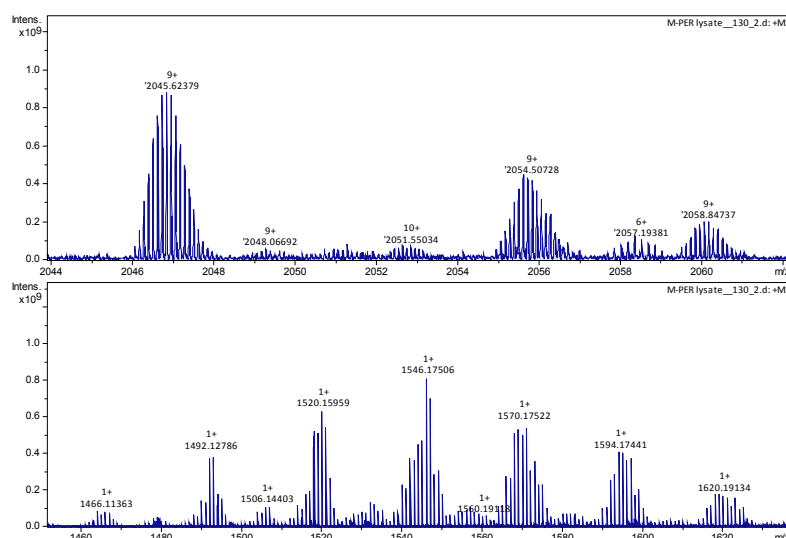
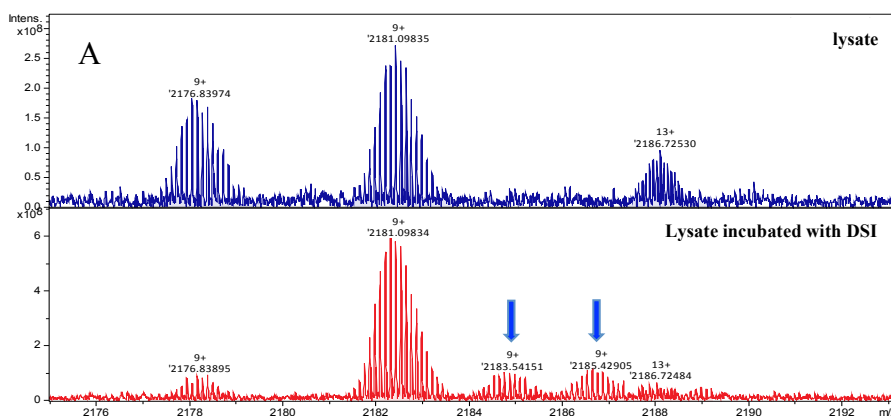


**Figure 5.9** Spectra of native proteins (above) and peptides (below) extracted from the spectrum of the M-PER lysate (skimmer 1 = 130 V, time of flight = 2.0 ms).

Except for the peaks with charge state +1, as many as 194 peaks were detected with charge states from +2 to +14 (**Appendix II**). Some of them were peptides, and the majority were identified as native proteins. The denature proteins were rarely observed. Their molecular weights distributed in a range from 1129 to 47210 Da.

The proteins in a cell lysate have a very broad distribution from several kDa to several hundred kDa. However, the molecular weights of the proteins in this experiment were in a narrow range. The M-PER reagent used for the lysis might be one reason because it extracts only nuclear and cytoplasmic proteins, and is unable to retrieve membrane protein with high molecular weight. The other reason is that the lysate was so complicated that one set of optimized parameters for FT-MS could not cover the proteins with different properties. As we mentioned above, proteins with high  $m/z$  need longer times of flight. Other parameters also might impact the resolution for different proteins.

A detailed examination of two spectra revealed three “extra” peaks that were only observed in the lysate incubated with DSI, the peaks of  $m/z$  2183.09834 and 2185.42905 both with charge state 9+ (**Fig. 5.10A**), and  $m/z$  1965.29045 with charge state 10+ (**Fig. 5.10B**). These peaks theoretically corresponded to the plausible protein-ligand complexes. Based on the  $m/z$  and charge state of three “extra” peaks, the calculation indicated that the putative proteins should appear at  $m/z$  2152.62, 2154.51, and 1937.46, respectively.



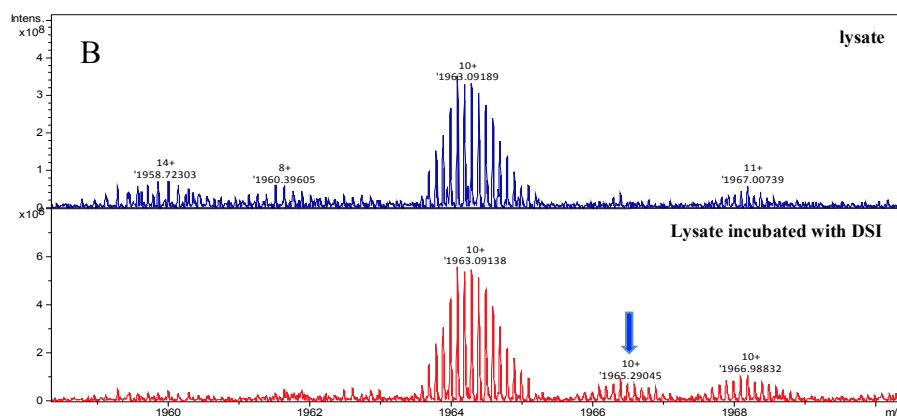


**Figure 5.10** Expanded spectra of the lysate (blue) and the lysate incubated with DSI (red) containing the “extra” peaks. (skimmer 1 = 130 V, time of flight = 2.0 ms, incubation time = 24 h).

Searching the range from  $m/z$  2,150 to 2,190 revealed that putative proteins corresponding in mass to  $m/z$  2152.62 and 2154.51 were not detected both in the lysate and the lysate incubated with DSI (**Fig. 5.11**). It might be ascribed to the unstable proteins to which DSI was bound, or the poor resolution of the mass spectrometry for minor proteins with low intensity. It is mostly likely that the small molecule bound to the minor proteins rather than the primary proteins of the cell lysate. Due to the limitation of the mass spectrometry, the intensity of such proteins was too low to be detected.

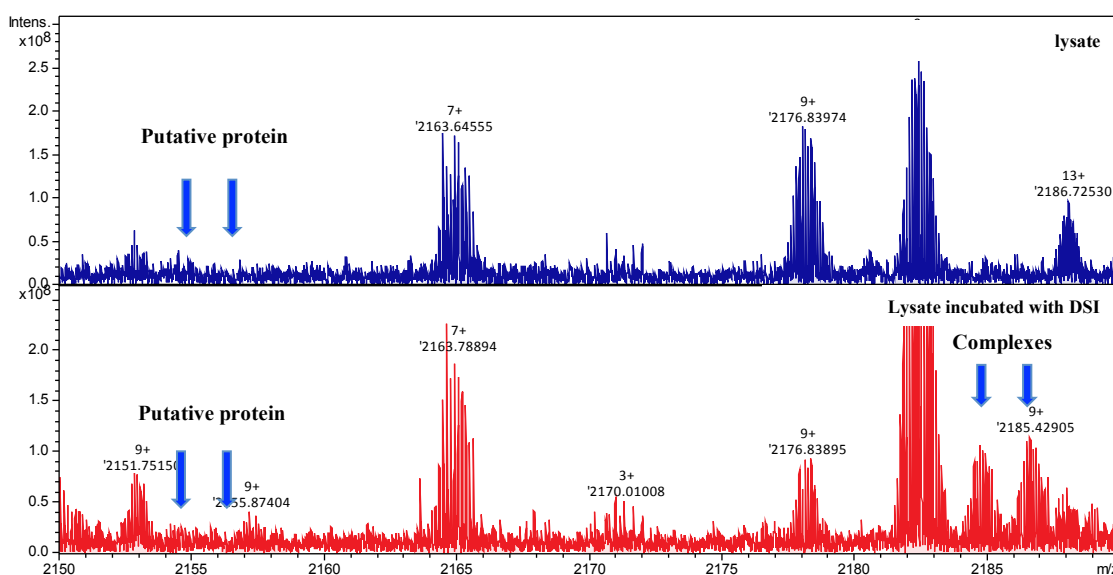


**Figure 5.11** Expanded spectra ( $m/z$  2,150-2,190) of the lysate (blue) and the lysate incubated with DSI (red) containing the “extra” peaks. (skimmer 1 = 130 V, time of flight = 2.0 ms, incubation time = 24 h).

Searching the range from  $m/z$  1,935 to 1,970 revealed that there were several

protein peaks around  $m/z$  1937.46 detected both in the lysate and the lysate incubated with DSI (**Fig. 5.12A**). The spectrum of the lysate gave  $m/z$  1936.57760 with charge state 10+ while that of the lysate incubated with DSI showed  $m/z$  1937.61067 with charge state 6+.

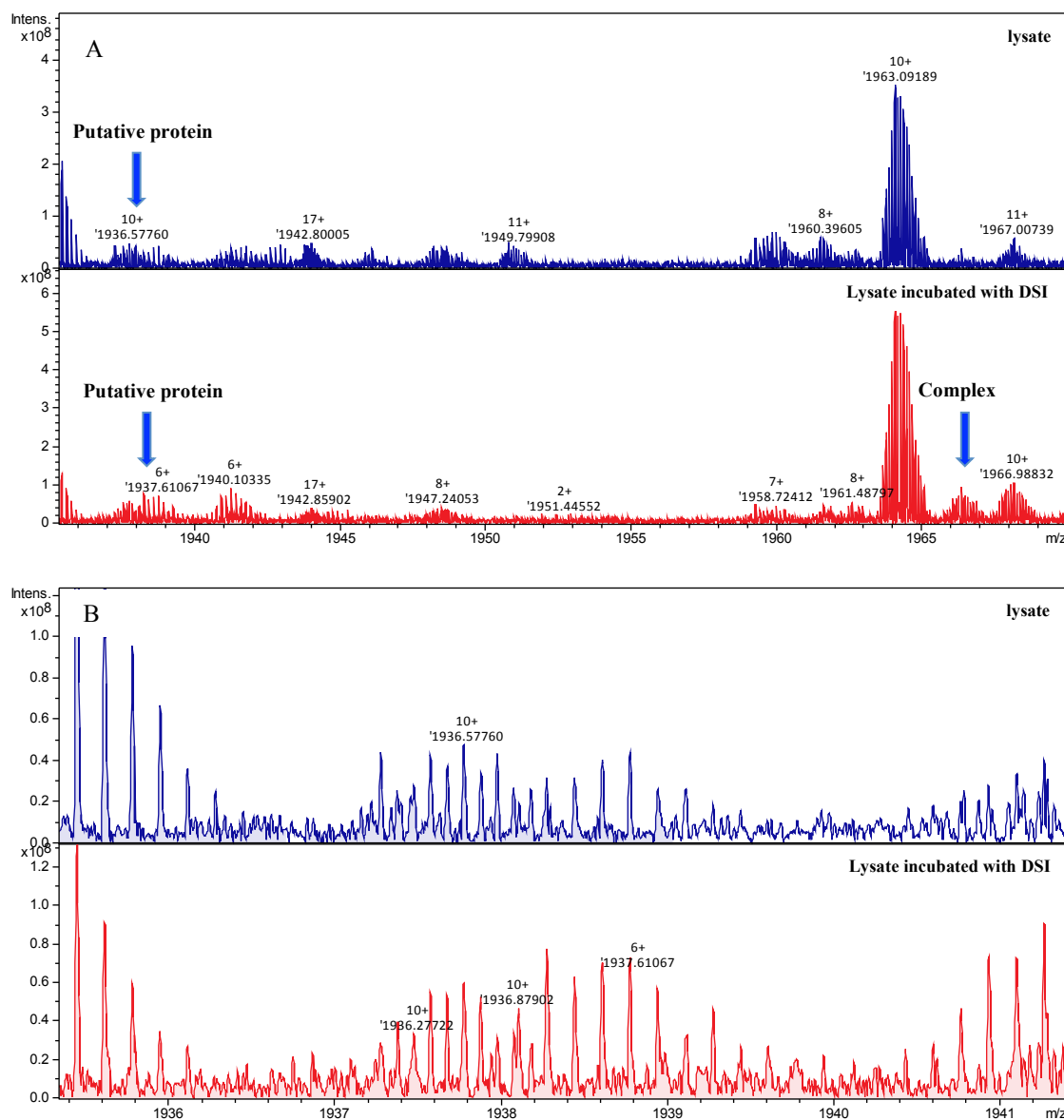


**Figure 5.12** Expanded spectra ( $m/z$  1,935-1,970) of the lysate (blue) and the lysate incubated with DSI (red) containing the “extra” peaks. (skimmer 1 = 130 V, time of flight = 2.0 ms, incubation time = 24 h).

Expanded spectra of these peaks (**Fig. 5.12B**) show that there were at least three proteins partially overlapping in this area, and two of them have charge states 10+. Due to the low intensity of these proteins, it is hard to identify the accurate number of proteins, their accurate  $m/z$  and charge state. However, these data strongly supported the

existence of the putative protein at  $m/z$  1937.61067 with charge state 10+.

These results indicated that the protein-ligand complexes could be detected from the whole lysate. It is feasible to identify a protein by using a bait molecule. However, due to the limitation of the mass spectrometry, some proteins or protein-ligand complexes with low intensity could hardly be detected. Therefore, the simplified samples from the cell lysate were required in order to get a better resolution for minor proteins.

Fractionation of the cell lysate by size exclusive column or ion exchange chromatography will be an important step before searching for noncovalent complex. The simplification of the sample can increase greatly the resolution for minor proteins and their complexes. On the other hand, it is easier to find the optimized mass conditions for every fraction of the lysate. In addition, the voltage of the skimmer 1 could be optimized to a lower value, which can decrease the complex dissociation, and increase the possibility to detect the weak complexes at the same time.

## **5.4 Future work**

The results presented in the chapter proved the feasibility to use a molecule with specific biological effect as a bait to identify target proteins from the cell lysate through native mass spectrometry. Based on these data, detailed and in-depth research is of great practicability. Some further work can be reasonably drawn from the results.

1. More lysis methods should be tried in order to find a more complete and efficient way to get as many native proteins as possible from the living cells, especially those membrane proteins.
2. Although FT-MS showed high sensitivity and high resolution in the experiment, the proteins in the lysate were so complex. A fractionation of the cell lysate by size exclusive column or ion exchange chromatography should

be performed to increase the resolution for proteins and protein-ligand complexes with low intensity.

3. Optimization of FT-MS instrument parameters should be done for every sample obtained through fractionation.
4. The Bruker Solarix 12T FT-ICR mass spectrometer includes the ECD features. Electron capture dissociation (ECD) experiments should be performed to identify the proteins having noncovalent bindings with the bait molecule. The identified proteins could then provide pivotal information to unveil the possible target proteins and disclose the plausible acting pathways.

## 5.5 References

1. Zheng, W. L.; Li, G.; Li, X. Y., Affinity purification in target identification: the specificity challenge. *Arch. Pharmacol. Res.* **2015**, 38, (9), 1661-1685.
2. Hofstadler, S. A.; Sannes-Lowery, K. A., Applications of ESI-MS in drug discovery: interrogation of noncovalent complexes. *Nat. Rev. Drug Discov.* **2006**, 5, (7), 585-595.
3. Hofstadler, S. A.; Sannes-Lowery, K. A., Applications of ESI-MS in drug discovery: interrogation of noncovalent complexes. *Nat. Rev. Drug Discov.* **2006**, 5, (7), 585-95.
4. Pacholarz, K. J.; Garlish, R. A.; Taylor, R. J.; Barran, P. E., Mass spectrometry based tools to investigate protein-ligand interactions for drug discovery. *Chem. Soc. Rev.* **2012**, 41, (11), 4335-4355.
5. Chowdhury, S. K.; Katta, V.; Chait, B. T., Probing conformational changes in proteins by mass spectrometry. *J. Am. Chem. Soc.* **1990**, 112, (24), 9012-9013.
6. Shin, Y. G.; Van Breemen, R. B., Analysis and screening of combinatorial libraries using mass spectrometry. *Biopharm. Drug Dispos.* **2001**, 22, (7-8), 353-372.
7. Johnson, B. M.; Nikolic, D.; Van Breemen, R. B., Applications of pulsed ultrafiltration-mass spectrometry. *Mass Spectrom. Rev.* **2002**, 21, (2), 76-86.
8. Nikolic, D.; Habibi-Goudarzi, S.; Corley, D. G.; Gafner, S.; Pezzuto, J. M.; Van Breemen, R. B., Evaluation of cyclooxygenase-2 inhibitors using pulsed ultrafiltration mass spectrometry. *Anal. Chem.* **2000**, 72, (16), 3853-3859.
9. Cummins, L. L.; Chen, S.; Blyn, L. B.; Sannes-Lowery, K. A.; Drader, J. J.; Griffey, R. H.; Hofstadler, S. A., Multitarget affinity/specificity screening of natural products: finding and characterizing high-affinity ligands from complex mixtures by using high-performance mass spectrometry. *J. Nat. Prod.* **2003**, 66, (9), 1186-1190.
10. Gao, H.; Leary, J.; Carroll, K. S.; Bertozzi, C. R.; Chen, H., Noncovalent complexes of APS reductase from *M. tuberculosis*: Delineating a mechanistic model using ESI-FTICR MS. *J. Am. Soc. Mass. Spectrom.* **2007**, 18, (2), 167-178.
11. Vu, H.; Quinn, R. J., Direct screening of natural product extracts using mass spectrometry. *J. Biomol. Screen* **2008**, 13, (4), 265-275.
12. Vu, H.; Roullier, C.; Campitelli, M.; Trenholme, K. R.; Gardiner, D. L.; Andrews, K. T.; Skinner-Adams, T.; Crowther, G. J.; Van Voorhis, W. C.; Quinn, R. J., Plasmodium Gametocyte Inhibition Identified from a Natural-Product-Based Fragment Library. *ACS*

*Chem. Biol.* **2013**, 8, (12), 2654-2659.

13. Whittingham, J. L.; Leal, I.; Nguyen, C.; Kasinathan, G.; Bell, E.; Jones, A. F.; Berry, C.; Benito, A.; Turkenburg, J. P.; Dodson, E. J., dUTPase as a platform for antimalarial drug design: structural basis for the selectivity of a class of nucleoside inhibitors. *Structure* **2005**, 13, (2), 329-338.
14. Griffey, R. H.; Sannes-Lowery, K. A.; Drader, J. J.; Mohan, V.; Swayze, E. E.; Hofstadler, S. A., Characterization of low-affinity complexes between RNA and small molecules using electrospray ionization mass spectrometry. *J. Am. Chem. Soc.* **2000**, 122, (41), 9933-9938.
15. Pedro, L.; Van Voorhis, W. C.; Quinn, R. J., Optimization of Electrospray Ionization by Statistical Design of Experiments and Response Surface Methodology: Protein-Ligand Equilibrium Dissociation Constant Determinations. *J. Am. Soc. Mass. Spectrom.* **2016**, 27, (9), 1520-30.
16. Murata, H.; Takao, T.; Shimonishi, Y., Optimization of Skimmer Voltages of an Electrospray Ion-Source Coupled with a Magnetic-Sector Instrument. *Rapid Commun. Mass Spectrom.* **1994**, 8, (2), 205-210.
17. Yang, B.; Feng, Y. J.; Vu, H.; McCormick, B.; Rowley, J.; Pedro, L.; Crowther, G. J.; Van Voorhis, W. C.; Forster, P. I.; Quinn, R. J., Bioaffinity Mass Spectrometry Screening. *J. Biomol. Screen* **2016**, 21, (2), 194-200.

## CHAPTER 6 General conclusions and perspectives

### 6.1 General conclusions

The thesis presented a proof-of-concept to translate traditional Chinese medicines to modern medicines through a variety of modern chemical and biological technologies.

The first step was data mining of accumulative knowledge of TCMs in ancient medicinal books and literatures. The long history of TCMs in clinical practices provided a selection of herbs and herb pairs with definite therapeutic effects on the neurodegenerative diseases. Physicochemical analysis, ChemGPS-NP, and *in silico* BBB prediction were used for an in-depth analysis of major compounds from the selected herbal materials. An amazing convergence between the TCM components and current small molecule drugs was found from the perspective of physicochemical properties. The results laid a solid foundation for further investigations.

In the following, three levels of samples, extract, fraction and compounds, were prepared and analyzed using HPLC-ELSD, LC-MS, and LC-NMR. Also some artificial mixtures that mimicked the chemical composition of extract or fraction were produced. With definite chemical composition, these samples were further screened on the established multidimensional phenotypic screening platform. Detailed analysis of the biological data revealed that the screened TCM samples showed high correlation with lysosome. The results were consistent with the fact that these TCM samples were prepared from the selected herb and herb pairs with known therapeutic effect, and vindicated that lysosome is highly correlated with brain perturbations.

The results further guide towards the identification of targets of a plausible, common lysosome-related mechanism or pathway underlying the neurodegenerative diseases. By using native mass spectrometry ESI-FTICR-MS, a molecule showing the strongest effects from phenotypic assay was used as a bait to identify the non-covalent complexes from the cell lysate. The feasibility of the novel strategy has been tentatively proven, and more work will continue until the related proteins are identified.

From ancient knowledge to modern drugs, the concept has been proven rationale and feasible. Physicochemical analysis, chemical profiling, phenotypic screening or target identification, all these technologies and relevant tools build a bridge between ancient TCMs and modern medicines.

## **6.2 Integration of new technologies will benefit TCM research**

The integration of the above-mentioned tools and technologies has been proven an important and efficient way when investigating the complex TCMs. Every tool or technique has its own advantages, and their integration contributes to new findings.

TCM features the usage of mixtures. Phenotypic screening can give an overall biological effect for a sample no matter it is a mixture (extract/fraction) or a pure compound. HPLC analysis can reveal the chemical composition of a mixture. The combination of chemical and biological data facilitates detailed investigations of a mixture and its individual components at the same time. The technologies helped us disclose the existence of synergistic effect, antagonistic effect and additive effect of the mixtures, and are believed to unlock more from different perspectives.

The investigation of mechanism or biological targets of a mixture is a challenging task. Phenotypic screening provides a platform bridging mixture and pure compound. In our study, the compound, showing the same phenotypic signature with a mixture, was used as a representative sample to disclose the mechanism or identify the target. This

new strategy can be regarded as a breakthrough to study the mechanism of a mixture by treating it as a whole rather than a collection of compounds.

Additionally, native mass spectrometry ESI-FTICR-MS is an excellent tool. Its simplicity, high sensitivity and high resolution determine its potential usage in complicate samples like the cell lysate. The spectrum generated by FT-MS exhibits visible signals of non-covalent complexes, and a simple comparison of spectrum of a lysate with that of the lysate spiked with a ligand will easily unveil the existence of the complex. With the help from technologies such as ECD, subsequent work will lead to the identification of the corresponding protein revolved in pathways underlying the disease. Native mass spectrometry is a powerful tool to explore the unknown or novel mechanism.

The research work described in this thesis is an integrated approach and a starting point. These technologies provide possibilities for a better understanding of TCM from the perspective of systems biology.

At the moment, although more people outside China have gradually accepted TCM as an alternative medicine, the lack of scientific evidence to support efficacy and safety is still a major reason that keeps TCM from widespread recognition. Different from western medicine, TCM features the usage of mixtures, all kinds of extracts from individual herbs or formulas. This makes it more difficult to explain TCM than western medicine. Fortunately, the development of modern technologies has shed light on this complex system. That is exactly the problems that this thesis has addressed. This integrated approach to TCM will allow the ancient knowledge and wisdom to be vindicated and accepted globally. Traditional Chinese medicines can coexist with western medicine. The usage of them in a complementary way will definitely benefit the health of human beings.

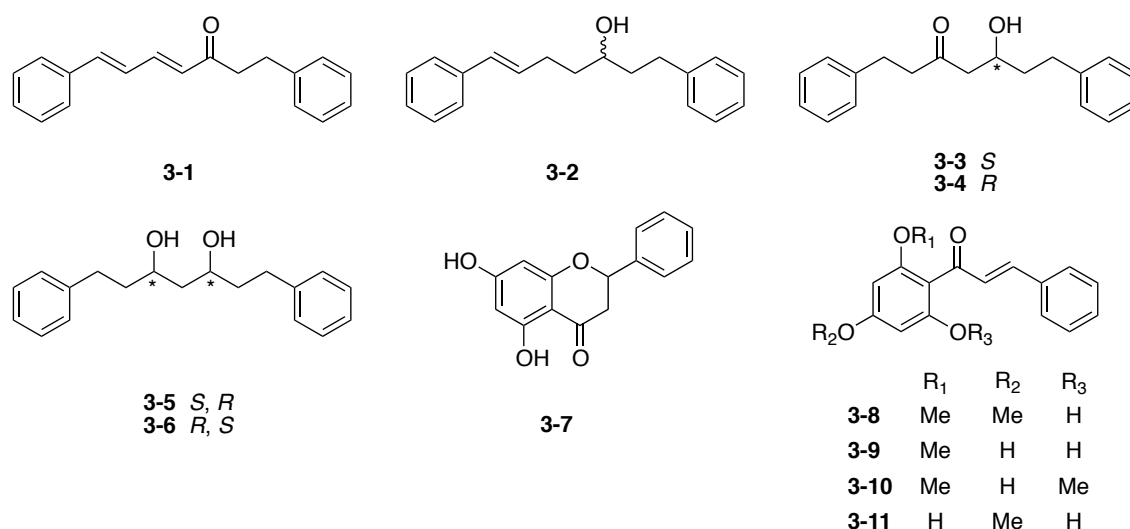


## Supporting Information

### Isolation and structural elucidation of compounds from the selected herbs

#### S1 Curcumins, flavonoids, and chalcones from Amomi Fructus Rotundus

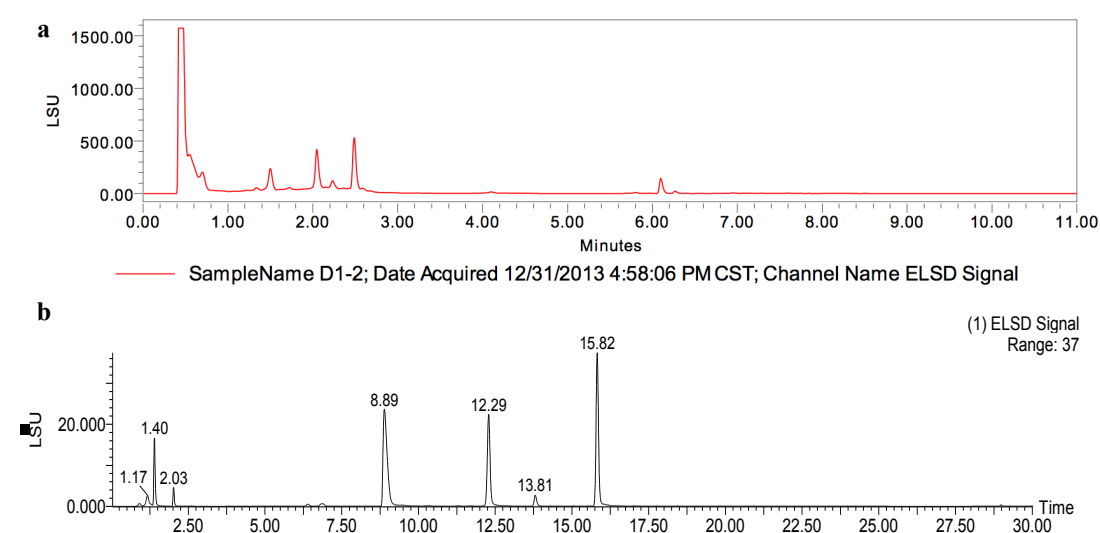
Dried fruits (10 kg) of *A. compactum* was ground and extracted three times (4 days each) with acetone (5 L) at room temperature. After concentration of the combined percolate under reduced pressure, the crude extract was suspended in water (40°C), and then partitioned with petroleum ether (PE), CH<sub>2</sub>Cl<sub>2</sub>, and EtOAc, successively. The CH<sub>2</sub>Cl<sub>2</sub> extract (600 g) was subjected to silica gel column chromatography (CC) elution with PE/acetone (10:1–0:1, in a stepwise manner) to give 14 fractions. The repeated CC combined with the preparative HPLC yielded the isolation of 11 compounds including diarylheptanoids<sup>1-5</sup>, flavonoids<sup>6</sup>, and chalcones<sup>7-10</sup>. Their structures were identified by extensive analysis of spectroscopic data and comparison with data in literature shown in **Fig. S.1**.



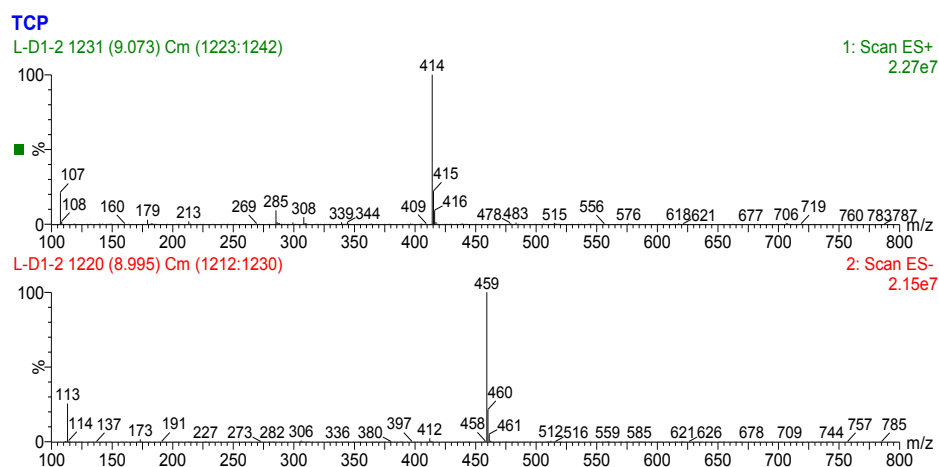
**Figure S.1** Structures of diarylheptanoids, flavonoids, and chalcones from Amomi Fructus Rotundus.

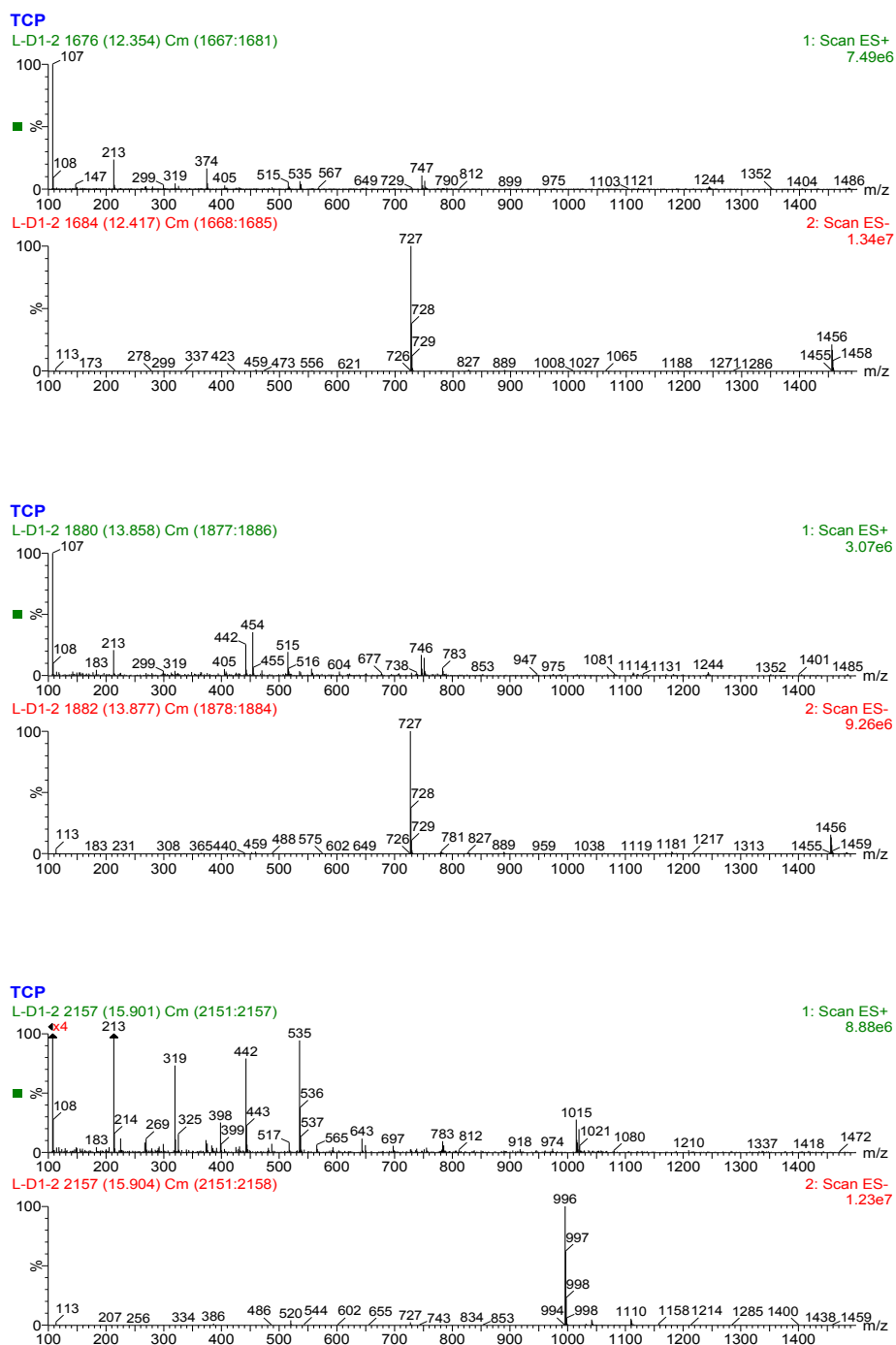
## S2 Parishines from Gastrodiae Rhizoma

The HPLC chromatogram of the de-sugar fraction of Gastrodiae Rhizoma showed that there are four major peaks from RT 1.5 min to RT 2.5 min. To obtain these four compounds, the HPLC condition was optimized (**Fig. S.2**) and the molecular weight of these four peaks were obtained on a LC-MS run. The molecular weights of peaks 1-4 are shown in **Fig. S.3**.



**Figure S.2** (a) The HPLC chromatogram of the de-sugar fraction of Gastrodiae Rhizoma; (b) The optimized LC-MS chromatogram containing four major compounds.

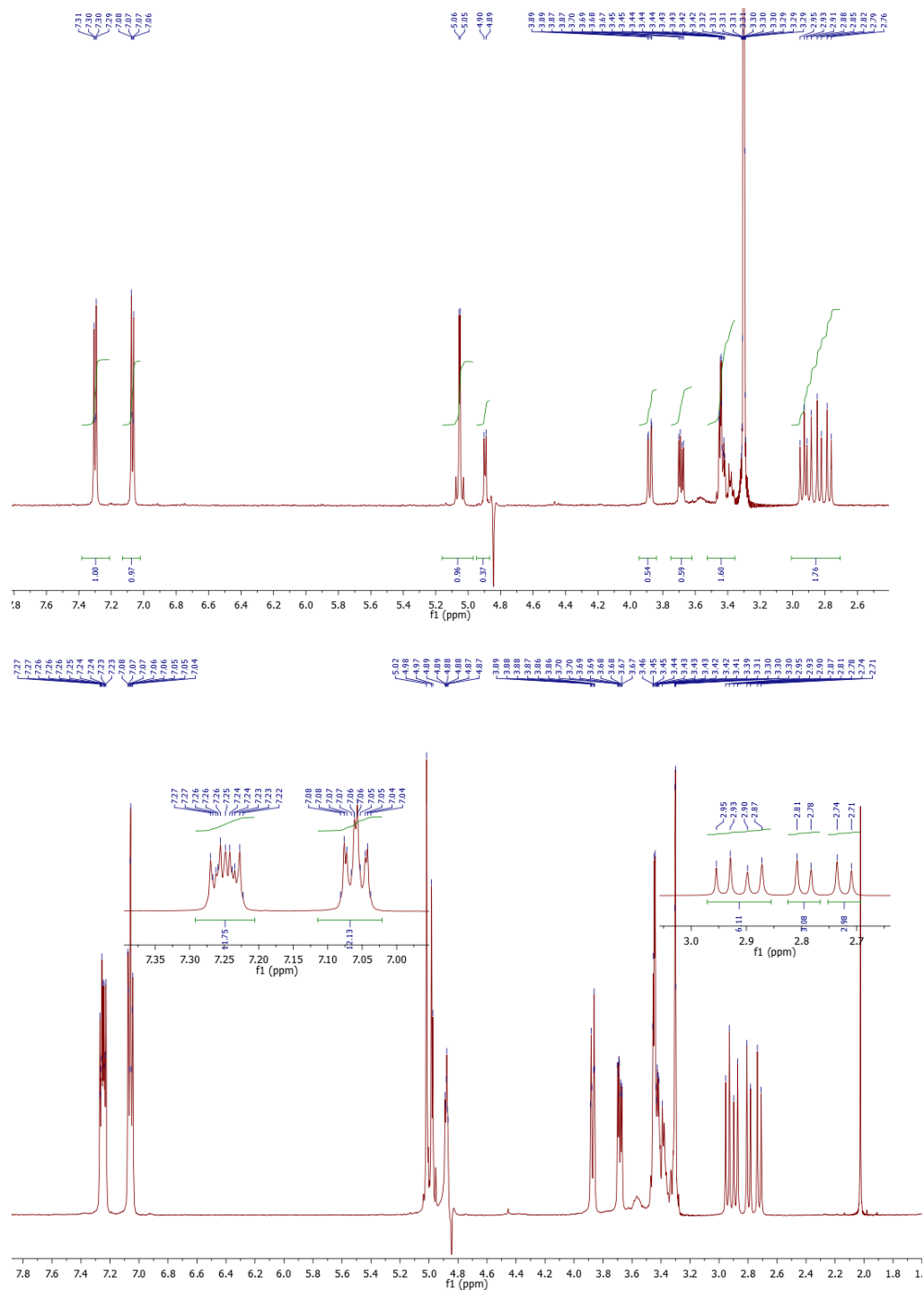




**Figure S.3** Positive and negative ion chromatogram of peaks 1-4.

1.1g of the fat-soluble fraction was dissolved in a mixture of 15 mL MeOH, 10 mL water, and 5 mL DMF, and then subjected to preparative HPLC. Four peaks at the retention times around 37, 53, 57, and 65 min were collected, respectively. The solutions were concentrated and gave four compounds-peak1 (74 mg), peak 2 (48 mg), peak 3 (10 mg), and peak 4 (70 mg).

At the same time, 20 mg of the fat-soluble fraction was dissolved in 2 mL of methanol and then run on the LC-NMR in a stop-flow mode.  $^1\text{H}$  NMR, HSQC and HMBC spectra were acquired for all four peaks. The  $^1\text{H}$  NMR spectra of peaks 1-4 are shown in **Fig. S.4**.



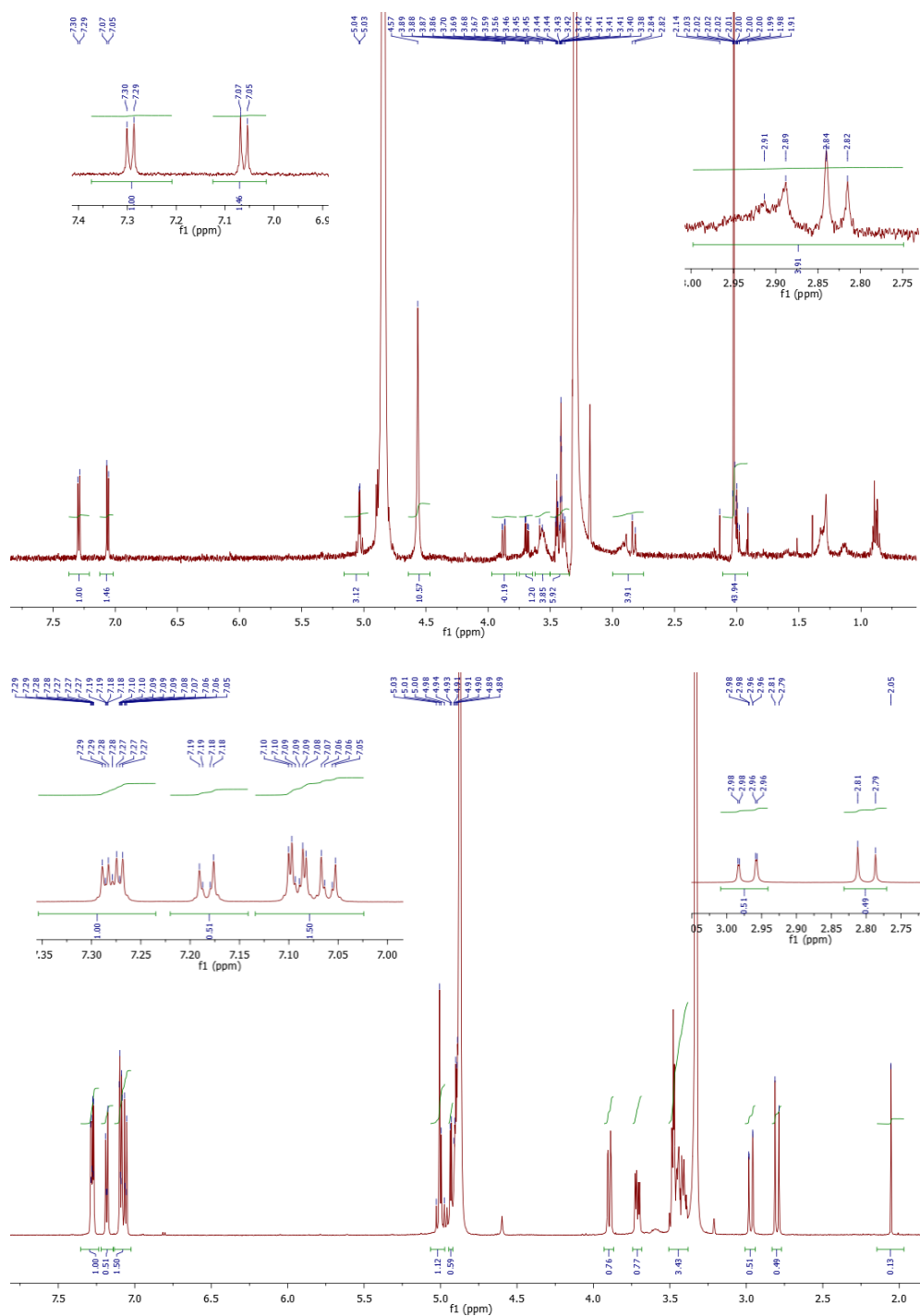


**Figure S.4**  $^1\text{H}$  NMR spectra of peaks 1-4.

The structures of these four peaks (**Fig. 3.7**) were finally determined as parishine derivatives by extensive analysis of their MS and the spectroscopic data, and comparison with data in literature as well.<sup>11, 12</sup>

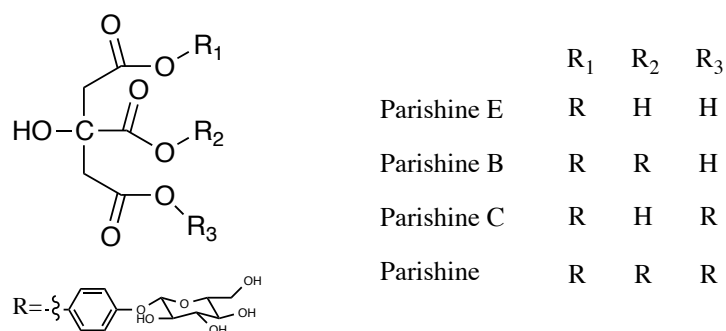


**Figure S.5** Structures of parishine derivatives from Gastrodiae Rhizoma.

### S3 Experimental

Preparative HPLC was performed on a Varian PrepStar system with an Alltech 3300 ELSD detector. Chromatographic separations were carried out on a Waters Sunfire<sup>®</sup> RP C<sub>18</sub>, 5  $\mu$ m, 30 mm  $\times$  150 mm column. The gradient table was shown as follows.

	Time (min)	Flow (mL/min)	%A	%B	Curve
1	0.01	25.00	2.0	98.0	6
2	10.00	25.00	2.0	98.0	6
3	100.0	25.00	30.0	70.0	6

A = 0.1% TFA in CH<sub>3</sub>CN; B = 0.1% TFA in Water

LC-NMR was performed on a Bruker ACE LC-SPE NMR instrument (LC: Agilent 1260 Infinity, SPE: Bruker PROSPEKT 2), and data were processed with Hystar 3.2 for LC and Bruker TopSpin 3.2 for NMR. The column for chromatographic separations and the gradient table were the same with those for preparative HPLC.

## References

1. Holscher, D.; Brand, S.; Wenzler, M.; Schneider, B., NMR-based metabolic profiling of Anigozanthos floral nectar. *Journal of natural products* **2008**, 71, (2), 251-7.
2. Claeson, P.; Panthong, A.; Tuchinda, P.; Reutrakul, V.; Kanjanapothi, D.; Taylor, W. C.; Santisuk, T., Three non-phenolic diarylheptanoids with anti-inflammatory activity from *Curcuma xanthorrhiza*. *Planta Med.* **1993**, 59, (5), 451-4.
3. Kimura, Y.; Takahashi, S.; Yoshida, I., [Studies on the constituents of *Alpinia*. XII. On the constituents of the seeds of *Alpinia katsumadai* Hayata. I. The structure of cardamomin]. *Yakugaku Zasshi* **1968**, 88, (2), 239-41.
4. Romanski, J.; Nowak, P.; Chapuis, C.; Jurczak, J., Total synthesis of (5S)-dihydroyashabushiketol. *Tetrahedron-Asymmetry* **2011**, 22, (7), 787-790.
5. Narasimhulu, M.; Reddy, T. S.; Mahesh, K. C.; Krishna, A. S.; Rao, J. V.; Venkateswarlu, Y., Synthesis of yashabushidiol and its analogues and their cytotoxic activity against cancer cell lines. *Bioorg. Med. Chem. Lett.* **2009**, 19, (11), 3125-3127.
6. Huang, Y.-L.; Chen, C.-C.; Hsu, F.-L.; Chen, C.-F., Two Tannins from *Phyllanthus tenellus*. *J. Nat. Prod.* **1998**, 61, (4), 523-524.
7. Boeck, P.; Bandeira Falcao, C. A.; Leal, P. C.; Yunes, R. A.; Filho, V. C.; Torres-Santos, E. C.; Rossi-Bergmann, B., Synthesis of chalcone analogues with increased antileishmanial activity. *Bioorg. Med. Chem.* **2006**, 14, (5), 1538-45.
8. Ngo, K. S.; Brown, G. D., Stilbenes, monoterpenes, diarylheptanoids, labdanes and chalcones from *Alpinia katsumadai*. *Phytochemistry* **1998**, 47, (6), 1117-1123.
9. Kuo, Y. C.; Yang, L. M.; Lin, L. C., Isolation and immunomodulatory effect of flavonoids from *Syzygium samarangense*. *Planta Med.* **2004**, 70, (12), 1237-1239.
10. Malek, N. A.; Phang, C. W.; Ibrahim, H.; Wahab, N. A.; Sim, K. S., Phytochemical and Cytotoxic Investigations of *Alpinia mutica* Rhizomes. *Molecules* **2011**, 16, (1), 583-589.
11. Lin, J. H.; Liu, Y. C.; Hau, J. P.; Wen, K. C., Parishins B and C from rhizomes of *Gastrodia elata*. *Phytochemistry* **1996**, 42, (2), 549-551.
12. Yang, X.-D.; Zhu, J.; Yang, R.; Liu, J.-P.; Li, L.; Zhang, H.-B., Phenolic constituents from the rhizomes of *Gastrodia elata*. *Natural Product Research* **2007**, 21, (2), 180-186.

## Appendix I

Details of 171 samples for phenotypic screening including SN number, biocluster and which herb or herb pair it came from.

SN Number	Which of Which	Compound Names	No	Biocluster
SN00827874	Compound 1 of Herb 3	paeoniflorin	32	6
SN00827875	Compound 2 of Herb 3	albiflorin	33	6
SN00811372	Ethanol extract of Herb 3			6
SN00811373	Water-soluble fraction of ethanol extract of Herb 3			2
SN00811374	Fat-soluble fraction of ethanol extract of Herb 3			6
SN00827878	Compound 1 of Herb 15	curcumin	88	5
SN00827879	Compound 2 of Herb 15	bisdemethoxycurcumin	89	5
SN00827880	Compound 3 of Herb 15	cardamonin	90	5
SN00811378	Ethanol extract of Herb 15			6
SN00811379	Water-soluble fraction of ethanol extract of Herb 15			6
SN00811380	Fat-soluble fraction of ethanol extract of Herb 15			2
SN00834693	Artificial mixture of compounds of Herb 13			4
SN00827916	Compound 1 of Herb 13	arachidonic acid	81	5
SN00827917	Compound 2 of Herb 13	oleic acid	82	7
SN00827918	Compound 3 of Herb 13	linoleic acid	83	6
SN00827919	Compound 4 of Herb 13	linolenic acid	84	3
SN00811399	Ethanol extract of Herb 13			6
SN00811400	Water-soluble fraction of ethanol extract of Herb 13			2
SN00811401	Fat-soluble fraction of ethanol extract of Herb 13			
SN00834695	Artificial mixture of compounds of Herb 8			6
SN00827881	Compound 1 of Herb 8	ligustilide	49	7
SN00827882	Compound 2 of Herb 8	ferulic acid	50	6
SN00827883	Compound 3 of Herb 8	caffeic acid	51	4

SN00827884	Compound 4 of Herb 8	levistilide A	52	3
SN00827885	Compound 5 of Herb 8	senkyunolide A	53	5
SN00827886	Compound 6 of Herb 8	butylphthalide	54	7
SN00827887	Compound 7 of Herb 8	ligustrazine	55	6
SN00827888	Compound 8 of Herb 8	senkyunolide I	56	6
SN00811381	Ethanol extract of Herb 8			3
SN00811382	Water-soluble fraction of Ethanol Extract of Herb 8			6
SN00811383	Fat-soluble fraction of Ethanol Extract of Herb 8			2
SN00827926	Water extract of Herb 8			5
SN00827927	Water-soluble fraction of Water Extract of Herb 8			6
SN00827928	Fat-soluble fraction of Water Extract of Herb 8			7
SN00827900	Compound 1 of Herb 9	cryptotanshinone	57	6
SN00827901	Compound 2 of Herb 9	salviandic acid B	58	6
SN00827902	Compound 3 of Herb 9	dihydrotanshinone I	59	6
SN00827903	Compound 4 of Herb 9	rosmarinic acid	60	4
SN00827904	Compound 5 of Herb 9	danshensu	61	7
SN00827905	Compound 6 of Herb 9	tanshinone IIA	62	5
SN00827906	Compound 7 of Herb 9	tanshinone I	63	5
SN00827907	Compound 8 of Herb 9	salviandic acid A	64	3
SN00827908	Compound 9 of Herb 9	3,4-dihydroxydenhyde	65	6
SN00827909	Compound 10 of Herb 9	3,4-dihydrobenzonic acid	66	6
SN00827910	Compound 11 of Herb 9	lithospermic acid	67	
SN00811393	Ethanol extract of Herb 9			4
SN00811394	Water-soluble fraction of ethanol extract of Herb 9			6
SN00811395	Fat-soluble fraction of ethanol extract of Herb 9			2
SN00827860	Compound 1 of Herb 2	lobetyolin	31	6
SN00811357	Ethanol extract of Herb 2			6
SN00811358	Water-soluble fraction of Ethanol Extract of Herb 2			6
SN00811359	Fat-soluble fraction of Ethanol Extract of Herb 2			6
SN00827920	Water extract of Herb 2			3
SN00827921	Water-soluble fraction of Water Extract of Herb 2			6

SN00827922	Fat-soluble fraction of Water Extract of Herb 2			<b>6</b>
SN00827897	Compound 1 of Herb 14	daidzin	<b>85</b>	
SN00827898	Compound 2 of Herb 14	puerarin	<b>86</b>	<b>6</b>
SN00827899	Compound 3 of Herb 14	daidzein	<b>87</b>	<b>2</b>
SN00811390	Ethanol extract of Herb 14			<b>6</b>
SN00811391	Water-soluble fraction of ethanol extract of Herb 14			<b>6</b>
SN00811392	Fat-soluble fraction of ethanol extract of Herb 14			<b>6</b>
SN00834691	Artificial mixture 1 of compounds of Herb pair 14+9			<b>6</b>
SN00827944	Ethanol Extract of Herb Pair 14+9			<b>2</b>
SN00827945	Water-soluble fraction of ethanol extract of Herb Pair 14+9			<b>6</b>
SN00827946	Fat-soluble fraction of ethanol extract of Herb Pair 14+9			<b>2</b>
SN00827876	Compound 1 of Herb 7	rhynchophylline	<b>47</b>	<b>6</b>
SN00827877	Compound 2 of Herb 7	isorhynchophylline	<b>48</b>	
SN00811375	Ethanol extract of Herb 7			<b>6</b>
SN00811376	Water-soluble fraction of ethanol extract of Herb 7			
SN00811377	Fat-soluble fraction of ethanol extract of Herb 7			<b>2</b>
SN00827889	Compound 1 of Herb 4	aloe emodin	<b>34</b>	<b>5</b>
SN00827890	Compound 2 of Herb 4	chrysophanol	<b>35</b>	<b>6</b>
SN00827891	Compound 3 of Herb 4	physcion	<b>36</b>	
SN00827892	Compound 4 of Herb 4	emodin	<b>37</b>	<b>6</b>
SN00827893	Compound 5 of Herb 4	2,3,5,4'-tetrahydrosystilbene-2-O- $\beta$ -D-glucopyranoside	<b>38</b>	<b>7</b>
SN00811384	Ethanol extract of Herb 4			
SN00811385	Water-soluble fraction of ethanol extract of Herb 4			<b>3</b>
SN00811386	Fat-soluble fraction of ethanol extract of Herb 4			<b>2</b>
SN00811402	Compound 1 of Herb 1	R-ginsenoside Rh2	<b>19</b>	<b>6</b>
SN00811403	Compound 2 of Herb 1	S-ginsenoside Rh1	<b>21</b>	<b>6</b>

SN00811404	Compound 3 of Herb 1	Ginsenoside Rb3	7	6
SN00811405	Compound 4 of Herb 1	Ginsenoside Ro	24	
SN00811406	Compound 5 of Herb 1	Ginsenoside Rb1	5	6
SN00811407	Compound 6 of Herb 1	Ginsenoside Rc	8	2
SN00811408	Compound 7 of Herb 1	Panaxatriol	14	3
SN00811409	Compound 8 of Herb 1	Ginsenoside CK	1	6
SN00811410	Compound 9 of Herb 1	Pseudoginsenoside F11	15	1
SN00811411	Compound 10 of Herb 1	Ginsenoside F1	4	6
SN00811412	Compound 11 of Herb 1	Ginsenoside Re	10	2
SN00811413	Compound 12 of Herb 1	R-ginsenoside Rg3	17	6
SN00811414	Compound 13 of Herb 1	Ginsenoside Rg1	11	1
SN00811415	Compound 14 of Herb 1	Panaxadiol	13	2
SN00811416	Compound 15 of Herb 1	Ginsenoside Rd	9	6
SN00811417	Compound 16 of Herb 1	Ginsenoside F2	2	6
SN00811418	Compound 17 of Herb 1	Ginsenoside Rk1	12	6
SN00811419	Compound 18 of Herb 1	Ginsenoside Rb2	6	2
SN00811420	Compound 19 of Herb 1	R-ginsenoside Rg2	28	6
SN00811421	Compound 20 of Herb 1	Ginsenoside Rf	3	5
SN00811422	Compound 21 of Herb 1	Pseudoginsenoside RT5	16	5
SN00811423	Compound 22 of Herb 1	Protopanaxatriol	20	1
SN00811424	Compound 23 of Herb 1	Ginsenoside F3	25	6
SN00811425	Compound 24 of Herb 1	R-ginsenoside Rh1	18	6
SN00811426	Compound 25 of Herb 1	S-ginsenoside Rh2	22	6
SN00811427	Compound 26 of Herb 1	S-protopanaxadiol	23	6
SN00811428	Compound 27 of Herb 1	Ginsenoside Rg2	27	6
SN00811429	Compound 28 of Herb 1	S-ginsenoside Rg3	29	
SN00811430	Compound 29 of Herb 1	Ginsenoside Rg6	26	5
SN00811431	Compound 30 of Herb 1	R-protopanaxatriol	30	6
SN00811369	Ethanol extract of Herb 1			
SN00811370	Water-soluble fraction of ethanol extract of Herb 1			1
SN00811371	Fat-soluble fraction of ethanol extract of Herb 1			6
SN00827865	Compound 1 of Herb 10	eugenol	68	2

SN00827866	Compound 2 of Herb 10	$\alpha$ -asarone	<b>69</b>	<b>2</b>
SN00827867	Compound 3 of Herb 10	methyleugenol	<b>70</b>	<b>4</b>
SN00827868	Compound 4 of Herb 10	methyl isoeugenol	<b>71</b>	<b>2</b>
SN00811363	Ethanol extract of Herb 10			<b>6</b>
SN00811364	Water-soluble fraction of ethanol extract of Herb 10			<b>3</b>
SN00811365	Fat-soluble fraction of ethanol extract of Herb 10			
SN00827938	Ethanol Extract of Herb Pair 10+11			<b>2</b>
SN00827939	Water-soluble fraction of ethanol extract of Herb Pair 10+11			<b>6</b>
SN00827940	Fat-soluble fraction of ethanol extract of Herb Pair 10+11			<b>6</b>
SN00827894	Compound 1 of Herb 5	catalpol	<b>39</b>	<b>6</b>
SN00827895	Compound 2 of Herb 5	acetoside	<b>40</b>	<b>6</b>
SN00827896	Compound 3 of Herb 5	5-hydroxymethyl-2-furaldehyde	<b>41</b>	<b>6</b>
SN00811387	Ethanol extract of Herb 5			<b>3</b>
SN00811388	Water-soluble fraction of ethanol extract of Herb 5			<b>2</b>
SN00811389	Fat-soluble fraction of ethanol extract of Herb 5			<b>2</b>
SN00834694	Artificial mixture of compounds of Herb Pair 12+13			<b>6</b>
SN00827941	Ethanol extract of Herb Pair 12+13			<b>6</b>
SN00827942	Water-soluble fraction of ethanol extract of Herb Pair 12+13			<b>2</b>
SN00827943	Fat-soluble fraction of ethanol extract of Herb Pair 12+13			<b>6</b>
SN00834692	Artificial mixture of compounds of Herb 12			<b>6</b>
SN00827861	Compound 1 of Herb 12	nuciferine	<b>77</b>	<b>6</b>
SN00827862	Compound 2 of Herb 12	jujuboside A	<b>78</b>	<b>6</b>
SN00827863	Compound 3 of Herb 12	spinosin	<b>79</b>	<b>6</b>
SN00827864	Compound 4 of Herb 12	jujuboside B	<b>80</b>	<b>6</b>
SN00811360	Ethanol extract of Herb 12			<b>6</b>

SN00811361	Water-soluble fraction of ethanol extract of Herb 12			
SN00811362	Fat-soluble fraction of ethanol extract of Herb 12			4
SN00834698	Artificial mixture 1 of compounds of Herb 6			6
SN00834696	Artificial mixture 2 of compounds of Herb 6			6
SN00827869	Compound 1 of Herb 6	gastrodin	42	6
SN00827870	Compound 2 of Herb 6	parishin E	43	6
SN00827871	Compound 3 of Herb 6	parishin B	44	6
SN00827872	Compound 4 of Herb 6	parishin C	45	5
SN00827873	Compound 5 of Herb 6	parishin	46	4
SN00811366	Ethanol Extract of Herb 6			
SN00811367	Water-soluble fraction of Ethanol Extract of Herb 6			6
SN00811368	Fat-soluble fraction of Ethanol Extract of Herb 6			2
SN00827923	Water Extract of Herb 6			
SN00827924	Water-soluble fraction of Water Extract of Herb 6			6
SN00827925	Fat-soluble fraction of Water Extract of Herb 6			5
SN00834699	Artificial mixture 1 of compounds of Herb Pair 6+8			6
SN00834697	Artificial mixture 2 of compounds of Herb Pair 6+8			6
SN00827932	Ethanol Extract of Herb pair 6+8			3
SN00827933	Water-soluble fraction of Ethanol Extract of Herb Pair 6+8			2
SN00827934	Fat-soluble fraction of Ethanol Extract of Herb Pair 6+8			2
SN00827929	Water Extract of Herb Pair 6+8			4
SN00827930	Water-soluble fraction of Water Extract of Herb Pair 6+8			2
SN00827931	Fat-soluble fraction of Water Extract of Herb Pair 6+8			7
SN00827935	Ethanol Extract of Herb Pair 6+7			6
SN00827936	Water-soluble fraction of Herb Pair 6+7			6
SN00827937	Fat-soluble fraction of Herb Pair 6+7			6
SN00827911	Compound 1 of Herb 11	senegenin	72	7

SN00827912	Compound 2 of Herb 11	tenuifolin	<b>73</b>	<b>6</b>
SN00827913	Compound 3 of Herb 11	onjisaponine B	<b>74</b>	
SN00827914	Compound 4 of Herb 11	Polygalaxanthone III	<b>75</b>	<b>6</b>
SN00827915	Compound 5 of Herb 11	3,6'-disinapoyl sucrose	<b>76</b>	<b>7</b>
SN00811396	Ethanol Extract of Herb 11			<b>6</b>
SN00811397	Water-soluble fraction of Ethanol Extract of Herb 11			<b>5</b>
SN00811398	Fat-soluble fraction of Ethanol Extract of Herb 11			<b>6</b>

## Appendix II

Peaks with charge states from +2 to +14 detected in the spectrum of the lysate incubated with DSI.

<i>m/z</i>	Charge state	MW	<i>m/z</i>	Charge state	MW
564.84532	2	1129.69064	2058.84737	9	18529.62633
570.30024	2	1140.60048	1853.06326	10	18530.6326
731.10346	2	1462.20692	2120.30257	9	19082.72313
1137.83716	2	2275.67432	1930.87458	10	19308.7458
1303.4129	2	2606.8258	1936.5776	10	19365.776
1746.81759	2	3493.63518	2176.83974	9	19591.55766
1346.98628	3	4040.95884	2181.09835	9	19629.88515
2467.75949	2	4935.51898	1963.09189	10	19630.9189
1645.50971	3	4936.52913	1784.7209	11	19631.9299
1234.38548	4	4937.54192	2197.5423	9	19777.8807
2481.23472	2	4962.46944	2199.71448	9	19797.43032
1654.49809	3	4963.49427	2487.25464	8	19898.03712
1241.12593	4	4964.50372	2211.01053	9	19899.09477
1382.58188	6	8295.49128	1990.0104	10	19900.104
1690.1162	5	8450.581	1809.1916	11	19901.1076
1408.59863	6	8451.59178	2215.33756	9	19938.03804
1422.2874	7	9956.0118	1993.80812	10	19938.0812
3362.43182	3	10087.29546	2008.3169	10	20083.169
2522.07471	4	10088.29884	2241.73248	9	20175.59232
2017.86217	5	10089.31085	2252.36185	9	20271.25665
1681.71993	6	10090.31958	2027.22558	10	20272.2558
1441.61937	7	10091.33559	2028.6537	10	20286.537
1261.54361	8	10092.34888	2051.55034	10	20515.5034
2527.57238	4	10110.28952	2324.62439	9	20921.61951
2022.2593	5	10111.2965	2092.26227	10	20922.6227
1685.38326	6	10112.29956	2125.80481	10	21258.0481
2531.56133	4	10126.24532	2144.6761	10	21446.761
2025.44993	5	10127.24965	1949.79908	11	21447.78988
1724.70695	6	10348.2417	1967.00739	11	21637.08129
1478.46487	7	10349.25409	2452.32252	9	22070.90268
2675.67005	4	10702.6802	2207.19599	10	22071.9599
3629.27934	3	10887.83802	2006.63433	11	22072.97763
1863.26635	6	11179.5981	1839.49845	12	22073.9814
1597.37408	7	11181.61856	1698.07613	13	22074.98969
1906.5257	6	11439.1542	2219.09302	10	22190.9302
1634.30962	7	11440.16734	2237.70002	10	22377.0002
2320.33416	5	11601.6708	2034.36819	11	22378.05009
1933.78169	6	11602.69014	3777.53077	6	22665.18462
1657.66965	7	11603.68755	3785.59693	6	22713.58158
1669.30861	7	11685.16027	2321.89576	10	23218.9576
1678.68403	7	11750.78821	3789.77715	7	26528.44005
1969.67297	6	11818.03782	3316.19154	8	26529.53232
1688.43725	7	11819.06075	2947.84322	9	26530.58898
2057.19381	6	12343.16286	2653.1695	10	26531.695
1717.83306	8	13742.66448	3810.22072	7	26671.54504

3655.28428	4	14621.13712	1574.26448	17	26762.49616
2924.42614	5	14622.1307	2682.66885	10	26826.6885
1827.77137	8	14622.17096	2438.88011	11	26827.68121
2437.19021	6	14623.14126	2235.72249	12	26828.66988
2089.16635	7	14624.16445	2741.80018	10	27418.0018
1828.14688	8	14625.17504	1958.72303	14	27422.12242
2094.72897	7	14663.10279	2535.06347	11	27885.69817
2493.58413	6	14961.50478	2368.87202	12	28426.46424
2137.50421	7	14962.52947	2186.7253	13	28427.4289
1870.44008	8	14963.52064	2030.60224	14	28428.43136
1662.72716	9	14964.54444	1895.29729	15	28429.45935
1496.55516	10	14965.5516	2595.23118	11	28547.54298
1873.18788	8	14985.50304	2379.04446	12	28548.53352
2143.06509	7	15001.45563	2867.45416	10	28674.5416
1875.31049	8	15002.48392	2606.87436	11	28675.61796
1884.18978	8	15073.51824	2389.72401	12	28676.68812
2163.64555	7	15145.51885	2614.84153	11	28763.25683
1893.31833	8	15146.54664	1929.37906	15	28940.6859
3805.50717	4	15222.02868	2457.9887	12	29495.8644
2203.71657	7	15426.01599	3787.36543	8	30298.92344
1928.25349	8	15426.02792	3790.78864	8	30326.30912
1960.39605	8	15683.1684	3822.22271	8	30577.78168
1978.84373	8	15830.74984	3825.88539	8	30607.08312
1759.082	9	15831.738	2201.70532	15	33025.5798
2264.71461	7	15853.00227	2064.16287	16	33026.60592
1981.75141	8	15854.01128	1942.80005	17	33027.60085
1761.66898	9	15855.02082	3257.82843	11	35836.11273
2660.7727	6	15964.6362	2986.44245	12	35837.3094
2074.41632	8	16595.33056	2756.7935	13	35838.3155
2077.68104	8	16621.44832	2559.95166	14	35839.32324
2103.43066	8	16827.44528	2989.51846	12	35874.22152
2413.41824	7	16893.92768	2759.71471	13	35876.29123
3387.3075	5	16936.5375	3001.51926	12	36018.23112
2419.80545	7	16938.63815	2770.79102	13	36020.28326
2117.45318	8	16939.62544	3041.37226	12	36496.46712
1912.43637	9	17211.92733	3317.93683	11	36497.30513
1974.46552	9	17770.18968	2810.6921	13	36538.9973
2234.72555	8	17877.8044	2753.31834	14	38546.45676
1986.53495	9	17878.81455	2965.25608	13	38548.32904
2239.9787	8	17919.8296	2970.29578	13	38613.84514
2256.35745	8	18050.8596	2758.20525	14	38614.8735
2005.76662	9	18051.89958	3184.41216	13	41397.35808
2629.79279	7	18408.54953	2957.10008	14	41399.40112
2301.20206	8	18409.61648	3188.64948	13	41452.44324
2045.62379	9	18410.61411	3203.65775	13	41647.55075
1841.16123	10	18411.6123	3245.72247	13	42194.39211
1673.8758	11	18412.6338	3840.58164	11	42246.39804
2048.06692	9	18432.60228	3249.95453	13	42249.40889
2311.19209	8	18489.53672	3137.67306	15	47065.0959
2054.50728	9	18490.56552	3368.289	14	47156.046
1849.15975	10	18491.5975	3370.21976	14	47183.07664
2316.07485	8	18528.5988	3372.14708	14	47210.05912